



January 8, 2017

Lambda global polarization in AuAu collisions at $\sqrt{s_{NN}} = 7.7, 11.5, 14.5, 19.6, 27, \text{ and } 39 \text{ GeV}$ from the STAR experiment

5

Isaac Upsilon¹

1. The Ohio State University, Columbus, USA

Email: upsal.1@osu.edu

Abstract

Lambda global polarization results are shown for the BES energies

10 **Contents**

1	Introduction	10
2	Quality Assurance	15
15	2.1 Event QA	15
	2.2 Event Plane determination	26
	2.2.1 Event plane resolution	35
	2.3 Track QA	37
	2.4 Lambda reconstruction	40
	2.4.1 Daughter PID	40
	2.4.2 Lambda topological cuts	50
20	3 Data analysis	54
	3.1 Resolution Correction	55
	3.2 Mass background	56
	3.3 Detector acceptance correction	61
25	3.3.1 Detector acceptance correction explanation	61
	3.3.2 Detector acceptance correction results	62
	3.4 Helicity efficiency	63
	3.4.1 Helicity efficiency description	64
	3.4.2 Helicity efficiency effect	73
	3.5 Feed-down correction	84
30	3.5.1 Abstract for feeddown	84
	3.5.2 Correction procedure and definitions	84
	3.5.3 Which particles are included?	84
	3.5.4 Feed-down matrices	85
	3.5.5 Application to STAR data	85
35	3.5.6 Acknowledgements	88
	3.5.7 Extracting feed-down fractions from Bill Llope's THERMUS file	88
	3.5.8 Communication with Jean Cleymans	107
	3.5.9 Sanity check	109
	3.5.10 HIJING efficiency	109
40	3.5.11 Old feed-down correction using only Σ^0 s	110
	3.6 Discussion of statistical error	111

4 Systematic errors	112
4.1 Topological cut dependencies	112
4.1.1 Covariance method idea	112
45 4.1.2 Mass purity	114
4.1.3 Results	119
4.1.4 Simple cut variation	124
4.2 Residual effect	126
4.3 Scaling errors	129
50 4.4 Conservation of momentum effects on event plane resolution	130
4.5 Feeddown	135
 5 Systematic Dependencies	 136
5.1 Centrality	136
5.2 Energy	158
55 5.3 Rapidity	164
5.4 Azimuthal angle	173
 6 Signal falsification	 176
6.1 Simulation comparison	176
6.2 Rotated pions	176
 60 7 STAR 2007 results	 179

List of Figures

1	$P_H^{\Lambda,\bar{\Lambda}}$	11
2	schematic of collision	12
3	Lambda in event with black background schematic	13
65	4 overview of the STAR detector	14
5	Reference multiplicity	17
6	Z Vertex	17
7	ToF Multiplicity	18
8	BBC East ADC sum	18
70	9 BBC West ADC sum	19
10	7GeV R Vertex	20
11	11GeV R Vertex	21
12	15GeV R Vertex	22
13	19GeV R Vertex	23
75	14 27GeV R Vertex	24
15	39GeV R Vertex	25
16	BBC numbering scheme	26
17	STAR Coordinates	27
18	7GeV Ψ_1 distribution	29
80	19 11GeV Ψ_1 distribution	29
20	15GeV Ψ_1 distribution	30
21	19GeV Ψ_1 distribution	30
22	27GeV Ψ_1 distribution	31
23	39GeV Ψ_1 distribution	31
85	24 7GeV $\Psi_{1,W}$ vs. $\Psi_{1,E}$	32
25	11GeV $\Psi_{1,W}$ vs. $\Psi_{1,E}$	32
26	15GeV $\Psi_{1,W}$ vs. $\Psi_{1,E}$	33
27	19GeV $\Psi_{1,W}$ vs. $\Psi_{1,E}$	33
28	27GeV $\Psi_{1,W}$ vs. $\Psi_{1,E}$	34
90	29 39GeV $\Psi_{1,W}$ vs. $\Psi_{1,E}$	34
30	Resolution Correction	35
31	Charged track p_T	37
32	Charged track η	38

33	Charged track N _{Hits Possible}	38
95	34 Charged track N _{Hits}	39
35 Charged track Fit Ratio	39	
36 7GeV dE/dx vs. p	40	
37 7GeV 1/β vs. p	41	
38 7GeV m^2 vs. p	41	
100	39 11GeV dE/dx vs. p	42
40 11GeV 1/β vs. p	42	
41 11GeV m^2 vs. p	43	
42 15GeV dE/dx vs. p	43	
43 15GeV 1/β vs. p	44	
105	44 15GeV m^2 vs. p	44
45 19GeV dE/dx vs. p	45	
46 19GeV 1/β vs. p	45	
47 19GeV m^2 vs. p	46	
48 27GeV dE/dx vs. p	46	
110	49 27GeV 1/β vs. p	47
50 27GeV m^2 vs. p	47	
51 39GeV dE/dx vs. p	48	
52 39GeV 1/β vs. p	48	
53 39GeV m^2 vs. p	49	
115	54 Lambda reconstruction diagram	50
55 Proton DCA distribution	51	
56 Pion DCA distribution	51	
57 Daughter DCA distribution	52	
58 Lambda DCA distribution	52	
120	59 Lambda decay length distribution	53
60 Lambda mass distribution	53	
61 Resolution effect 0-80%	55	
62 Resolution effect 20-50%	55	
63 Λ off mass distribution	56	
125	64 Λ off mass comparison ($m_{\text{inv}} > m_{\Lambda}$)	57
65 Λ off mass comparison ($m_{\text{inv}} < m_{\Lambda}$)	58	

66	$\bar{\Lambda}$ off mass comparison ($m_{\text{inv}} > m_{\Lambda}$)	58
67	$\bar{\Lambda}$ off mass comparison ($m_{\text{inv}} < m_{\Lambda}$)	59
68	Λ purity correction comparison	60
130	69 $\bar{\Lambda}$ purity correction comparison	60
70	Helicity efficiency diagram	63
71	Helicity Efficiency Data	64
72	Helicity Efficiency Simulation	65
73	Helicity efficiency effect (39GeV Λ)	66
135	74 Helicity efficiency effect (39GeV $\bar{\Lambda}$)	67
75	Helicity efficiency effect (27GeV Λ)	67
76	Helicity efficiency effect (27GeV $\bar{\Lambda}$)	68
77	Helicity Efficiency Simulation	69
78	S_y asymmetry η slices	70
140	79 S_y asymmetry with STAR η cut	71
80	S_y asymmetry with helicity efficiency	72
81	Helicity efficiency effect presentation p1	73
82	Helicity efficiency effect presentation p2	74
83	Helicity efficiency effect presentation p3	75
145	84 Helicity efficiency effect presentation p4	76
85	Helicity efficiency effect presentation p5	77
86	Helicity efficiency effect presentation p6	78
87	Helicity efficiency effect presentation p7	79
88	Helicity efficiency effect presentation p8	80
150	89 Helicity efficiency effect presentation p9	81
90	Helicity efficiency effect presentation p10	82
91	Helicity efficiency effect presentation p11	83
92	Invariant mass as a function of pion DCA	114
93	Lambda invariant mass purity as a function of pion DCA	115
155	94 Lambda invariant mass purity as a function of proton DCA	115
95	Lambda invariant mass purity as a function of daughter DCA	116
96	Lambda invariant mass purity as a function of Lambda DCA	116
97	Lambda invariant mass purity as a function of Lambda decay length	117
98	Λ polarization covariance with cut quantities for each Λ cut index	119

160	99	Λ polarization covariance with cut quantities for each Λ cut index; zoomed in	119
	100	Λ polarization “slope” from covariance with cut quantities for each Λ cut index	120
	101	Λ polarization “slope” from covariance with cut quantities for each Λ cut index	120
	102	Λ polarization “slope” from covariance with cut quantities for each Λ cut index; zoomed in	121
	103	Λ polarization “slope” from covariance with cut quantities for each Λ cut index	122
165	104	Λ polarization “slope” from covariance with cut quantities for each Λ cut index; zoomed in	122
	105	Λ polarization “slope” from covariance with cut quantities for each Λ cut index	123
	106	Λ polarization “slope” from covariance with cut quantities for each Λ cut index; zoomed in	123
	107	Λ cut comparison	124
	108	$\bar{\Lambda}$ cut comparison	124
170	109	Yadav’s study of MC effects on resolution p1	130
	110	Yadav’s study of MC effects on resolution p2	130
	111	Yadav’s study of MC effects on resolution p3	131
	112	Yadav’s study of MC effects on resolution p4	131
	113	Yadav’s study of MC effects on resolution p5	132
175	114	Yadav’s study of MC effects on resolution p6	132
	115	Yadav’s study of MC effects on resolution p7	133
	116	Yadav’s study of MC effects on resolution p8	133
	117	Yadav’s study of MC effects on resolution p9	134
	118	Yadav’s study of MC effects on resolution p10	134
180	119	Λ more peripheral centrality	136
	120	Λ more central centrality	137
	121	Λ cut into halves of centrality	137
	122	Λ cut into thirds of centrality	138
	123	Λ for mid-centrality	138
185	124	Λ for bins of 20% centrality	139
	125	Λ for 0-20% and 20-80% centrality	139
	126	Λ right of mass peak ($m_{\text{inv}} > m_{\Lambda}$) more peripheral centrality	140
	127	Λ right of mass peak ($m_{\text{inv}} > m_{\Lambda}$) more central centrality	140
	128	Λ right of mass peak ($m_{\text{inv}} > m_{\Lambda}$) cut into halves of centrality	141
190	129	Λ right of mass peak ($m_{\text{inv}} > m_{\Lambda}$) cut into thirds of centrality	141
	130	Λ right of mass peak ($m_{\text{inv}} > m_{\Lambda}$) for mid-centrality	142
	131	Λ right of mass peak ($m_{\text{inv}} > m_{\Lambda}$) for bins of 20% centrality	142

132	Λ right of mass peak ($m_{\text{inv}} > m_{\Lambda}$) for 0-20% and 20-80% centrality	143
133	Λ left of mass peak ($m_{\text{inv}} < m_{\Lambda}$) more peripheral centrality	143
195	Λ left of mass peak ($m_{\text{inv}} < m_{\Lambda}$) more central centrality	144
135	Λ left of mass peak ($m_{\text{inv}} < m_{\Lambda}$) cut into halves of centrality	144
136	Λ left of mass peak ($m_{\text{inv}} < m_{\Lambda}$) cut into thirds of centrality	145
137	Λ left of mass peak ($m_{\text{inv}} < m_{\Lambda}$) for mid-centrality	145
138	Λ left of mass peak ($m_{\text{inv}} < m_{\Lambda}$) for bins of 20% centrality	146
200	139 Λ left of mass peak ($m_{\text{inv}} < m_{\Lambda}$) for 0-20% and 20-80% centrality	146
140	$\bar{\Lambda}$ more peripheral centrality	147
141	$\bar{\Lambda}$ more central centrality	147
142	$\bar{\Lambda}$ cut into halves of centrality	148
143	$\bar{\Lambda}$ cut into thirds of centrality	148
205	144 $\bar{\Lambda}$ for mid-centrality	149
145	$\bar{\Lambda}$ for bins of 20% centrality	149
146	$\bar{\Lambda}$ for 0-20% and 20-80% centrality	150
147	$\bar{\Lambda}$ right of mass peak ($m_{\text{inv}} > m_{\Lambda}$) more peripheral centrality	150
148	$\bar{\Lambda}$ right of mass peak ($m_{\text{inv}} > m_{\Lambda}$) more central centrality	151
210	149 $\bar{\Lambda}$ right of mass peak ($m_{\text{inv}} > m_{\Lambda}$) cut into halves of centrality	151
150	$\bar{\Lambda}$ right of mass peak ($m_{\text{inv}} > m_{\Lambda}$) cut into thirds of centrality	152
151	$\bar{\Lambda}$ right of mass peak ($m_{\text{inv}} > m_{\Lambda}$) for mid-centrality	152
152	$\bar{\Lambda}$ right of mass peak ($m_{\text{inv}} > m_{\Lambda}$) for bins of 20% centrality	153
153	$\bar{\Lambda}$ right of mass peak ($m_{\text{inv}} > m_{\Lambda}$) for 0-20% and 20-80% centrality	153
215	154 $\bar{\Lambda}$ left of mass peak ($m_{\text{inv}} < m_{\Lambda}$) more peripheral centrality	154
155	$\bar{\Lambda}$ left of mass peak ($m_{\text{inv}} < m_{\Lambda}$) more central centrality	154
156	$\bar{\Lambda}$ left of mass peak ($m_{\text{inv}} < m_{\Lambda}$) cut into halves of centrality	155
157	$\bar{\Lambda}$ left of mass peak ($m_{\text{inv}} < m_{\Lambda}$) cut into thirds of centrality	155
158	$\bar{\Lambda}$ left of mass peak ($m_{\text{inv}} < m_{\Lambda}$) for mid-centrality	156
220	159 $\bar{\Lambda}$ left of mass peak ($m_{\text{inv}} < m_{\Lambda}$) for bins of 20% centrality	156
160	$\bar{\Lambda}$ left of mass peak ($m_{\text{inv}} < m_{\Lambda}$) for 0-20% and 20-80% centrality	157
161	Λ polarization dependence on energy (2 bins)	158
162	Λ polarization dependence on energy (3 bins)	158
163	Λ right of mass peak ($m_{\text{inv}} > m_{\Lambda}$) polarization dependence on energy (2 bins)	159
225	164 Λ right of mass peak ($m_{\text{inv}} > m_{\Lambda}$) polarization dependence on energy (3 bins)	159

165	Λ left of mass peak ($m_{\text{inv}} < m_{\Lambda}$) polarization dependence on energy (2 bins)	160
166	Λ left of mass peak ($m_{\text{inv}} < m_{\Lambda}$) polarization dependence on energy (3 bins)	160
167	$\bar{\Lambda}$ polarization dependence on energy (2 bins)	161
168	$\bar{\Lambda}$ polarization dependence on energy (3 bins)	161
230	169 $\bar{\Lambda}$ right of mass peak ($m_{\text{inv}} > m_{\Lambda}$) polarization dependence on energy (2 bins)	162
170	$\bar{\Lambda}$ right of mass peak ($m_{\text{inv}} > m_{\Lambda}$) polarization dependence on energy (3 bins)	162
171	$\bar{\Lambda}$ left of mass peak ($m_{\text{inv}} < m_{\Lambda}$) polarization dependence on energy (2 bins)	163
172	$\bar{\Lambda}$ left of mass peak ($m_{\text{inv}} < m_{\Lambda}$) polarization dependence on energy (3 bins)	163
173	Λ polarization dependence on rapidity (2 bins)	164
235	174 Λ polarization dependence on rapidity (3 bins)	164
175	Λ polarization dependence on rapidity sign	165
176	Λ right of mass peak ($m_{\text{inv}} > m_{\Lambda}$) polarization dependence on rapidity (2 bins)	165
177	Λ right of mass peak ($m_{\text{inv}} > m_{\Lambda}$) polarization dependence on rapidity (3 bins)	166
178	Λ right of mass peak ($m_{\text{inv}} > m_{\Lambda}$) polarization dependence on rapidity sign	166
240	179 Λ left of mass peak ($m_{\text{inv}} < m_{\Lambda}$) polarization dependence on rapidity (2 bins)	167
180	Λ left of mass peak ($m_{\text{inv}} < m_{\Lambda}$) polarization dependence on rapidity (3 bins)	167
181	Λ Left of mass peak ($m_{\text{inv}} < m_{\Lambda}$) polarization dependence on rapidity sign	168
182	$\bar{\Lambda}$ polarization dependence on rapidity (2 bins)	168
183	$\bar{\Lambda}$ polarization dependence on rapidity (3 bins)	169
245	184 $\bar{\Lambda}$ polarization dependence on rapidity sign	169
185	$\bar{\Lambda}$ right of mass peak ($m_{\text{inv}} > m_{\Lambda}$) polarization dependence on rapidity (2 bins)	170
186	$\bar{\Lambda}$ right of mass peak ($m_{\text{inv}} > m_{\Lambda}$) polarization dependence on rapidity (3 bins)	170
187	$\bar{\Lambda}$ right of mass peak ($m_{\text{inv}} > m_{\Lambda}$) polarization dependence on rapidity sign	171
188	$\bar{\Lambda}$ left of mass peak ($m_{\text{inv}} < m_{\Lambda}$) polarization dependence on rapidity (2 bins)	171
250	189 $\bar{\Lambda}$ left of mass peak ($m_{\text{inv}} < m_{\Lambda}$) polarization dependence on rapidity (3 bins)	172
190	$\bar{\Lambda}$ Left of mass peak ($m_{\text{inv}} < m_{\Lambda}$) polarization dependence on rapidity sign	172
191	Λ polarization dependence on azimuthal angle	173
192	Λ right of mass peak ($m_{\text{inv}} > m_{\Lambda}$) polarization dependence on azimuthal angle	173
193	Λ left of mass peak ($m_{\text{inv}} < m_{\Lambda}$) polarization dependence on azimuthal angle	174
255	194 $\bar{\Lambda}$ polarization dependence on azimuthal angle	174
195	$\bar{\Lambda}$ right of mass peak ($m_{\text{inv}} > m_{\Lambda}$) polarization dependence on azimuthal angle	175
196	$\bar{\Lambda}$ left of mass peak ($m_{\text{inv}} < m_{\Lambda}$) polarization dependence on azimuthal angle	175
197	Λ and $\bar{\Lambda}$ polarization with rotated pions	177

198	Λ off mass polarization with rotated pions	177
-----	--	-----

260	199 $\bar{\Lambda}$ off mass polarization with rotated pions	178
-----	--	-----

1 Introduction

The analysis is performed for the BES energies: 7.7, 11.5, 14.5, 19.6, 27, and 39 GeV.

Peripheral collisions have large angular momentum ($\sim 10^4 - 10^5 \hbar$) which can be transferred, in part, to the fireball at mid-rapidity. In principle this could be related to baryon stopping. A partial thermalization
265 of the angular degrees of freedom inside the fireball would lead to hadronic spin alignment with the angular momentum of the system. This spin alignment is the global polarization of the hadrons. The vorticity is the curl of a fluid's velocity field $\vec{\omega} \equiv \nabla \times \vec{v}$. In a hydrodynamic description the vorticity of the fluid is probed by the global polarization, which is largely unexplored in current transport models.

Lambda baryons are self analyzing which means that the daughter protons are preferentially emitted in
270 the direction of the Lambda's spin (note that the proton is emitted opposite the spin for the antiparticle, the $\bar{\Lambda}$). The distribution of emitted protons follows the following distribution

$$\frac{1}{N} \frac{dN}{d\Omega^*} = \frac{1}{4\pi} \left(1 + \alpha \vec{S}_\Lambda^* \cdot \hat{p}_p^* \right), \quad (1)$$

where the * denotes the rest frame of the Λ , \vec{S}_Λ^* is the Lambda spin direction, \hat{p}_p^* is the daughter proton momentum direction.

The self analyzing nature of the Λ s allows us to make a measurement of the global Λ polarization. The
275 global polarization is measured by looking to see if the spin of the Λ points preferentially in the direction of the angular momentum of the system \hat{L} . \hat{L} is found via the first order event plane, Ψ_1 , which is found by using the BBC. Our measure of polarization is

$$\frac{8}{\pi\alpha} \langle \sin(\phi_p^* - \Psi_1) \rangle \quad (2)$$

where ϕ_p^* is the proton's azimuthal angle.

Initially we planned on extracting the polarization due to the magnetic field and vorticity separately. We
280 are no longer doing this now that we have switched from a PRL to a Nature paper. Plots and discussion from this are littered throughout. We plan on a followup PRC which will include this so I don't want to remove it.

The final plot for Λ and $\bar{\Lambda}$ polarization

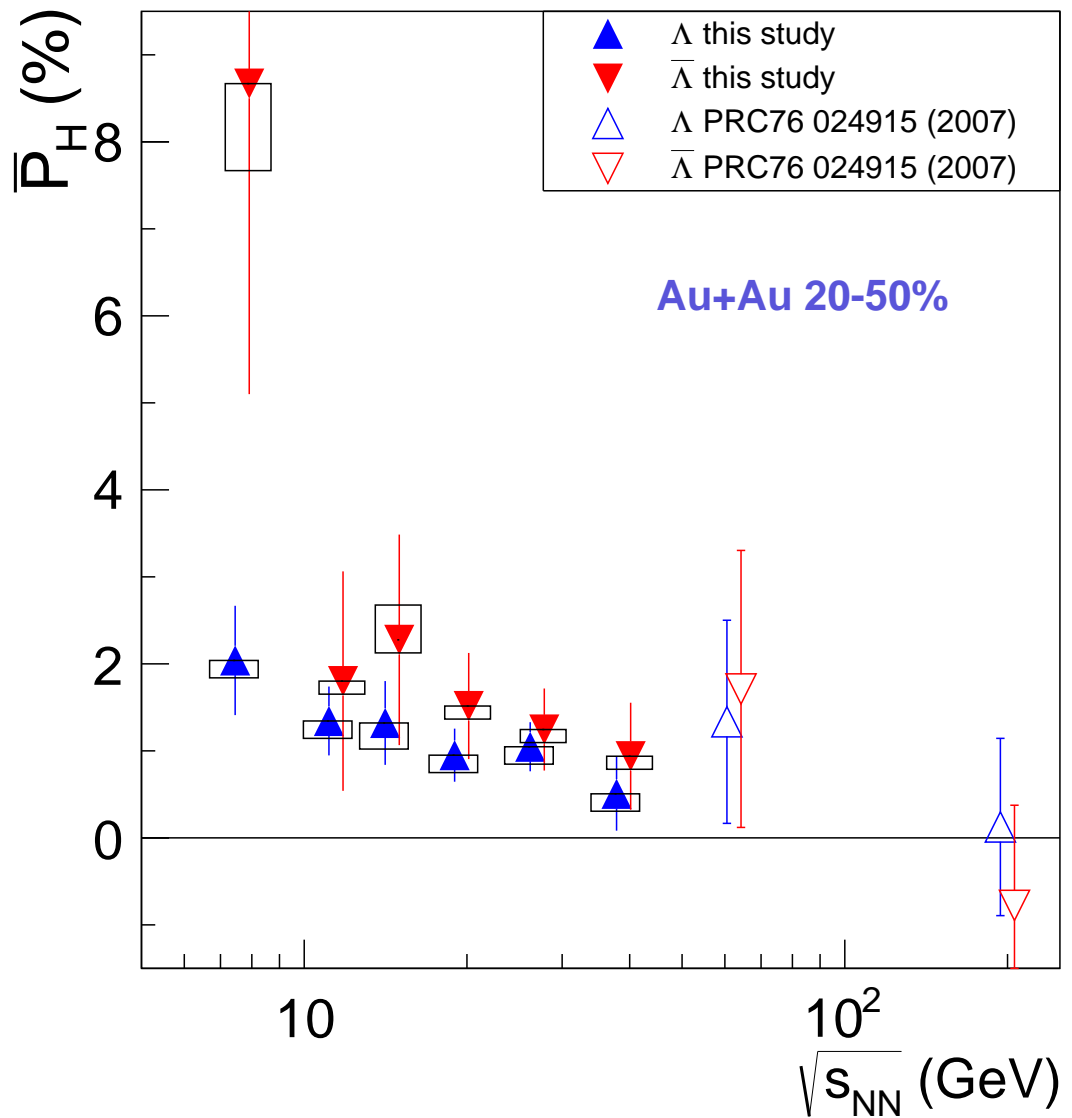


Fig. 1: $\left\langle \frac{8}{\pi\alpha} \sin(\Psi_1 - \phi_{\Lambda,\bar{\Lambda}}^*) \right\rangle$ vs. $\sqrt{s_{NN}}$ for 20-50% centrality

The supporting plots are

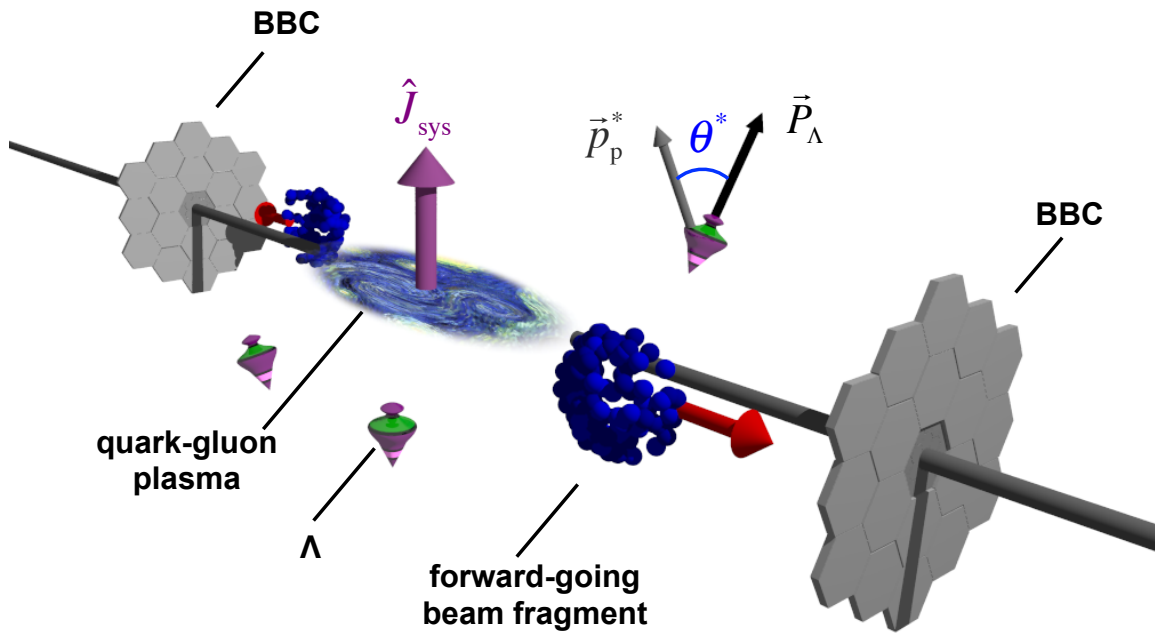


Fig. 2: schematic of collision.

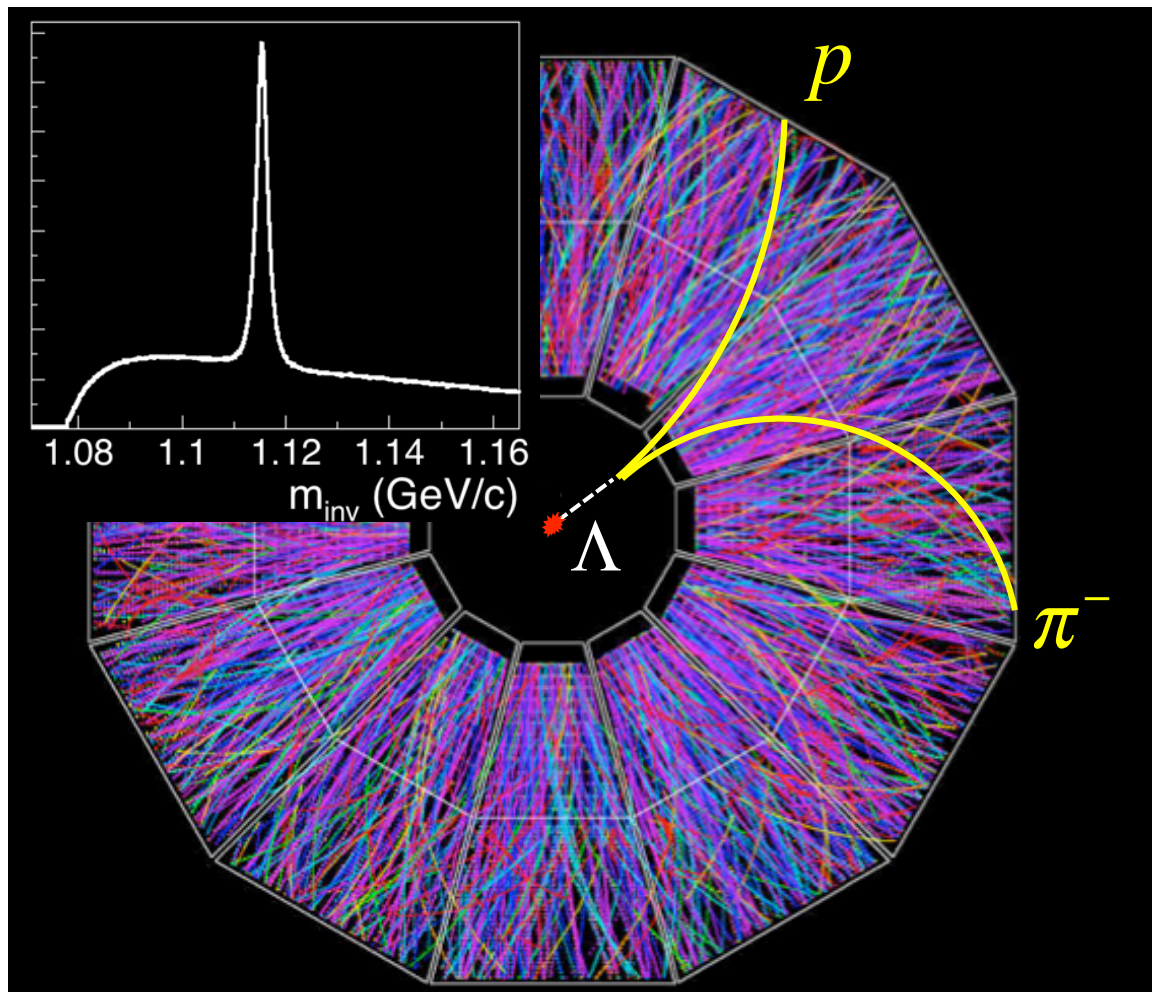


Fig. 3: Lambda in event with black background schematic.

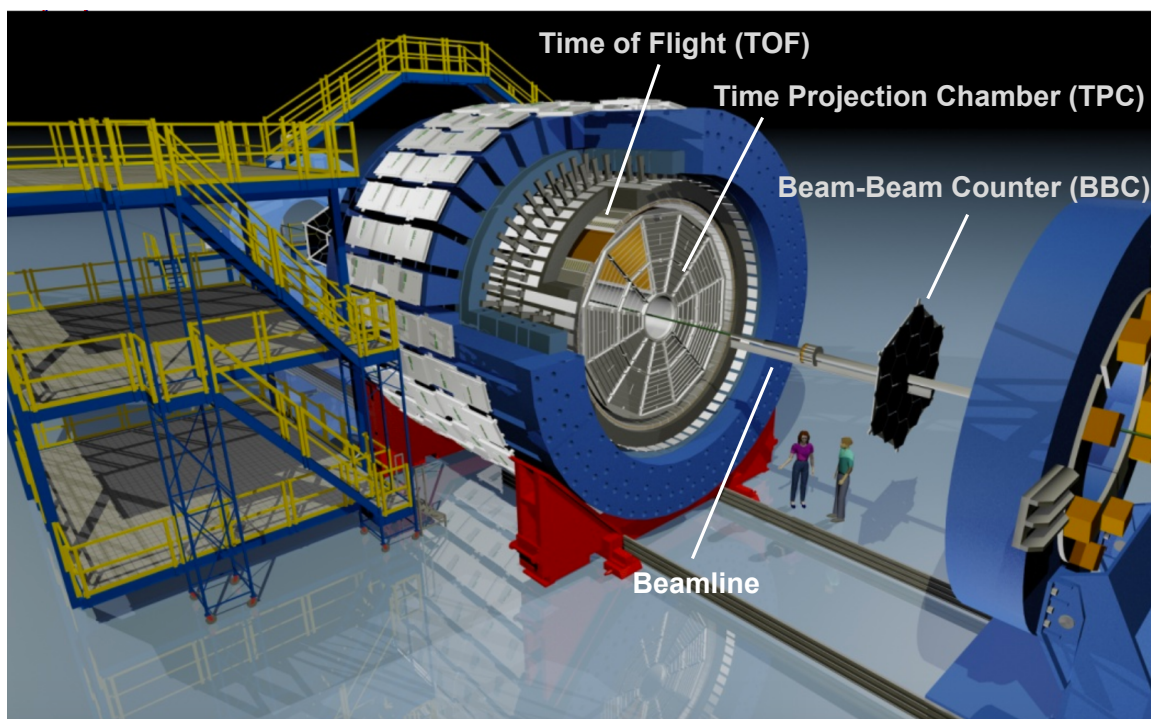


Fig. 4: overview of the STAR detector.

285 **2 Quality Assurance**

2.1 Event QA

The events used in the analysis have the following cuts

- The magnitude of the z component of the primary vertex is $\leq 70\text{cm}$. At 39GeV this is a 40cm cut and at 11GeV this is 50cm cut.
- 290 – Tof multiplicity ≥ 1
- the R vertex component is required to be less than 2cm except in the case of 15GeV where it is less than 1cm and centered at (0, -0.89) cm.
- The adc sum for the East and West BBC are separately required to be ≥ 75
- Additionally there is an η symmetry cut so that $|(N_{\eta>0} - N_{\eta>0}) / N_{\text{total}}| \leq 5$
- 295 – The centrality ID that we get from StRefMultCorr must be ≥ 0

The trigger list for each energy is

- 7.7GeV: 290001, 290004
- 11.5GeV: 310004, 310014
- 14.5GeV: 440005, 440015
- 300 – 19.6GeV: 340001, 340011, 340021
- 27GeV: 360001, 360002
- 39GeV: 280001, 280002

Additionally there is a list of rejected runs which is

- 7.7GeV: 11199124, 11100002, 11100045, 11101046, 11102012, 11102051, 11102052, 11102053, 11102054, 11102055, 11102058, 11103035, 11103056, 11103058, 11103092, 11103093, 11105052, 11105053, 11105054, 11105055, 11107007, 11107042, 11107057, 11107061, 11107065, 11107074, 11108101, 11109013, 11109077, 11109088, 11109090, 11109127, 11110013, 11110034, 11110073, 11110076, 11111084, 11111085
- 305 – 11.5GeV: 11148039, 11148045, 11149001, 11149008, 11149010, 11149011, 11149015, 11149047, 11150016, 11150025, 11150028, 11151036, 11151040, 11151050, 11152016, 11152036, 11152078, 11153032, 11153042, 11155001, 11155009, 11156003, 11156009, 11157012, 11158006, 11158022, 11158024
- 310 – 14.5GeV: 15046073, 15046089, 15046094, 15046096, 15046102, 15046103, 15046104, 15046105, 15046106, 15046107, 15046108, 15046109, 15046110, 15046111, 15047004, 15047015, 15047016, 15047019, 15047021, 15047023, 15047024, 15047026, 15047027, 15047028, 15047029, 15047030, 15047039, 15047040, 15047041, 15047044, 15047047, 15047050, 15047052, 15047053, 15047056, 15047057, 15047061, 15047062, 15047063, 15047064, 15047065, 15047068, 15047069, 15047070, 15047071, 15047072, 15047074, 15047075, 15047082, 15047085, 15047086, 15047087, 15047093, 15047096, 15047097, 15047098, 15047100, 15047102, 15047104, 15047106, 15048003, 15048004,

320 15048012, 15048013, 15048014, 15048016, 15048017, 15048018, 15048019, 15048020, 15048021,
 15048023, 15048024, 15048025, 15048026, 15048028, 15048029, 15048030, 15048031, 15048033,
 15048034, 15048074, 15048075, 15048076, 15048077, 15048078, 15048079, 15048080, 15048081,
 15048082, 15048083, 15048084, 15048085, 15048086, 15048087, 15048088, 15048089, 15048091,
 15048092, 15048093, 15048094, 15048095, 15048096, 15048097, 15048098, 15049002, 15049003,
 325 15049009, 15049013, 15049014, 15049015, 15049016, 15049017, 15049018, 15049019, 15049020,
 15049021, 15049022, 15049023, 15049025, 15049026, 15049027, 15049028, 15049030, 15049031,
 15049032, 15049033, 15049037, 15049038, 15049039, 15049040, 15049041, 15049074, 15049077,
 15049083, 15049084, 15049085, 15049086, 15049087, 15049088, 15049089, 15049090, 15049091,
 330 15049092, 15049093, 15049094, 15049096, 15049097, 15049098, 15049099, 15050001, 15050002,
 15050003, 15050004, 15050005, 15050006, 15050010, 15050011, 15050012, 15050013, 15050014,
 15050015, 15050016, 15051131, 15051132, 15051133, 15051134, 15051137, 15051141, 15051144,
 15051146, 15051147, 15051148, 15051149, 15051156, 15051157, 15051159, 15051160, 15052001,
 15052004, 15052005, 15052006, 15052007, 15052008, 15052009, 15052010, 15052011, 15052014,
 335 15052015, 15052016, 15052017, 15052018, 15052019, 15052020, 15052021, 15052022, 15052023,
 15052024, 15052025, 15052026, 15052040, 15052041, 15052042, 15052043, 15052060, 15052061,
 15052062, 15052063, 15052064, 15052065, 15052066, 15052067, 15052068, 15052069, 15052070,
 15052073, 15052074, 15052075, 15053027, 15053028, 15053029, 15053034, 15053035, 15053052,
 15053054, 15053055, 15054053, 15054054, 15055018, 15055137, 15056117, 15057055, 15057059,
 15058006, 15058011, 15058021, 15059057, 15059058, 15061001, 15061009, 15062006, 15062069,
 340 15065012, 15065014, 15066070, 15068013, 15068014, 15068016, 15068018, 15069036, 15070008,
 15070009, 15070010

- 19.6GeV: 12113091, 12114007, 12114035, 12114078, 12114092, 12114116, 12115009, 12115014,
 12115015, 12115016, 12115018, 12115019, 12115020, 12115022, 12115023, 12115062, 12115073,
 12115093, 12115094, 12116012, 12116054, 12117010, 12117016, 12117020, 12117065, 12119040,
 12119042, 12120017, 12120026, 12121017, 12121022, 12121034, 12121050, 12121067, 12122019
- 27GeV: 12172050, 12172051, 12172055, 12173030, 12173031, 12173032, 12173033, 12173034,
 12174067, 12174085, 12175062, 12175087, 12175113, 12175114, 12175115, 12176001, 12176044,
 12176054, 12176071, 12177015, 12177061, 12177092, 12177099, 12177101, 12177106, 12177107,
 12177108, 12178003, 12178004, 12178005, 12178006, 12178013, 12178099, 12178120
- 39GeV: 11199124, 11100002, 11100045, 11101046, 11102012, 11102051, 11102052, 11102053,
 11102054, 11102055, 11102058, 11103035, 11103056, 11103058, 11103092, 11103093, 11105052,
 11105053, 11105054, 11105055, 11107007, 11107042, 11107057, 11107061, 11107065, 11107074,
 11108101, 11109013, 11109077, 11109088, 11109090, 11109127, 11110013, 11110034, 11110073,
 11110076, 11111084, 11111085

355 In addition to the bad runs list 15GeV events are taken only from running days 53-70.

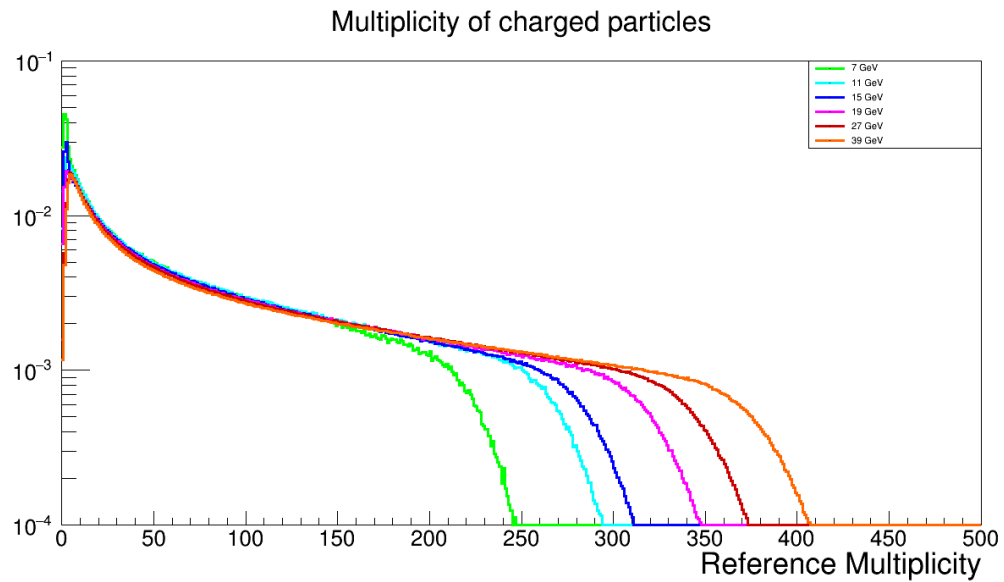


Fig. 5: Multiplicity of charged tracks (normalized)

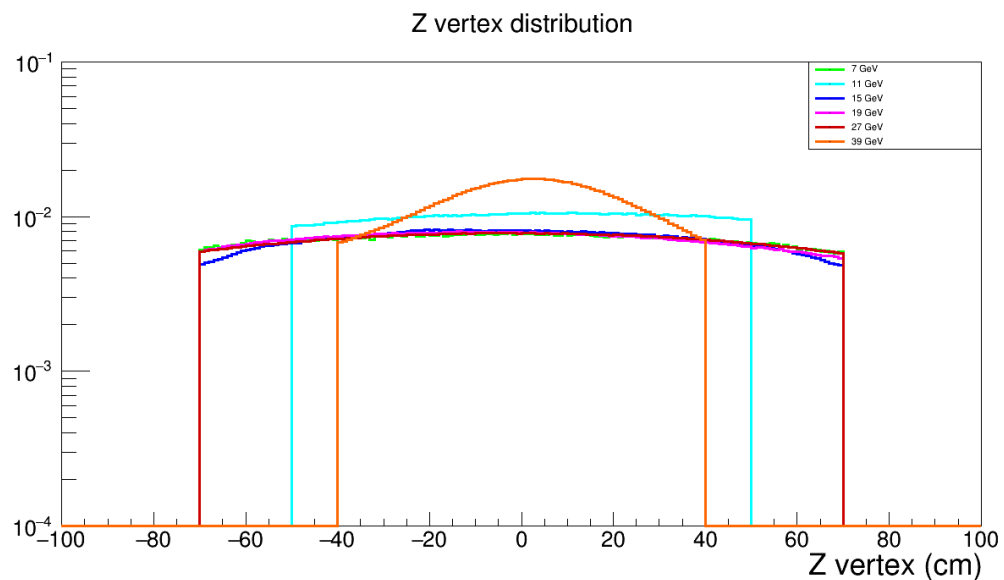


Fig. 6: Z component of event vertex (normalized)

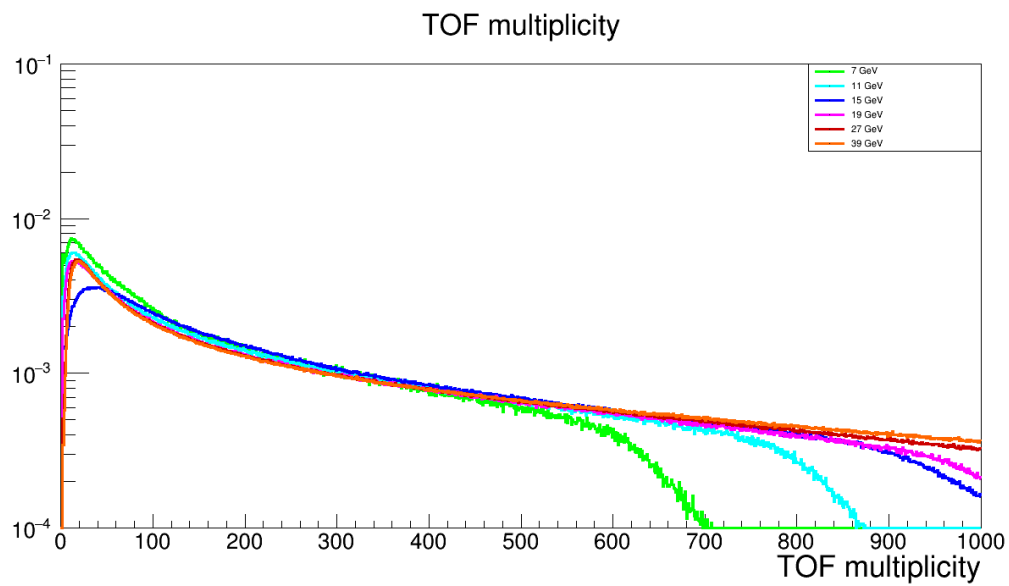


Fig. 7: TofMultiplicity (normalized)

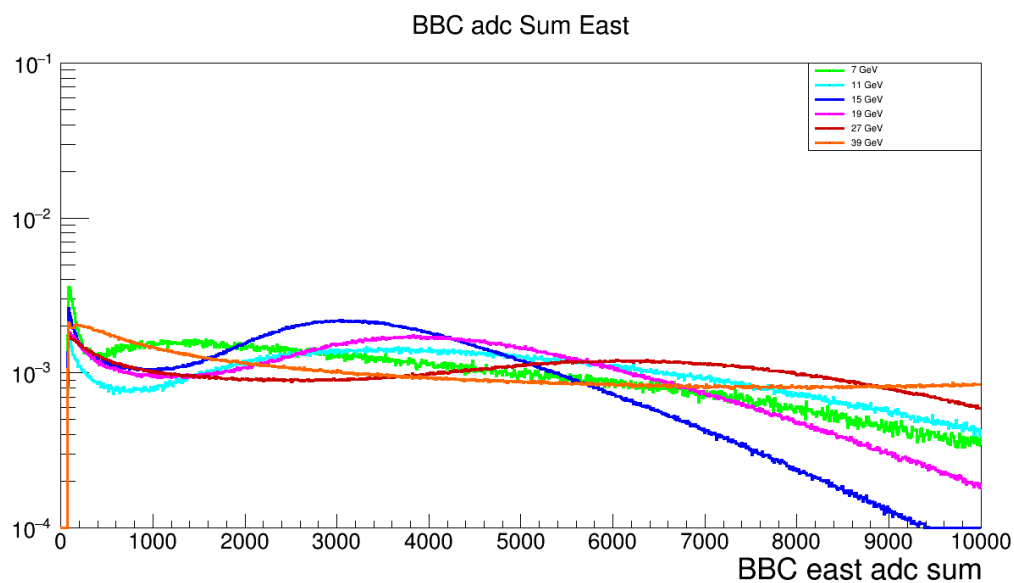


Fig. 8: BBC East ADC sum (normalized)

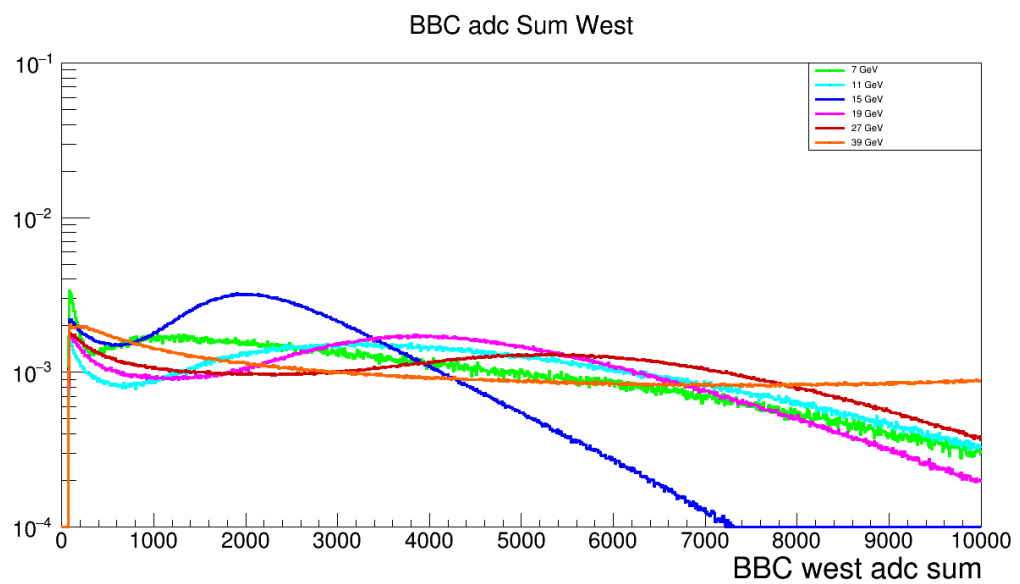


Fig. 9: BBC West ADC sum (normalized)

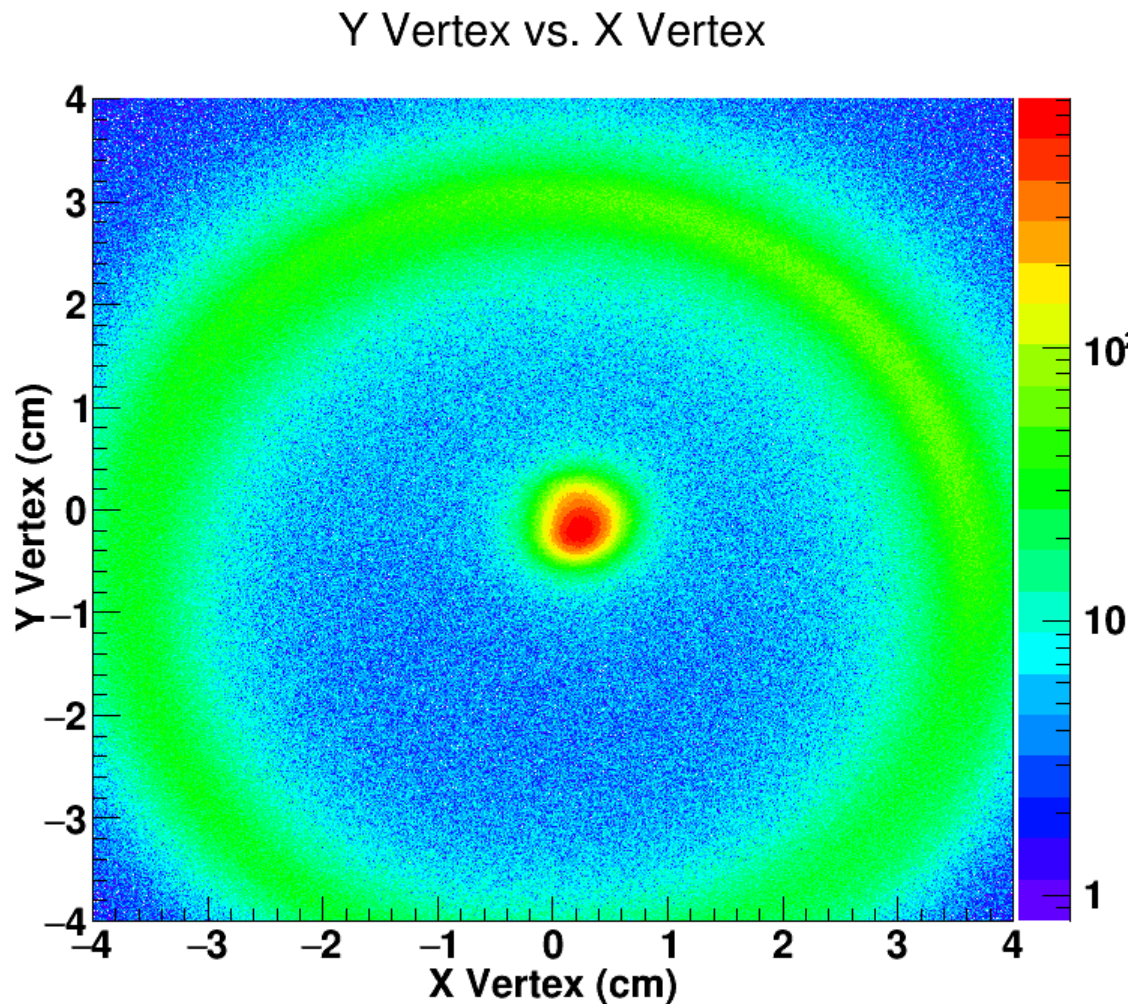


Fig. 10: y component of primary vertex vs. x component of primary vertex for 7GeV

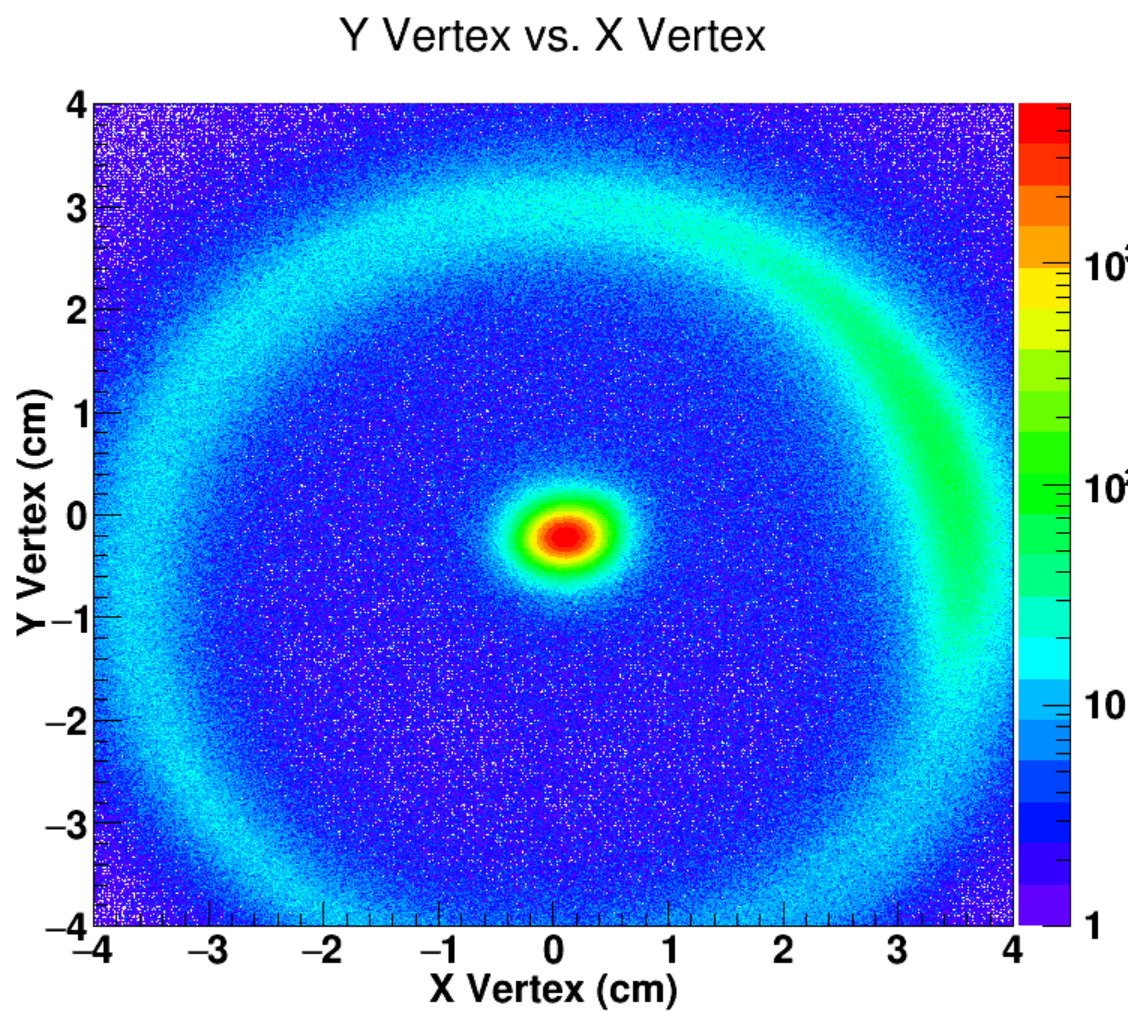


Fig. 11: y component of primary vertex vs. x component of primary vertex for 11GeV

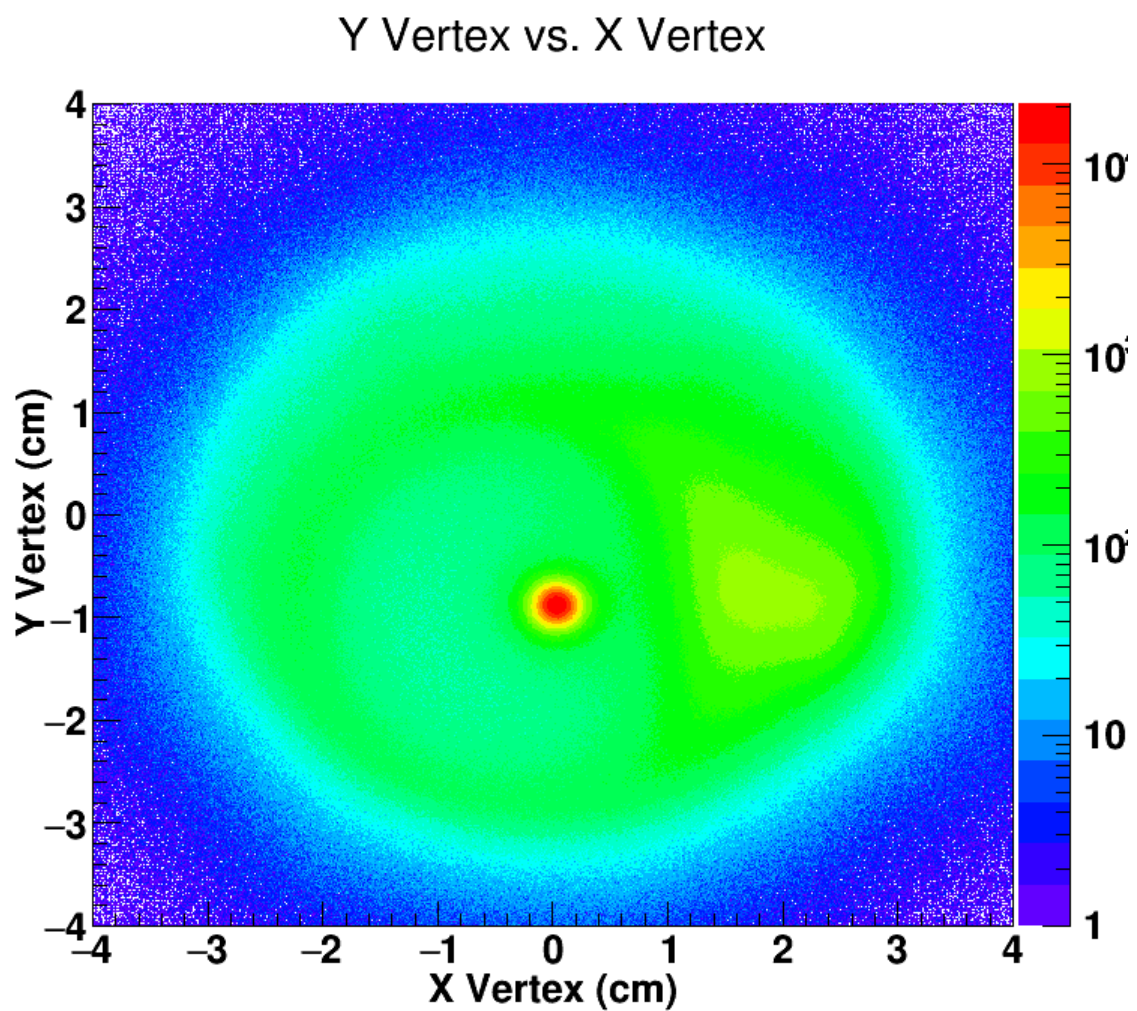


Fig. 12: y component of primary vertex vs. x component of primary vertex for 15GeV

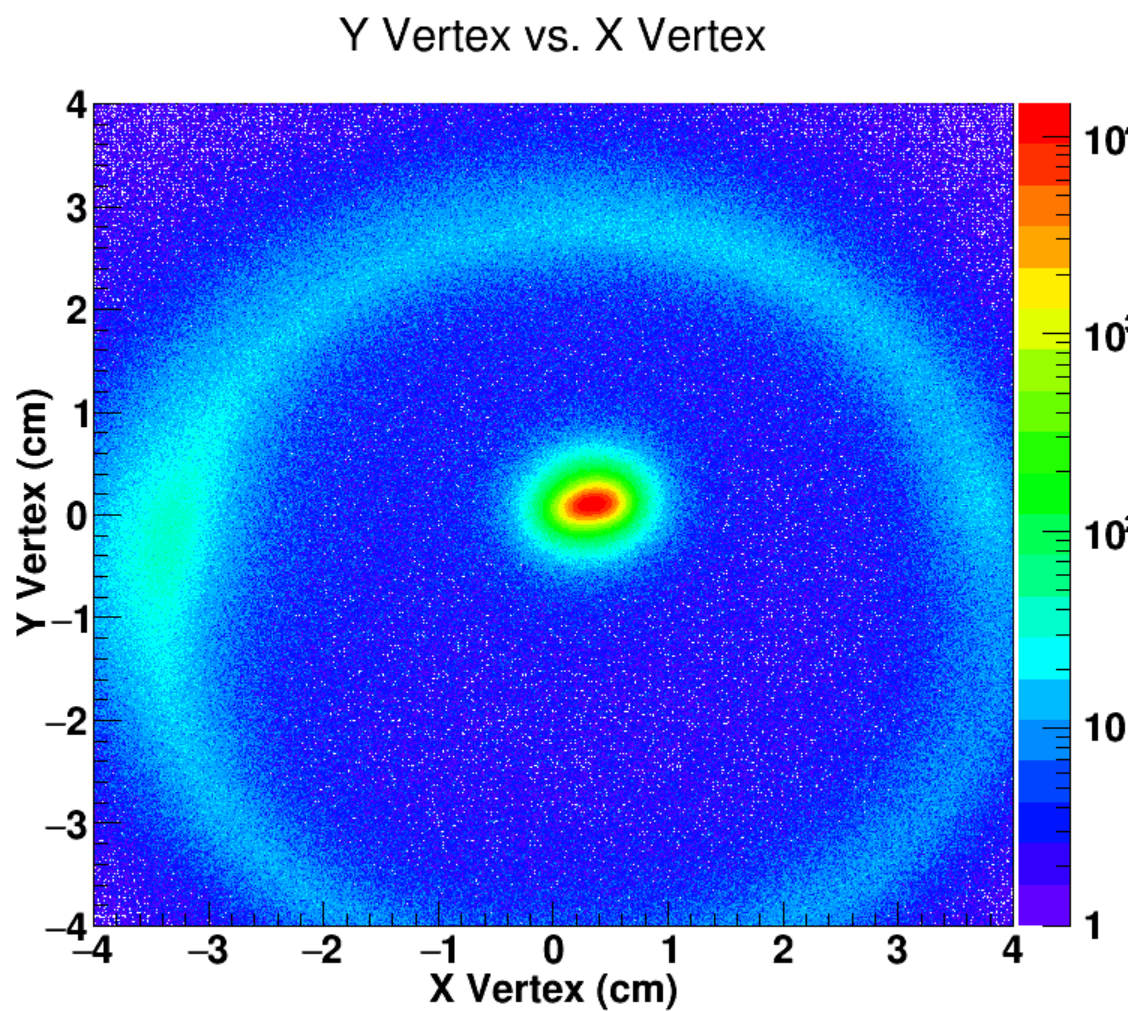


Fig. 13: y component of primary vertex vs. x component of primary vertex for 19GeV

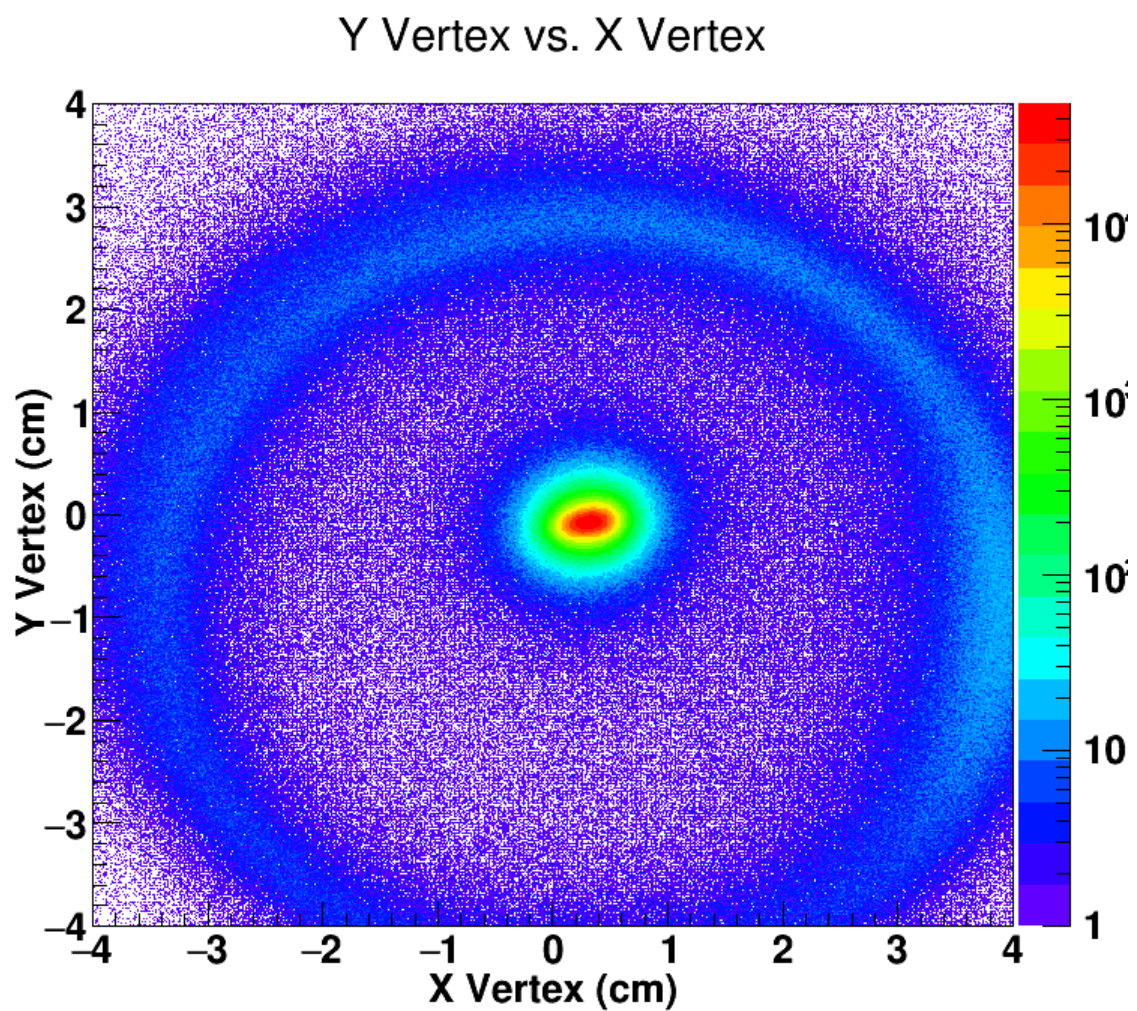


Fig. 14: y component of primary vertex vs. x component of primary vertex for 27GeV

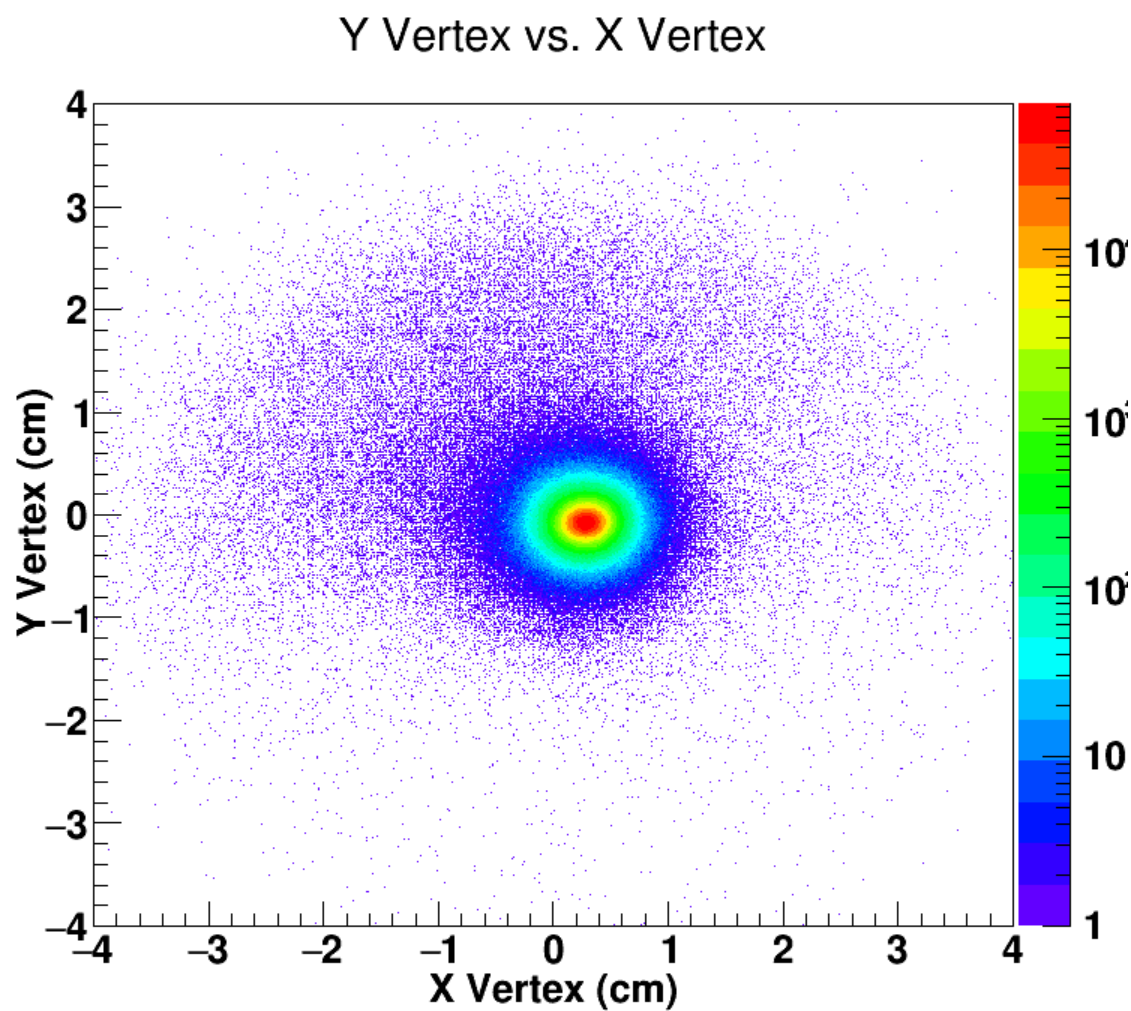


Fig. 15: y component of primary vertex vs. x component of primary vertex for 39GeV

2.2 Event Plane determination

The analysis uses the first order event plane, Ψ_1 , determined by the east and west BBCs (beam beam counters). Generally the event plane is found by weighting the tile geometry by the ADC value for that given tile. The numbering scheme for the inner tiles of the detector (only the inner tiles are used) is shown below for one looking a very large $|z|$

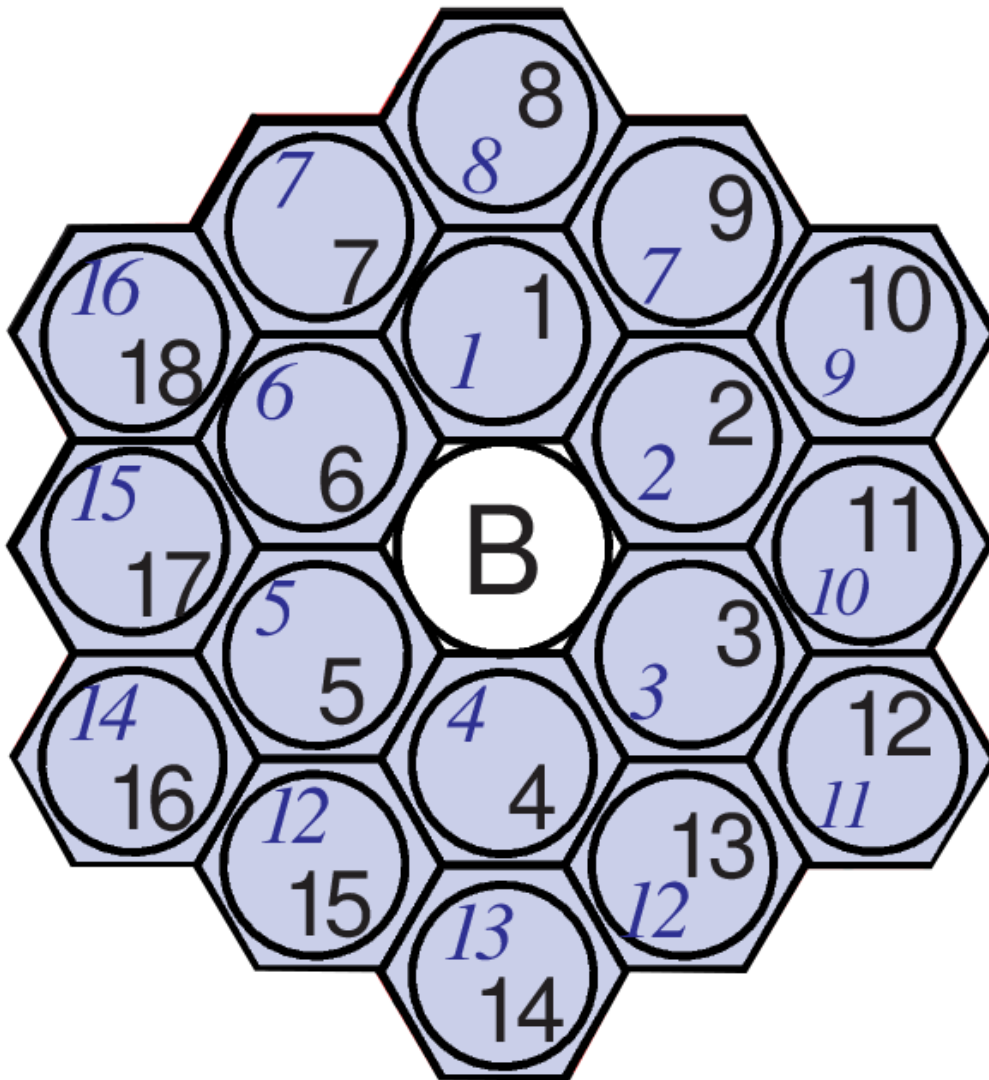


Fig. 16: BBC numbering scheme looking at very large $|z|$. Black numbers represent tile number while blue numbers represent PMT number.

Tiles 7 and 9 (13 and 15) share PMTs which means it is impossible to tell whether one was hit or the other. Many analyses deal with this by randomly ambiguity by assigning the ADC value in its entirety to tile 7 (13) XOR tile 9 (15). I prefer to count the tile pair's contribution as being between them so $\pi/2$ ($3\pi/2$). I think that this scheme makes more sense and certainly makes comparisons with ones own code or the code of others much easier. In practice I have not seen a noticeable difference between the two methods. Note that either way the tiles are mirrored about the x axis but not the y axis so that a line parallel to the z axis might go through tile 11 on the West BBC and tile 17 on the East BBC while such a line could go through both tile 8s.

365

$v_1 * y > 0$ by conventions most reasonable to the STAR event plane. Therefore the west BBC reconstructs the "right" event plane. Spectators on the east side BBC hit a position which is 180° in $x - y$ from those that hit the west. This means that there is a negative sign for the east BBC event plane. More simply $Psi_E = 0 \implies Q_{x,West} = x_{STAR}$ which would mean $Psi_E = \pi \implies Q_{x,East} = -x_{STAR}$. A particularly nice picture of the STAR coordinate system (<https://drupal.star.bnl.gov/STAR/public/img/SketchUpSTAR>) is

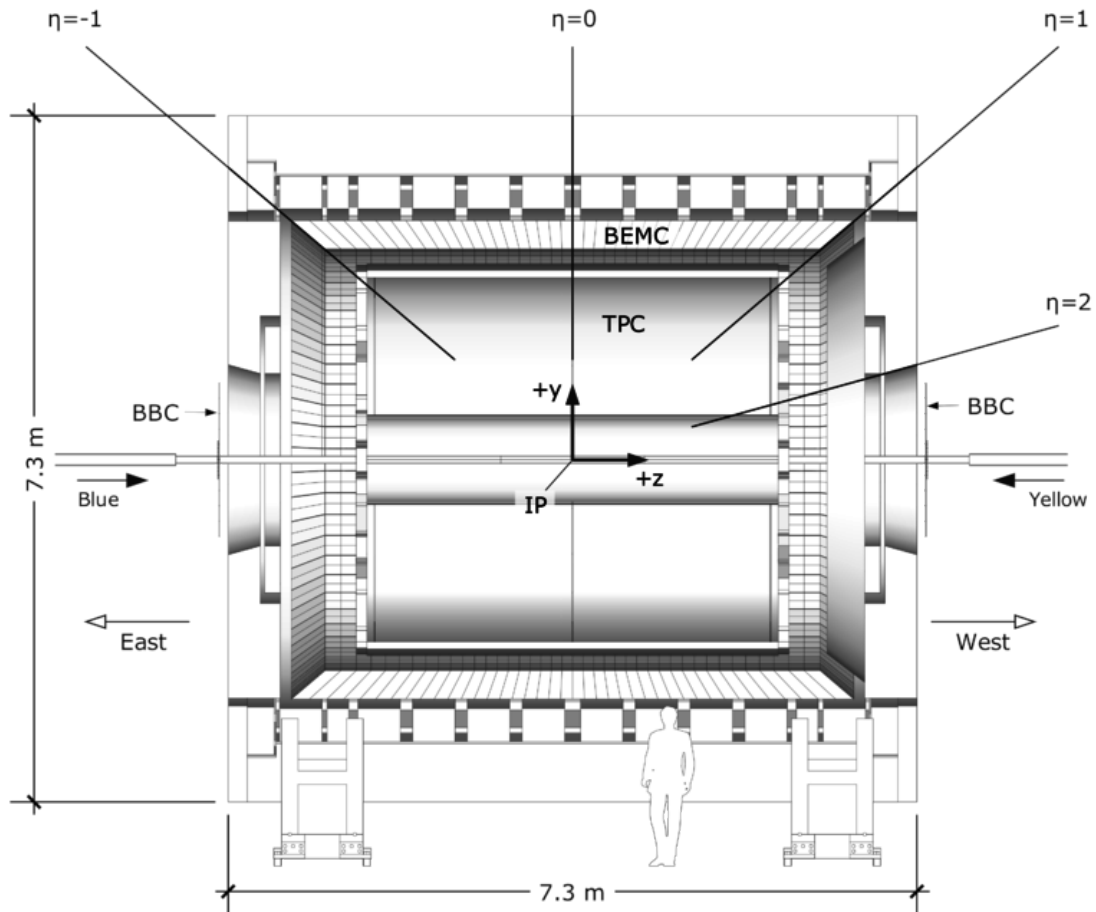


Fig. 17: STAR coordinate system

The "raw" (uncorrected) event plane is found by weighting tile geometry by the ADC for the relevant tile. This sum over the ADC channels creates a standard flow Q vector, $Q_1 = (\sum_{i=1}^{16} ADC_i * \cos(\phi_i), \sum_{i=1}^{16} ADC_i * \sin(\phi_i))$. We make (and correct) Q vectors for east and west separately which allows us to get a resolution correction later. The Q vector for the full event plane is basically made by taking $Q_{1,W} - Q_{1,E}$. After this raw event plane is found we do a series of corrections to the event plane. The corrections are done in the following order:

- Gain correction: The idea of the gain correction is that not all BBC tiles may output the same adc value for the same hit, some can be hot/cold. To correct for this we normalize the number of hits in each tile by the amount that tile fired relative to the other tiles making sure that the bank of "other tiles" is equally likely to be hit. So, innermost tiles 1-6 are normalized together while, separately tiles 7-18 are normalized together. This normalization should be done over enough time to get reasonable statistics and a small enough time that the normalization is relevant. I do this normalization for each new run number.
- Recentering correction: The Q vector averaged over all events has to be zero since, of course, there is no preferred impact parameter. Even with the gain correction it is possible that the Q vector doesn't average to zero since adcs can saturate and it is possible that a particular adc is more likely to saturate than the others. In principal the recentering correction well motivated, in practice this correction tends to be minimally impactful
- Ψ shift correction: This is the least well motivated of the corrections. In principal the event plane distributions should all be flat since there is no preferred event plane, this correction takes each Psi distribution (full/east/west) and applies a flattening method which flattens in harmonics of the distribution (decomposed into sines and cosines). The harmonics of the distribution are then subtracted off. Typically only the first few harmonics are non-zero. This is a steamroller that runs over the distribution. The best justification for why the shift correction is okay is the Ψ_E vs Ψ_W plot where the Ψ_E vs Ψ_W are separately corrected. In such a plot the correlation is seen to be better after the shifting. We have done nothing, in such a case, to require that to happen. The correction is done to 20th order, this is overkill but it isn't expensive to do.

The following plots show the event plane distributions as they are corrected for all relevant energies

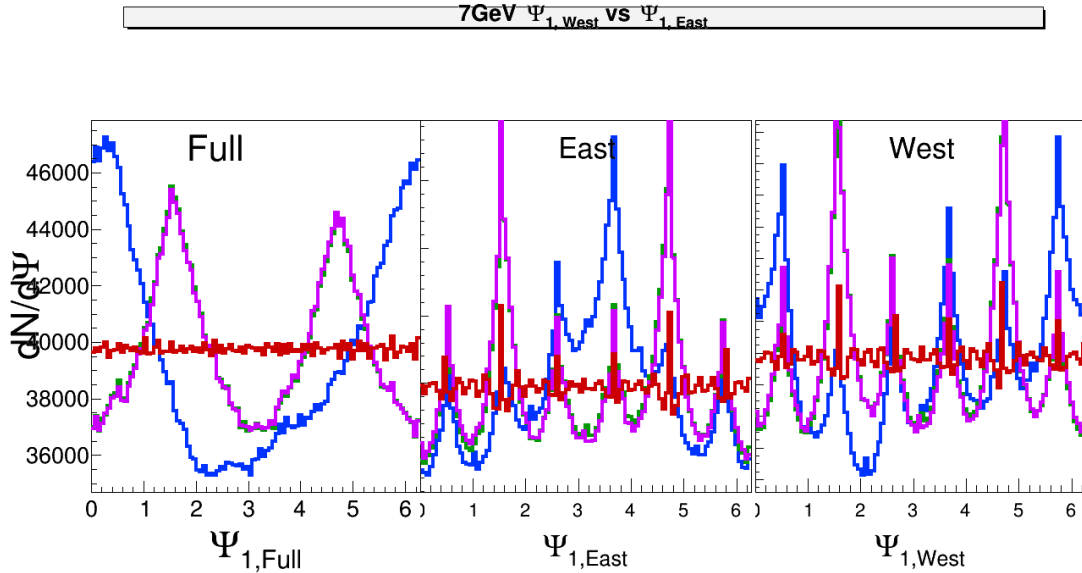


Fig. 18: 7GeV Ψ_1 distribution as corrections are applied. Blue - Raw, Green - Gain corrected, Violet - Recentered, Red - Shifted.

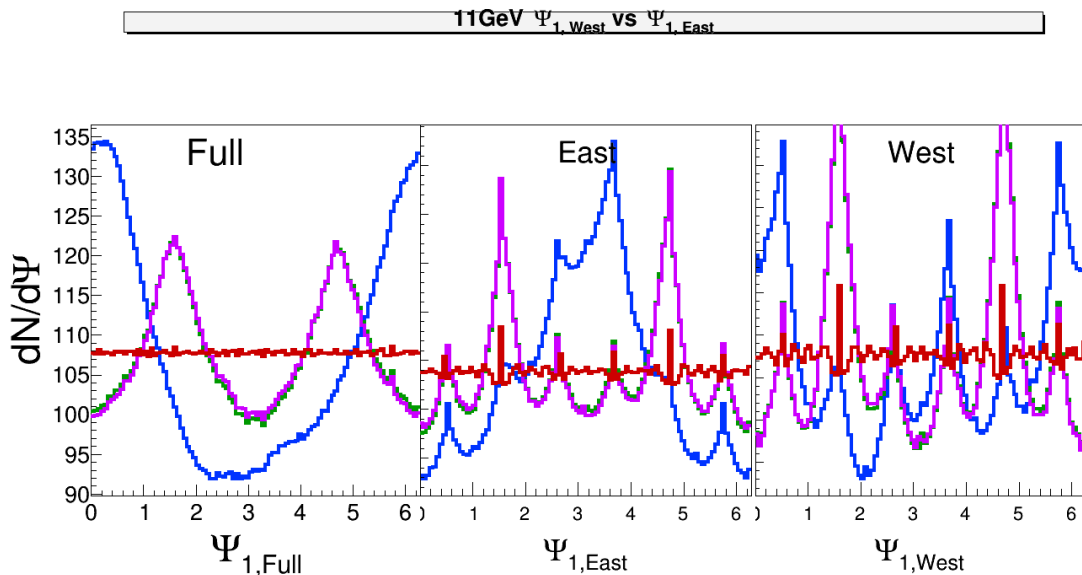


Fig. 19: 11GeV Ψ_1 distribution as corrections are applied. Blue - Raw, Green - Gain corrected, Violet - Recentered, Red - Shifted.

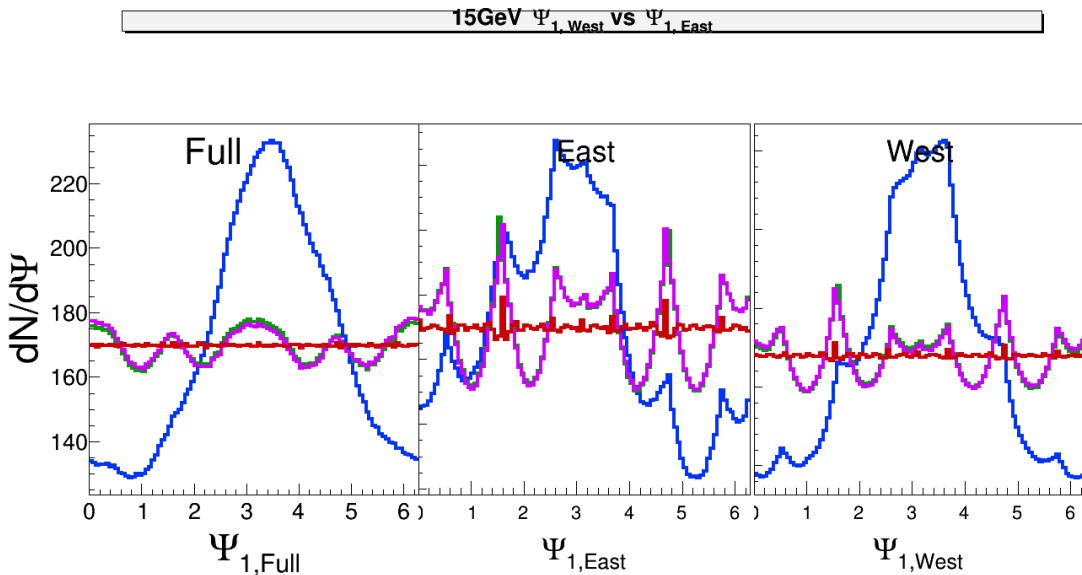


Fig. 20: 15GeV Ψ_1 distribution as corrections are applied. Blue - Raw, Green - Gain corrected, Violet - Recentered, Red - Shifted.

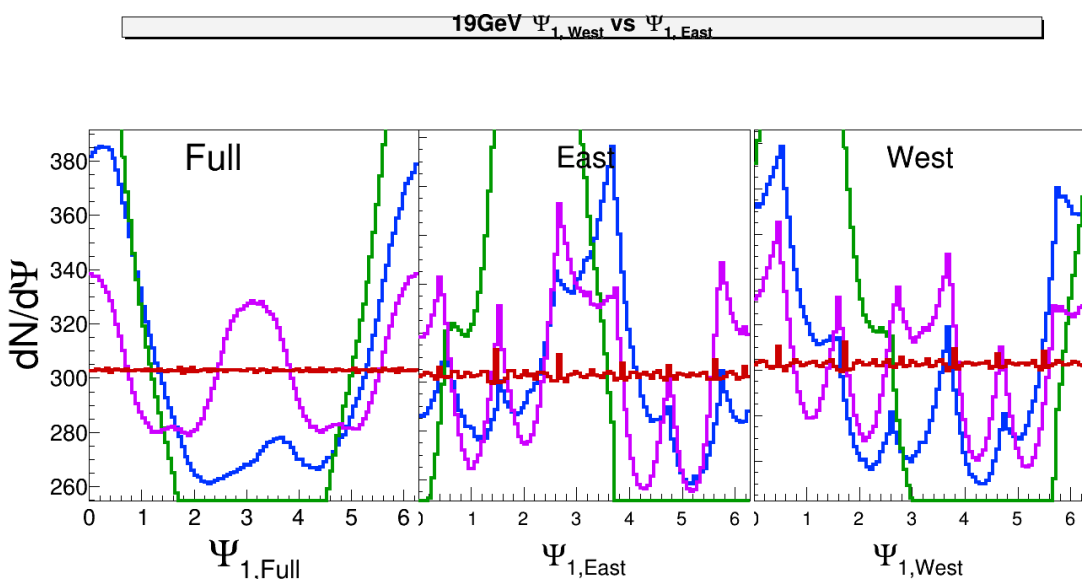


Fig. 21: 19GeV Ψ_1 distribution as corrections are applied. Blue - Raw, Green - Gain corrected, Violet - Recentered, Red - Shifted.

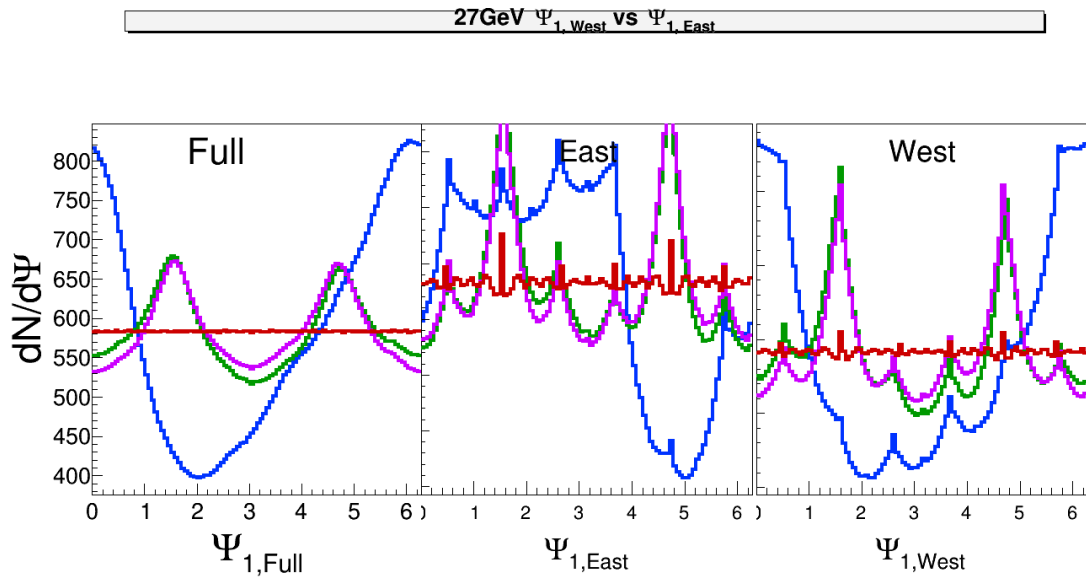


Fig. 22: 27GeV Ψ_1 distribution as corrections are applied. Blue - Raw, Green - Gain corrected, Violet - Recentered, Red - Shifted.

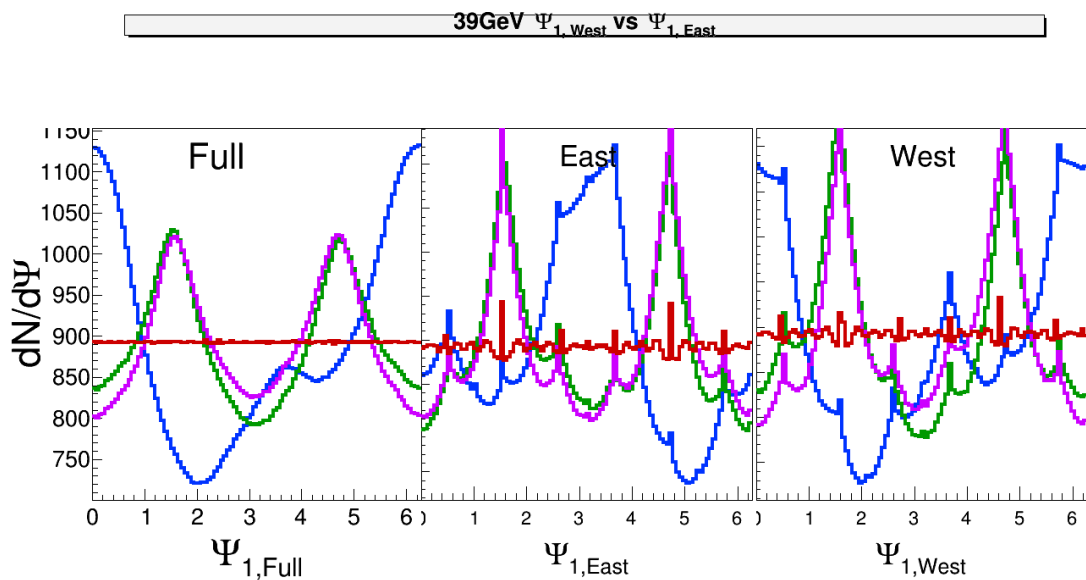


Fig. 23: 39GeV Ψ_1 distribution as corrections are applied. Blue - Raw, Green - Gain corrected, Violet - Recentered, Red - Shifted.

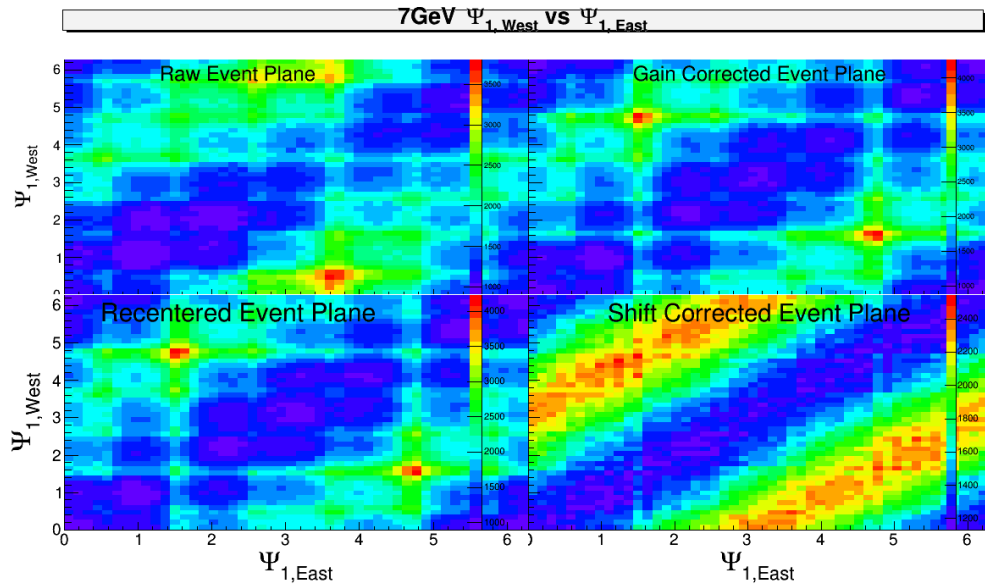


Fig. 24: BBC West Ψ_1 vs. BBC East Ψ_1 for 7GeV as corrections are applied

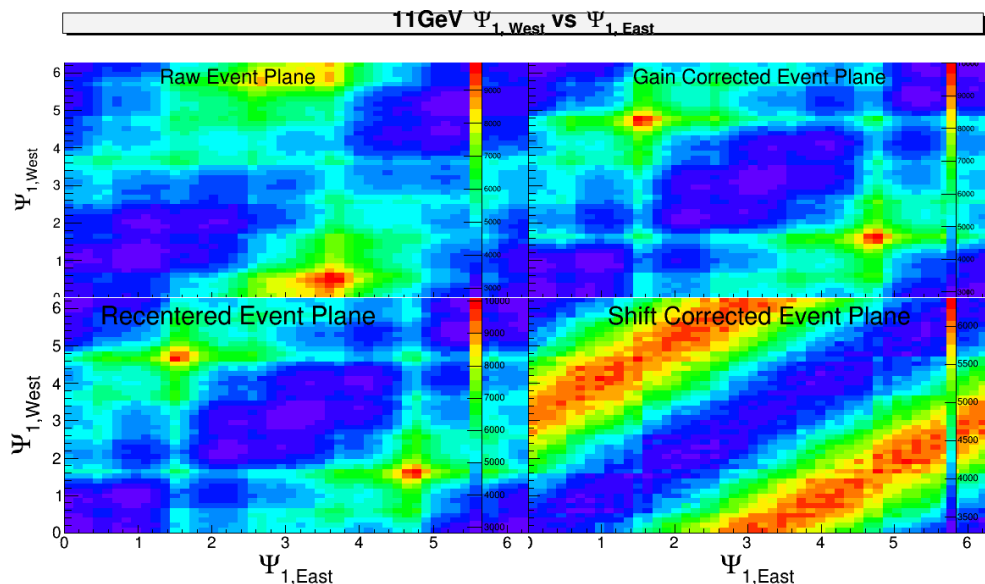


Fig. 25: BBC West Ψ_1 vs. BBC East Ψ_1 for 11GeV as corrections are applied

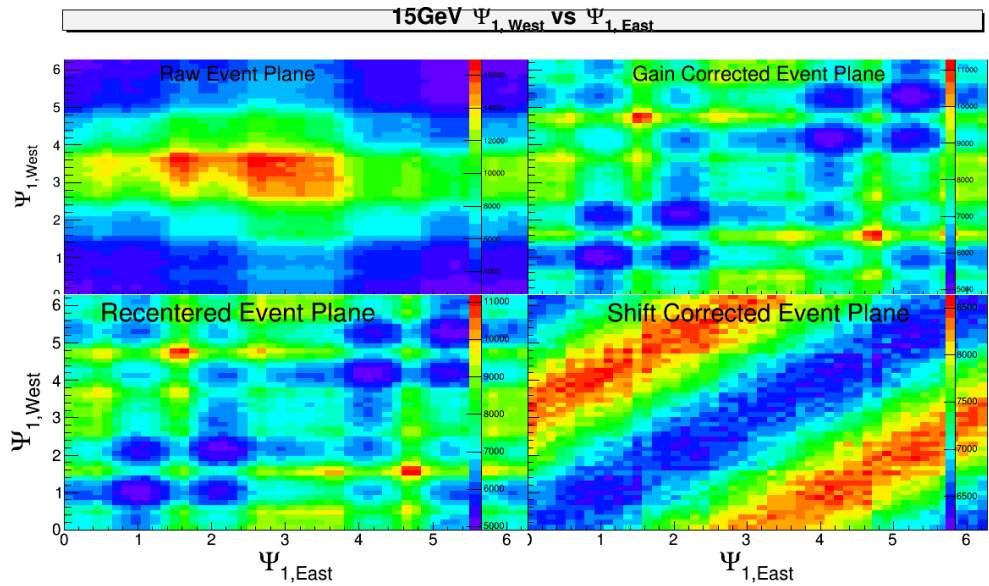


Fig. 26: BBC West Ψ_1 vs. BBC East Ψ_1 for 15GeV as corrections are applied

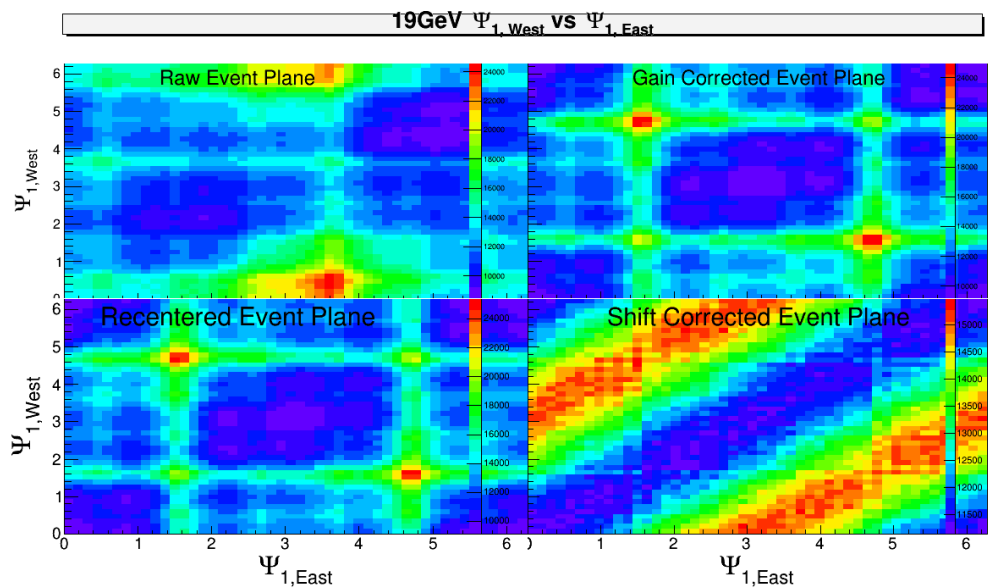


Fig. 27: BBC West Ψ_1 vs. BBC East Ψ_1 for 19GeV as corrections are applied

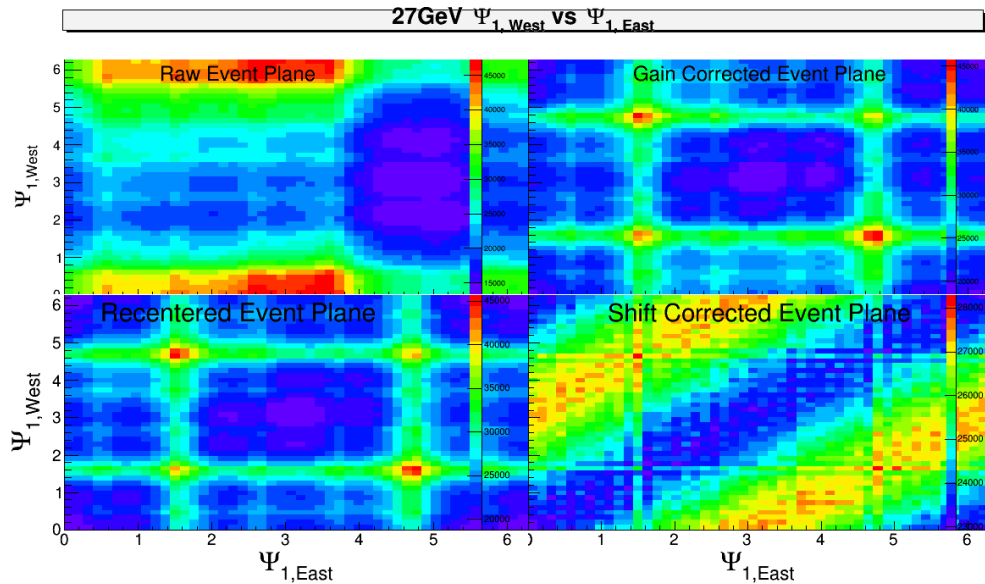


Fig. 28: BBC West Ψ_1 vs. BBC East Ψ_1 for 27GeV as corrections are applied

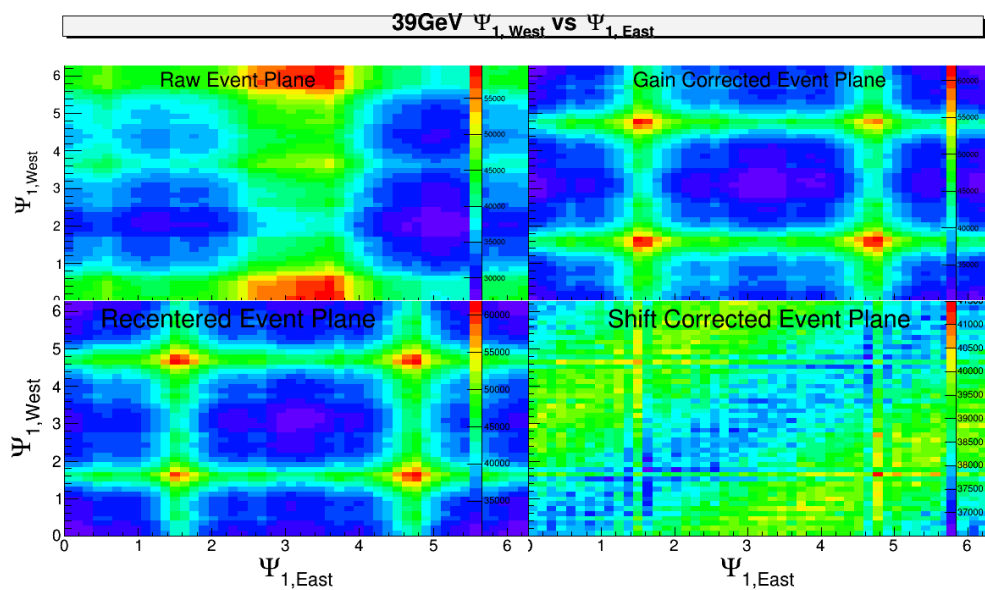


Fig. 29: BBC West Ψ_1 vs. BBC East Ψ_1 for 39GeV as corrections are applied

2.2.1 Event plane resolution

Finally we have a resolution correction factor which is found in the typical way outlined here (<http://arxiv.org/abs/0809.4051>). The relative magnitude of the corrections is the correlator of the east and west planes: $\cos(\Psi_{1,W} - \Psi_{1,E})$, the actual values are found by inverting Bessel equations (eq. 10 of this paper) using the sub event plane resolution. This resolution is solved for each central value of the sub event plane resolution as well as the statistical error bars. Of course the statistical error bars of the sub-event plane resolution are symmetric, but this is not guaranteed when they are put through the root finding algorithm. If the sizes of the up and down error bars differed by less than a percent I just defined the error bar to be the average of them. In fact the difference was less than 1% every time (it could have been smaller but I don't remember the factor) so I never had to consider what to do in case of asymmetry. The values are

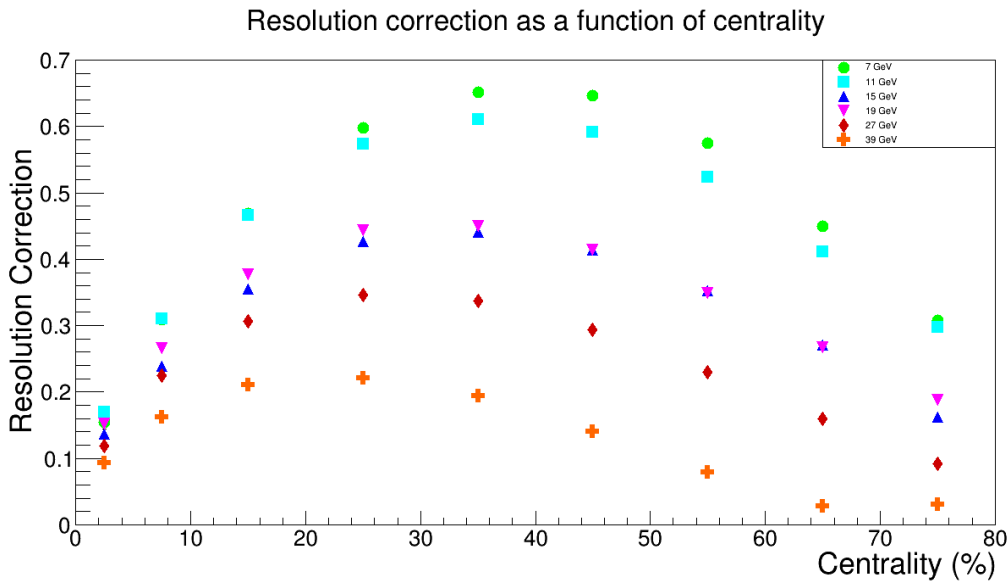


Fig. 30: Resolution correction as a function of centrality

I started putting all of this information in a table but that is both very time consuming and not as useful as arrays. The “values” below are resolution and the “errors” are the errors on the resolution

//resolution as a function of centrality in order 70-80, 60-70, 50-60, 40-50, 30-40, 20-30, 10-20, 5-10, 0-5:

```

float Value7[9] = {0.307486, 0.449667, 0.574805, 0.646084, 0.651441, 0.597433, 0.468886, 0.309121, 0.154215};

float Error7[9] = {0.00350804, 0.0018571, 0.00128989, 0.00101399, 0.000984015, 0.00120613, 0.00178403, 0.00439411, 0.00936414};

float Value11[9] = {0.297083, 0.41103, 0.523299, 0.591951, 0.610235, 0.573203, 0.466745, 0.310846, 0.170367};

float Error11[9] = {0.00216346, 0.0013164, 0.000902906, 0.000735164, 0.000702311, 0.000788124, 0.00108837, 0.0026144, 0.00496451};

float Value15[9] = {0.162577, 0.270896, 0.352444, 0.41449, 0.440722, 0.426715, 0.35558, 0.238906, 0.136717};

float Error15[9] = {0.00319226, 0.00177016, 0.00119992, 0.000993054, 0.000897895, 0.000969794, 0.00125653, 0.00294766, 0.00530565};

float Value19[9] = {0.187944, 0.266781, 0.348138, 0.414074, 0.449791, 0.443808, 0.377452, 0.265421,

```

```
0.151509};  
430 float Error19[9] = {0.00208176, 0.00127301, 0.000934693, 0.000738721, 0.00067166, 0.000690424,  
0.000881327, 0.00196368, 0.00349595};  
float Value27[9] = {0.0915621, 0.159324, 0.230443, 0.294388, 0.337777, 0.346737, 0.306512, 0.225316,  
0.118245};  
float Error27[9] = {0.00294643, 0.00154611, 0.00108434, 0.000810682, 0.00070117, 0.000693721,  
0.000825761, 0.00167731, 0.00329719};  
435 float Value39[9] = {0.0304321, 0.0277353, 0.0795904, 0.140791, 0.193922, 0.220535, 0.211103, 0.162255,  
0.093857};  
float Error39[9] = {0.00737913, 0.0081295, 0.00258267, 0.00147021, 0.00104289, 0.000912287, 0.000975987,  
0.0018576, 0.00328591};
```

440 **2.3 Track QA**

The cuts I use to select tracks

- Track flag ≥ 0
- $0.15\text{GeV} < p_T < 10\text{GeV}$
- $|\eta| < 1$
- 445 – NHitsPossible ≥ 5
- $15 < \text{Number of hits} < 100$
- NHitsFit/NHitsPossible ≥ 0.52

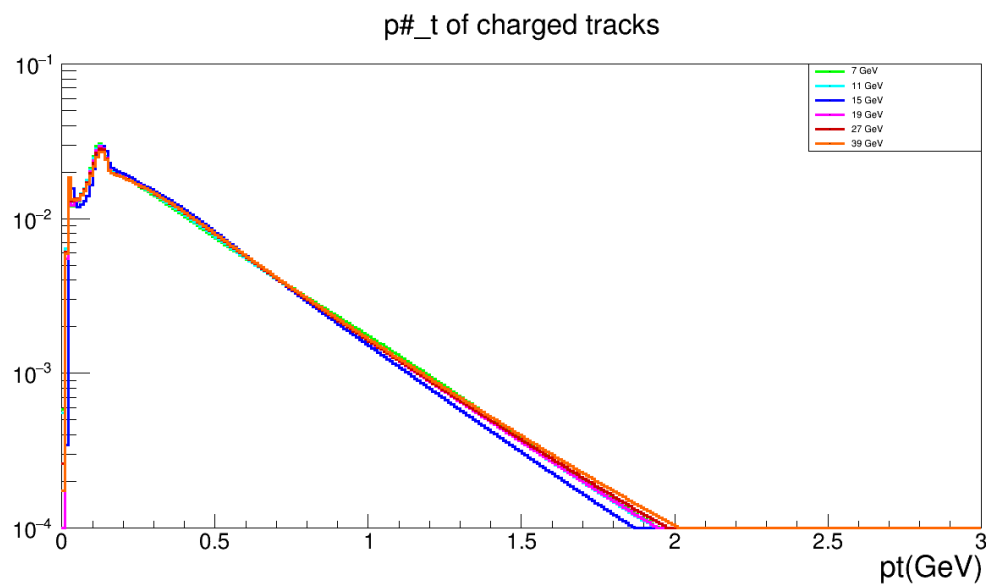


Fig. 31: $\frac{dN}{d(p_T)}$ vs p_T

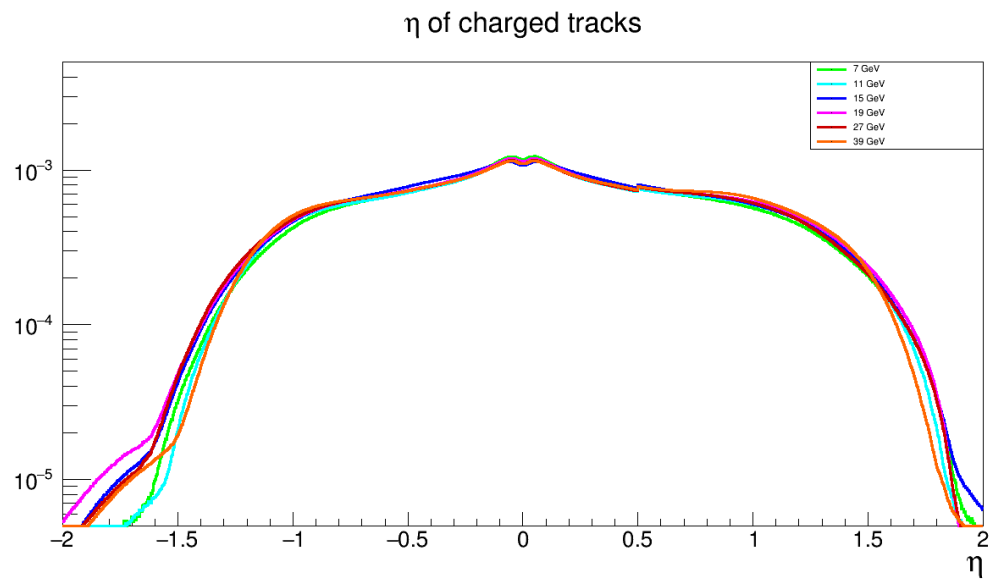


Fig. 32: $\frac{dN}{d\eta}$ vs η

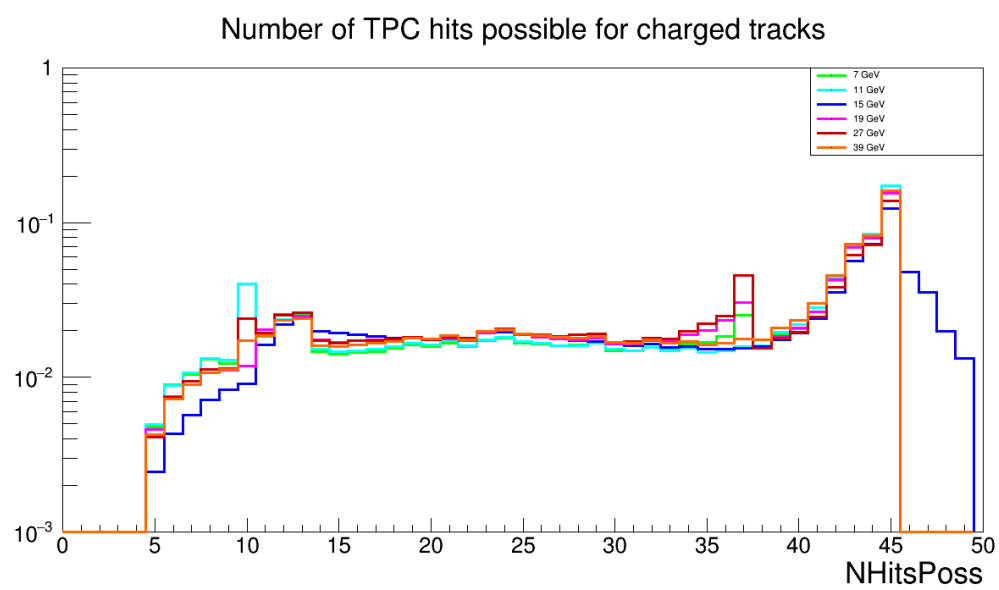


Fig. 33: $\frac{dN}{dN_{\text{Hits Possible}}}$ vs $N_{\text{Hits Possible}}$

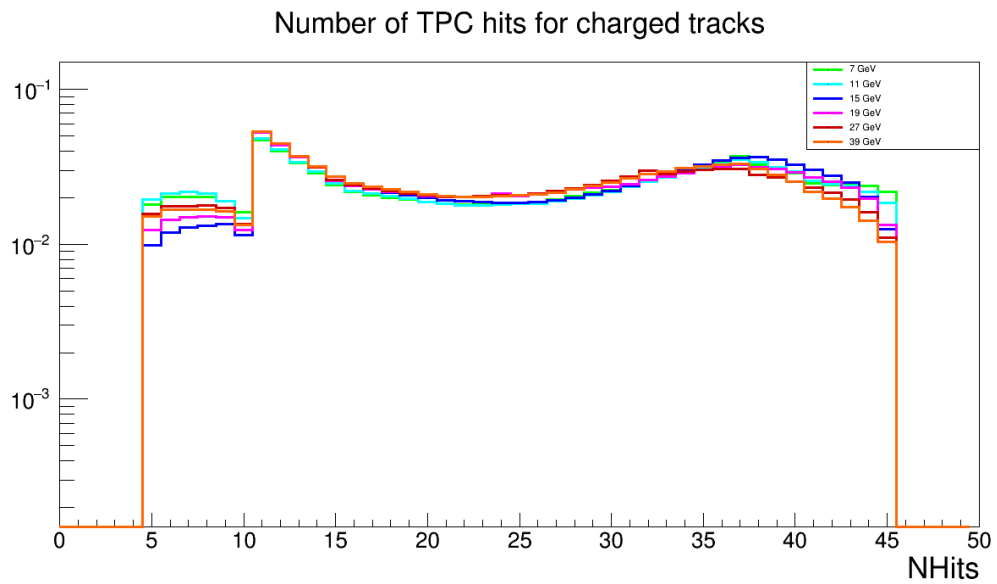


Fig. 34: $\frac{dN}{dN_{\text{Hits}}}$ vs N_{Hits}

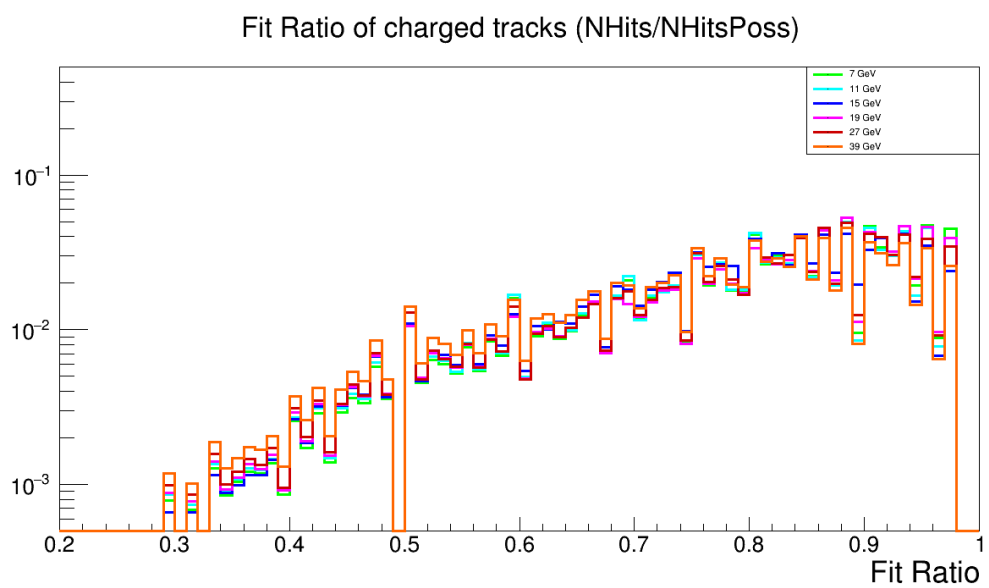


Fig. 35: $\frac{dN}{d(\text{Fit Ratio})}$ vs Fit Ratio

2.4 Lambda reconstruction

2.4.1 Daughter PID

450 Of course Lambdas are reconstructed from proton and pion tracks, so the first step in the reconstruction is the proton and pion track particle identification. This analysis uses TPC dE/dx and the ToF 1/β for PID. ToF information is not required so the ToF mass cuts are only used if the information exists. The cuts are as follows

- Proton: $|N_{\sigma, \text{proton}}| < 3$
- 455 – Proton: $0.5\text{GeV}^2 < m_{\text{ToF}}^2 < 1.5\text{GeV}^2$
- Pion: $|N_{\sigma, \text{pion}}| < 3$
- Pion: $0.017\text{GeV}^2 - 0.013\text{GeV}^2 * p < m_{\text{ToF}}^2 < 0.04\text{GeV}$

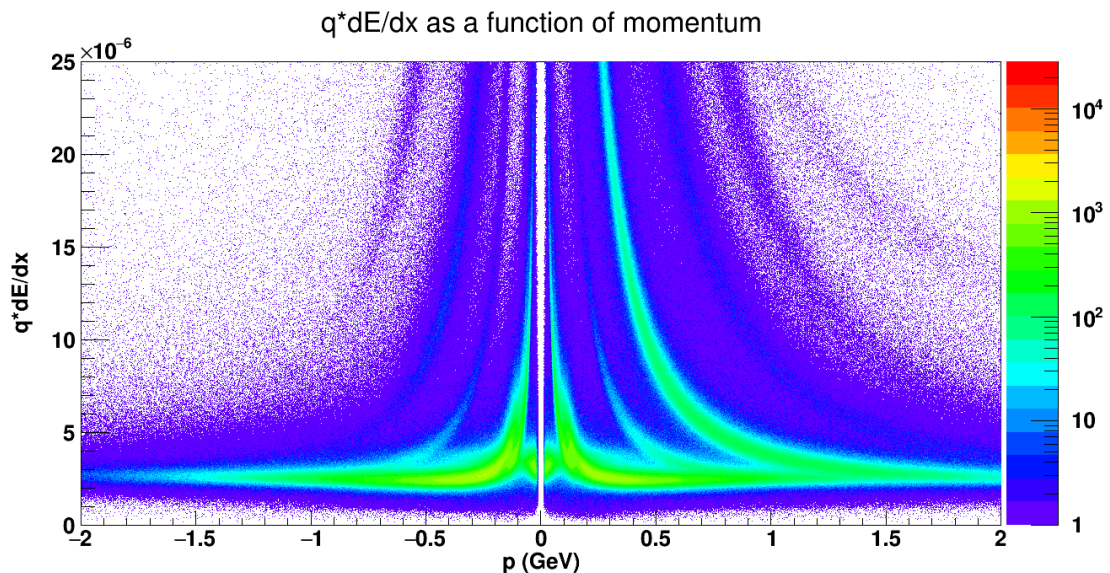


Fig. 36: 7GeV charged track dE/dx vs. p from the TPC

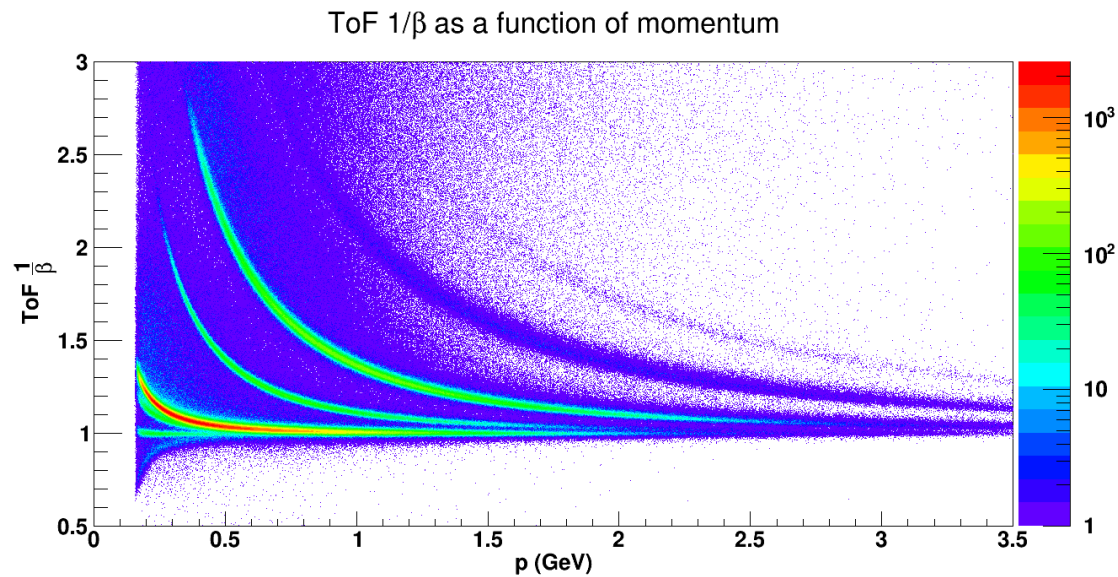


Fig. 37: 7GeV charged track $1/\beta$ vs. p from the ToF

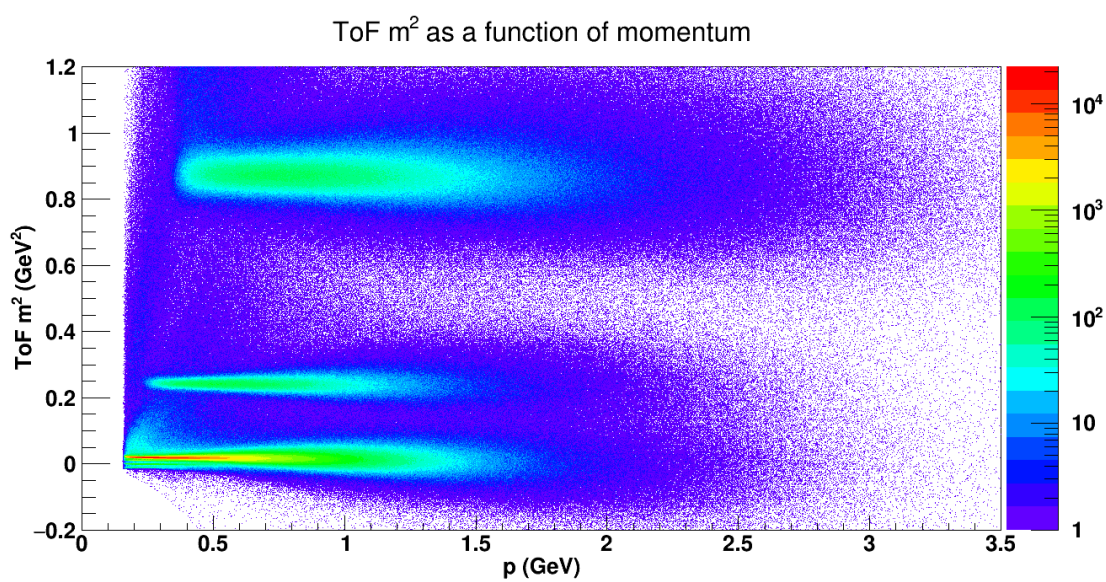


Fig. 38: 7GeV charged track m^2 vs p from the ToF

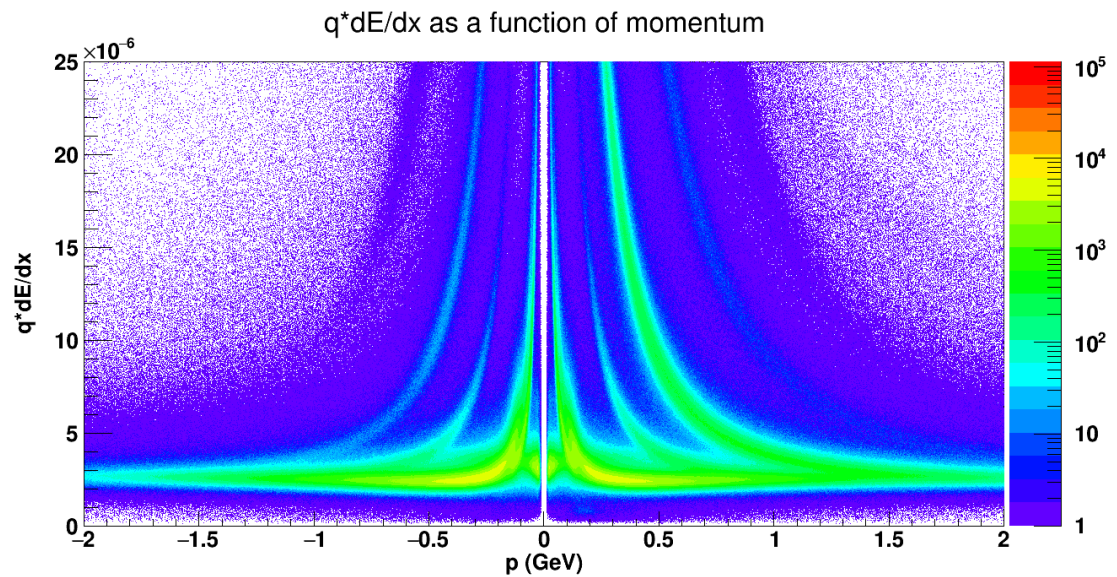


Fig. 39: 11GeV charged track dE/dx vs. p from the TPC

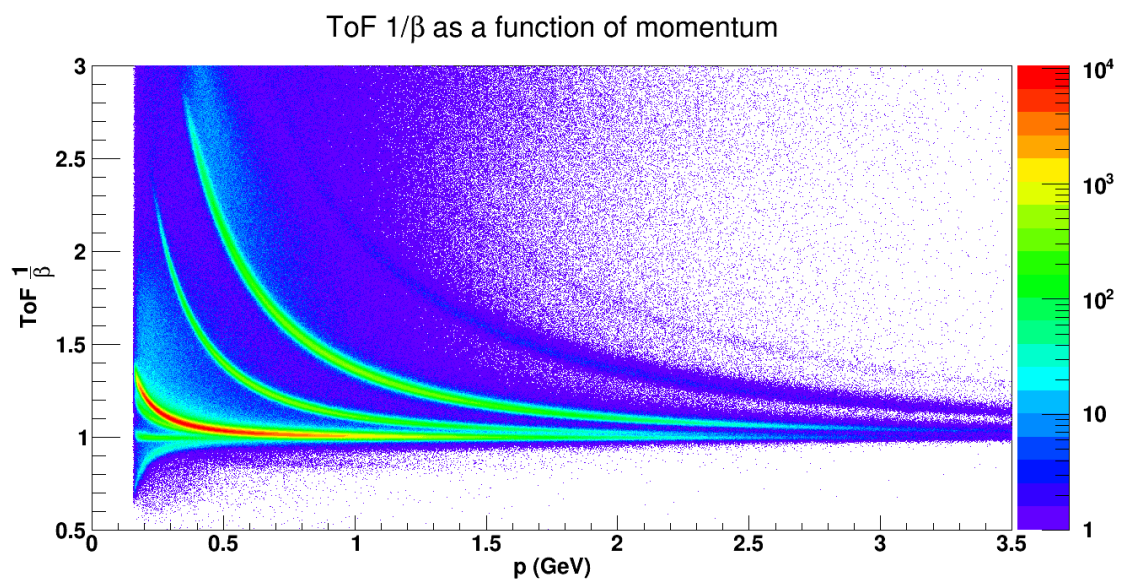


Fig. 40: 11GeV charged track $1/\beta$ vs. p from the ToF

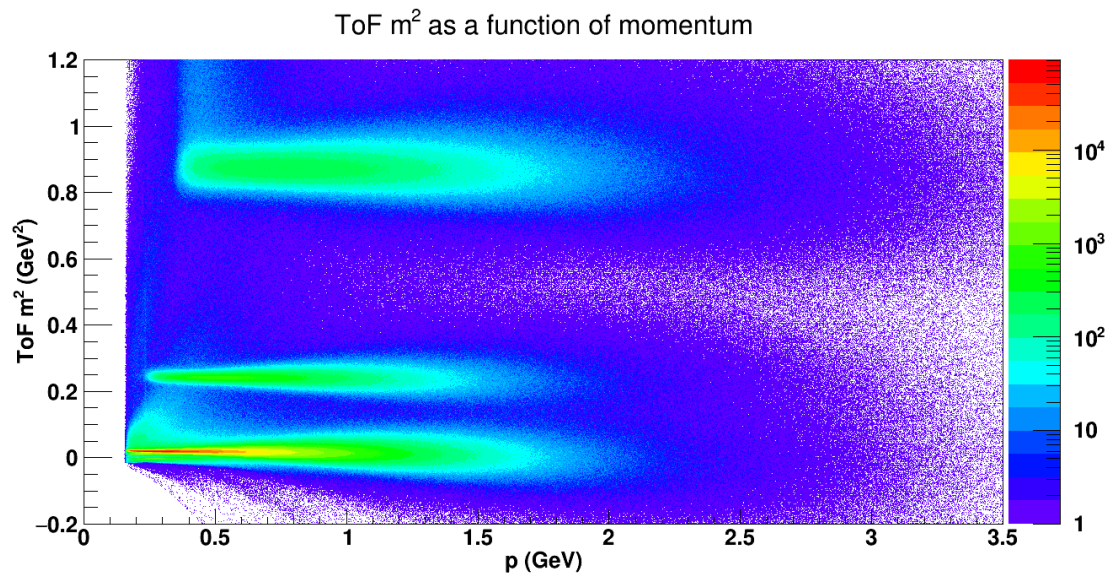


Fig. 41: 11GeV charged track m^2 vs p from the ToF

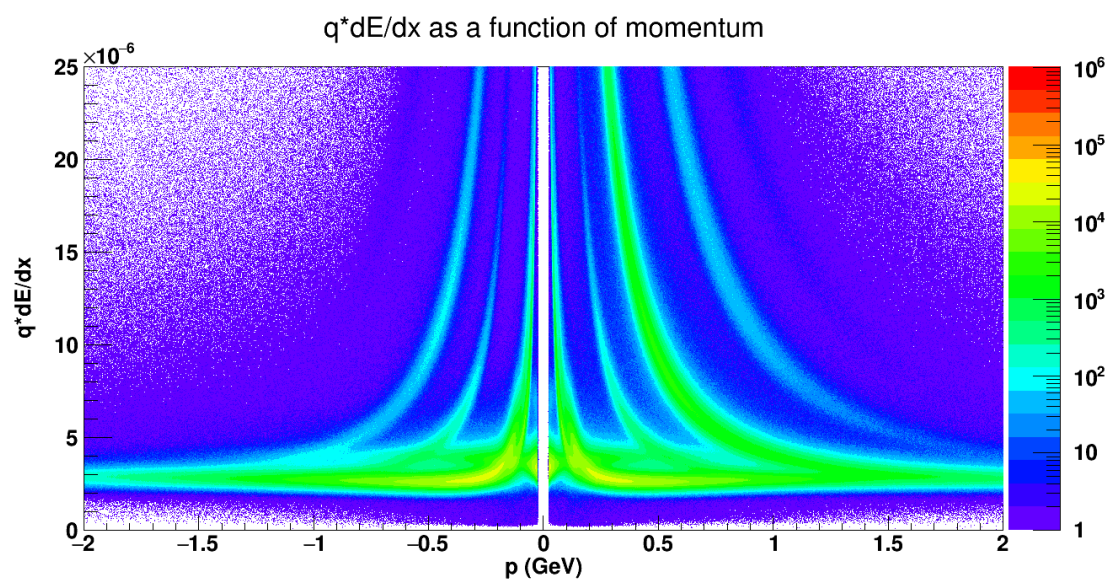


Fig. 42: 15GeV charged track dE/dx vs. p from the TPC

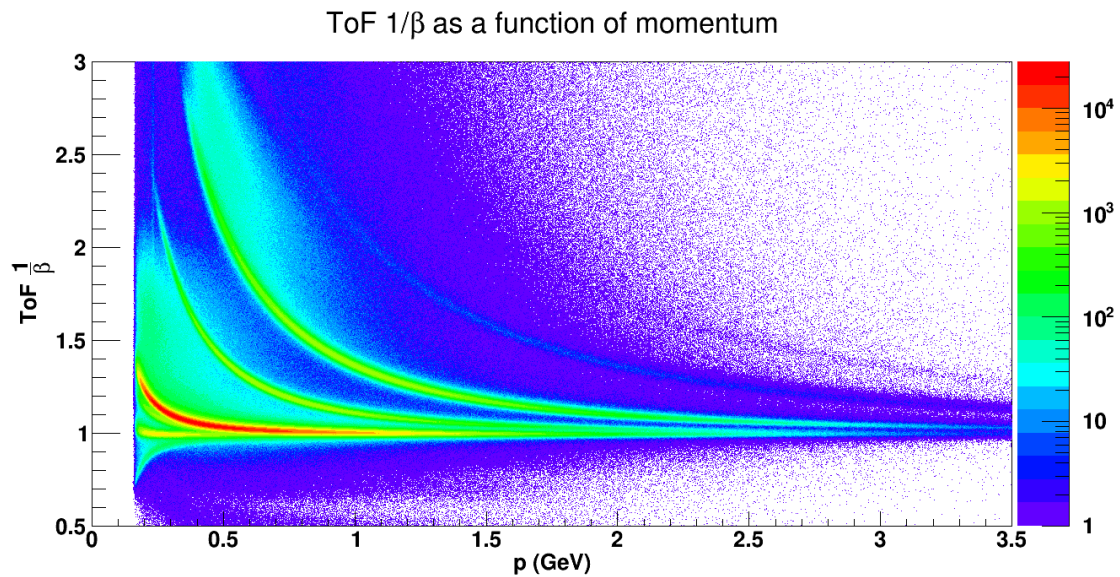


Fig. 43: 15GeV charged track $1/\beta$ vs. p from the ToF

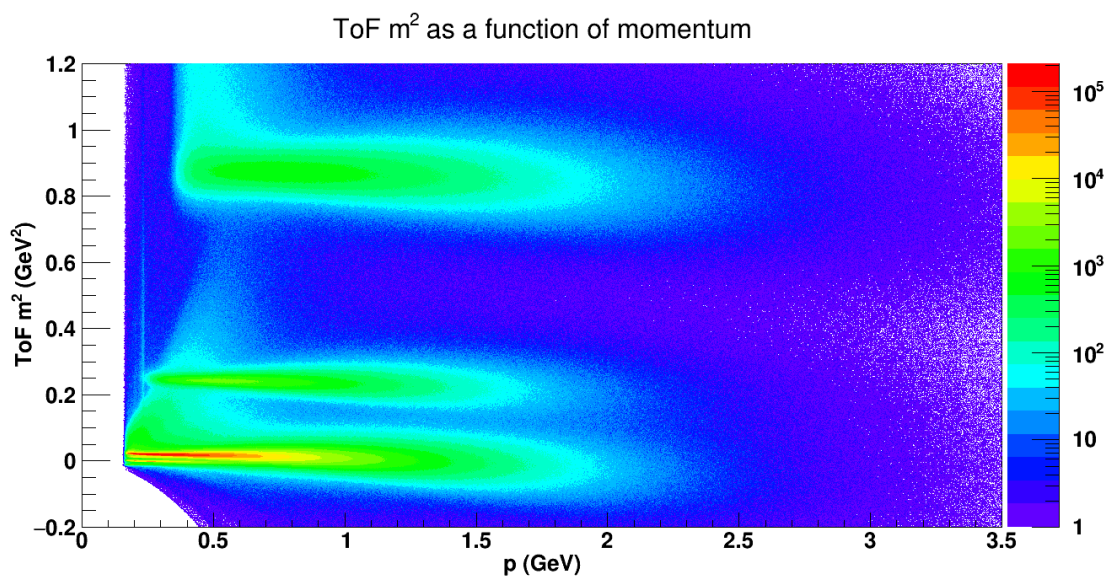


Fig. 44: 15GeV charged track m^2 vs p from the ToF

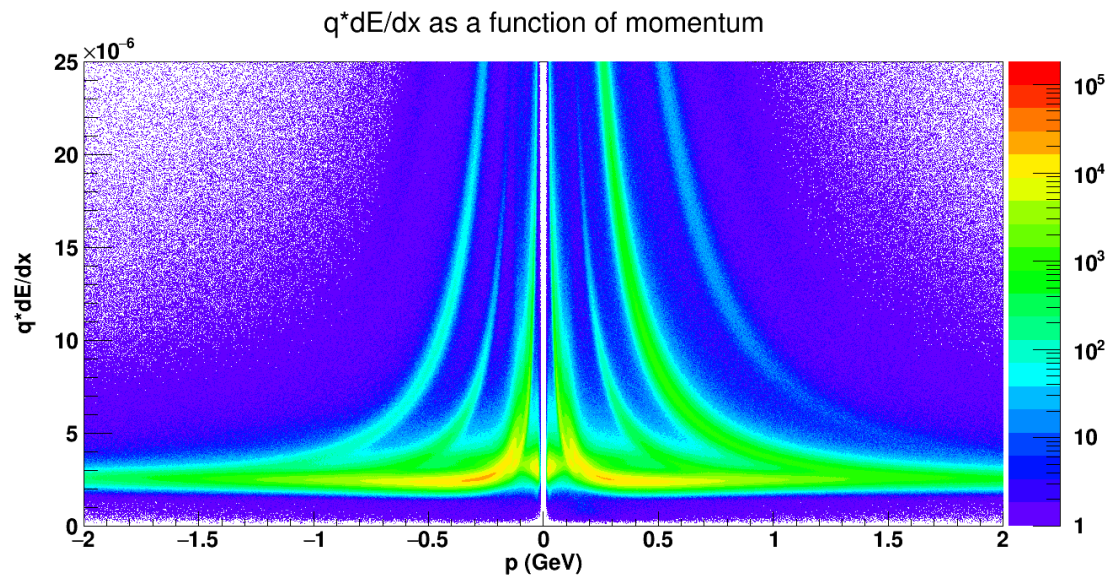


Fig. 45: 19GeV charged track dE/dx vs. p from the TPC

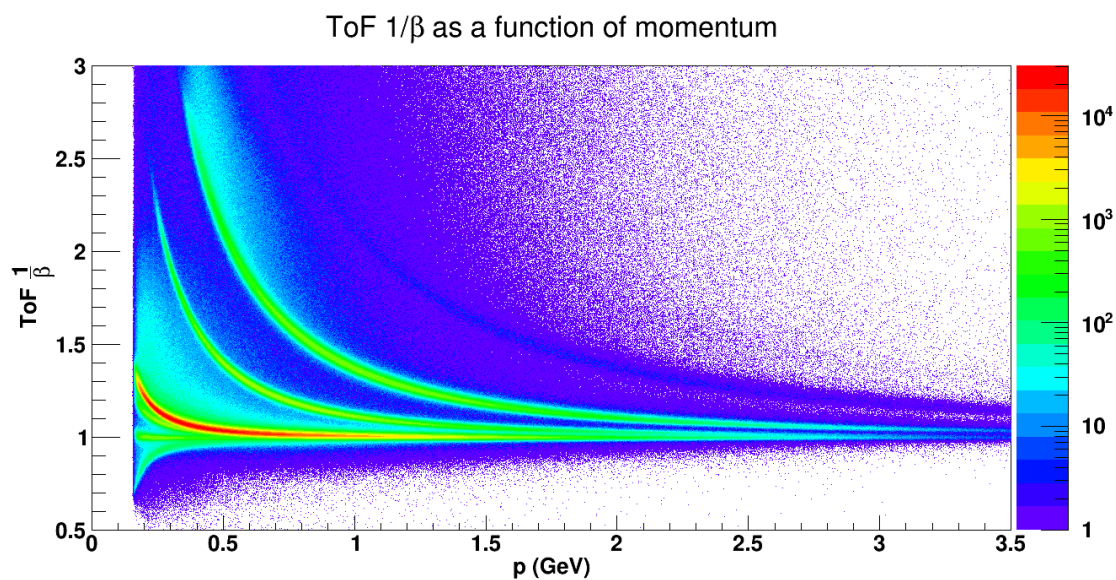


Fig. 46: 19GeV charged track $1/\beta$ vs. p from the ToF

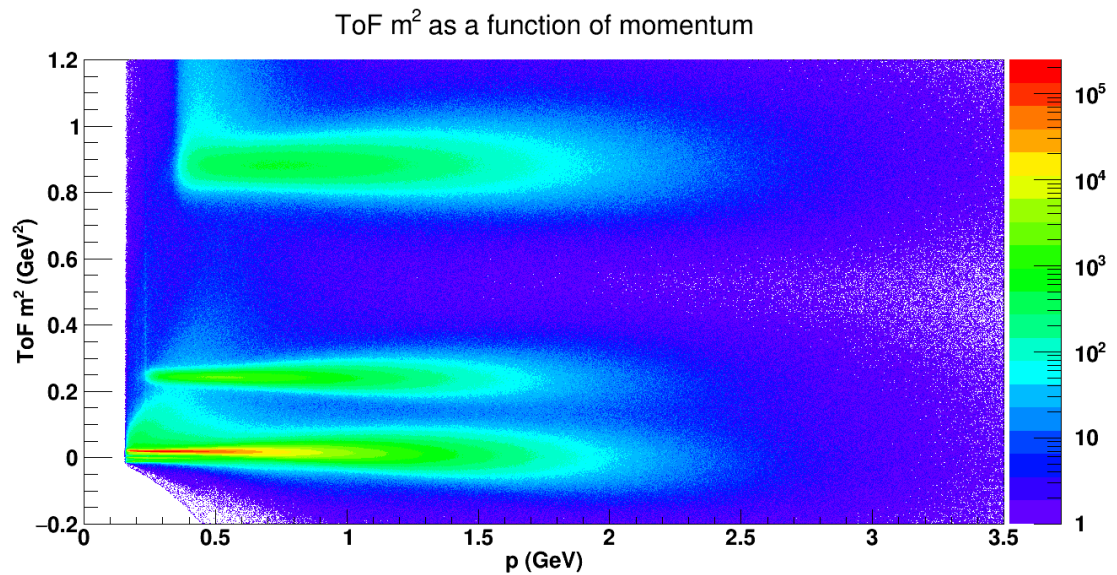


Fig. 47: 19GeV charged track m^2 vs p from the ToF

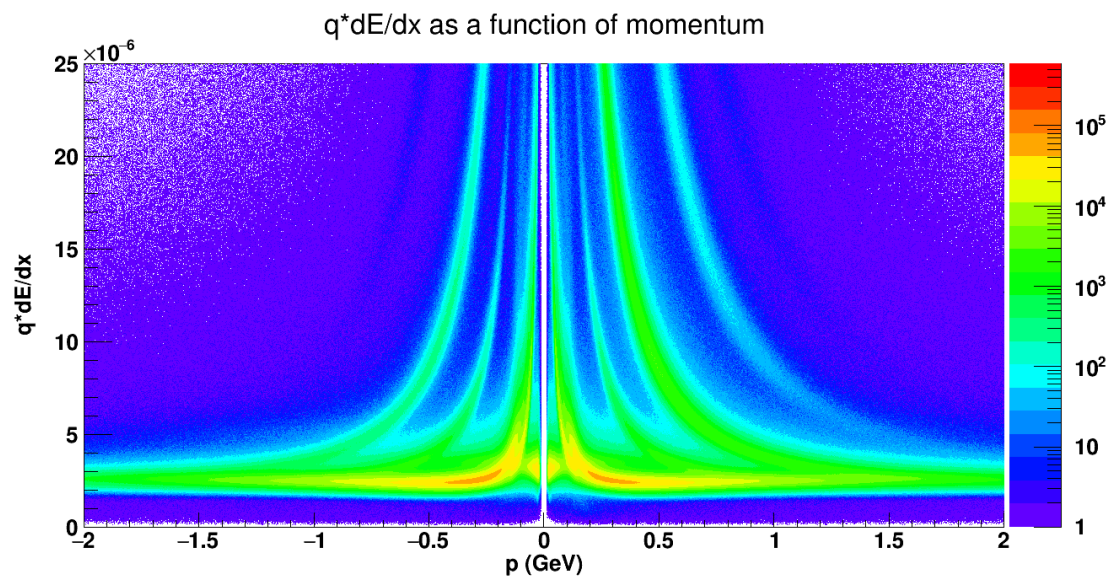


Fig. 48: 27GeV charged track dE/dx vs. p from the TPC

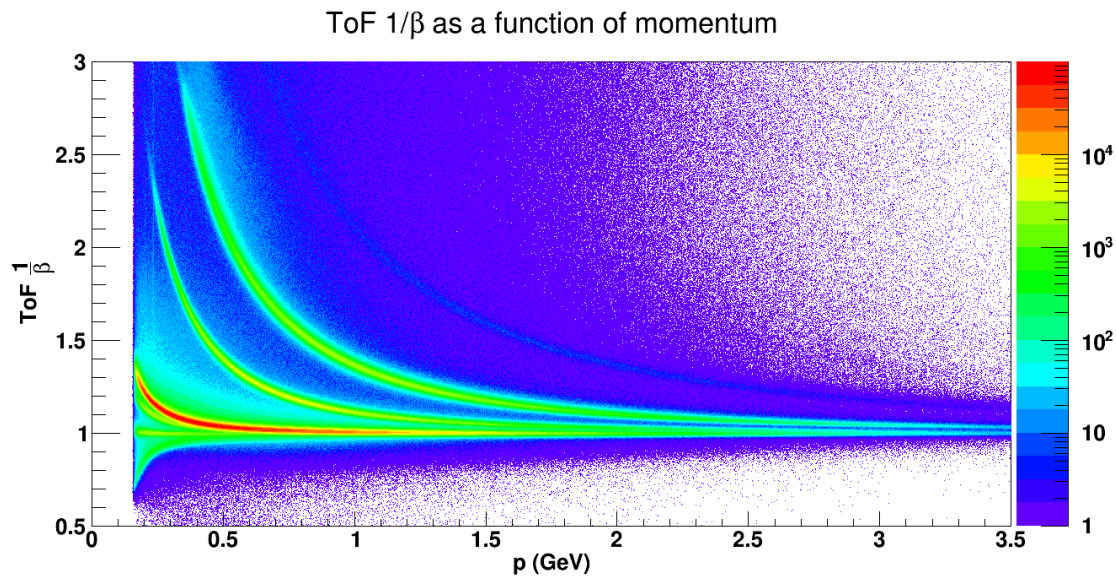


Fig. 49: 27GeV charged track $1/\beta$ vs. p from the ToF

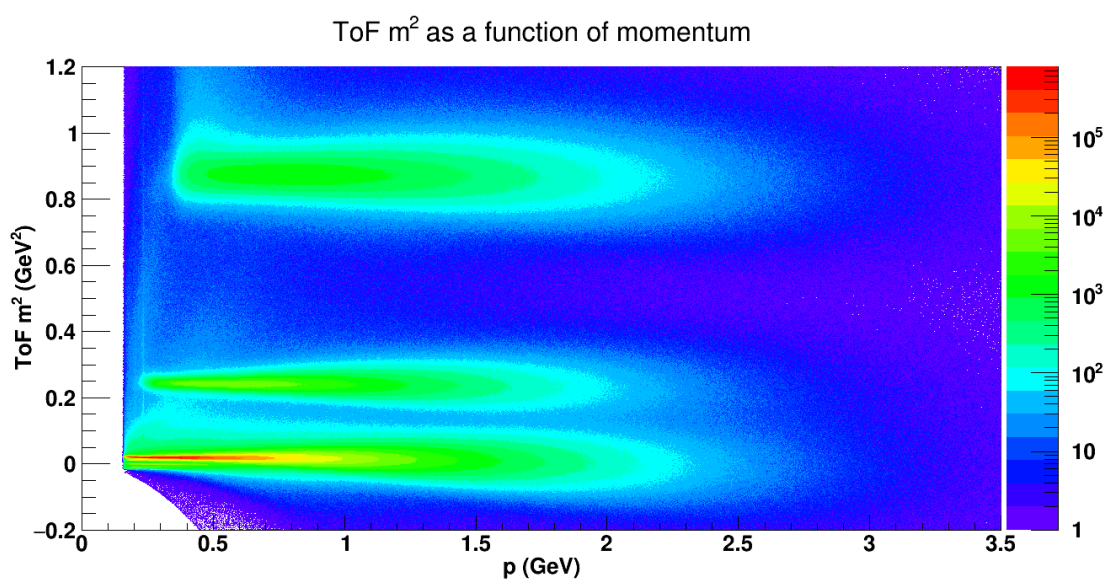


Fig. 50: 27GeV charged track m^2 vs p from the ToF

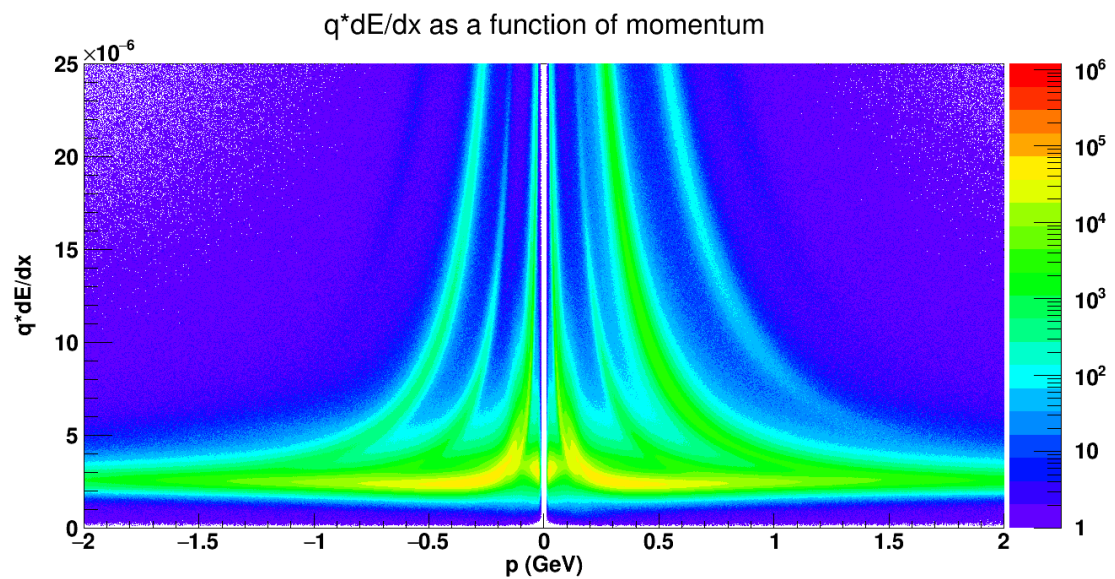


Fig. 51: 39GeV charged track dE/dx vs. p from the TPC

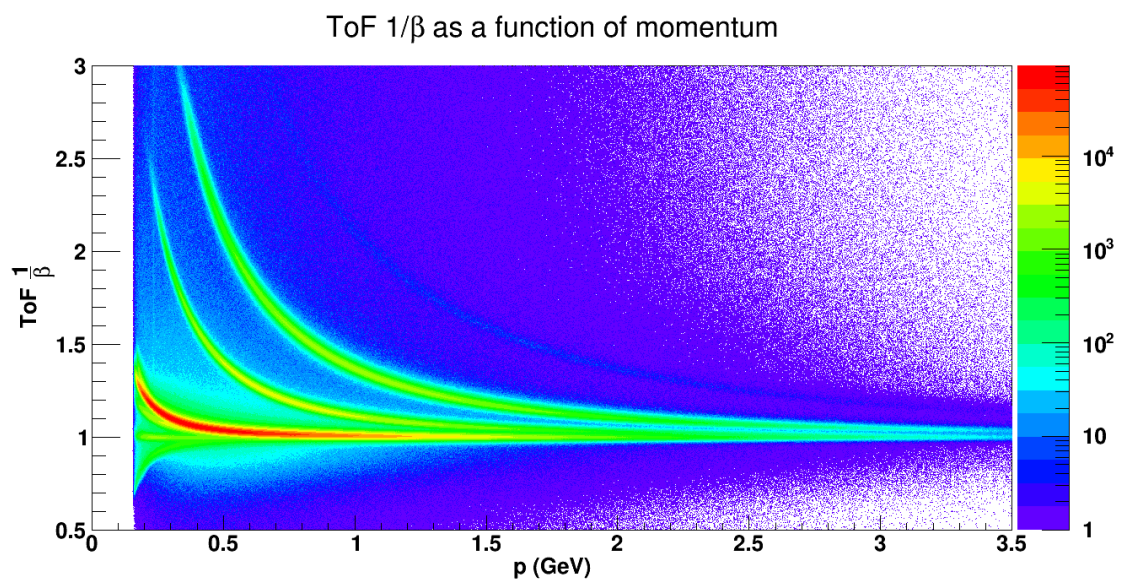


Fig. 52: 39GeV charged track 1/β vs. p from the ToF

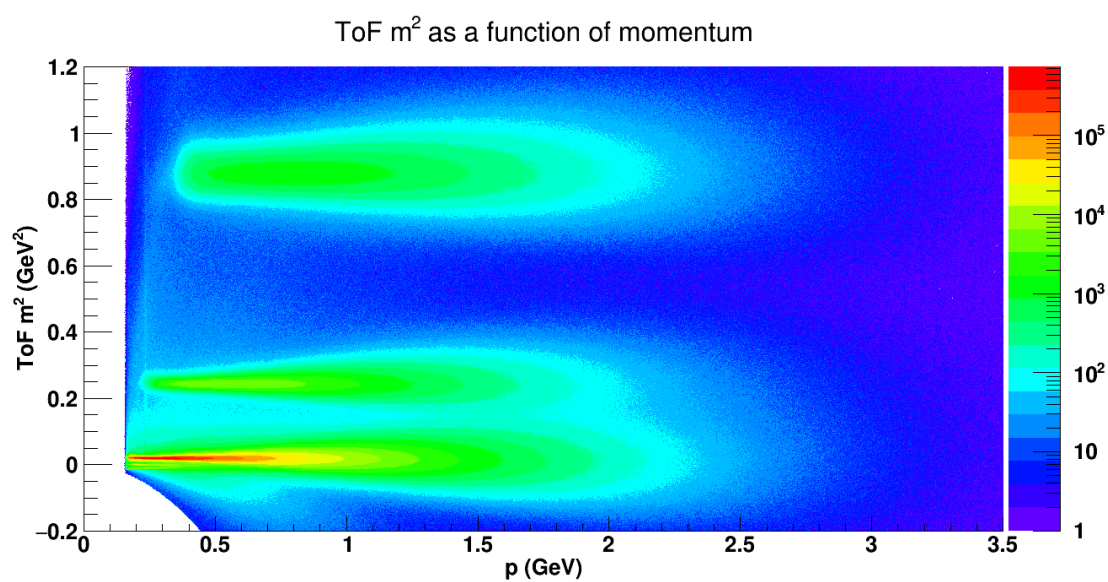


Fig. 53: 39GeV charged track m^2 vs p from the ToF

2.4.2 Lambda topological cuts

Lambdas are reconstructed from the protons and pions using a series of topological cuts. The scheme for the cuts is rather complicated as the cut values themselves depend on whether or not the candidate proton and pion separately have ToF information.

- (Proton ToF and Pion ToF, Proton ToF and !Pion ToF, !Proton ToF and Pion ToF, !Proton ToF and !Pion ToF)

– Proton DCA to PV $\geq (0.1, 0.15, 0.5, 0.6)$ cm

– Pion DCA to PV $\geq (0.7, 0.8, 1.5, 1.7)$ cm

– Lambda DCA to PV $\leq (1.3, 1.2, 0.75, 0.75)$ cm

– Lambda decay length $\geq (2, 2.5, 3.5, 4)$ cm

– Proton to Pion DCA to each other ≤ 1 cm

– Finally there is a cut ensuring that the Lambda is moving away from the primary vertex.

– Lambdas are taken in the mass window (1.115683 ± 0.005) GeV

– As described in section 4.1 for systematic error reasons we actually do not include Lambdas for which the pion has ToF data and the proton does not

- Proton DCA is a cut on a minimum (DCA > x)

- Pion DCA is a cut on a minimum

- Proton to Pion DCA is a cut on a maximum

- Λ DCA is a cut on a maximum

- Λ Decay Length is a cut on a minimum

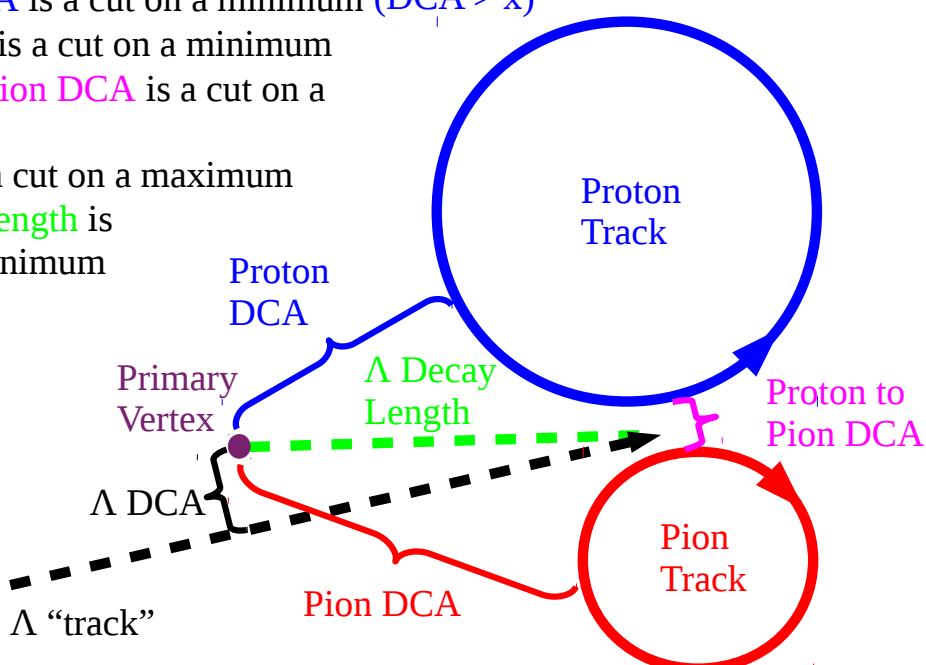


Fig. 54: Diagram of how cuts are applied to reconstruct lambdas

It should be mentioned here that the quantities I am plotting below are made by greatly loosening, though not eradicating, the cuts. Therefore all such plots display quantities after all of the cuts, in some form, have been applied to them. This means that there will be some non-trivial structure. I will come back with plots for this later.

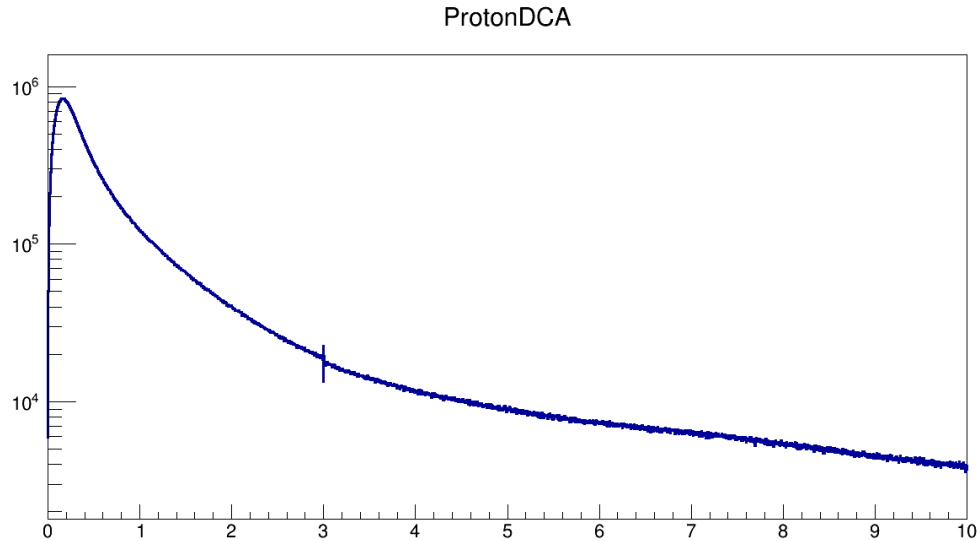


Fig. 55: Counts vs. proton DCA to the primary vertex (cm)

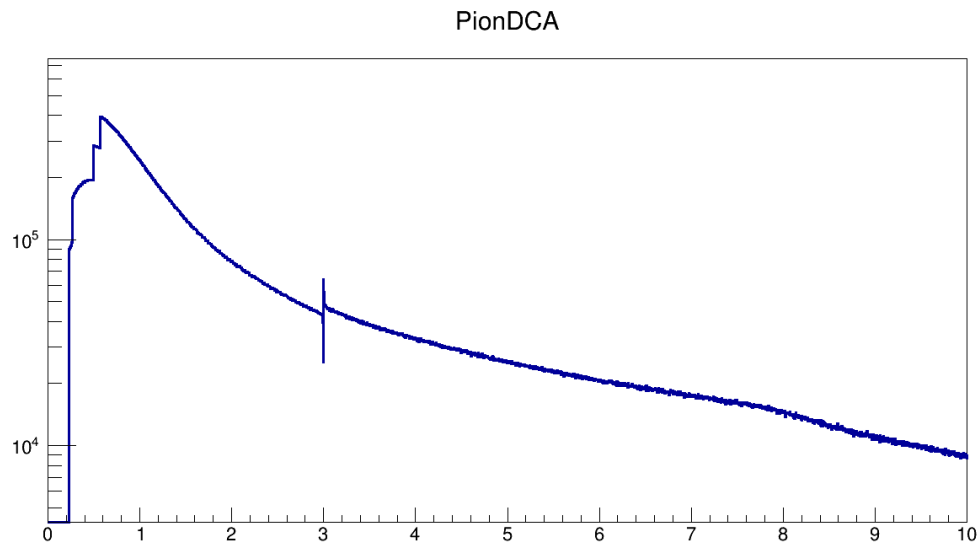


Fig. 56: Counts vs. pion DCA to the primary vertex (cm)

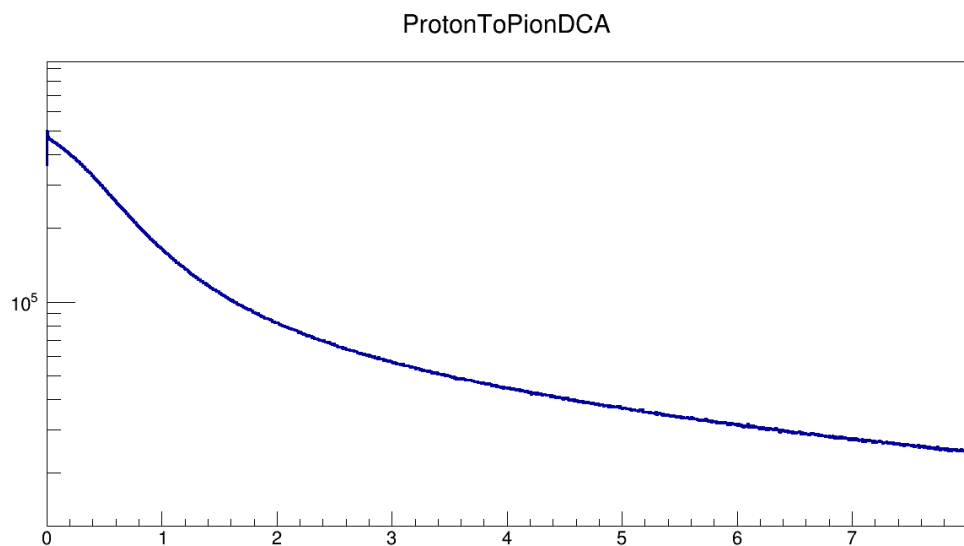


Fig. 57: DCA of one daughter track to another (cm)

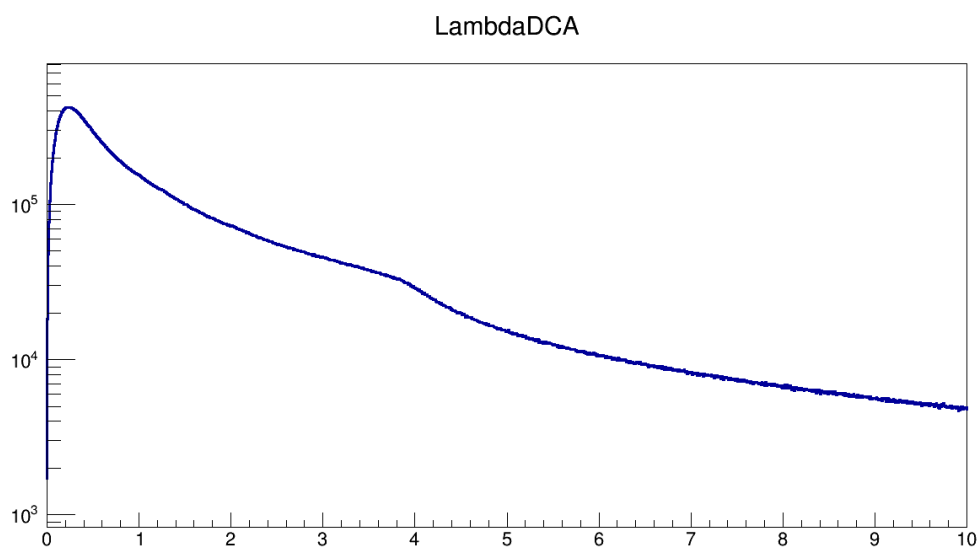


Fig. 58: Counts vs. Lambda DCA to the primary vertex (cm)

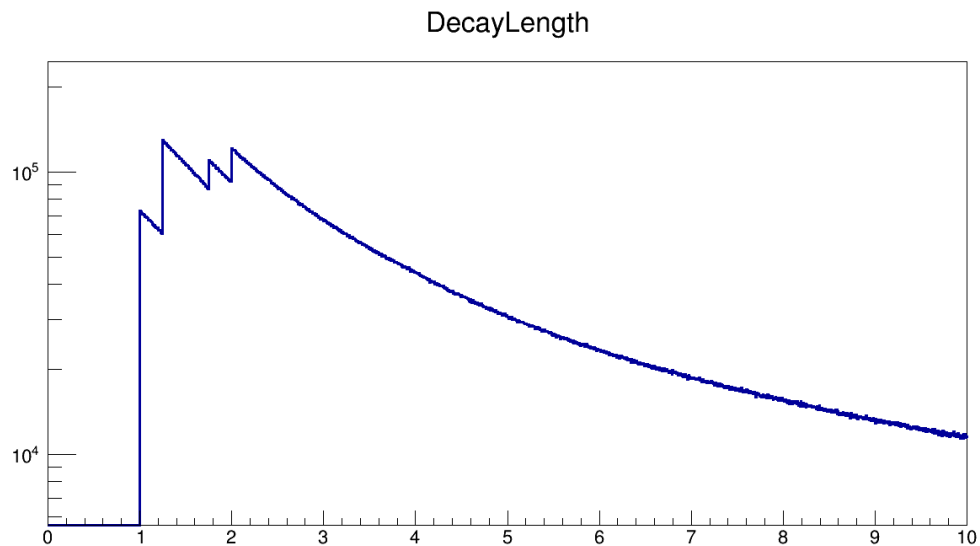


Fig. 59: Counts vs. Lambda decay length (cm)

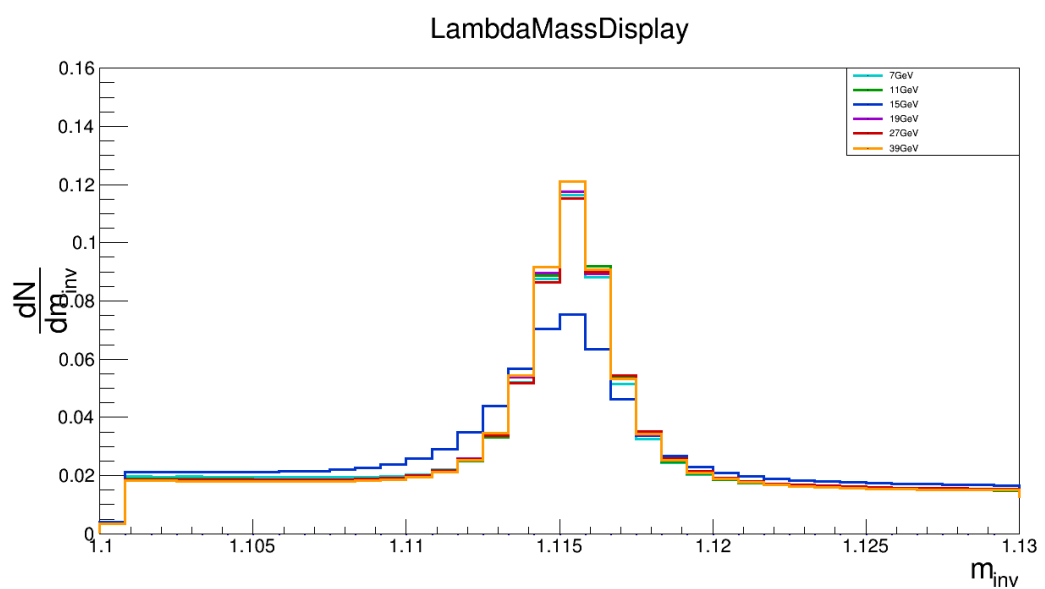


Fig. 60: $\frac{dN}{dm_\Lambda}$ vs. m_Λ (GeV). Note the strange mass distribution at 15GeV, probably from the HFT

3 Data analysis

The idea of the measurement is described in the introduction. In this section I'll include some final and corrected results, explain what corrections are made, and talk about some efficiency and reconstruction issues that occur in the measurement. Aside from the final result and unless otherwise mentioned most plots depict $\langle \sin(\Psi_1 - \phi_{\Lambda}^*) \rangle$ with a resolution correction, which neglects the constant factor $\frac{8}{\pi\alpha}$. The general idea of this section is to provide both the steps to doing this analysis and to explain issues that are deemed fundamentally important to the QA of the analysis. In order what is done is

- Apply event cuts (sec. 2.1)
- Determine the event plane (sec. 2.2)
- Make arrays of tracks which pass track cuts (sec. 2.3)
- Loop over track arrays and apply Lambda topological cuts to find Lambda candidates (sec. 2.4.2)
- Fill TProfiles with $\sin(\Psi_1 - \phi_{\Lambda}^*)$ (that is average) for each centrality
- Divide by resolution correction, R and multiply by $\frac{8}{\pi\alpha}$ (sec. 2.2.1)
- Apply mass purity correction (sec. 3.2)
- Apply acceptance correction (sec. 3.3)
- Apply helicity efficiency correction (sec. 3.4.2) – these are the final P_H values
- Separate into vortical and magnetic components with feed-down correction (3.5)

See sec. 3.6 for a brief discussion of the statistical errors and sec 4 for a discussion of the systematic errors. Note that in the above table the decay parameter α_H is taken to be 0.647 ± 0.013 for both the Λ and $\bar{\Lambda}$ results. This is the decay parameter of the Λ . This may seem an odd choice as $\alpha_{\bar{\Lambda}}$ has been measured independently. It is of fundamental interest whether these values differ but measured values have consistently found to be the same within statistical errors and it is largely assumed that they are, in fact, identical. Using different values would be confusing in as far as we are looking for differences in the data between Λ and $\bar{\Lambda}$ polarization and would be endorsing the more unlikely scenario that they are different. At any rate it is evident that the difference is small and the errors in the α_H are nearly negligible compared to the relatively large statistical uncertainty in the measure.

3.1 Resolution Correction

Since $\langle \sin(\Psi_1 - \phi_\Lambda^*) \rangle$ is a cululant it has the same resolution correction as any flow parameter v_n which is to say it is divided, centrality bin by centrality bin, by the values in Fig. 2.2.1 ($\langle \sin(\Psi_1 - \phi_\Lambda^*) \rangle / R$).⁵⁰⁵ On the centrality bin by centrality bin basis this is a constant scale so the significance of the result is preserved. However, since the resolution is not uniform over all centrality ranges, the significance of the result may be changed. A comparison to illustrate this is below.

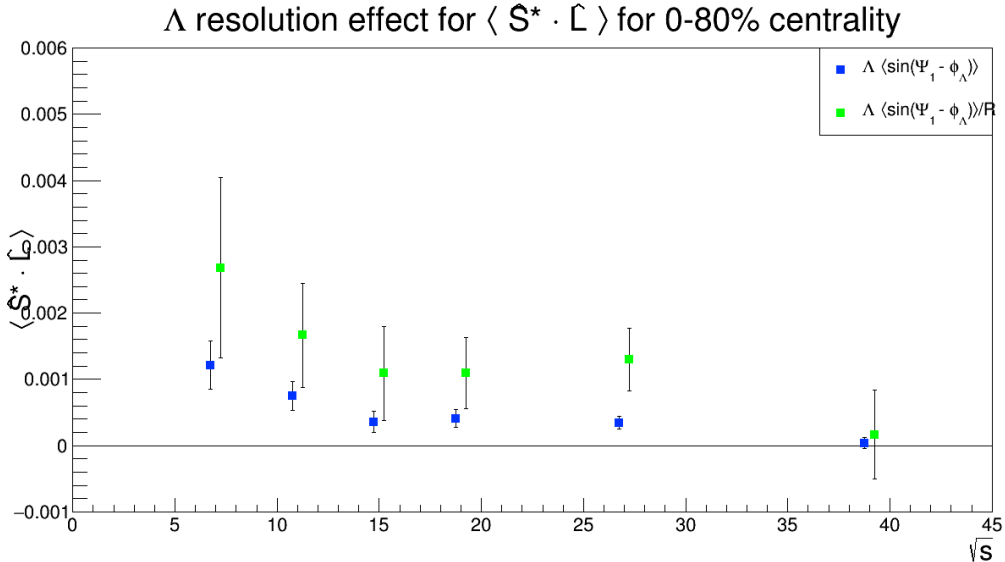


Fig. 61: Effect of resolution correction at effect 0-80% this is really $\langle \sin(\Psi_1 - \phi_\Lambda^*) \rangle / R$, not what the axis claims.

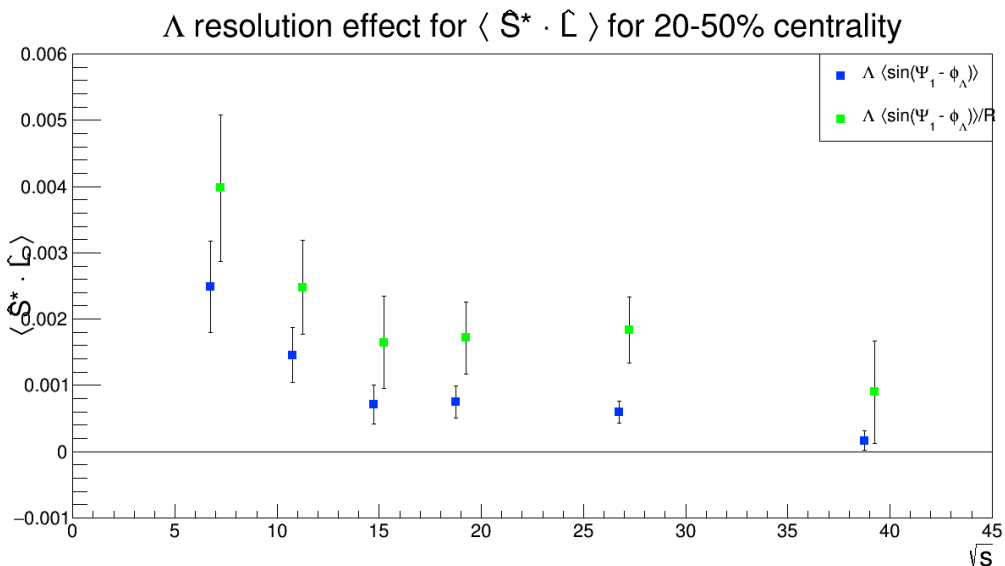


Fig. 62: Effect of resolution correction at effect 20-50% this is really $\langle \sin(\Psi_1 - \phi_\Lambda^*) \rangle / R$, not what the axis claims.

3.2 Mass background

510 A natural place to look for signal falsification is the wings of the Lambda mass distribution. In principle proton and pion pairs sufficiently away from the mass peak are not daughters of real Lambdas and thus should have no preference for the proton's momentum in the pair rest frame. We split our Lambda candidates into three categories: on mass peak, left of the mass peak ($m_{\text{inv}} < m_{\Lambda}$), pairs with invariant mass right of the mass peak ($m_{\text{inv}} > m_{\Lambda}$). The purity of the on peak Lambda candidates is estimated from
 515 the mass distribution by simply assuming a linear trend of the background between the points 1.108GeV and 1.125GeV and getting the counts. Obviously this is problematic for the 15GeV data, but changing procedure will complicate things. We leave a gap between the distributions so that the mass distribution used looks like this

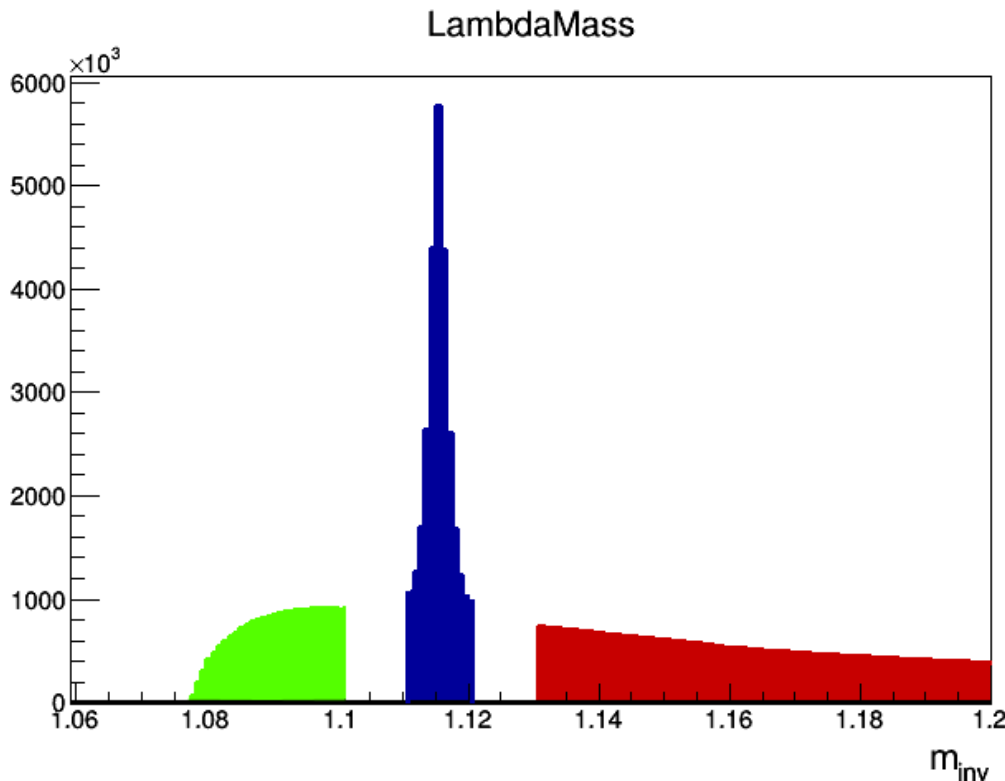


Fig. 63: Lambda mass distribution showing the regions right and left of the mass peak that are used in the analysis.

The signal for the Lambda polarization could leak into the mass wings via protons which are real Lambda daughters being paired with pions which are not their siblings. This effect is difficult to quantify but it isn't as incredible as it might sound. Proton DCA cuts are designed to pick only non-primary protons, the majority of which should come from Lambdas. The off mass signals we see have turned out not to be anomalies, as they persist through systematic checks of signal dependencies (as in different regions of E_Λ , y_Λ , centrality, ϕ_Λ , and the suit of topology cuts). If the height of the signal of the mass distribution is S and the height of the background is B we can do a similar subtraction of the off mass component as a flow measurement would do. In the final analysis we do not take this scaling into account (we assume zero background) but this calculation is important for the systematic errors. The off mass component is averaged from the $m_{\text{inv}} > m_\Lambda$ and the $m_{\text{inv}} > m_\Lambda$ component. Looking at the on mass peak Lambdas we measure

$$\langle \sin(\Psi_1 - \phi_\Lambda^*) \rangle_{\text{On Peak}} = \frac{S \langle \sin(\Psi_1 - \phi_\Lambda^*) \rangle_\Lambda + B \langle \sin(\Psi_1 - \phi_\Lambda^*) \rangle_{\text{Off Peak}}}{S + B} \quad (3)$$

Of course we want to know the Λ portion of the above equation so the mass corrected value takes the form (note that $(S+B)/S \sim 1.2$)

$$\langle \sin(\Psi_1 - \phi_\Lambda^*) \rangle_\Lambda = \frac{S+B}{S} \langle \sin(\Psi_1 - \phi_\Lambda^*) \rangle_{\text{On Peak}} - \frac{B}{S} \langle \sin(\Psi_1 - \phi_\Lambda^*) \rangle_{\text{Off Peak}} \quad (4)$$

The on peak results compared to the off peak results can be seen below

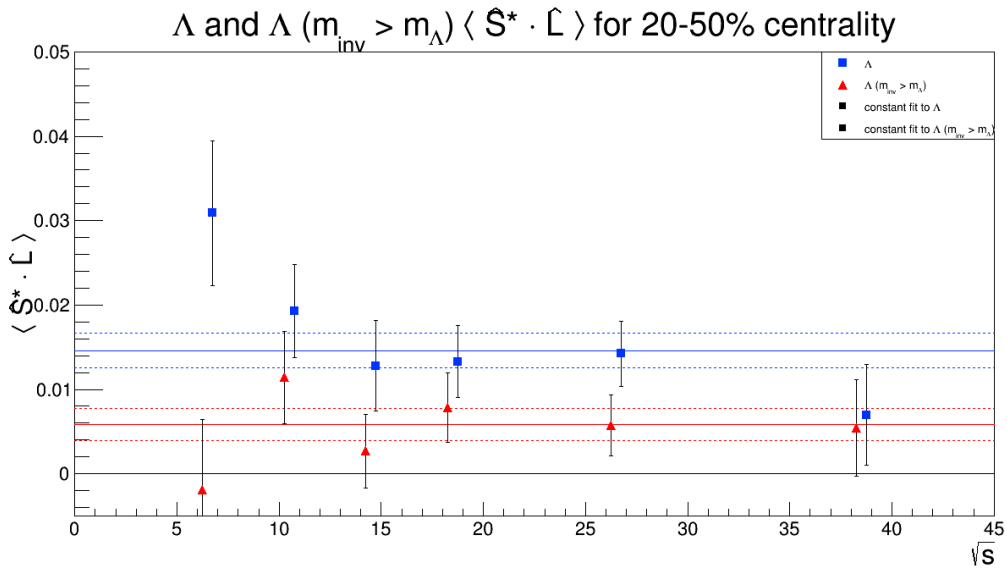


Fig. 64: Λ on peak result compared to this result $m_{\text{inv}} > m_\Lambda$. In order to show that the off mass results are significantly lower than the on peak results the two sets of data have been fit with a constant function, with error bars in dashed lines.

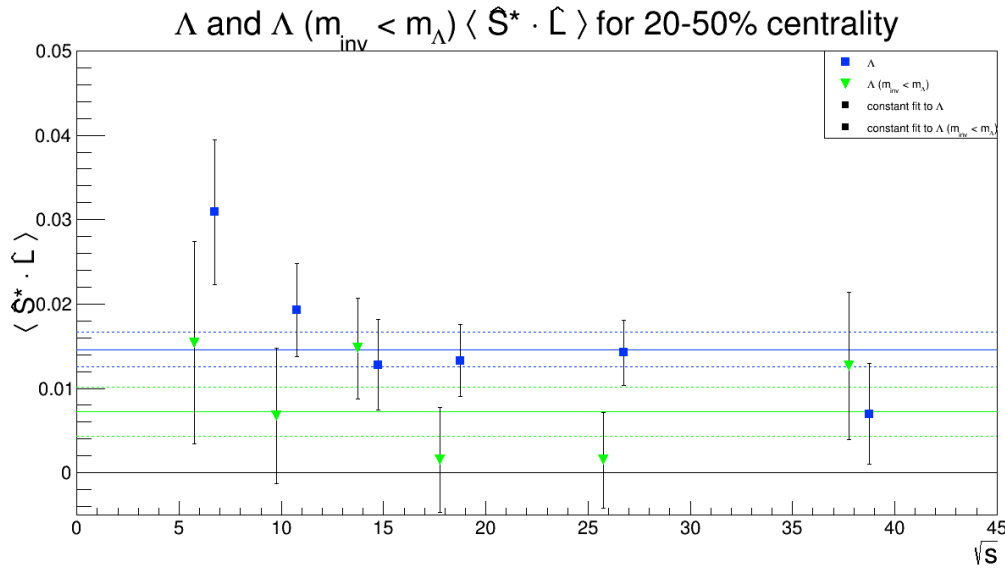


Fig. 65: Λ on peak result compared to this result $m_{inv} < m_\Lambda$. In order to show that the off mass results are significantly lower than the on peak results the two sets of data have been fit with a constant function, with error bars in dashed lines.

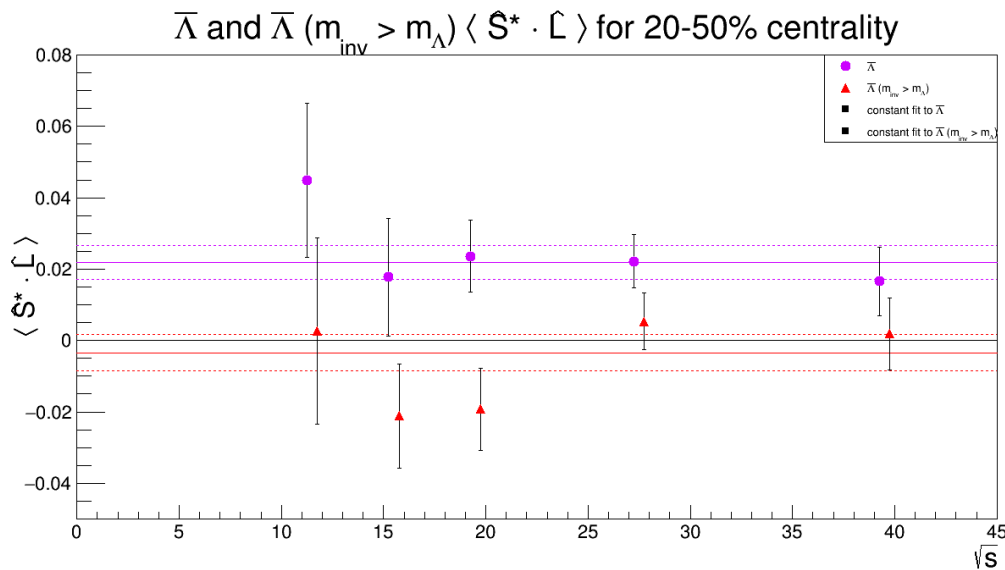


Fig. 66: $\bar{\Lambda}$ on peak result compared to this result $m_{inv} > m_\Lambda$. In order to show that the off mass results are significantly lower than the on peak results the two sets of data have been fit with a constant function, with error bars in dashed lines.

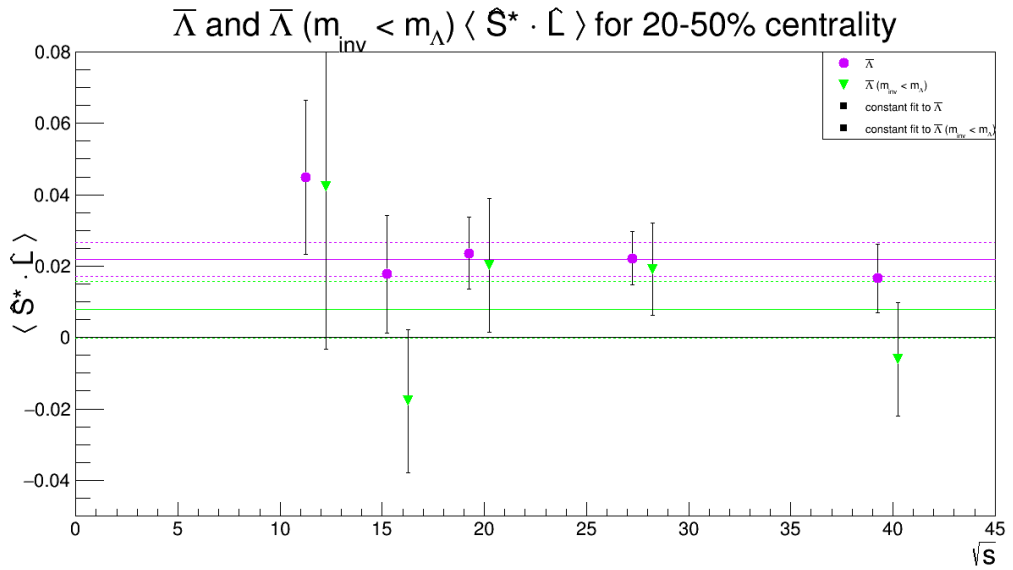


Fig. 67: $\bar{\Lambda}$ on peak result compared to this result $m_{inv} < m_\Lambda$. In order to show that the off mass results are significantly lower than the on peak results the two sets of data have been fit with a constant function, with error bars in dashed lines.

535

We can do the corrections described in equation 4 including this off-mass term and not including the off mass term (that is taking zero for the second term) and compare them. In the further analysis we assume the off-mass contribution is zero. This difference is a source of systematic errors in the analysis.

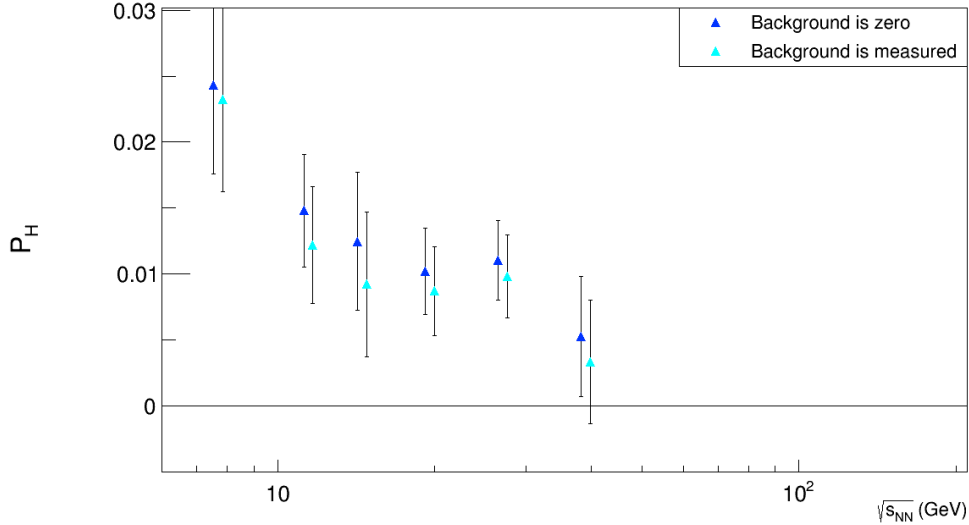


Fig. 68: Λ polarization results corrected for purity in the mass background. Results are corrected assuming the second term of eq. 4 is zero and by taking that second term from the data (measured).

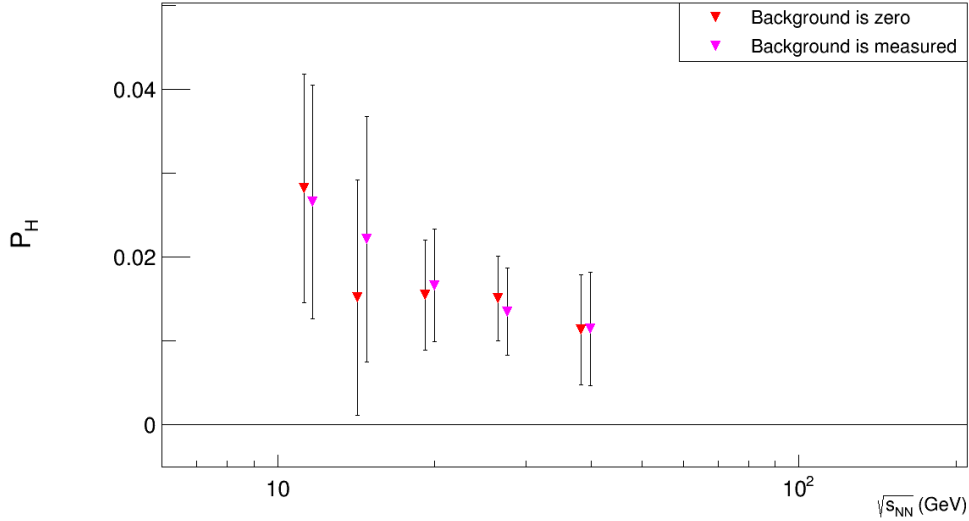


Fig. 69: $\bar{\Lambda}$ polarization results corrected for purity in the mass background. Results are corrected assuming the second term of eq. 4 is zero and by taking that second term from the data (measured).

3.3 Detector acceptance correction

Much of this section is the same as section C in the 2007 global polarization paper by STAR. Keep in mind that the negative sign error in that paper is propagated here as a substitution $\phi_p^* - \Psi_{RP} \longrightarrow \Psi_{RP} - \phi_p^*$.

3.3.1 Detector acceptance correction explanation

⁵⁴⁰ The polarization as $\langle \sin(\Psi_{RP} - \phi_p^*) \rangle$ assumes a perfect detector. To correctly take into account the detector acceptance we note that the integral over the solid angle (for the proton boosted into the Lambda's rest frame) $d\Omega_p^* = d\phi_p^* \sin(\theta_p^*) d\theta_p^*$. What we actually get when we consider detector acceptance is

$$\langle \sin(\Psi_{RP} - \phi_p^*) \rangle = \int \frac{d\Omega_p^*}{4\pi} \frac{d\phi_H^*}{2\pi} A(\mathbf{p}_H, \mathbf{p}_p^*) \int_0^{2\pi} \frac{d\Psi_{RP}}{2\pi} \sin(\Psi_{RP} - \phi_p^*) [1 + \alpha_H P_H(\mathbf{p}_H; \Psi_{RP}) \sin \theta_p^* \cdot \sin(\Psi_{RP} - \phi_p^*)] \quad (5)$$

⁵⁴⁵ where \mathbf{p}_H is the hyperon 3-momentum and $A(\mathbf{p}_H, \mathbf{p}_p^*)$ is a function to account for the acceptance; the integral of which is unity. Since the polarization can, in principle, depend on the Lambda's azimuthal angle and the detector is even with respect to ϕ we can expand the polarization into a sum over even harmonics:

$$P_H(\Psi_{RP} - \phi_p^*, p_T^H, \eta^H) = \sum_{n=0}^{\infty} P_H^{(2n)}(p_T^H, \eta^H) \cos \{2n[\Psi_{RP} - \phi_p^*]\}. \quad (6)$$

In this paper the we are not quoting any such azimuthal dependence of the signal so we quote the polarization averaged over all possible values of $\phi_H - \Psi_{RP}$:

$$P_H(p_T^H, \eta^H) \equiv \overline{P_H(\Psi_{RP} - \phi_p^*, p_T^H, \eta^H)} = P_H^{(0)}(p_T^H, \eta^H) \quad (7)$$

By substituting eq.6 into eq.5 and integrating over the reaction plane we get

$$\langle \sin(\Psi_{RP} - \phi_p^*) \rangle = \frac{\alpha_H}{2} \int \frac{d\Omega_p^*}{4\pi} \frac{d\phi_H^*}{2\pi} A(\mathbf{p}_H, \mathbf{p}_p^*) \sin \theta_p^* \left[P_H(p_T^H, \eta^H) - \frac{1}{2} \cos[2(\phi_H - \phi_p^*)] P_H^{(2)}(p_T^H, \eta^H) \right]. \quad (8)$$

⁵⁵⁰ From here the observable $P_H = \frac{8}{\pi \alpha_H} \langle \sin(\Psi_{RP} - \phi_p^*) \rangle$ can be written

$$\begin{aligned} \frac{8}{\pi \alpha_H} \langle \sin(\Psi_{RP} - \phi_p^*) \rangle &= \frac{4}{\pi} \overline{\sin \theta_p^*} P_H(p_T^H, \eta^H) - \frac{2}{\pi} \overline{\sin \theta_p^* \cos[2(\phi_H - \phi_p^*)]} P_H^{(2)}(p_T^H, \eta^H) \\ &= A_0(p_T^H, \eta^H) P_H(p_T^H, \eta^H) - A_2(p_T^H, \eta^H) P_H^{(2)}(p_T^H, \eta^H), \end{aligned} \quad (9)$$

where the functions $A_0(p_T^H, \eta^H)$ and $A_2(p_T^H, \eta^H)$ are defined by the average of $\sin \theta_p^*$ and $\sin \theta_p^* \cos[2(\phi_H - \phi_p^*)]$ over the detector acceptance according to

$$A_0(p_T^H, \eta^H) = \frac{4}{\pi} \overline{\sin \theta_p^*} \equiv \frac{4}{\pi} \int \frac{d\Omega_p^*}{4\pi} \frac{d\phi_H^*}{2\pi} A(\mathbf{p}_H, \mathbf{p}_p^*) \sin \theta_p^* \quad (10)$$

$$A_2(p_T^H, \eta^H) = \frac{2}{\pi} \overline{\sin \theta_p^* \cos[2(\phi_H - \phi_p^*)]} \equiv \frac{2}{\pi} \int \frac{d\Omega_p^*}{4\pi} \frac{d\phi_H^*}{2\pi} A(\mathbf{p}_H, \mathbf{p}_p^*) \sin \theta_p^* \cos[2(\phi_H - \phi_p^*)]. \quad (11)$$

$\sqrt{s_{NN}}$	A_0	A_0 error
$7.7GeV$	1.034	2.56e-4
$11.5GeV$	1.032	1.59e-4
$14.5GeV$	1.026	1.23e-4
$19.6GeV$	1.027	9.26e-5
$27GeV$	1.026	6.45e-5
$39GeV$	1.022	5.75e-5

Table 1: A_0 averaged over p_T^H and η^H

3.3.2 Detector acceptance correction results

Here are the numerical results for A_0 averaged over p_T^H and η^H . We do not look at the dependencies for this measurement since the quoted values for the measurement itself already are integrated over p_T^H and η^H . The polarization is divided by these numbers to arrive at the acceptance corrected values.

3.4 Helicity efficiency

An efficiency issue which is important for this analysis has to do with the direction the Lambda daughters are emitted in the rest frame of the Lambda with respect to the momentum of the Lambda in the lab frame.
⁵⁶⁰ If we end up with a Lambda daughter pion with very low momentum it is unlikely to be measured in the detector. Since protons are much more massive even protons with low momentum (relative, of course, to other protons) are likely to be measured. Since the proton is emitted preferentially in the direction of (opposite to) the Λ 's ($\bar{\Lambda}$'s) spin in its rest frame, \hat{S}^* , we measure more positive (negative) than negative (positive) helicity Λ s ($\bar{\Lambda}$ s). A schematic is shown below.

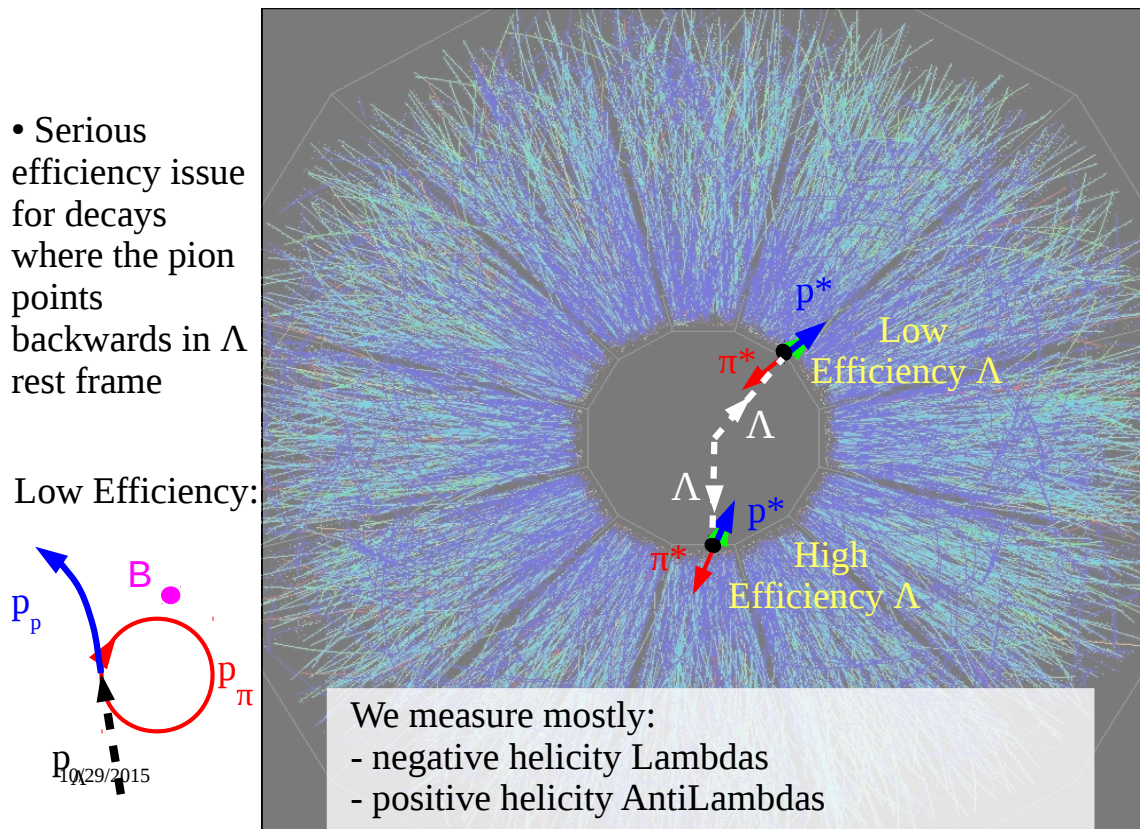


Fig. 70: Diagram to show the poor efficiency of Lambdas with low momentum pion daughters as compared to Lambdas with low momentum proton daughters.

⁵⁶⁵ Primarily this effect will not effect the data analysis and will be discussed in more detail in sec. 3.4.1. However a real polarization signal can, in fact, receive a small modification due to this efficiency. This modification is discussed in 3.4.2

3.4.1 Helicity efficiency description

⁵⁷⁰ This effect can be seen in data as well as simulation. If the measurement of $\sin(\Psi_1 - \phi_{\Lambda,\bar{\Lambda}}^*)$ is conducted azimuthally insensitively then this effect averages out but if one wants to take the measurement that is azimuthally dependent it is essential that the effect is known. To look at this effect and its cause I'll plot $\hat{p}_{\text{proton}}^* \cdot \hat{p}_\Lambda$ for data and HIJING.

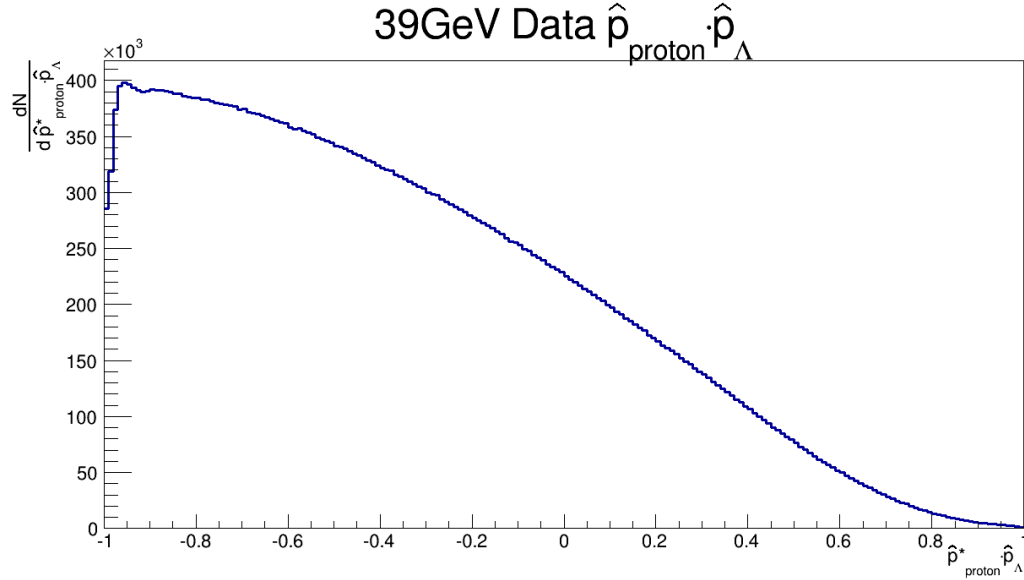


Fig. 71: Despite some of the axes this is $\hat{p}_{\text{proton}}^* \cdot \hat{p}_\Lambda$ for 39GeV. This is essentially the same for all $\sqrt{s_{NN}}$. Naturally, physically, this plot should be totally flat since there should be no preffered direction for proton momentum (ignoring some sort of coupling of polarization with emission angle and Lambda yields - which we can basically ignore).

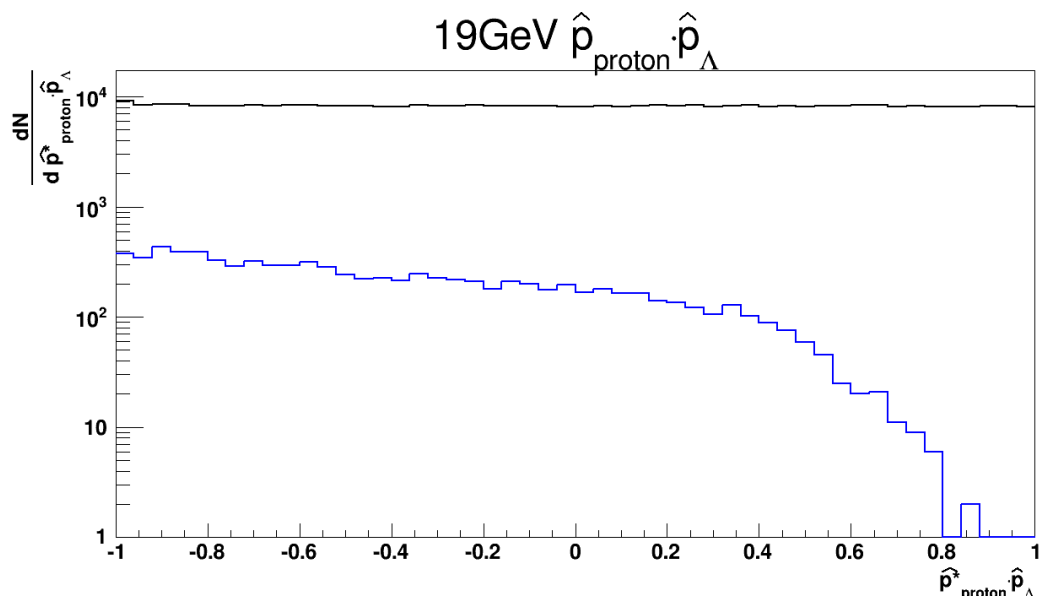


Fig. 72: This is the same as Fig. 3.4.1, but made using HIJING data. The black curve is from pure simulation Λ s. The blue curve is made from requiring basic reconstruction cuts (those which are possible: proton p_T , pion p_T , proton DCA, pion DCA, and Lambda decay length) of these simulated Λ s. By far the most (actually only!) important cut to this plot is the minimum pion p_T which causes this shape.

To see how this effects the data one can look at $\sin(\Psi_1 - \phi_{\Lambda,\bar{\Lambda}}^*)$ vs. $\Psi_1 - \phi_{\Lambda,\bar{\Lambda}}$. In the following plots the label of “Polarization” means $-\sin(\Psi_1 - \phi_{\Lambda,\bar{\Lambda}}^*)$. At the time of making these plots there were a few negative signs that I had not correctly accounted for. Much like the previous STAR paper on this polarization I had a negative sign in my definition of \hat{L} which is where the negative sign above comes from. Additionally there is a negative sign in how I determined Ψ_1 , this and the previous mistake cancel out. Finally I also had a sign error in the $\bar{\Lambda}$ result since the antiproton is emitted opposite the $\bar{\Lambda}$ spin, which I did not first realize. The summary of the previous points on sign errors is that in the following two plots the Λ results are okay but the results for $\bar{\Lambda}$ s should be flipped about the y axis. Due to an incorrect definition early in the analysis (the same as in the 2007 STAR paper) there is a sign error in the Λ results. There are two sign errors in the $\bar{\Lambda}$ results that cancel. Therefore the Λ plots should simply be flipped about the y axis. Remember that the angular momentum points in negative y and that the efficiency is such that we are more likely to reconstruct (Anti)Lambdas with negative (positive) helicity!!

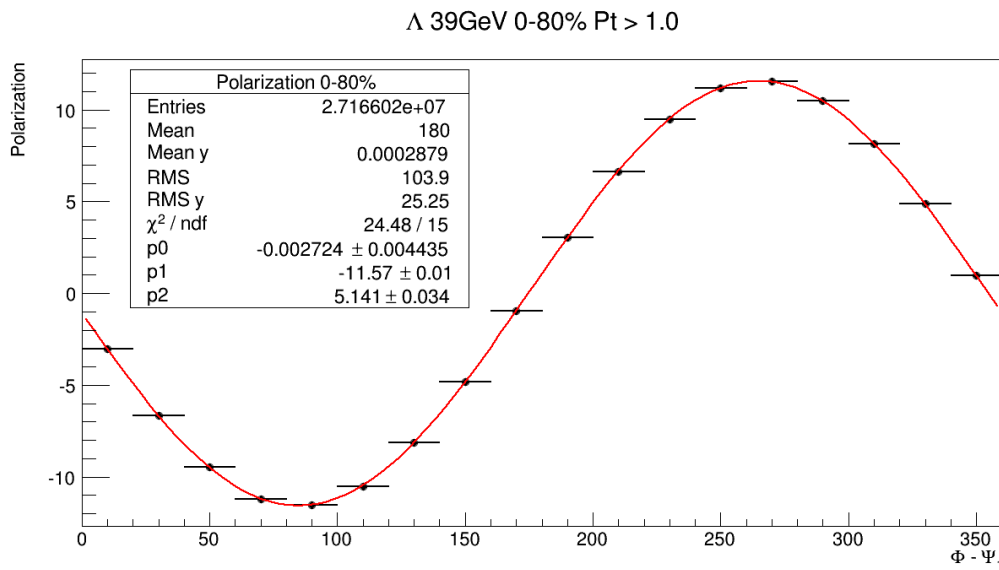


Fig. 73: $\sin(\Psi_1 - \phi_{\Lambda}^*)$ vs. $\Psi_1 - \phi_{\Lambda}$ for 39GeV Λ s with $p_T > 1\text{GeV}$. The data have been fit by the function $p_0 + p_1 * \sin(x + p_2)$. The overall sinusoidal shape comes from the effect mentioned above and seen in Fig. 3.4.1. The specific phase shift comes from the STAR magnetic field which increases with p_T . 39GeV data has a RFF field alignment. There is a sign error in the Λ results.

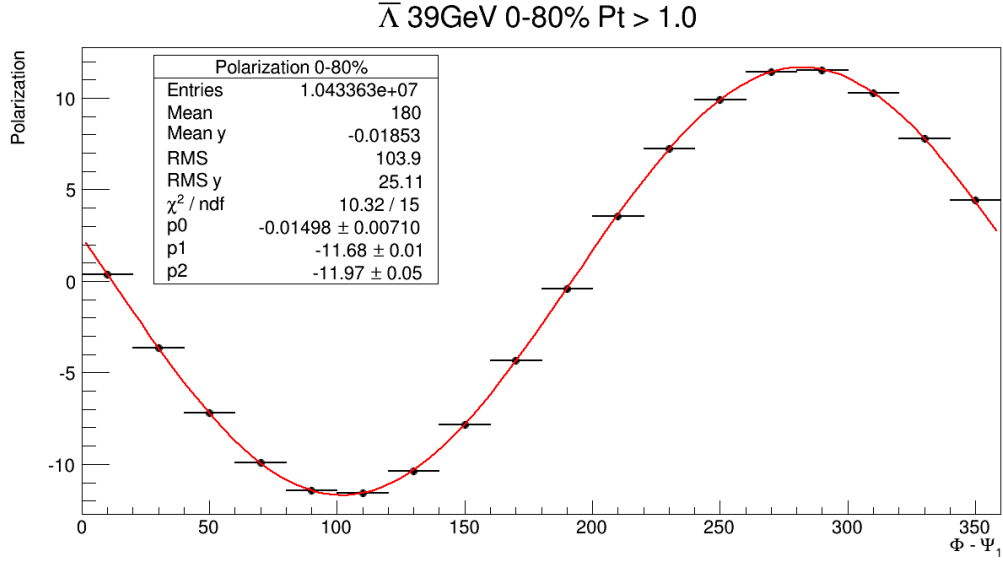


Fig. 74: $\sin(\Psi_1 - \phi_{\bar{\Lambda}}^*)$ vs. $\Psi_1 - \phi_{\bar{\Lambda}}$ for 39GeV $\bar{\Lambda}$ s with $p_T > 1\text{GeV}$. The data have been fit by the function $p0 + p1^*\sin(x+p2)$. The overall sinusoidal shape comes from the effect mentioned above and seen in Fig. 3.4.1. The specific phase shift comes from the STAR magnetic field which increases with p_T . 39GeV data has a RFF field alignment. Note that the phase is opposite in sign to what is seen in Fig. 3.4.1.

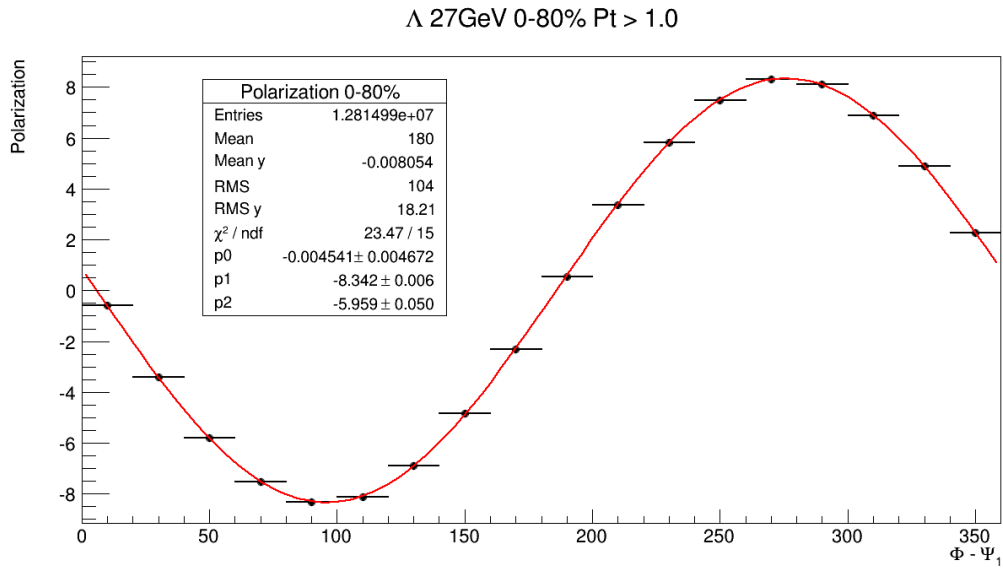


Fig. 75: $\sin(\Psi_1 - \phi_{\Lambda}^*)$ vs. $\Psi_1 - \phi_{\Lambda}$ for 27GeV Λ s with $p_T > 1\text{GeV}$. The data have been fit by the function $p0 + p1^*\sin(x+p2)$. The overall sinusoidal shape comes from the effect mentioned above and seen in Fig. 3.4.1. The specific phase shift comes from the STAR magnetic field which increases with p_T . 27GeV data has a FF field alignment. Note that the phase is opposite in sign to what is seen in Fig. 3.4.1. **There is a sign error in the Λ results.**

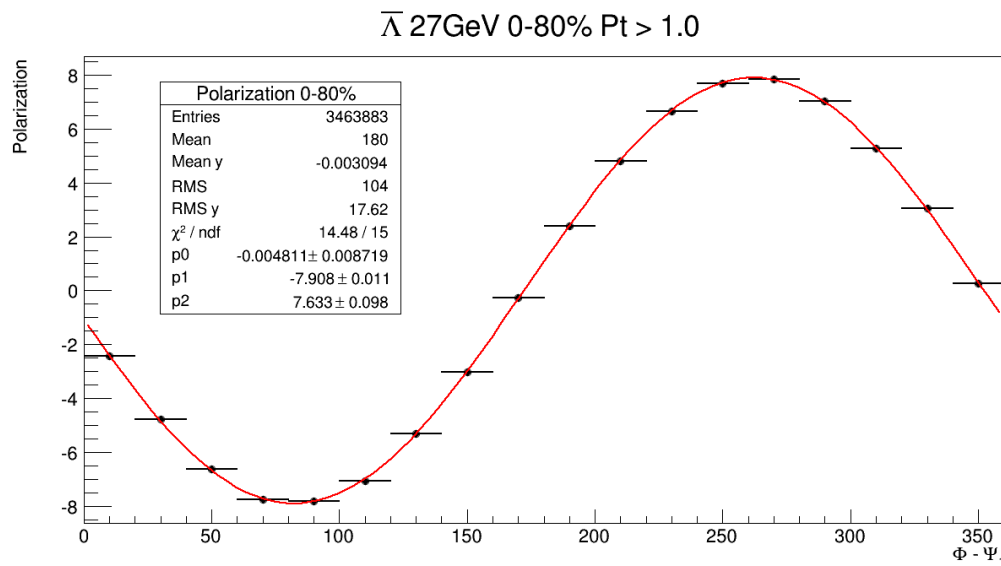


Fig. 76: $\sin(\Psi_1 - \phi_{\bar{\Lambda}}^*)$ vs. $\Psi_1 - \phi_{\bar{\Lambda}}$ for 27GeV $\bar{\Lambda}$ s with $p_T > 1\text{GeV}$. The data have been fit by the function $p_0 + p_1 \sin(x + p_2)$. The overall sinusoidal shape comes from the effect mentioned above and seen in Fig. 3.4.1. The specific phase shift comes from the STAR magnetic field which increases with p_T . 27GeV data has a RFF field alignment. Note that the phase is opposite in sign to what is seen in Fig. 3.4.1.

585 Knowing that we tend to see the Lambdas with backwards going protons means that we will see this sinusoidal behavoir. Ignore, for now, the phase shift and focus just on the overall sine shape seen above. Also, in the following discussion, assume that there is no global polarization so that an azimuthally integrated measure would give a null result. Finally take \hat{L} to be pointing in $\pi/2$ with respect to the event plane. For a $\Lambda(\bar{\Lambda})$ with $\phi_\Lambda - \Psi_1 = 0$ the helicity efficiency should have no effect since $\sin(\Psi_1 - \phi_\Lambda^*)$
 590 vs. $\Psi_1 - \phi_{\bar{\Lambda}}$ for $\phi_\Lambda - \Psi_1 = \pi$ is also zero. The same thing is effectively true for a Lambda emitted in $\phi_\Lambda - \Psi_1 = \pi$. If, however the $\Lambda(\bar{\Lambda})$ is emitted such that $0 < \phi_\Lambda - \Psi_1 < \pi$ the efficiency will generate a large negative (positive) $\sin(\Psi_1 - \phi_\Lambda^*)$. Naturally the opposite is true for emission in $\pi < \phi_\Lambda - \Psi_1 < \pi$.

Let's start over with a Λ with $\phi_\Lambda - \Psi_1 = 0$ decaying with the STAR magnetic field on FF (as we have in 27GeV data). The decay point resolution of the Lambda is finite so we do not know exactly where the
 595 proton daughter was born. The magnetic field points in $+\hat{z}$ so the proton will appear to be bent slightly towards positive \hat{y} which means negative \hat{L} . This imperfection leads to a negative value of $\sin(\Psi_1 - \phi_\Lambda^*)$ for such Λ s. This effect is the same for $\bar{\Lambda}$ s since the antiproton curves the opposite direction and also denotes the opposite direction of spin - so two negatives cancel. This effect persists as you go about ϕ^* so at Λ with $\phi_\Lambda - \Psi_1 = \pi$ you end up with a positive number from the magnetic field.

600 Finally I want to compare these results to HIJING data

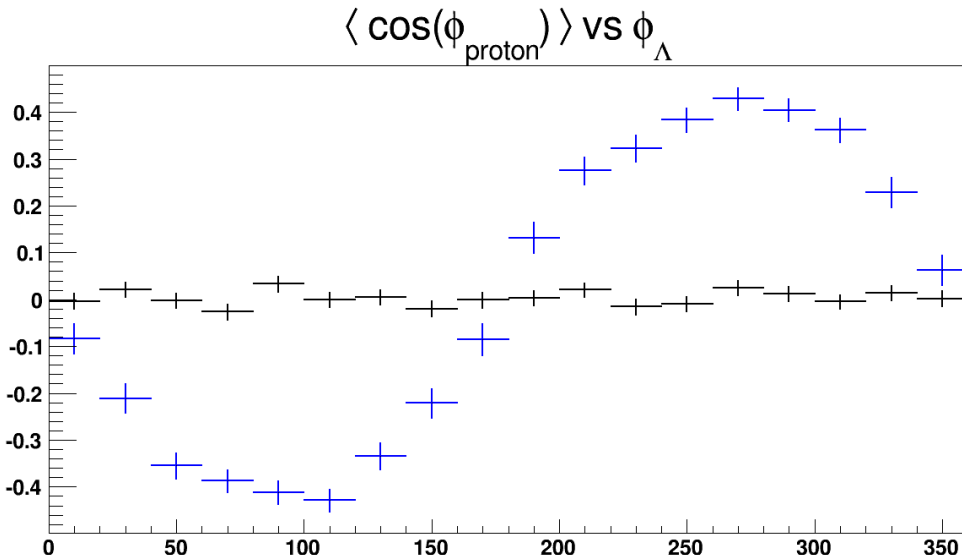


Fig. 77: As in Fig. 3.4.1 the black curve is from pure simulation Λ s. The blue curve is made from requiring basic reconstruction cuts. This has the assumption that the $\Psi_1 = 0$. **The same sign error is in these HIJING results.**

To understand how this efficiency creates an asymmetry in the final results see the flowing plots which show the η_Λ dependence of our polarization parameter. In this version I am plotting $S_y = \vec{S}_\Lambda \cdot \hat{L}$ which differs by a factor of two from $\sin(\Psi_1 - \phi_\Lambda^*)$ and also includes a boosting of the spin vector. In principle this could make a difference but in practice the S_y results have been consistent (accounting for the factor 605 of two) with $\sin(\Psi_1 - \phi_\Lambda^*)$, so it seems to be an ignorable difference. At the very least I am confident that the qualitative arguments presented here are correct.

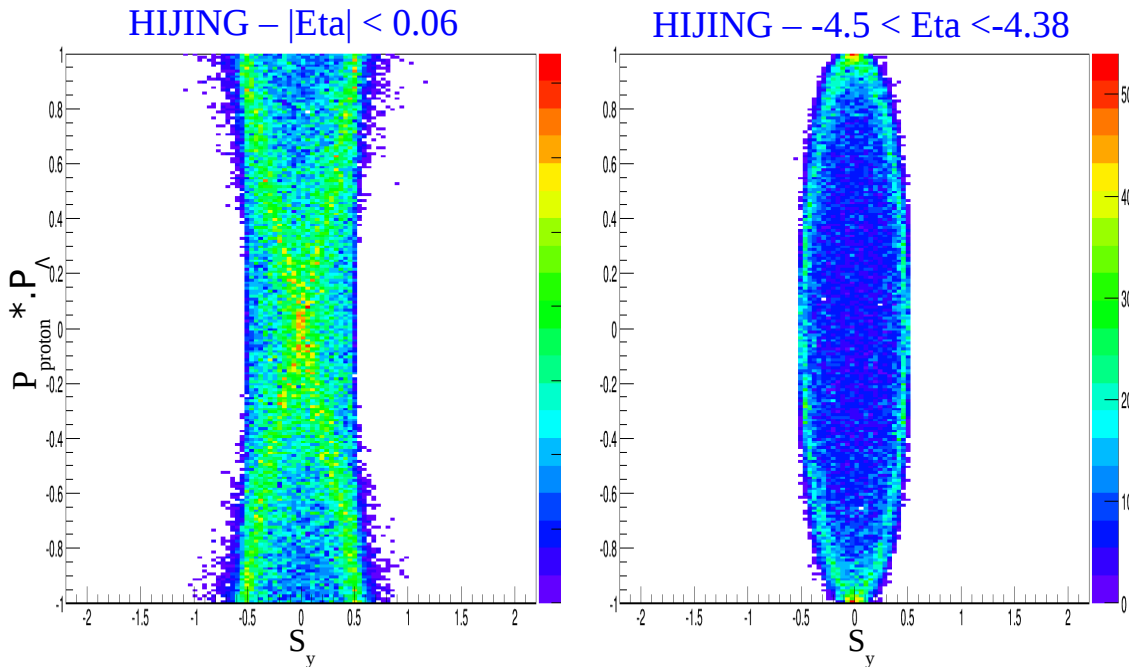


Fig. 78: As in Fig. 3.4.1 The figure on the left is a S_y for a narrow slice η_Λ at mid-rapidity while the figure on the right is a narrow slice very backward in η . For the first case the Λ is emitted in the same $x - y$ plane as \hat{L} in the second figure it is almost perpendicular to \hat{L} . Since the proton tends to be emitted with basically the same momentum as the Lambda these tendencies make sense. **The same sign error is in these HIJING results.**

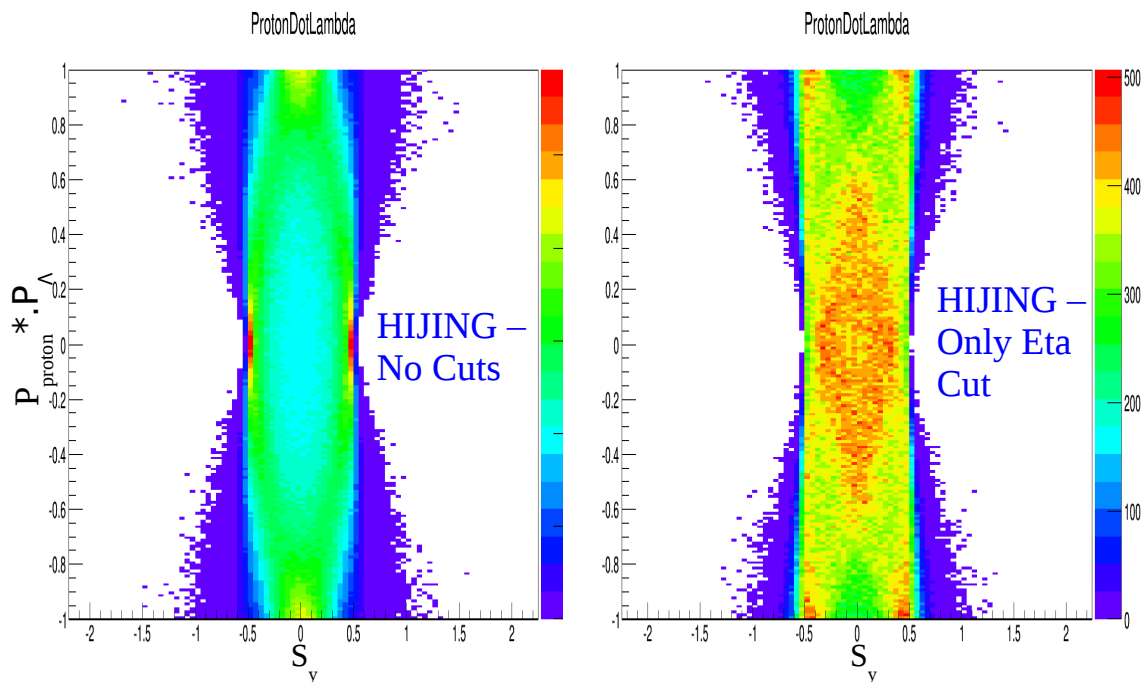


Fig. 79: As in Fig. 3.4.1 Fig. 3.4.1 tells us how looking at S_y within the STAR η range changes the underlying distribution. The same sign error is in these HIJING results.

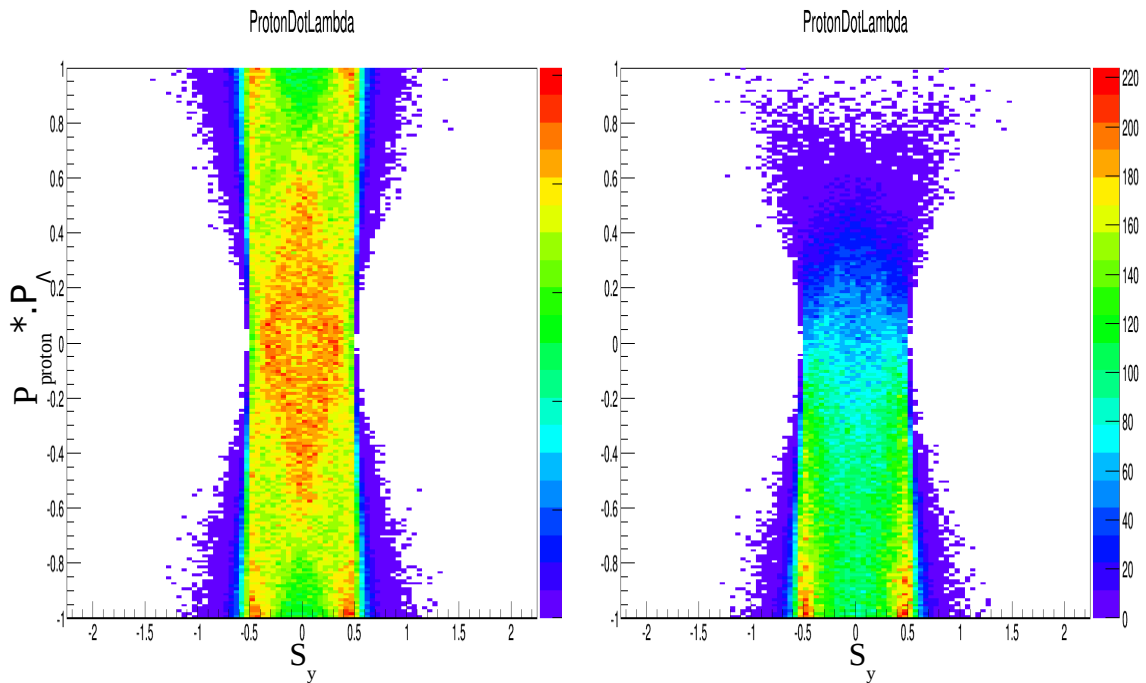


Fig. 80: Finally we see what the effect the helicity efficiency (Fig 3.4.1) has on the underlying distribution (Fig. 3.4.1). Now we see an asymmetry in the S_y distribution from the efficiency. **The same sign error is in these HIJING results.**

3.4.2 Helicity efficiency effect

In the previous section I described the helicity efficiency should average out when performing the analysis over all Lambda ϕ . Something which may not be immediately obvious is that there is essentially a coupling at higher harmonics of the ϕ distribution between the polarization (a zeroth order in trigonometric functions) and the aforementioned efficiency (a first order in trigonometric functions). Naturally I am assuming that the polarization is not phi dependant - an assumption which is seemingly born out in data (it is at least fair to say that such a dependance, if it exists, must be small compared to the phi-averaged polarization measured here).

Remember first that the sign of fig. 3.4.1 is wrong. we know from fig. 3.4.1 that negative (positive) helicity Lambdas (AntiLambdas) will have higher efficiency. If the Lambdas are actually polarized then a sample of Lambdas at $\pi/2$ has polarization in $-\hat{y}$ as well as an efficiency (independant of polarization) that tends to align spins along $-\hat{y}$. This will lead to an *increased* efficiency relative to Lambdas from any other ϕ . Similarly Lambdas at $-\pi/2$ have polarization anti-aligning with the efficiency effect, and thus a *decreased* efficiency. This coupling will make the first hump in 3.4.1 larger and the second hump smaller which means averaged over all of ϕ the polarization you will measure is *larger* than the nominal polarization of the sample.

Attached is a BulkCorr presentation detailing a simple simulation. In the simulation the azimuthal distribution of the Lambda daughters are chosen by sampling the polarization distribution with a given polarization. Additionally there are minimum p_T cuts on the daughters to get the efficiency effect (the Lambda momentum is chosen by sampling a real Lambda momentum distribution).

The result of all of this is a 7% scaling (that is a division of 1.07) for the polarization measure.

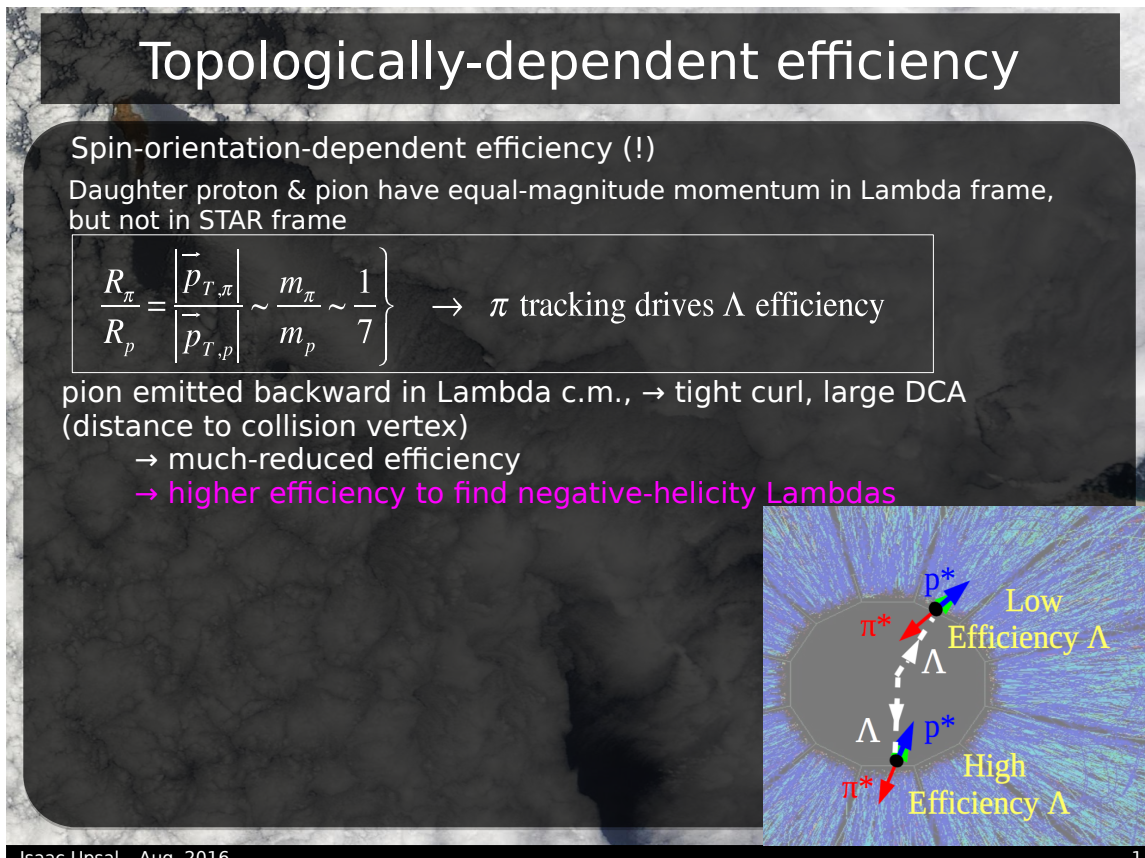


Fig. 81: Presentation on the effect of helicity efficiency on the polarization analysis p1.

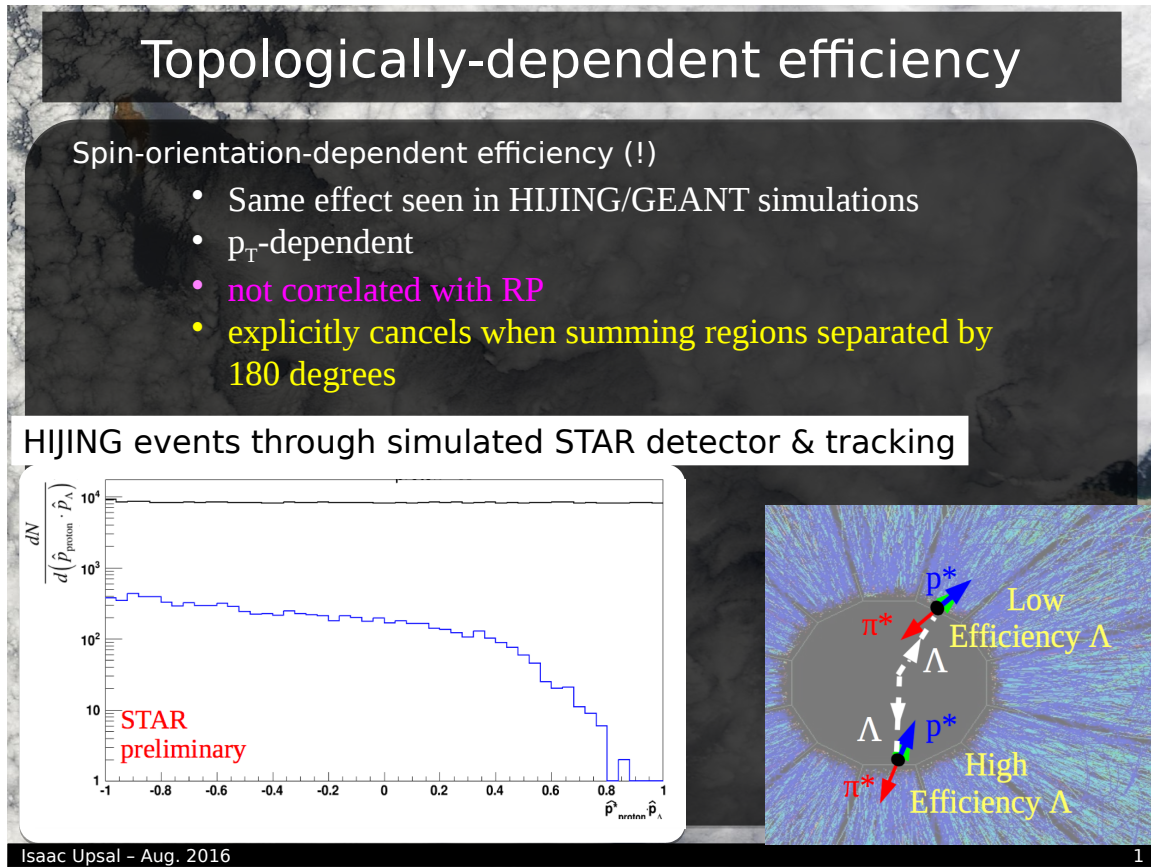


Fig. 82: Presentation on the effect of helicity efficiency on the polarization analysis p2.

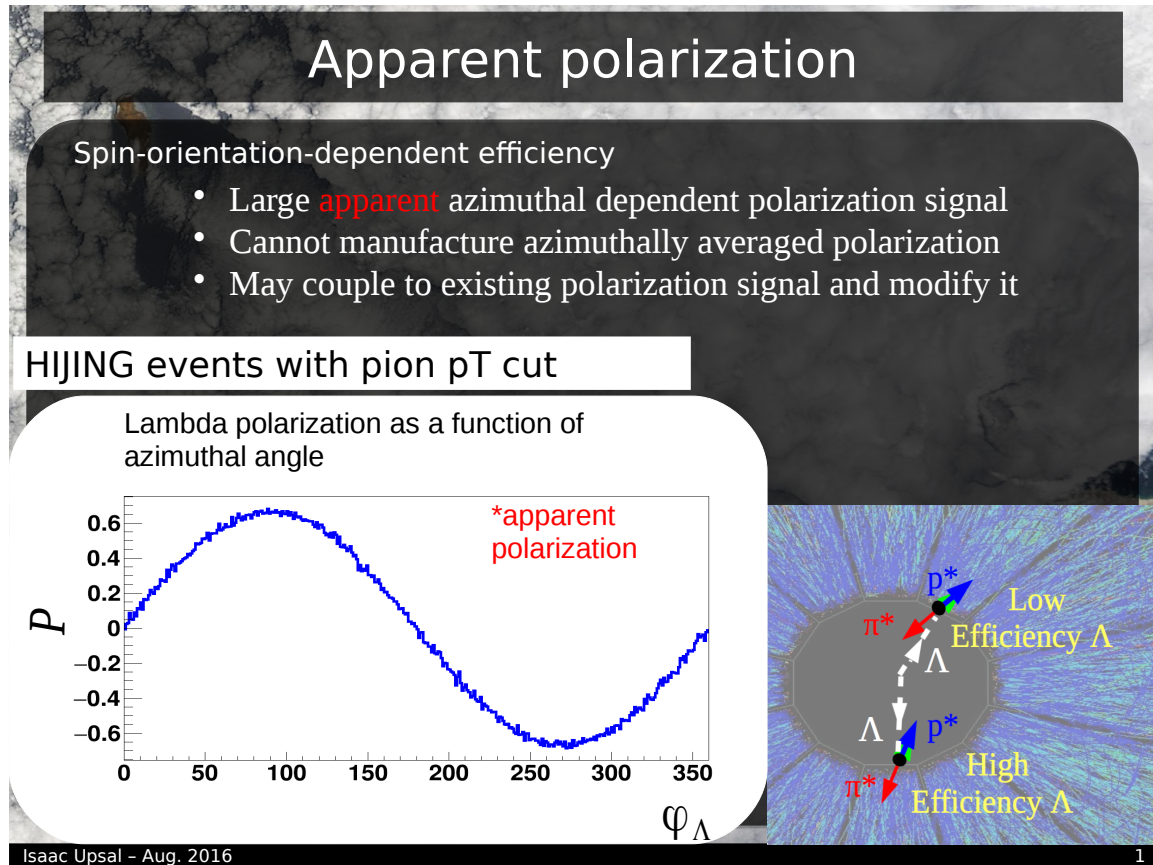


Fig. 83: Presentation on the effect of helicity efficiency on the polarization analysis p3.

Spin alignment from polarization

- Azimuthally independent polarization
- No detector!
- Spins in **ensemble** align with \hat{L}
- True for any ensemble of φ_Λ

Isaac Upsilon - Aug. 2016

1

Fig. 84: Presentation on the effect of helicity efficiency on the polarization analysis p4.

Spin alignment from efficiency

- No real polarization – only detector effects
- Lose Lambdas with spins in **ensemble** which align with \hat{p}

Isaac Upsal - Aug. 2016

1

Fig. 85: Presentation on the effect of helicity efficiency on the polarization analysis p5.

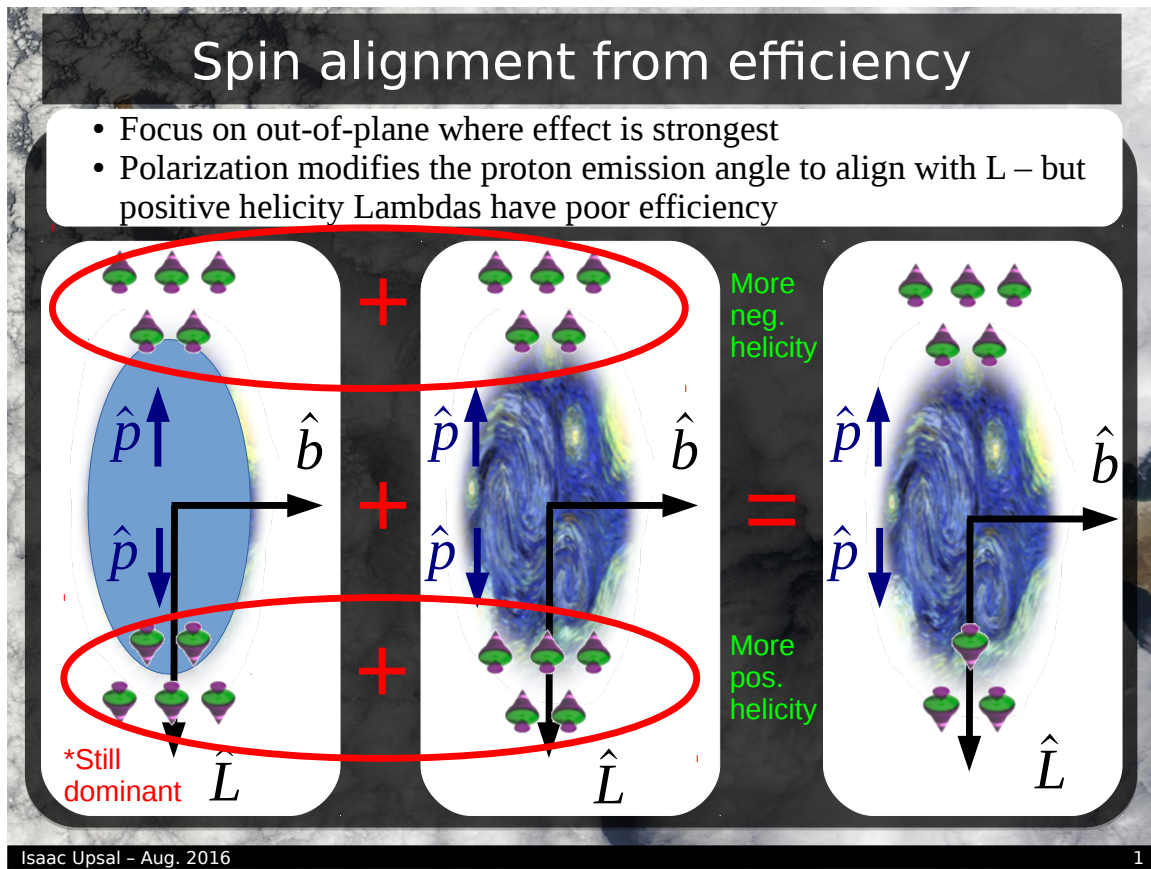


Fig. 86: Presentation on the effect of helicity efficiency on the polarization analysis p6.

Spin alignment from efficiency

- Introduces azimuthally dependent efficiency
- More Lambdas with spins aligning with angular momentum than anti-aligned
- Makes **real** polarization signal look bigger
- For AntiLambdas flip spins and efficiencies – ultimately the same effect
- Scaling and systematic error

Isaac Upsilon - Aug. 2016

1

Fig. 87: Presentation on the effect of helicity efficiency on the polarization analysis p7.

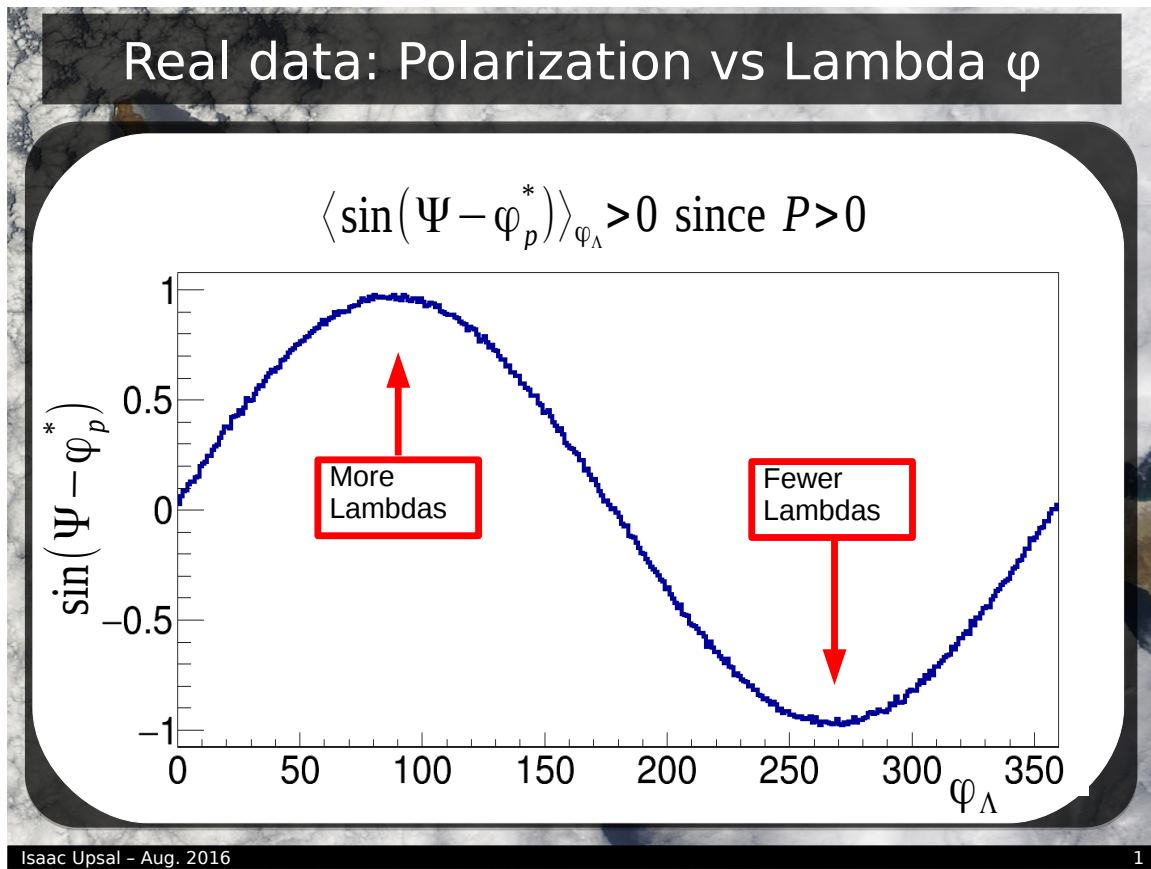


Fig. 88: Presentation on the effect of helicity efficiency on the polarization analysis p8.

Test consequence of efficiency

- Simple simulation, get proton decay direction by sampling distribution for different polarizations
$$1 + \alpha P \cos(\theta^*)$$
- Then make pion pt cut and check and compare “measured” polarization to input polarization

Isaac Upsal - Aug. 2016

1

Fig. 89: Presentation on the effect of helicity efficiency on the polarization analysis p9.

Test consequence of efficiency

- Effect is flat WRT polarization input
- Strong dependence on the value of the pt cut
 - Looks approx. linear
- Scale the data points by the value at $0.2 - 1/1.07$
- Reasonable cuts are all around 0.2GeV – should remove most of STAR tracking effect
 - Systematic error of 3.5%

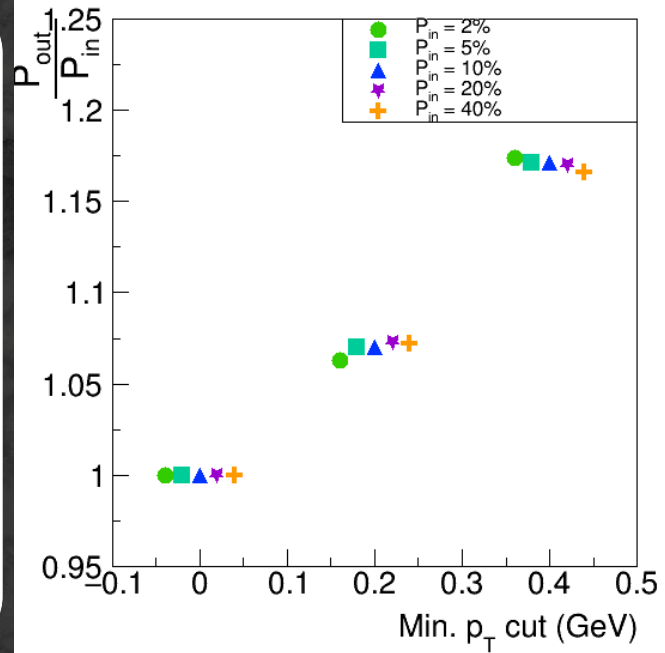


Fig. 90: Presentation on the effect of helicity efficiency on the polarization analysis p10.

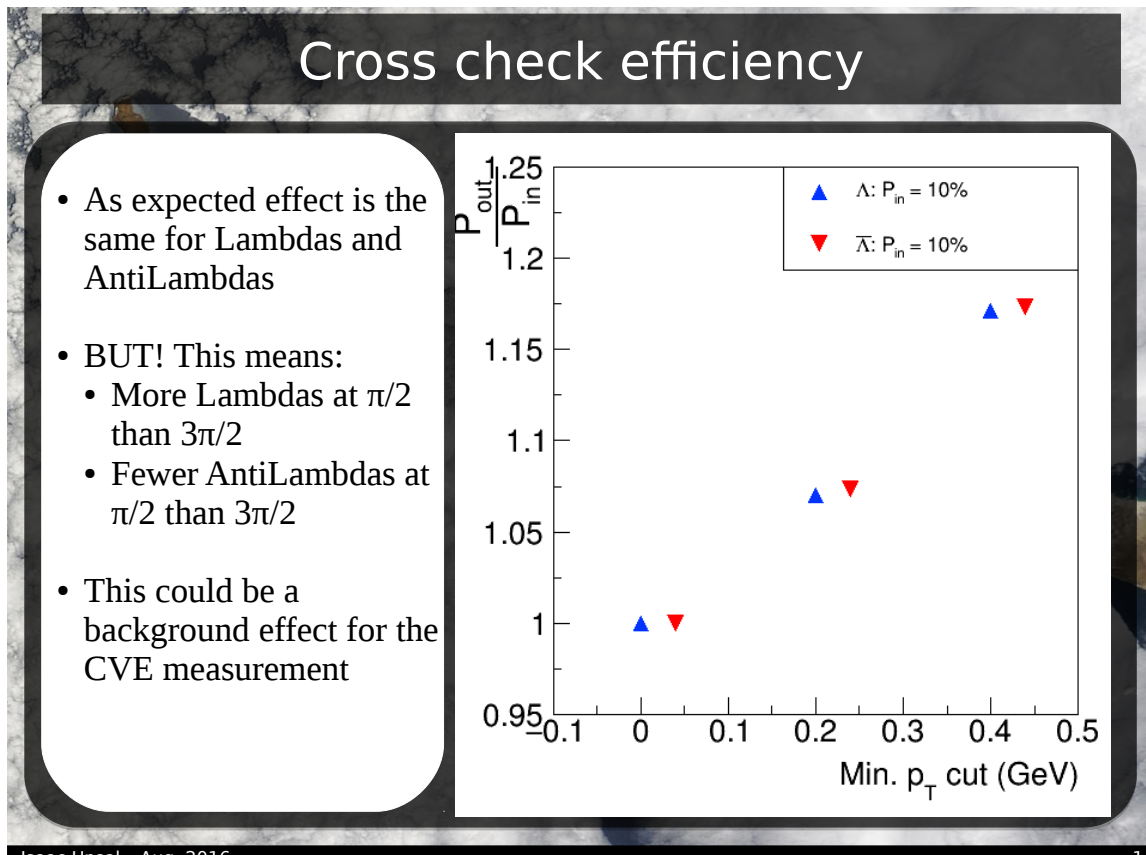


Fig. 91: Presentation on the effect of helicity efficiency on the polarization analysis p11.

3.5 Feed-down correction

This section is about feed-down correction which only applies to separating the vortical/magnetic components of the polarization. Perhaps the best resource is a paper we wrote along with Francesco Becattini and Iurii Karpenko specifically to address this:

<https://arxiv.org/abs/1610.02506>

I'm basically going to just copy down a document Mike wrote about this as part of communications for the paper writing process. Because of this there is a possibility that certain statements make sense more in that context than this one. I'm going to copy the subsections of the document as well. I also plan on posting a document called "FeeddownCorrection.pdf" which has the same information as this section.

3.5.1 Abstract for feeddown

A majority ($\sim 75\%$) of Λ ($\bar{\Lambda}$) hyperons in our data sample are not primary particles, but rather feeddown daughters of heavier particles, especially Σ^0, Σ^*, Ξ . To extract vorticity and magnetic field from the data, we must account for this feeddown. The formalism to do this in a thermal model has recently been published by Becattini, Karpenko, Lisa, Uppsala and Voloshin. In this note, I detail how we use the THERMUS model yields to this effect.

3.5.2 Correction procedure and definitions

If vortical and/or magnetic effects generate polarization in Λ and $\bar{\Lambda}$ emitted from heavy ion collisions, then presumably all other hadrons are polarized, as well. Since more than 75% of measured Λ and $\bar{\Lambda}$ are daughters of other particles, we need to account for the effects of “polarized feed-down.”

The formalism for doing this has recently been published [?], and for small polarization the thermal vorticity $\bar{\omega}$ and magnetic field are related to the measured polarizations according to

$$\begin{pmatrix} \bar{\omega}_c \\ B_c/T \end{pmatrix} = \begin{bmatrix} \frac{2}{3} \sum_R (f_{\Lambda R} C_{\Lambda R} - \frac{1}{3} f_{\Sigma^0 R} C_{\Sigma^0 R}) S_R (S_R + 1) & \frac{2}{3} \sum_R (f_{\Lambda R} C_{\Lambda R} - \frac{1}{3} f_{\Sigma^0 R} C_{\Sigma^0 R}) (S_R + 1) \mu_R \\ \frac{2}{3} \sum_{\bar{R}} (f_{\bar{\Lambda} \bar{R}} C_{\bar{\Lambda} \bar{R}} - \frac{1}{3} f_{\bar{\Sigma}^0 \bar{R}} C_{\bar{\Sigma}^0 \bar{R}}) S_{\bar{R}} (S_{\bar{R}} + 1) & \frac{2}{3} \sum_{\bar{R}} (f_{\bar{\Lambda} \bar{R}} C_{\bar{\Lambda} \bar{R}} - \frac{1}{3} f_{\bar{\Sigma}^0 \bar{R}} C_{\bar{\Sigma}^0 \bar{R}}) (S_{\bar{R}} + 1) \mu_{\bar{R}} \end{bmatrix}^{-1} \begin{pmatrix} P_{\Lambda}^{\text{meas}} \\ P_{\bar{\Lambda}}^{\text{meas}} \end{pmatrix}. \quad (12)$$

Here, $f_{\Lambda R}$ ($f_{\bar{\Lambda} \bar{R}}$) is the fraction of measured Λ s ($\bar{\Lambda}$ s) that arise from the direct decay of a baryon $R \rightarrow \Lambda + X$ ($\bar{R} \rightarrow \bar{\Lambda} + X$). Similarly, $f_{\Sigma^0 R}$ ($f_{\bar{\Sigma}^0 \bar{R}}$) is the fraction of measured Λ s ($\bar{\Lambda}$ s) that arise from the direct decay $R \rightarrow \Sigma^0 + X \rightarrow \Lambda + \gamma + X$ ($\bar{R} \rightarrow \bar{\Sigma}^0 + X \rightarrow \bar{\Lambda} + \gamma + X$). (Note carefully the last sentence: $f_{\Sigma^0 R}$ does not give the fraction of *Sigmas* coming from parent R , but the fraction of *Lambdas* coming from (grand)parent R .) The branching ratio for $\Sigma^0 \rightarrow \Lambda + \gamma$ is essentially 100%.

The constants C are the spin transfer coefficients, listed in table 2, and S_R and μ_R are the spin and magnetic moment of particle R . For the antibaryons, $S_{\bar{R}} = S_R$, $C_{\bar{X}Y} = C_{XY}$, and $\mu_{\bar{R}} = -\mu_R$.

The sums in equation 12 are understood to include the contributions of *primary* Λ s and Σ^0 s, too.

3.5.3 Which particles are included?

The number of individual contributors to the measured Λ yield is huge. However, the primary ones are listed in table 3. Primary Λ s make up about 25% of that yield. The daughters from Ξ, Σ^0, Σ^* make up another 60% and then there are $\sim 15\%$ more, which we will call “other.” These include things like $\Lambda(1405)$ and $\Lambda(1530)$. In fact, these two that I mention each contribute about 1% of the yield. Others contribute less. (Bill Llope’s files list the contributors in decreasing order of contribution, and these two are the last ones he lists before truncating.)

Decay	C
parity-conserving: $\frac{1}{2}^+ \rightarrow \frac{1}{2}^+ 0^-$	-1/3
parity-conserving: $\frac{1}{2}^- \rightarrow \frac{1}{2}^+ 0^-$	1
parity-conserving: $\frac{3}{2}^+ \rightarrow \frac{1}{2}^+ 0^-$	1/3
parity-conserving: $\frac{3}{2}^- \rightarrow \frac{1}{2}^+ 0^-$	-1/5
$\Xi^0 \rightarrow \Lambda + \pi^0$	+0.900
$\Xi^- \rightarrow \Lambda + \pi^-$	+0.927
$\Sigma^0 \rightarrow \Lambda + \gamma$	-1/3

Table 2: Polarization transfer factors C for important decays $X \rightarrow \Lambda(\Sigma)\pi$

This 15% we will consider as unpolarized. If there were no magnetic field, but only vortical-induced polarization, we [?] have checked that the alternating signs of the spin transfer coefficients C effectively make all their contributions cancel each other out; so, our assumption of (effective) zero polarization is justified. To definitively say what would happen if there *is* a magnetic field, we would have to know the magnetic moments of these contributors, and they are not measured. It is very reasonable to assume, however, that, as in the vortical case, they would effectively cancel each other out. In any event, these “other” parents are assumed to be a zero-polarization component to the measured Λ s. Hence, they suppress the signal by “diluting” it by $\sim 15\%$.

The relevant values of $f_{\Lambda R}$, $f_{\bar{\Lambda}R}$, $f_{\Sigma^0 R}$, and $f_{\bar{\Sigma}^0 R}$, using the THERMUS yields, are given in table 4. Appendix 3.5.7 discusses how to extract these constants f from the THERMUS files.

index i	particle	J^P	$\mu (\mu_N)$	BR $\rightarrow \Lambda + X$	BR $\rightarrow \Sigma^0 + X$
0	Λ'	$\frac{1}{2}^+$	-0.613 [?]	(100%)	-
1	Σ^0	$\frac{1}{2}^+$	+0.79 (quark model [?])	100%	-
2	Ξ^-	$\frac{1}{2}^+$	-0.651 [?]	100%	0
3	Ξ^0	$\frac{1}{2}^+$	-1.25 [?]	100%	0
4	Σ^{*-}	$\frac{3}{2}^+$	-2.41 [?]	87%	7%
5	Σ^{*0}	$\frac{3}{2}^+$	+0.30 [?]	87%	1%
6	Σ^{*+}	$\frac{3}{2}^+$	+3.02 [?]	87%	7%

Table 3: Particles that may feed down to our Λ sample. Λ' refers to primary Λ s. The index, i , is used in the computer code implementation of this calculation; it is included just for reference. Magnetic moments, μ , are given in units of the nuclear magneton, μ_N . Branching ratios to Λ and Σ^0 baryons are needed to calculate f factors in equation 12.

3.5.4 Feed-down matrices

The numbers in table 4 may be plugged into equation 12, to get the matrix elements listed in table 5. To be very clear, these are the matrix elements of the *inverted* matrix. In other words, to get the physical quantities of interest, use equation 13, below, with the values of a, b, c, d from table 5.

$$\begin{pmatrix} \bar{\omega}_c \\ B_c/T \end{pmatrix} = \begin{bmatrix} a & b \\ c & d \end{bmatrix} \begin{pmatrix} P_\Lambda^{\text{meas}} \\ P_{\bar{\Lambda}}^{\text{meas}} \end{pmatrix}. \quad (13)$$

3.5.5 Application to STAR data

The STAR measurements on hyperon polarization are listed in table 6. Applying equation 13 with the matrix elements listed in table 5 yields the physical parameters, listed in table 7.

f	7.7 GeV	11.5 GeV	14.5 GeV	19.6 GeV	27 GeV	39 GeV	62.4 GeV	200 GeV
$f_{\Lambda'}$	2.800e-01	2.492e-01	2.418e-01	2.350e-01	2.313e-01	2.273e-01	2.239e-01	2.183e-01
$f_{\Lambda\Sigma^0}$	1.806e-01	1.666e-01	1.627e-01	1.591e-01	1.569e-01	1.547e-01	1.524e-01	1.493e-01
$f_{\Lambda\Sigma^{*+}}$	1.044e-01	1.052e-01	1.045e-01	1.037e-01	1.027e-01	1.022e-01	1.007e-01	9.984e-02
$f_{\Lambda\Sigma^{*0}}$	1.039e-01	1.047e-01	1.040e-01	1.032e-01	1.023e-01	1.017e-01	1.002e-01	9.938e-02
$f_{\Lambda\Sigma^{*-}}$	1.018e-01	1.028e-01	1.020e-01	1.013e-01	1.004e-01	9.987e-02	9.840e-02	9.763e-02
$f_{\Lambda\Xi^0}$	4.056e-02	4.992e-02	5.438e-02	5.842e-02	6.208e-02	6.464e-02	6.970e-02	7.308e-02
$f_{\Lambda\Xi^-}$	3.906e-02	4.822e-02	5.256e-02	5.649e-02	6.004e-02	6.254e-02	6.743e-02	7.073e-02
$f_{\Sigma^0\Sigma^{*+}}$	8.402e-03	8.466e-03	8.405e-03	8.343e-03	8.267e-03	8.220e-03	8.099e-03	8.033e-03
$f_{\Sigma^0\Sigma^{*0}}$	1.194e-03	1.204e-03	1.195e-03	1.186e-03	1.175e-03	1.169e-03	1.152e-03	1.142e-03
$f_{\Sigma^0\Sigma^{*-}}$	8.188e-03	8.268e-03	8.211e-03	8.154e-03	8.080e-03	8.036e-03	7.917e-03	7.855e-03
$f_{\Lambda,\text{other}}$	1.319e-01	1.555e-01	1.602e-01	1.650e-01	1.667e-01	1.696e-01	1.701e-01	1.746e-01
$\bar{f}_{\Lambda'}$	2.327e-01	2.192e-01	2.162e-01	2.143e-01	2.153e-01	2.144e-01	2.175e-01	2.159e-01
$\bar{f}_{\Lambda\Sigma^0}$	1.502e-01	1.465e-01	1.455e-01	1.451e-01	1.461e-01	1.459e-01	1.480e-01	1.477e-01
$\bar{f}_{\Lambda\Sigma^{*+}}$	8.681e-02	9.254e-02	9.341e-02	9.454e-02	9.567e-02	9.638e-02	9.774e-02	9.871e-02
$\bar{f}_{\Lambda\Sigma^{*0}}$	8.636e-02	9.210e-02	9.297e-02	9.409e-02	9.522e-02	9.593e-02	9.729e-02	9.826e-02
$\bar{f}_{\Lambda\Sigma^{*-}}$	8.461e-02	9.037e-02	9.126e-02	9.239e-02	9.350e-02	9.421e-02	9.555e-02	9.652e-02
$\bar{f}_{\Lambda\Xi^0}$	1.071e-01	9.659e-02	9.200e-02	8.909e-02	8.565e-02	8.373e-02	7.931e-02	7.675e-02
$\bar{f}_{\Lambda\Xi^+}$	1.031e-01	9.329e-02	8.892e-02	8.614e-02	8.283e-02	8.100e-02	7.672e-02	7.428e-02
$\bar{f}_{\Sigma^0\Sigma^{*+}}$	6.985e-03	7.446e-03	7.516e-03	7.606e-03	7.697e-03	7.754e-03	7.864e-03	7.942e-03
$\bar{f}_{\Sigma^0\Sigma^{*0}}$	9.926e-04	1.059e-03	1.069e-03	1.082e-03	1.094e-03	1.103e-03	1.118e-03	1.129e-03
$\bar{f}_{\Sigma^0\Sigma^{*-}}$	6.807e-03	7.271e-03	7.343e-03	7.433e-03	7.523e-03	7.580e-03	7.688e-03	7.766e-03
$\bar{f}_{\Lambda,\text{other}}$	1.344e-01	1.536e-01	1.637e-01	1.683e-01	1.694e-01	1.719e-01	1.713e-01	1.751e-01

Table 4: f's from THERMUS.

f	7.7 GeV	11.5 GeV	14.5 GeV	19.6 GeV	27 GeV	39 GeV	62.4 GeV	200 GeV
a	1.4601	1.4260	1.4038	1.3856	1.3635	1.3512	1.3195	1.3029
b	1.0462	1.0930	1.1274	1.1513	1.1752	1.1913	1.2230	1.2456
c	-1.7853	-1.9134	-1.9357	-1.9539	-1.9616	-1.9722	-1.9709	-1.9877
d	1.7928	1.9162	1.9503	1.9676	1.9726	1.9817	1.9757	1.9898

Table 5: The matrix elements of the INVERTED matrix. Multiply this by the polarization “vector” as per equation 13.

In table 8 are listed the physical parameters *if feeddown is neglected*. This is obviously for comparison only. In this case, $f_{\Lambda'} = \bar{f}_{\Lambda'} = 1$ and all other f s are zero, so that for every energy, the matrix is

$$\begin{bmatrix} a & b \\ c & d \end{bmatrix}_{\text{no feeddown}} = \begin{bmatrix} 0.5 & -0.613 \\ 0.5 & 0.613 \end{bmatrix}^{-1} = \begin{bmatrix} 1 & 1 \\ -0.8157 & +0.8157 \end{bmatrix} \quad (14)$$

Comparing tables 7 and 8 shows that accounting for feed-down increases $\bar{\omega}$ by $\sim 20\%$, and increases B by a factor of 2.

⁶⁸⁵ **About units** As is common, we have been using units such that $\hbar = c = k_B = 1$. Furthermore, we've used $\mu_N = 1$. In this case, $\bar{\omega}_c = \omega_c/T$ and B/T are both dimensionless. That's why they are quantified in percentages in the second and third columns of tables 7 and 8.

In human units, vorticity is measured in s^{-1} (usually not written as Hz) and B in Tesla. In order to get to these units, we will need to assume a temperature. Here, we will assume $k_B T = 160 \text{ MeV}$.

The conversions are

$$\omega [\text{in s}^{-1}] = (k_B T) \cdot \left(\frac{\omega}{T} [\text{dimensionless}] \right) / \hbar \quad (15)$$

$$B [\text{in Tesla}] = (k_B T) \cdot \left(\frac{B}{T} [\text{dimensionless}] \right) / \mu_N \quad (16)$$

Explicitly, $\hbar = 6.58 \times 10^{-22} \text{ MeV} \cdot \text{s}$ and $\mu_N = 3.15 \times 10^{-14} \text{ MeV/Tesla}$.

(To make the connection to equation 12, the $\frac{2}{3}$ in front of everything is basically $1/(S_\Lambda + 1)$. The units of this cancel with the $(S_R + 1)$ factor found inside of every sum. That leaves S_R in the left columns; this is the spin of particle R . In our matrix, we have been using, e.g., $S_{\Sigma^*} = \frac{3}{2}$, when in reality it is $S_{\Sigma^*} = \frac{3}{2}\hbar$. Likewise, in our matrix, we have been using, e.g. $\mu_{\Sigma^{*+}} = +3.02$, when in reality it is $\mu_{\Sigma^{*+}} = +3.02\mu_N$.)

$\sqrt{s_{NN}}$ (GeV)	\bar{P}_Λ (%)	$\bar{P}_{\bar{\Lambda}}$ (%)
7.7	2.27 +/- 0.63	7.56 +/- 3.61
11.5	1.38 +/- 0.40	2.63 +/- 1.27
14.5	1.17 +/- 0.49	1.42 +/- 1.31
19.6	0.96 +/- 0.31	1.45 +/- 0.61
27.0	1.03 +/- 0.28	1.41 +/- 0.47
39.0	0.49 +/- 0.42	1.06 +/- 0.61
62.4	1.25 +/- 1.09	1.60 +/- 1.49
200.0	0.12 +/- 0.95	-0.73 +/- 1.08

Table 6: STAR measurements on polarization for 20-50% centrality Au+Au collisions.

$\sqrt{s_{NN}}$ (GeV)	$\bar{\omega}_c$ (%)	B/T (%)	ω (s^{-1})	B (Tesla)
7.7	11.23 +/- 3.89	9.49 +/- 6.58	2.7e+22 +/- 9.5e+21	4.8e+14 +/- 3.3e+14
11.5	4.85 +/- 1.50	2.40 +/- 2.55	1.2e+22 +/- 3.7e+21	1.2e+14 +/- 1.3e+14
14.5	3.24 +/- 1.63	0.51 +/- 2.73	7.9e+21 +/- 4.0e+21	2.6e+13 +/- 1.4e+14
19.6	2.99 +/- 0.82	0.98 +/- 1.34	7.3e+21 +/- 2.0e+21	5.0e+13 +/- 6.8e+13
27.0	3.06 +/- 0.68	0.76 +/- 1.09	7.5e+21 +/- 1.6e+21	3.8e+13 +/- 5.5e+13
39.0	1.93 +/- 0.93	1.13 +/- 1.48	4.7e+21 +/- 2.3e+21	5.8e+13 +/- 7.5e+13
62.4	3.60 +/- 2.32	0.70 +/- 3.64	8.8e+21 +/- 5.6e+21	3.6e+13 +/- 1.8e+14
200.0	-0.75 +/- 1.83	-1.68 +/- 2.86	-1.8e+21 +/- 4.4e+21	-8.5e+13 +/- 1.5e+14

Table 7: The vorticities and magnetic fields extracted from STAR polarization data, using equation 13 and the matrix elements from table 5.

$\sqrt{s_{NN}}$ (GeV)	$\bar{\omega}_c$ (%)	B/T (%)	ω (s^{-1})	B (Tesla)
7.7	9.83 +/- 3.67	4.31 +/- 2.99	2.4e+22 +/- 8.9e+21	2.2e+14 +/- 1.5e+14
11.5	4.02 +/- 1.33	1.02 +/- 1.09	9.8e+21 +/- 3.2e+21	5.2e+13 +/- 5.5e+13
14.5	2.58 +/- 1.40	0.21 +/- 1.14	6.3e+21 +/- 3.4e+21	1.0e+13 +/- 5.8e+13
19.6	2.40 +/- 0.68	0.40 +/- 0.56	5.8e+21 +/- 1.7e+21	2.0e+13 +/- 2.8e+13
27.0	2.44 +/- 0.55	0.31 +/- 0.45	5.9e+21 +/- 1.3e+21	1.6e+13 +/- 2.3e+13
39.0	1.55 +/- 0.75	0.46 +/- 0.61	3.8e+21 +/- 1.8e+21	2.4e+13 +/- 3.1e+13
62.4	2.85 +/- 1.84	0.29 +/- 1.50	6.9e+21 +/- 4.5e+21	1.5e+13 +/- 7.6e+13
200.0	-0.61 +/- 1.44	-0.69 +/- 1.17	-1.5e+21 +/- 3.5e+21	-3.5e+13 +/- 6.0e+13

Table 8: The vorticities and magnetic fields extracted from STAR polarization data, using equation 13 but a matrix that ignores feeddown, i.e. $f_{\Lambda'} = \bar{f}_{\bar{\Lambda}'} = 1$ and all other f_s are zero. The matrix used is given in equation 14. See text for details.

695 **3.5.6 Acknowledgements**

We thank Bill Llope for producing and interpreting UrQMD and THERMUS yields for all energies used here.

3.5.7 Extracting feed-down fractions from Bill Llope's THERMUS file

700 Bill Llope very kindly produced UrQMD and THERMUS output files for us, putting in way more work than we should have asked of him as a non-PA. Since the contribution of Σ^* is very important, and this information is not retained in the UrQMD files, I will focus on the THERMUS files.

Getting the f_i values from these files is non-trivial, so here I explain the procedure in excruciating detail. In subsubsections 3.5.7 and 3.5.7, I discuss extracting the fractions for the baryons and antibaryons explicitly. I will refer to the numbers for the 7.7 GeV calculation in this discussion.

705 In subsubsection 3.5.7, I provide the THERMUS file verbatim. And if you are still up for it, I include the actual root macro code used to extract the f values and the matrix elements in subsubsection 3.5.7.

Baryons

Primary Λ s The way Bill formatted these files was to give the primary yield of every particle *per primary Λ* . The rate (number per event) of primary Λ s for 7.7 GeV collisions is 0.00410527, as given by 710 the line

rate information: Primary Lambda = 0.00410527

From primary Σ^0 s The line 7.7 20 Sigma0 0.645168

tells us that there are 0.645168 Σ^0 per primary Λ ; i.e. $0.645168 \times 0.00410527 = 0.00264858883536 \Sigma^0$ s per event.

715 Since the branching ratio for $\Sigma^0 \rightarrow \Lambda + \gamma$ is 100%, that means there are 0.00264858883536 Λ s originating from primary Σ^0 per event, consistent with the line

rate information: Lambda<-Sigma0 = 0.00264859 running decay total (%) = 28.2045.)

Primary Σ^* contributions to Λ , both directly and through Σ^0 Bill puts his line numbers in kind of a weird order, but lower down, we see the same information for Σ^{*-} ,

720 7.7 103 Sigma*- 0.417829

which gives the number of Σ^{*-} per primary Λ , per event.

Now then, Σ^* will contribute to the Λ yield two ways: (1) directly and (2) through the Σ^0 . As discussed above, we deal with these separately.

The BR for $\Sigma^* \rightarrow \Lambda + \pi$ is 87%, meaning that the number of Λ coming *directly* from Σ^* decay is $0.87 \times 725 0.417829 \times 0.00410527 = 0.00149231174718$.

The BR for $\Sigma^* \rightarrow \Sigma + \pi$ is 11.7%. However, we only care about the $\Sigma^* \rightarrow \Sigma^0$ decay, since Σ^\pm does not decay to Λ . Unfortunately, the PDG does not specify the BR for $\Sigma^* \rightarrow \Sigma^0 + \pi$, so I had to do a little fiddling with numbers to figure out that the BRs that THERMUS uses are

$$BR[\Sigma^{*\pm} \rightarrow \Sigma^0 + \pi^\pm] = 7\% \quad \text{and} \quad BR[\Sigma^{*0} \rightarrow \Sigma^0 + \pi^0] = 1\%$$

That means the rate of Λ s coming from $\Sigma^{*-} \rightarrow \Sigma^0 \rightarrow \Lambda$ is $0.07 \times 0.417829 \times 0.00410527 = 0.00012007106012$.

Now then, when THERMUS reports the contribution of a parent (like Σ^{*-}) to a stable daughter (like Λ), it includes all multi-generational branches. (See the email from Jean Cleymans in subsubsection 3.5.8.) Therefore, to check consistency with the line

730 rate information: Lambda<-Sigma*- = 0.00161238 running decay total (%) = 79.4

we have to *add* these two routes: $0.00149231174718 + 0.00012007106012 = 0.0016123828073$, and find that it is, indeed, consistent.

Primary $\Xi \rightarrow \Lambda$ contributions Isaac's simulations say that the DCA cuts do almost nothing to discriminate Λ s coming from the weak decay $\Xi \rightarrow \Lambda + \pi$, so we need to use the line

735 7.7 22 Xi0 0.14489.

The branching ratio for $\Xi \rightarrow \Lambda + \pi$ is 100%, so the Ξ^0 rate is $0.14489 \times 0.00410527 = 0.0005948125703$.

Since THERMUS treats weakly-decaying particles as stable, there is no line that begins rate information: Lambda<-Xi0 =

"Other" contributions As discussed in subsubsection 3.5.3, anything beyond the Σ^* we consider as

740 "other." There is a large number of such parents, and they individually contribute a few percent or less to the Λ yield.

We now have to discuss the so-called "**running decay total**" that one sees in Bill's files. As he lists decay contributions, he is keeping a running tally of the percentage of *strong and electromagnetic decay* contributions that have been listed up until that point. In other words, the lines

745 rate information: Lambda<-Sigma0 = 0.00290201 running decay total (%) = 25.5247
 rate information: Lambda<-Sigma*+ = 0.00198037 running decay total (%) = 42.9432
 rate information: Lambda<-Sigma*0 = 0.00184499 running decay total (%) = 59.1709
 rate information: Lambda<-Sigma*- = 0.00193394 running decay total (%) = 76.181
 rate information: Lambda<-Lambda(1405) = 0.00025601 running decay total (%) = 82.1262
 750 rate information: Lambda<-Lambda(1520) = 0.000198498 running decay total (%) = 84.24
 tell us that the Σ^0 contributes 25.5247% of the Λ s that originate from strong and EM decay. And that the $Sigma^{*+}$ and Σ^0 together account for 42.9432% of the Λ s that originate from strong and EM decay. Et cetera.

So, the percentage of the Λ s that originate from strong and EM decay "beyond" Σ^{*-} is $100\% - 76.181\% = 23.819\%$. The rate of "other," then, is

$$\text{other rate} = \frac{100\% - 76.181\%}{76.181\%} \times (0.00290201 + 0.00198037 + 0.00184499 + 0.00193394) = 0.002708$$

The most significant contributor is $\Lambda(1405)$, which contributes $84.24\% - 82.162\% = 2.078\%$ of the Λ s,

755 as one finds by examining these lines:

rate information: Lambda<-Lambda(1405) = 0.00025601 running decay total (%) = 82.1262
 rate information: Lambda<-Lambda(1520) = 0.000198498 running decay total (%) = 84.24

Getting fs Okay, from subsubsections 3.5.7-3.5.7, we see how to get the *rates*. The value of a given

760 fraction (f) listed in table 4 is simply the rate divided by the sum of all the rates.

$\bar{\Lambda}$ hyperons For $\bar{\Lambda}$, the situation is slightly more complex, since for the lines that do not begin with "rate information", the yield is *always* given as a fraction of the number of primary Λ , not $\bar{\Lambda}$. So,

$$\text{rate for: } \bar{\Lambda} \leftarrow \Xi^0 = \underbrace{0.00863487}_{\#\bar{\Xi}^0/\#\Lambda} \times \underbrace{0.0187703^{-1}}_{(\#\bar{\Lambda}/\#\Lambda)^{-1}} \times \underbrace{7.70574e-05}_{\text{primary } \bar{\Lambda} \text{ rate}} = 0.00003544858801$$

$$\text{rate for: } \bar{\Lambda} \leftarrow \Xi^+ = \underbrace{0.00831551}_{\#\bar{\Xi}^+/\#\Lambda} \times \underbrace{0.0187703^{-1}}_{(\#\bar{\Lambda}/\#\Lambda)^{-1}} \times \underbrace{7.70574e-05}_{\text{primary } \bar{\Lambda} \text{ rate}} = 0.00003413752471$$

But as far as everything else, it is the same as for the Λ s.

765
+-----
root-s = 7.7
770 +-----
rate information: Primary Lambda = 0.00410527
rate information: Lambda<-Sigma0 = 0.00264859 running decay total (%) =
775 28.2045
rate information: Lambda<-Sigma*+ = 0.00165448 running decay total (%) =
45.8229
780 rate information: Lambda<-Sigma*0 = 0.00154073 running decay total (%) =
62.2299
rate information: Lambda<-Sigma*- = 0.00161238 running decay total (%) = 79.4
785 rate information: Lambda<-Lambda(1405) = 0.00025601 running decay total (%) =
82.1262
rate information: Lambda<-Lambda(1520) = 0.000198498 running decay total (%) =
84.24
790 7.7 19 Sigma+ 0.657359
7.7 20 Sigma0 0.645168
795 7.7 21 Sigma- 0.627637
7.7 22 Xi0 0.14489
7.7 23 Xi- 0.139531
800 7.7 24 Omega- 0.0158781
7.7 26 Antilambda 0.0187703
805 rate information: Primary Antilambda = 7.70574e-05
rate information: Antilambda<-Antisigma0 = 4.9715e-05 running decay total (%) =
26.9547
810 rate information: Antilambda<-AntiSigma*- = 3.10552e-05 running decay total (%) =
43.7924
rate information: Antilambda<-AntiSigma*0 = 2.89201e-05 running decay total (%) =
59.4724
815 rate information: Antilambda<-AntiSigma*+ = 3.0265e-05 running decay total (%) =
75.8816

```
rate information: Antilambda<-AntiLambda(1405) = 4.8054e-06 running decay total  
820 (%) = 78.487  
  
rate information: Antilambda<-AntiLambda(1520) = 3.72587e-06 running decay total  
(% ) = 80.5071  
  
825 7.7 27 Antisigma- 0.0123389  
7.7 28 Antisigma0 0.01211  
7.7 29 Antisigma+ 0.011781  
830 7.7 30 Antixi0 0.00863487  
7.7 31 Antixi+ 0.00831551  
835 7.7 32 Antiomega+ 0.00300444  
7.7 101 Sigma*+ 0.428739  
7.7 102 Sigma*0 0.426484  
840 7.7 103 Sigma*- 0.417829  
7.7 -101 AntiSigma*- 0.00804757  
845 7.7 -102 AntiSigma*0 0.00800526  
7.7 -103 AntiSigma*+ 0.00784279  
7.7 111 Lambda(1405) 0.187103  
850 7.7 112 Lambda(1520) 0.191493  
7.7 -111 AntiLambda(1405) 0.00351199  
855 7.7 -112 AntiLambda(1520) 0.00359439  
+-----  
root-s = 11.5  
860 +-----  
  
rate information: Primary Lambda = 0.00434062  
  
865 rate information: Lambda<-Sigma0 = 0.00290201 running decay total (%) =  
25.5247  
  
rate information: Lambda<-Sigma*+ = 0.00198037 running decay total (%) =  
42.9432  
870 rate information: Lambda<-Sigma*0 = 0.00184499 running decay total (%) =  
59.1709
```

```
rate information: Lambda<-Sigma*- = 0.00193394    running decay total (%) =
875      76.181

rate information: Lambda<-Lambda(1405) = 0.000309771   running decay total (%) =
880      78.9056

rate information: Lambda<-Lambda(1520) = 0.000253256   running decay total (%) =
885      81.1331

11.5 19 Sigma+      0.68017

885 11.5 20 Sigma0     0.668569

11.5 21 Sigma-      0.651854

11.5 22 Xi0       0.200347

890 11.5 23 Xi-       0.19352

11.5 24 Omega-      0.0327139

895 11.5 26 Antilambda  0.0684347

rate information: Primary Antilambda = 0.000297049

rate information: Antilambda<-Antisigma0 = 0.000198598   running decay total (%)

900      = 24.5241

rate information: Antilambda<-AntiSigma*- = 0.000135526   running decay total (%)

905      = 41.2598

rate information: Antilambda<-AntiSigma*0 = 0.000126262   running decay total (%)

910      = 56.8513

rate information: Antilambda<-AntiSigma*+ = 0.000132349   running decay total (%)

915      = 73.1946

rate information: Antilambda<-AntiLambda(1405) = 2.11991e-05   running decay total (%)

920      = 75.8124

rate information: Antilambda<-AntiLambda(1520) = 1.73315e-05   running decay total (%)

925      = 77.9526

11.5 27 Antisigma-    0.0465472

11.5 28 Antisigma0     0.0457533

920 11.5 29 Antisigma+    0.0446094

11.5 30 Antixi0      0.03016

925 11.5 31 Antixi+     0.0291322

11.5 32 Antiomega+    0.0108331

11.5 101 Sigma*+      0.485364
```

930 11.5 102 Sigma*0 0.483015
 11.5 103 Sigma*- 0.473984

935 11.5 -101 AntiSigma*- 0.0332157
 11.5 -102 AntiSigma*0 0.033055
 11.5 -103 AntiSigma*+ 0.032437

940 11.5 111 Lambda(1405) 0.214118
 11.5 112 Lambda(1520) 0.231072

945 11.5 -111 AntiLambda(1405) 0.0146531
 11.5 -112 AntiLambda(1520) 0.0158133

+-----
950 root-s = 14.5

+-----

955 rate information: Primary Lambda = 0.00377269

 rate information: Lambda<-Sigma0 = 0.00253881 running decay total (%) =
 24.9878

960 rate information: Lambda<-Sigma*+ = 0.00176082 running decay total (%) =
 42.3184

 rate information: Lambda<-Sigma*0 = 0.00164057 running decay total (%) =
 58.4654

965 rate information: Lambda<-Sigma*- = 0.00172018 running decay total (%) =
 75.396

 rate information: Lambda<-Lambda(1405) = 0.000275975 running decay total (%) =
970 78.1122

 rate information: Lambda<-Lambda(1520) = 0.000227828 running decay total (%) =
 80.3546

975 14.5 19 Sigma+ 0.684432
 14.5 20 Sigma0 0.672946
 14.5 21 Sigma- 0.656389

980 14.5 22 Xi0 0.224899
 14.5 23 Xi- 0.217355

985 14.5 24 Omega- 0.0417916

14.5 26 Antilambda 0.120935
rate information: Primary Antilambda = 0.000456251
990 rate information: Antilambda<-Antisigma0 = 0.000307032 running decay total (%)
= 24.1397
rate information: Antilambda<-AntiSigma*- = 0.000212945 running decay total (%)
995 = 40.8821
rate information: Antilambda<-AntiSigma*0 = 0.000198403 running decay total (%)
= 56.4811
1000 rate information: Antilambda<-AntiSigma*+ = 0.000208031 running decay total (%)
= 72.8371
rate information: Antilambda<-AntiLambda(1405) = 3.33751e-05 running decay total (%)
1005 = 75.4612
rate information: Antilambda<-AntiLambda(1520) = 2.75524e-05 running decay total (%)
= 77.6274
14.5 27 Antisigma- 0.082772
1010 14.5 28 Antisigma0 0.0813828
14.5 29 Antisigma+ 0.0793805
1015 14.5 30 Antixi0 0.0514521
14.5 31 Antixi+ 0.0497262
14.5 32 Antiomega+ 0.018087
1020 14.5 101 Sigma*+ 0.496519
14.5 102 Sigma*0 0.494154
1025 14.5 103 Sigma*- 0.48506
14.5 -101 AntiSigma*- 0.0600467
14.5 -102 AntiSigma*0 0.0597606
1030 14.5 -103 AntiSigma*+ 0.0586609
14.5 111 Lambda(1405) 0.219474
1035 14.5 112 Lambda(1520) 0.239163
14.5 -111 AntiLambda(1405) 0.0265422
14.5 -112 AntiLambda(1520) 0.0289233
1040 +-----

```
root-s = 19.6

1045 +-----+
    rate information: Primary Lambda = 0.00332199
    rate information: Lambda<-Sigma0 = 0.0022491   running decay total (%) = 24.4789
1050
    rate information: Lambda<-Sigma*+ = 0.00158353   running decay total (%) =
        41.7138
    rate information: Lambda<-Sigma*0 = 0.0014755   running decay total (%) =
1055      57.7729
    rate information: Lambda<-Sigma*- = 0.00154753   running decay total (%) =
        74.616
    rate information: Lambda<-Lambda(1405) = 0.000248646   running decay total (%) =
        77.3222
    rate information: Lambda<-Lambda(1520) = 0.000207127   running decay total (%) =
        79.5766
1065
    19.6 19 Sigma+      0.688414
    19.6 20 Sigma0      0.677035
1070 19.6 21 Sigma-      0.660628
    19.6 22 Xi0         0.248538
    19.6 23 Xi-         0.240325
1075
    19.6 24 Omega-      0.0516924
    19.6 26 Antilambda   0.204605
1080
    rate information: Primary Antilambda = 0.000679694
    rate information: Antilambda<-Antisigma0 = 0.000460177   running decay total (%) =
        23.763
1085
    rate information: Antilambda<-AntiSigma*- = 0.000323998   running decay total (%) =
        40.4939
    rate information: Antilambda<-AntiSigma*0 = 0.000301894   running decay total (%) =
        56.0834
1090
    rate information: Antilambda<-AntiSigma*+ = 0.000316631   running decay total (%) =
        72.4339
    rate information: Antilambda<-AntiLambda(1405) = 5.08741e-05   running decay total (%)
        = 75.061
    rate information: Antilambda<-AntiLambda(1520) = 4.23792e-05   running decay total
```

(%) = 77.2494

1100 19.6 27 Antisigma- 0.140853

19.6 28 Antisigma0 0.138525

19.6 29 Antisigma+ 0.135168

1105 19.6 30 Antixi0 0.0850653

19.6 31 Antixi+ 0.0822541

1110 19.6 32 Antiomega+ 0.0295958

19.6 101 Sigma*+ 0.507108

19.6 102 Sigma*0 0.504729

1115 19.6 103 Sigma*- 0.495578

19.6 -101 AntiSigma*- 0.103757

1120 19.6 -102 AntiSigma*0 0.10327

19.6 -103 AntiSigma*+ 0.101398

19.6 111 Lambda(1405) 0.224568

1125 19.6 112 Lambda(1520) 0.246932

19.6 -111 AntiLambda(1405) 0.0459477

1130 19.6 -112 AntiLambda(1520) 0.0505235

+-----

root-s = 27

1135 +-----

rate information: Primary Lambda = 0.00295424

1140 rate information: Lambda<-Sigma0 = 0.00200409 running decay total (%) =
24.2655

rate information: Lambda<-Sigma*+ = 0.001418 running decay total (%) = 41.4346

1145 rate information: Lambda<-Sigma*0 = 0.00132129 running decay total (%) =
57.4327

rate information: Lambda<-Sigma*- = 0.00138591 running decay total (%) =
74.2133

1150 rate information: Lambda<-Lambda(1405) = 0.000222788 running decay total (%) =
76.9109

rate information: Lambda<-Lambda(1520) = 0.000186136 running decay total (%) =
1155 79.1646

27 19 Sigma+ 0.689723

27 20 Sigma0 0.67838

1160 27 21 Sigma- 0.662023

27 22 Xi0 0.268434

1165 27 23 Xi- 0.259606

27 24 Omega- 0.0605516

27 26 Antilambda 0.284925

1170 rate information: Primary Antilambda = 0.000841737

rate information: Antilambda<-Antisigma0 = 0.000571017 running decay total (%)
= 23.7083

1175 rate information: Antilambda<-AntiSigma*- = 0.000404023 running decay total (%)
= 40.4832

1180 rate information: Antilambda<-AntiSigma*0 = 0.000376468 running decay total (%)
= 56.114

rate information: Antilambda<-AntiSigma*+ = 0.000394882 running decay total (%)
= 72.5092

1185 rate information: Antilambda<-AntiLambda(1405) = 6.34779e-05 running decay total
(%) = 75.1448

rate information: Antilambda<-AntiLambda(1520) = 5.30349e-05 running decay total
(%) = 77.3468

1190 27 27 Antisigma- 0.19652

27 28 Antisigma0 0.193288

1195 27 29 Antisigma+ 0.188627

27 30 Antixi0 0.113318

27 31 Antixi+ 0.109591

1200 27 32 Antiomega+ 0.0378719

27 101 Sigma*+ 0.510625

1205 27 102 Sigma*0 0.508241

27 103 Sigma*- 0.499072

27 -101 AntiSigma*- 0.14549

1210
27 -102 AntiSigma*0 0.144811
27 -103 AntiSigma*+ 0.142198

1215 27 111 Lambda(1405) 0.226262
27 112 Lambda(1520) 0.249531
27 -111 AntiLambda(1405) 0.0644677

1220
27 -112 AntiLambda(1520) 0.0710976

1225 root-s = 39

rate information: Primary Lambda = 0.00258929

1230 rate information: Lambda<-Sigma0 = 0.00176244 running decay total (%) =
23.9675

rate information: Lambda<-Sigma*+ = 0.00125746 running decay total (%) =
1235 41.0678

rate information: Lambda<-Sigma*0 = 0.00117175 running decay total (%) =
57.0025

1240 rate information: Lambda<-Sigma*- = 0.00122925 running decay total (%) =
73.7191

rate information: Lambda<-Lambda(1405) = 0.000197768 running decay total (%) =
1245 76.4085

rate information: Lambda<-Lambda(1520) = 0.000166061 running decay total (%) =
78.6668

39 19 Sigma+ 0.691946

1250 39 20 Sigma0 0.680664

39 21 Sigma- 0.664391

1255 39 22 Xi0 0.284404

39 23 Xi- 0.27513

39 24 Omega- 0.0684525

1260 39 26 Antilambda 0.430029

rate information: Primary Antilambda = 0.00111347

1265 rate information: Antilambda<-Antisigma0 = 0.0007579 running decay total (%) =

23.508

rate information: Antilambda<-AntiSigma*- = 0.000540746 running decay total (%)
= 40.2805

1270 rate information: Antilambda<-AntiSigma*0 = 0.000503886 running decay total (%)
= 55.9096

1275 rate information: Antilambda<-AntiSigma*+ = 0.000528614 running decay total (%)
= 72.3058

1280 rate information: Antilambda<-AntiLambda(1405) = 8.50459e-05 running decay total (%)
= 74.9437

39 27 Antisigma- 0.297557

1285 39 28 Antisigma0 0.292705

39 29 Antisigma+ 0.285708

39 30 Antixi0 0.167933

1290 39 31 Antixi+ 0.162457

39 32 Antiomega+ 0.0555001

1295 39 101 Sigma*+ 0.516638

39 102 Sigma*0 0.514246

39 103 Sigma*- 0.505046

1300 39 -101 AntiSigma*- 0.222169

39 -102 AntiSigma*0 0.221141

1305 39 -103 AntiSigma*+ 0.217185

39 111 Lambda(1405) 0.22916

39 112 Lambda(1520) 0.253995

1310 39 -111 AntiLambda(1405) 0.0985454

39 -112 AntiLambda(1520) 0.109225

1315 +-----

root-s = 62.4

+-----

1320 rate information: Primary Lambda = 0.00223124

```
rate information: Lambda<-Sigma0 = 0.00151873      running decay total (%) =
23.8575
1325
rate information: Lambda<-Sigma*+ = 0.00108358      running decay total (%) =
40.8793
1330
rate information: Lambda<-Sigma*0 = 0.00100972      running decay total (%) =
56.7408
rate information: Lambda<-Sigma*- = 0.00105927      running decay total (%) =
73.3807
1335
rate information: Lambda<-Lambda(1405) = 0.00017042  running decay total (%) =
76.0579
rate information: Lambda<-Lambda(1520) = 0.000143098  running decay total (%) =
78.3058
1340
62.4 19 Sigma+      0.691946
62.4 20 Sigma0      0.680664
1345 62.4 21 Sigma-      0.664391
62.4 22 Xi0      0.311249
62.4 23 Xi-      0.301099
1350
62.4 24 Omega-      0.0819849
62.4 26 Antilambda     0.591916
1355
rate information: Primary Antilambda = 0.00132071
rate information: Antilambda<-Antisigma0 = 0.000898958  running decay total (%)
= 23.6245
1360
rate information: Antilambda<-AntiSigma*- = 0.000641388  running decay total (%)
= 40.4801
rate information: Antilambda<-AntiSigma*0 = 0.000597668  running decay total (%)
= 56.1868
1365
rate information: Antilambda<-AntiSigma*+ = 0.000626998  running decay total (%)
= 72.6642
rate information: Antilambda<-AntiLambda(1405) = 0.000100874  running decay total
(%) = 75.3152
1370
rate information: Antilambda<-AntiLambda(1520) = 8.4702e-05  running decay total
(%) = 77.5412
1375 62.4 27 Antisigma-      0.409574
62.4 28 Antisigma0      0.402896
```

```
62.4 29 Antisigma+    0.393264
1380
62.4 30 Antixi0      0.215884

62.4 31 Antixi+      0.208844

1385 62.4 32 Antiomega+ 0.0666342

62.4 101 Sigma*+     0.516638

62.4 102 Sigma*0      0.514246
1390
62.4 103 Sigma*-     0.505046

62.4 -101 AntiSigma*- 0.305806

1395 62.4 -102 AntiSigma*0  0.30439

62.4 -103 AntiSigma*+  0.298945

62.4 111 Lambda(1405)  0.22916
1400
62.4 112 Lambda(1520)  0.253995

62.4 -111 AntiLambda(1405) 0.135643

1405 62.4 -112 AntiLambda(1520) 0.150344

+-----+
root-s = 200
1410
+-----+

rate information: Primary Lambda = 0.00209703

1415      rate information: Lambda<-Sigma0 = 0.00143445      running decay total (%) =
            23.413

rate information: Lambda<-Sigma*+ = 0.00103611      running decay total (%) =
            40.3242
1420
rate information: Lambda<-Sigma*0 = 0.000965538      running decay total (%) =
            56.0836

rate information: Lambda<-Sigma*- = 0.00101315      running decay total (%) =
            72.6201
1425

rate information: Lambda<-Lambda(1405) = 0.000163199  running decay total (%) =
            75.2838

1430      rate information: Lambda<-Lambda(1520) = 0.000138048  running decay total (%) =
            77.537

200 19 Sigma+        0.695232
```

1435 200 20 Sigma0 0.68404
200 21 Sigma- 0.667893
200 22 Xi0 0.334738
1440 200 23 Xi- 0.323959
200 24 Omega- 0.0958179
1445 200 26 Antilambda 0.824479

rate information: Primary Antilambda = 0.00172896

rate information: Antilambda<-Antisigma0 = 0.00118268 running decay total (%)
1450 = 23.3221

rate information: Antilambda<-AntiSigma*- = 0.000854248 running decay total (%)
= 40.1676

1455 rate information: Antilambda<-AntiSigma*0 = 0.000796066 running decay total (%)
= 55.8658

rate information: Antilambda<-AntiSigma*+ = 0.00083532 running decay total (%)
= 72.3381
1460
rate information: Antilambda<-AntiLambda(1405) = 0.000134554 running decay total (%) = 74.9915

rate information: Antilambda<-AntiLambda(1520) = 0.000113818 running decay total (%) = 77.236
1465

200 27 Antisigma- 0.573204
200 28 Antisigma0 0.563977
1470 200 29 Antisigma+ 0.550664
200 30 Antixi0 0.293143
1475 200 31 Antixi+ 0.283702
200 32 Antiomega+ 0.089128
200 101 Sigma*+ 0.525619
1480 200 102 Sigma*0 0.523216
200 103 Sigma*- 0.513973
1485 200 -101 AntiSigma*- 0.433362
200 -102 AntiSigma*0 0.431381
200 -103 AntiSigma*+ 0.42376

```

1490
200 111 Lambda(1405) 0.233495
200 112 Lambda(1520) 0.260714
1495 200 -111 AntiLambda(1405) 0.192511
200 -112 AntiLambda(1520) 0.214953

```

Mike's code to calculate f_s from Bill's THERMUS files Look, I know that what I have described is
 1500 a painful process, believe me. You might doubt that I did it right, and I wouldn't blame you for wanting to check. (If it makes you feel better, Jurii Karpenko did it also, though with a different thermal model (Becattini's) and no magnetic field and got very similar results.)

Here is the relevant snippet of code where I calculate the f_s and then the matrix elements. My philosophy here was to be super-explicit in the variable names, to make it as readable as possible. I fear that I overdid it. The variable names are too long. If I wasn't worrying about you, dear reader, then I would have made an array and done loops. As it is, I am doing explicit sums of variables with long names. I am aware that this is often a recipe for disaster, but I was super careful and double-checked my work along the way with an excel spreadsheet.

```

void MikeCodeSnippet() {
1510
    // this is simply the numbers from Bill Llope's files, distilled into a form amenable to
    // numeric manipulation
    // I extracted these numbers partially "by hand," being as careful as I could...
    Double_t roots[8]
1515    = {7.7      , 11.5     , 14.5     , 19.6     , 27       , 39       , 62.4     , 200
    };

    Double_t PrimaryLambdaRate[8]
    = {0.00410527, 0.00434062, 0.00377269, 0.00332199, 0.00295424, 0.00258929,
1520      0.00223124, 0.00209703};
    Double_t SigmaZeroToLambda[8]
    = {0.645168, 0.668569, 0.672946, 0.677035, 0.67838, 0.680664, 0.680664,
      0.68404 };
    Double_t SigmaStarPlusToLambda[8]
    = {0.428739, 0.485364, 0.496519, 0.507108, 0.510625, 0.516638, 0.516638,
      0.525619 };
    Double_t SigmaStarZeroToLambda[8]
    = {0.426484, 0.483015, 0.494154, 0.504729, 0.508241, 0.514246, 0.514246,
      0.523216 };
1530    Double_t SigmaStarMinusToLambda[8]
    = {0.417829, 0.473984, 0.48506, 0.495578, 0.499072, 0.505046, 0.505046,
      0.513973 };
    Double_t XiZeroToLambda[8]
    = {0.14489, 0.200347, 0.224899, 0.248538, 0.268434, 0.284404, 0.311249,
1535      0.334738 };
    Double_t XiMinusToLambda[8]
    = {0.139531, 0.19352, 0.217355, 0.240325, 0.259606, 0.27513, 0.301099,
      0.323959 };
    Double_t RunningDecayTotalAtSigmaStarMinus[8]
1540    = {79.4      , 76.181     , 75.396     , 74.616     , 74.2133    , 73.7191    , 73.3807    ,
      72.6201   };

```

```

Double_t AntiPrimaryLambdaToLambda[8]
= { 0.0187703 , 0.0684347 , 0.120935 , 0.204605 , 0.284925 , 0.430029 , 0.591916 ,
1545   0.824479 };
Double_t AntiSigmaZeroToLambda[8]
= { 0.01211 , 0.0457533 , 0.0813828 , 0.138525 , 0.193288 , 0.292705 , 0.402896 ,
0.563977 };
Double_t AntiSigmaStarMinusToLambda[8]
1550 = { 0.00804757 , 0.0332157 , 0.0600467 , 0.103757 , 0.14549 , 0.222169 , 0.305806 ,
0.433362 };
Double_t AntiSigmaStarZeroToLambda[8]
= { 0.00800526 , 0.033055 , 0.0597606 , 0.10327 , 0.144811 , 0.221141 , 0.30439 ,
0.431381 };
1555 Double_t AntiSigmaStarPlusToLambda[8]
= { 0.00784279 , 0.032437 , 0.0586609 , 0.101398 , 0.142198 , 0.217185 , 0.298945 ,
0.42376 };
Double_t AntiXiPlusToLambda[8]
= { 0.00831551 , 0.0291322 , 0.0497262 , 0.0822541 , 0.109591 , 0.162457 , 0.208844 ,
0.283702 };
1560 Double_t AntiXiZeroToLambda[8]
= { 0.00863487 , 0.03016 , 0.0514521 , 0.0850653 , 0.113318 , 0.167933 , 0.215884 ,
0.293143 };
Double_t RunningDecayTotalAtAntiSigmaStarPlus[8]
1565 = { 75.8816 , 74.0 , 72.8371 , 72.4339 , 72.5092 , 72.3058 , 72.6642 ,
72.3381 };

// okay now make the f's. This is more painful than one might guess.
1570 Double_t f_Lprimary[8],f_LSig0[8],f_LSigStarPlus[8],f_LSigStarZero[8],
f_LSigStarMinus[8],f_LXiZero[8],f_LXiMinus[8];
Double_t f_SSigStarMinus[8],f_SSigStarZero[8],f_SSigStarPlus[8],f_Lother[8];

1575 Double_t fBar_AntiLprimary[8],fBar_AntiLAntiSig0[8],fBar_AntiLAntiSigStarPlus[8],
fBar_AntiLAntiSigStarZero[8];
Double_t fBar_AntiLAntiSigStarMinus[8],fBar_AntiLAntiXiZero[8],fBar_AntiLAntiXiPlus[8];
Double_t fBar_AntiSASignStarMinus[8],fBar_AntiSASignStarZero[8],
fBar_AntiSASignStarPlus[8],fBar_AntiLother[8];
1580
for (Int_t iroots=0; iroots<8; iroots++) {
    Double_t sum=0.0;
    Double_t sum2=0.0;
    sum += f_Lprimary[iroots] = PrimaryLambdaRate[iroots];
1585    sum2 += f_LSig0[iroots] = SigmaZeroToLambda[iroots]*PrimaryLambdaRate[iroots];
    sum2 += f_LSigStarPlus[iroots] = SigmaStarPlusToLambda[iroots]*PrimaryLambdaRate[iroots
        ]*0.87;
    sum2 += f_LSigStarZero[iroots] = SigmaStarZeroToLambda[iroots]*PrimaryLambdaRate[iroots
        ]*0.87;
1590    sum2 += f_LSigStarMinus[iroots] = SigmaStarMinusToLambda[iroots]*PrimaryLambdaRate[iroots
        ]*0.87;
    sum2 += f_SSigStarPlus[iroots] = SigmaStarPlusToLambda[iroots]*PrimaryLambdaRate[iroots
        ]*0.07; // note 2-step decay thru Sigma0
    sum2 += f_SSigStarZero[iroots] = SigmaStarZeroToLambda[iroots]*PrimaryLambdaRate[iroots
        ]*0.01; // note 2-step decay thru Sigma0
1595    sum2 += f_SSigStarMinus[iroots] = SigmaStarMinusToLambda[iroots]*PrimaryLambdaRate[iroots
        ]*0.07; // note 2-step decay thru Sigma0
}

```

```

sum += sum2;
sum += f_LXiZero[iroots] = XiZeroToLambda[iroots]*PrimaryLambdaRate[iroots];
1600 sum += f_LXiMinus[iroots] = XiMinusToLambda[iroots]*PrimaryLambdaRate[iroots];
sum += f_Lother[iroots]
= sum2*(100.0-RunningDecayTotalAtSigmaStarMinus[iroots])/RunningDecayTotalAtSigmaStarMinus[iroots];

1605 f_Lprimary[iroots] /= sum;
f_LSig0[iroots] /= sum;
f_LSigStarPlus[iroots] /= sum;
f_LSigStarZero[iroots] /= sum;
f_LSigStarMinus[iroots] /= sum;
1610 f_SSigStarPlus[iroots] /= sum;
f_SSigStarZero[iroots] /= sum;
f_SSigStarMinus[iroots] /= sum;
f_LXiZero[iroots] /= sum;
f_LXiMinus[iroots] /= sum;
f_Lother[iroots] /= sum;

1615 }

1620
for (Int_t iroots=0; iroots<8; iroots++){
    Double_t sum=0.0;
    Double_t sum2=0.0;
    sum += fBar_AntiLprimary[iroots]
1625     = AntiPrimaryLambdaToLambda[iroots]*PrimaryLambdaRate[iroots];
    sum2 += fBar_AntiLAntiSig0[iroots]
        = AntiSigmaZeroToLambda[iroots]*PrimaryLambdaRate[iroots];
    sum2 += fBar_AntiLAntiSigStarPlus[iroots]
        = AntiSigmaStarPlusToLambda[iroots]*PrimaryLambdaRate[iroots]*0.87;
1630    sum2 += fBar_AntiLAntiSigStarZero[iroots]
        = AntiSigmaStarZeroToLambda[iroots]*PrimaryLambdaRate[iroots]*0.87;
    sum2 += fBar_AntiLAntiSigStarMinus[iroots]
        = AntiSigmaStarMinusToLambda[iroots]*PrimaryLambdaRate[iroots]*0.87;
    sum2 += fBar_AntiSASigStarPlus[iroots]
        = AntiSigmaStarPlusToLambda[iroots]*PrimaryLambdaRate[iroots]*0.07; // note 2-step
1635    decay thru Sigma0
    sum2 += fBar_AntiSASigStarZero[iroots]
        = AntiSigmaStarZeroToLambda[iroots]*PrimaryLambdaRate[iroots]*0.01; // note 2-step
            decay thru Sigma0
1640    sum2 += fBar_AntiSASigStarMinus[iroots]
        = AntiSigmaStarMinusToLambda[iroots]*PrimaryLambdaRate[iroots]*0.07; // note 2-step
            decay thru Sigma0
    sum += sum2;
    sum += fBar_AntiLAntiXiZero[iroots]
1645     = AntiXiZeroToLambda[iroots]*PrimaryLambdaRate[iroots];
    sum += fBar_AntiLAntiXiPlus[iroots]
        = AntiXiPlusToLambda[iroots]*PrimaryLambdaRate[iroots];
    sum += fBar_AntiLother[iroots]
        = sum2*(100.0-RunningDecayTotalAtAntiSigmaStarPlus[iroots])/RunningDecayTotalAtAntiSigmaStarPlus[iroots];

1650 fBar_AntiLprimary[iroots] /= sum;
fBar_AntiLAntiSig0[iroots] /= sum;

```

```

1655 fBar_AntiLAntiSigStarPlus[iroots] /= sum;
fBar_AntiLAntiSigStarZero[iroots] /= sum;
fBar_AntiLAntiSigStarMinus[iroots] /= sum;
fBar_AntiSAntiSigStarPlus[iroots] /= sum;
fBar_AntiSAntiSigStarZero[iroots] /= sum;
fBar_AntiSAntiSigStarMinus[iroots] /= sum;
1660 fBar_AntiLAntiXiZero[iroots] /= sum;
fBar_AntiLAntiXiPlus[iroots] /= sum;
fBar_AntiLother[iroots] /= sum;

}

1665

// Now let's make the matrix!

1670 //-----
Double_t a[8],b[8],c[8],d[8];

for (int i=0; i<8; i++) {
    a[i] = (2.0/3.0)*(1.0*(
1675          f_Lprimary[i]      * 1.0      * (3.0/4.0)
+ f_LSig0[i]        * (-1.0/3.0) * (3.0/4.0)
+ f_LSigStarPlus[i] * (1.0/3.0) * (15.0/4.0)
+ f_LSigStarZero[i] * (1.0/3.0) * (15.0/4.0)
+ f_LSigStarMinus[i] * (1.0/3.0) * (15.0/4.0)
1680          + f_LXiZero[i]     * (0.900)   * (3.0/4.0)
+ f_LXiMinus[i]    * (0.927)   * (3.0/4.0)
)
-(1.0/3.0)*(
          f_SSigStarPlus[i] * (1.0/3.0) * (15.0/4.0)
+ f_SSigStarZero[i] * (1.0/3.0) * (15.0/4.0)
+ f_SSigStarMinus[i] * (1.0/3.0) * (15.0/4.0)
)
);
1685

1690 b[i] = (2.0/3.0)*(1.0*(
          f_Lprimary[i]      * 1.0      * (3.0/2.0) * (-0.613)
+ f_LSig0[i]        * (-1.0/3.0) * (3.0/2.0) * (+0.79)
+ f_LSigStarPlus[i] * (1.0/3.0) * (5.0/2.0) * (+3.02)
+ f_LSigStarZero[i] * (1.0/3.0) * (5.0/2.0) * (+0.30)
1695          + f_LSigStarMinus[i] * (1.0/3.0) * (5.0/2.0) * (-2.41)
+ f_LXiZero[i]     * (0.900)   * (3.0/2.0) * (-1.25)
+ f_LXiMinus[i]    * (0.927)   * (3.0/2.0) * (-0.651)
)
-(1.0/3.0)*(
          f_SSigStarPlus[i] * (1.0/3.0) * (5.0/2.0) * (+3.02)
+ f_SSigStarZero[i] * (1.0/3.0) * (5.0/2.0) * (+0.30)
+ f_SSigStarMinus[i] * (1.0/3.0) * (5.0/2.0) * (-2.41)
)
);
1700

1705 c[i] = (2.0/3.0)*(1.0*(
          fBar_AntiLprimary[i]      * 1.0      * (3.0/4.0)
+ fBar_AntiLAntiSig0[i]        * (-1.0/3.0) * (3.0/4.0)
+ fBar_AntiLAntiSigStarPlus[i] * (1.0/3.0) * (15.0/4.0)

```

```

1710
+ fBar_AntiLAntiSigStarZero[i] * (1.0/3.0) * (15.0/4.0)
+ fBar_AntiLAntiSigStarMinus[i] * (1.0/3.0) * (15.0/4.0)
+ fBar_AntiLAntiXiZero[i]     * (0.900)   * (3.0/4.0)
+ fBar_AntiLAntiXiPlus[i]    * (0.927)   * (3.0/4.0)
)
1715 -(1.0/3.0)*(
fBar_AntiSAntiSigStarPlus[i] * (1.0/3.0) * (15.0/4.0)
+ fBar_AntiSAntiSigStarZero[i] * (1.0/3.0) * (15.0/4.0)
+ fBar_AntiSAntiSigStarMinus[i] * (1.0/3.0) * (15.0/4.0)
)
1720 );
d[i] = (2.0/3.0)*(1.0*(
fBar_AntiLprimary[i]      * 1.0      * (3.0/2.0) * (+0.613)
+ fBar_AntiLAntiSig0[i]    * (-1.0/3.0) * (3.0/2.0) * (-0.79)
1725 + fBar_AntiLAntiSigStarPlus[i] * (1.0/3.0) * (5.0/2.0) * (-3.02)
+ fBar_AntiLAntiSigStarZero[i] * (1.0/3.0) * (5.0/2.0) * (-0.30)
+ fBar_AntiLAntiSigStarMinus[i] * (1.0/3.0) * (5.0/2.0) * (+2.41)
+ fBar_AntiLAntiXiZero[i]   * (0.900)   * (3.0/2.0) * (+1.25)
+ fBar_AntiLAntiXiPlus[i]  * (0.927)   * (3.0/2.0) * (+0.651)
1730 )
-(1.0/3.0)*(
fBar_AntiSAntiSigStarPlus[i] * (1.0/3.0) * (5.0/2.0) *
(-3.02)
+ fBar_AntiSAntiSigStarZero[i] * (1.0/3.0) * (5.0/2.0) *
(-0.30)
+ fBar_AntiSAntiSigStarMinus[i] * (1.0/3.0) * (5.0/2.0) *
(+2.41)
)
1735 );
1740 }
1745 // ----- what we want is the INVERTED matrix -----
Double_t aInv[8],bInv[8],cInv[8],dInv[8];
for (Int_t i=0; i<8; i++){
  Double_t det = a[i]*d[i] - b[i]*c[i];
  aInv[i] = d[i]/det;
1750  bInv[i] = -b[i]/det;
  cInv[i] = -c[i]/det;
  dInv[i] = a[i]/det;
}
1755 }
```

3.5.8 Communication with Jean Cleymans

This subsubsection contains an email exchange with Jean Cleymans, the author of THERMUS. Basically, I wanted to make sure I understood how to interpret the output of the code. From this exchange, I understand that when I see the line

rate information: Lambda<-Lambda(1405) = 0.00025601 running decay total (%) = 82.1262
 that tells me the number of Λ s, per event, that have their origin as a *primary* $\Lambda(1405)$. That primary $\Lambda(1405)$ could be a parent, a grandparent, a great-grandparent, whatever.

At the end of Jean's mail, he tells me that he will get back to me "today," but he never did. Which is fine;
1765 I got the information I needed.

Dear Lisa,

Great to hear that you are finding THERMUS useful. The main author Spencer Wheaton
wrote the following:

1770 Yes, the grandparents are included too. Essentially, in the decay chain, all decay
products are allowed to decay down until they reach particles that are considered stable.

Regards
Spencer

1775 I will look more specifically at your question and get back to you later today.
With best regards
Jean

1780 From: Lisa, Michael <lisa@physics.osu.edu>
Sent: 13 July 2016 05:38:45 PM
To: Jean Cleymans
Subject: question about THERMUS

1785 Dear Jean,

We are using THERMUS for some feed-down studies, and it is incredibly useful!

1790 I have an important question that I hope you can answer. If I look at section 2.2
of your paper <https://arxiv.org/pdf/hep-ph/0407174v2.pdf>, you discuss that the code
will decay unstable hadrons to the stable ones (like pions, protons, Lambdas) which
is crucial for us experimentalists.

1795 So, Delta++ ---> p + pi+ will occur, and the pi+ distribution at the end will include
contributions from Delta++ decay. Great! My question is, what about multi-step decays,
for example Sigma(1775)-->Sigma(1385)+pi+ and then the Sigma(1385)-->Sigma+pi+, and
then Sigma-->Lambda+gamma.

1800 Equation (30) of your paper seems to say that there is a loop over primordial particles,
which are allowed to decay, but in the above example, the Sigma(1385) would not be
"primordial," correct? (I do understand that, naturally, there are ALSO primordial
Sigma(1385) baryons from the model.) And also the Sigma is not "primordial."

1805 My confusion comes from the text above equation (30) that reads "the primordial hadrons
are allowed to decay to particles considered stable..." as well as the "(prim)"
superscript
in equation (30) itself.

1810 My question may boil down to ask: in my above example, do the final Lambdas have the
contribution whose "grandparent" is Sigma(1775)?

I hope my question is clear. Can you help me understand?

1815 Thank you very much, and best regards,
Mike

3.5.9 Sanity check

For $\Xi^- \left[\frac{1}{2}^+ \right] \rightarrow \Lambda \left[\frac{1}{2}^+ \right] + \pi^- [0^-]$, parity is conserved for p-wave decay and violated for s-wave decay. In the weak decay of these baryons, the γ factor quantifies the degree by which parity is violated.

$$\gamma = \frac{S^2 - P^2}{S^2 + P^2} \quad (17)$$

¹⁸²⁰ As an electromagnetic process, $\Sigma^0 \rightarrow \Lambda + \gamma$ conserves parity, so is p-wave. This would correspond to $\gamma_{\Xi^-} = -1$, in which case $F_{\Xi^-} = -\frac{1}{3}$, which is the same as F_{Σ^0} . This is consistent with equation ??.

$\gamma_{\Xi^-} = +1$ corresponds to the parity-violating s-wave decay mode, for which the spin of the Λ daughter must point in the same direction as the Ξ^- parent ($F_{\Xi^-} = +1$), by angular momentum conservation. Again, this is consistent with equation ??.

¹⁸²⁵ 3.5.10 HIJING efficiency

We do not use the results of this section in the feed-down correction

Different particles have different decay kinematics which can lead to different efficiencies. Since the Σ^0 decay is electromagnetic the Λ daughter has basically the same decay kinematics as a primary Λ . On the other hand, weak decays like the Ξ^- , Ξ^0 , and the Ω^0 have lifetimes similar to the Λ . Because of this the the *apparent* decay length of the Λ which is a daughter of one of these multi-strange particles is longer than average decay length of actual primary Λ . Similarly such a secondary Λ would have a larger reconstructed DCA and (generally) larger DCA of each secondary Λ daughter to the primary vertex. In order to account for this effect we used HIJING data and compared the efficiency of the multi-strange hadrons to the efficiency of the Lambdas. This relative efficiency was used because the yields we got from UrQMD and THERMUS are with respect to Lambdas. Quoting the yields this way somewhat mitigates the tendency for models like UrQMD to underestimate strangeness. These efficiencies are taken into account when quoting yields in in section ??.

In order to get the efficiency for reconstructing a Ξ^- relative to reconstructing a primary Λ we first get a Ξ^- efficiency. This is accomplished by dividing the number of MC Ξ^- tracks in the HIJING by the number of HIJING Ξ^- 's that are associated via the association maker and pass our normal reconstruction cuts. This quantity is then divided by the same thing (# pure MC tracks/# reconstructed Λ) for primary Λ s. The corollary is done for antiparticles (that is efficiency is quoted with respect to the $\bar{\Lambda}$). All such efficiencies were calculated with STAR productionHIJING events at 19GeV. It is assumed that it should not vary significantly for different values of $\sqrt{s_{NN}}$. These final efficiencies can then be multiplied by the yields of Ξ^- per Λ that we have for the UrQMD and THERMUS.

Particle	relative efficiency
Ξ^-	1.12728
Ξ^0	1.01695
Ω^0	0.97769
Ξ^+	1.09458
Ξ^0	1.00359
Ω^0	1.00907

Table 9: Relative efficiency [(# Multi-strange particle passing cuts)/(# Multi-strange particle simulated)]/[(# primary Lambda passing cuts)/(# primary Lambda simulated)]

3.5.11 Old feed-down correction using only Σ^0 s

This section is obsolete. It explains how we used to do the feed-down correction when only Σ^0 s were considered.

One correction that has to be done is the effect of Sigma baryon feeddown from the electromagnetic decay
¹⁸⁵⁰ $\Sigma^0 \rightarrow \Lambda + \gamma$. The lifetime of the Sigma is $7.4 \cdot 10^{-20}$ s so it effectively doesn't change the decay topology of the Lambda. If a collection of Σ^0 has spin aligned in one direction the Λ daughter will, on average, receive a $-1/3$ of the spin of the Σ^0 because of the spin 1 photon. If the global Λ polarization originates from spin coupling in the fireball one would expect that all particles emitted from the fireball share this global polarization. Therefore the Lambda polarization we're measuring appears smaller than it actually
¹⁸⁵⁵ is due to this Σ^0 feeddown. In the following equation the subscript " Λ " means *primary* Lambdas - or at least those not from Σ^0 s - while " Σ^0 " means Lambdas from Σ^0 feeddown

$$\langle \sin(\Psi_1 - \phi_\Lambda^*) \rangle_{\text{Measured}} = \frac{N_\Lambda}{N_\Lambda + N_{\Sigma^0}} \langle \sin(\Psi_1 - \phi_\Lambda^*) \rangle_\Lambda + \frac{N_{\Sigma^0}}{N_\Lambda + N_{\Sigma^0}} \langle \sin(\Psi_1 - \phi_\Lambda^*) \rangle_{\Sigma^0} \quad (18)$$

As mentioned above

$$\langle \sin(\Psi_1 - \phi_\Lambda^*) \rangle_{\Sigma^0} = -\frac{1}{3} \langle \sin(\Psi_1 - \phi_\Lambda^*) \rangle_\Lambda \quad (19)$$

Therefore

$$\begin{aligned} \langle \sin(\Psi_1 - \phi_\Lambda^*) \rangle_\Lambda &= \frac{1 + \frac{N_{\Sigma^0}}{N_\Lambda}}{1 - \frac{1}{3} \frac{N_{\Sigma^0}}{N_\Lambda}} \langle \sin(\Psi_1 - \phi_\Lambda^*) \rangle_{\text{Measured}} \\ &\approx \frac{1 + e^{-\Delta m/T}}{1 - \frac{1}{3} e^{-\Delta m/T}} \langle \sin(\Psi_1 - \phi_\Lambda^*) \rangle_{\text{Measured}} \end{aligned} \quad (20)$$

Where in Eq. 20 we can approximate the ratio N_{Σ^0}/N_Λ using a simple thermal distribution so that
¹⁸⁶⁰ $\frac{N_{\Sigma^0}}{N_\Lambda} \sim e^{-\frac{m_{\Sigma^0} - m_\Lambda}{T}}$. The temperature should be about 140 MeV and deviations of ± 10 MeV seem to only alter the scaling by about 4%.

3.6 Discussion of statistical error

There is not much to discuss in this section but I want to clearly enumerate the sources of statiscal error. Systematic errors are discussed in sec. 4.

1865 Of course the first thing is the statistical error itself coming from filling the TProfiles as described in the bulleted list at the beginning of this section (sec. 3). Of course the error bars are appropriately scaled with the various scalings and corrections we do to the data. The errors on these scalings make up the systematic error of the measurement. A detailed discussion on the error for the mass purity correction can
1870 and the acceptance correction) all have associated errors which fall under systematics, and are discussed in sec. 4.3.

4 Systematic errors

Summary of systematic errors to be discussed in detail later in this section

- Mass purity/residual mass background correction (sec. 4.2). This is the primary source of errors.
- Error in α_H (sec. 4.3) – $\sim 2\%$ scaling error.
- Error in resolution correction (sec. 2.2.1 and 4.3) – $< 1\%$
- Error in A_0 determination (table 1 and 4.3) – $< 0.03\%$
- There is an error in the helicity efficiency effect on the data (sec. 3.4.2 and 4.3) – $< 3.5\%$
- Error in resolution correction from momentum conservation effects (sec. 4.4) – $\sim 2\%$
- For feed down corrected results (vorticity and magnetic field) there is a factor 2 systematic error coming from uncertainty in the temperature T (sec. 3.5)

4.1 Topological cut dependencies

A typical source of systematic errors in the cuts. In this section I'll go over the analysis to find systematic errors from the topology cuts we use to find Lambdas. The nominal cuts used in the analysis can be found in section 2.4.2. The first thing we tried doing was making each cut individually tighter or looser so we had $\pm 25\%$ of the number of Lambdas used in the analysis. The idea was that we could estimate the systematic error by comparing the tight-cut and the loose-cut results. The difference turned out to be possible contributable to statistical error (see section 4.1.4). In order to get a finer handle on this difference we tried to look at the covariance of the polarization with the topological cuts. The result from this study is that "systematic errors are smaller than statistical". The statistical fluctuations simply dominate any deviation from zero covariance that we can see

4.1.1 Covariance method idea

The covariance of two variables (say P for polarization and X for some cut quantity e.g. pion DCA) is defined to be

$$\text{Cov}(P, X) = \langle PX \rangle - \langle P \rangle \langle X \rangle. \quad (21)$$

This, of course, tells us how the cut quantities and the polarization measure co-vary. We look at each covariation with each variable separately. The advantage here is that we can use much more Lambda candidates that wouldn't pass the nominal cuts in order to understand a trend rather than a simple difference. What we really want to get systematic errors is a description of how the polarization depends on the variable. A slope parameter can be made that treats the variation as approximately linear

$$\begin{aligned} \text{Slope}(P(X)) &= \frac{\text{Covariance}(P, X)}{\text{Variance}(X)} \\ &= \frac{\langle PX \rangle - \langle P \rangle \langle X \rangle}{\langle X^2 \rangle - \langle X \rangle^2} \end{aligned} \quad (22)$$

Once we have a slope that describes the variation of the polarization with X we can get the systematic error by multiplying by a *reasonable* range in the cut quantity (ΔX)

$$\text{Error} = \Delta X * \text{Slope} \quad (23)$$

A reasonable range for ΔX is, for each cut, the difference between where you might make the a loose version and a tight version of the cut. As it happens the ΔX is just a scaling and, since we don't get a significant slope value, it is not necessary to use when we find no clear non-statistican deviation from zero for the slope.

There is a subtlety here I've glossed over which is that the apparent magnitude of the polarization depends on the purity of Lambda sample which, in turn, depends on the value of the quantity I'm cutting on. To account for this I can scale the slope by the purity of the mass distribution. Doing this requires a characterization of the slope of the purity distribution. For example suppose I want to know the covariance of the polarization with the pion DCA. If I look in bins of pion DCA for Lambda candidates the ones with the largest DCA have the purest Lambda distribution. Since we normally scale the measured polarization by $(S+B)/S$ (assuming zero polarization in the mass background) the polarization will be of a greater magnitude than that measured at low pion DCA. So we have done no purity correction to the data if it has the same positive polarization at a bin of low pion DCA as it does for a different bin a high pion DCA, the high pion DCA bin will have a larger *apparent* polarization and a positive covarianc will be seen. Given that we have a positive net polarization we might expect a trivial positive covariance for pion DCA to appear just from variation of the purity with pion DCA.

What we measure without correcting for the purity is the so called “measured” slope, we can recast 22 as

$$\text{Slope}(P(X))^M = \frac{d}{dX} P^M \quad (24)$$

where M denotes the “measured” quantity and T denotes a “true” quantity. We can relate this to the true polarization which we get from purity correcting the measured values, provided we assume that we can describe the variation of $S/(S+B)$ with X by a linear function with slope m_X

$$\begin{aligned} \text{Slope}(P(X))^M &= \frac{d}{dX} \left(\frac{S}{S+B} P^T \right) \\ &= \frac{S}{S+B} \frac{d}{dX} P^T + \left(\frac{d}{dX} \frac{S}{S+B} \right) P^T \\ &= \frac{S}{S+B} \text{Slope}^T + m_X P^T \\ &\approx \left\langle \frac{S}{S+B} \right\rangle \text{Slope}^T + m_X \langle P^T \rangle \end{aligned} \quad (25)$$

4.1.2 Mass purity

An example of purity changing with a cut quantity:

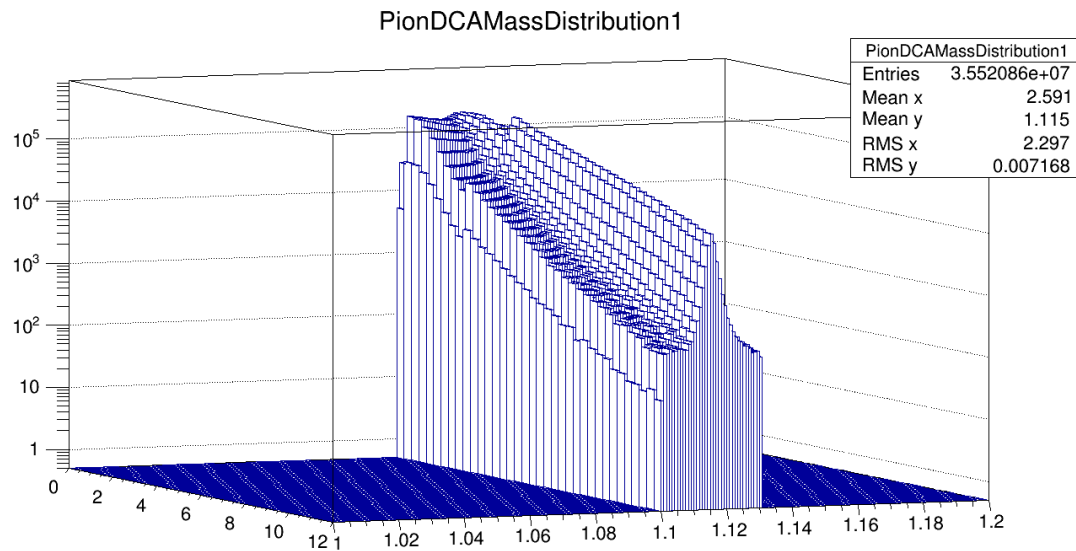


Fig. 92: Invariant mass (GeV – right axis) as a function of pion DCA (cm – left axis) for cut index 1 (proton has ToF info, pion does not). Vertical axis is counts. Cutoff in invariant mass is an artifact of what I save in my PicoDst files – higher/lower mass is not necessary for purity estimation.

1925 A linear fit of the purity for various quantities can be seen below

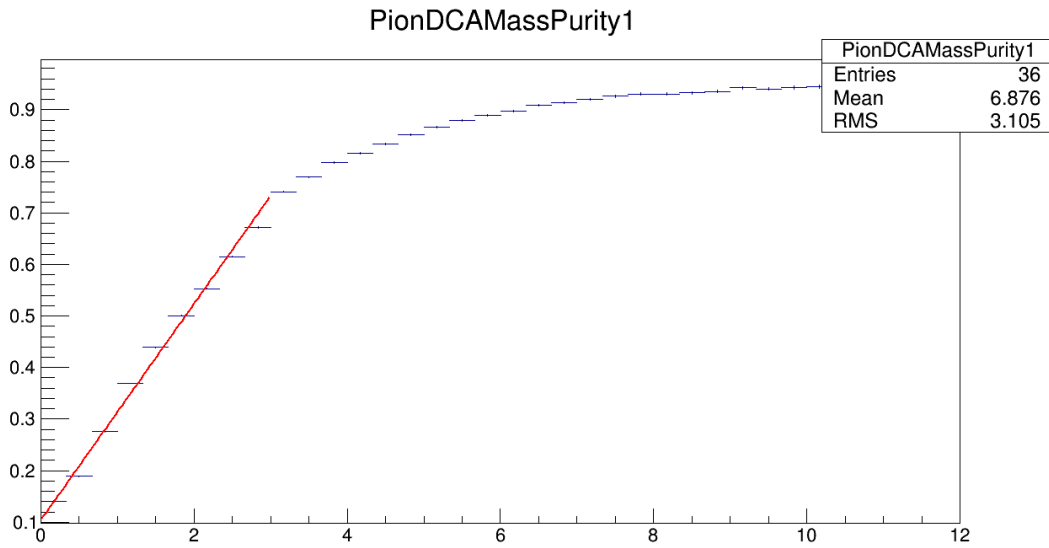


Fig. 93: Lambda invariant mass purity as a function of pion DCA fit with a linear function ($p_0 + p_1 * x$) for cut index 1

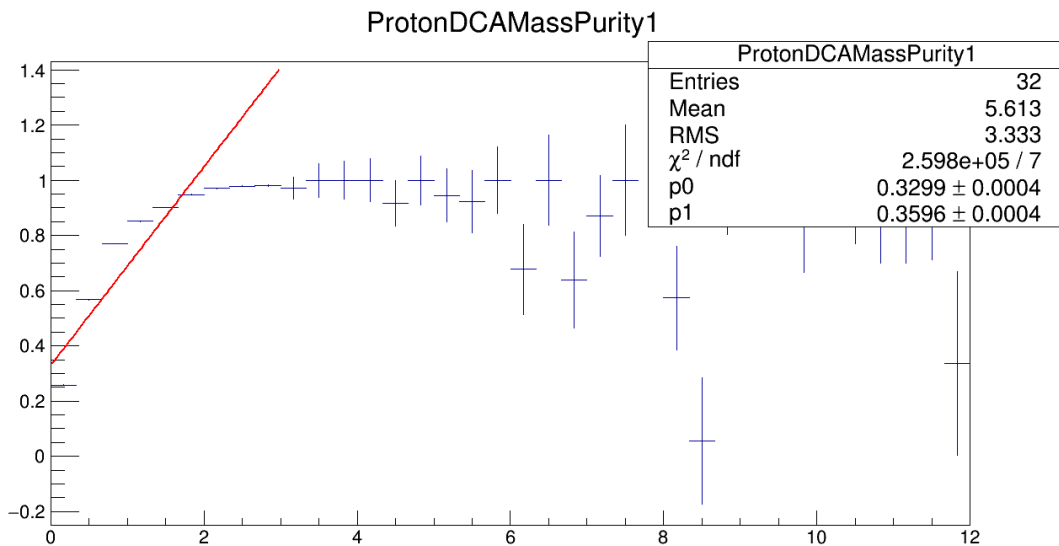


Fig. 94: Lambda invariant mass purity as a function of proton DCA fitted with a linear function ($p_0 + p_1 * x$) for cut index 1

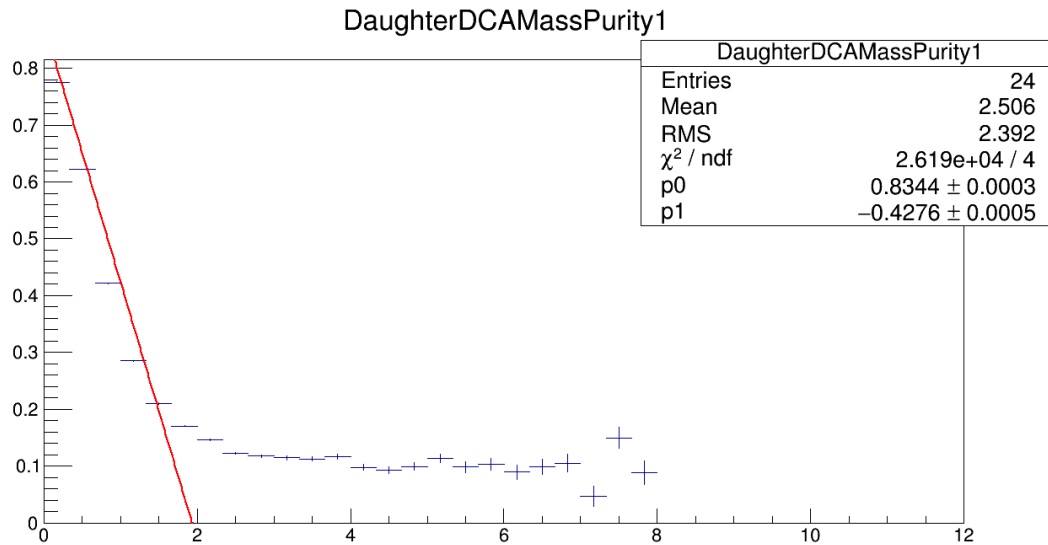


Fig. 95: Lambda invariant mass purity as a function of daughter DCA fit with a linear function ($p_0 + p_1 * x$) for cut index 1

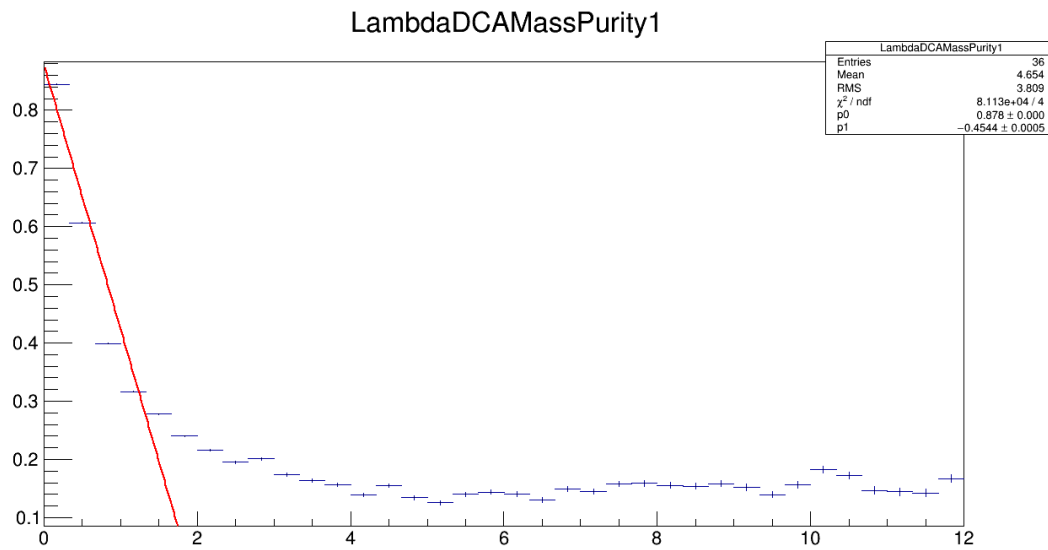


Fig. 96: Lambda invariant mass purity as a function of Lambda DCA fitted with a linear function ($p_0 + p_1 * x$) for cut index 1

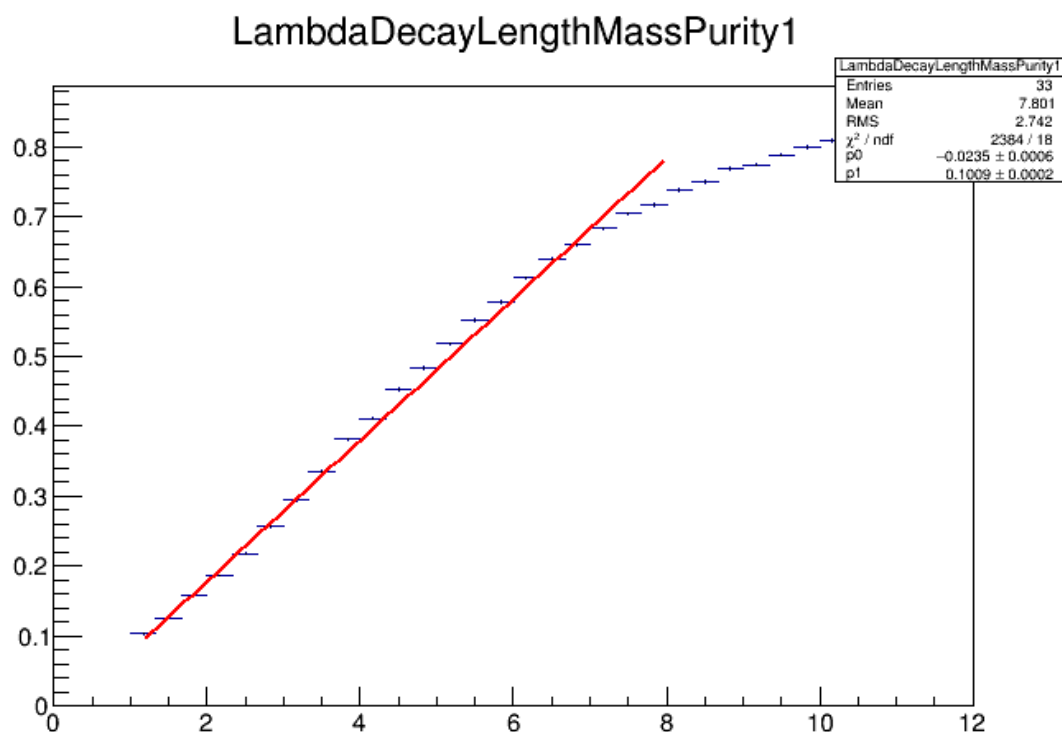


Fig. 97: Lambda invariant mass purity as a function of Lambda decay length fitted with a linear function ($p_0 + p_1 * x$) for cut index 1

Clearly a linear approximation is not ideal for several of these functions. The only thing to be done is to change the range over which the fit is done and try to overestimate m_X . The range was varied but the nominal fit range for these functions is (where Min. refers to the lower value of the cut and max refers to the upper value)

Cut description	cut index 0	cut index 1	cut index 2	cut index 3
PionDCA min	0.0	0.0	0.5	0.5
PionDCA max	3.0	3.0	3.0	3.0
ProtonDCA min	0.0	0.0	0.0	0.0
ProtonDCA max	3.0	3.0	3.0	3.0
DaughterDCA min	0.0	0.0	0.0	0.0
DaughterDCA max	2.0	2.0	2.0	2.0
LambdaDCA min	0.0	0.0	0.0	0.0
LambdaDCA max	2.0	2.0	2.0	2.0
LambdaDecayLength min	1.167	1.167	3.0	3.0
LambdaDecayLength max	8.0	8.0	8.0	8.0

Table 10: Range of linear fit of mass purity as a function of respective cut quantity

1930 4.1.3 Results

Since the error bars depend so much on which cut I'm considering and the cut index of the Lambda I may have to duplicate a few of the plots so zoomed in. What we're looking for is a clear non-statistical deviation of the slope. Each point on the following plots represents the covariance of the polarization with various cut quantities (e.g. pion DCA). There is a separate point for each type of Lambda (cut index 0, 1, 2, or 3).

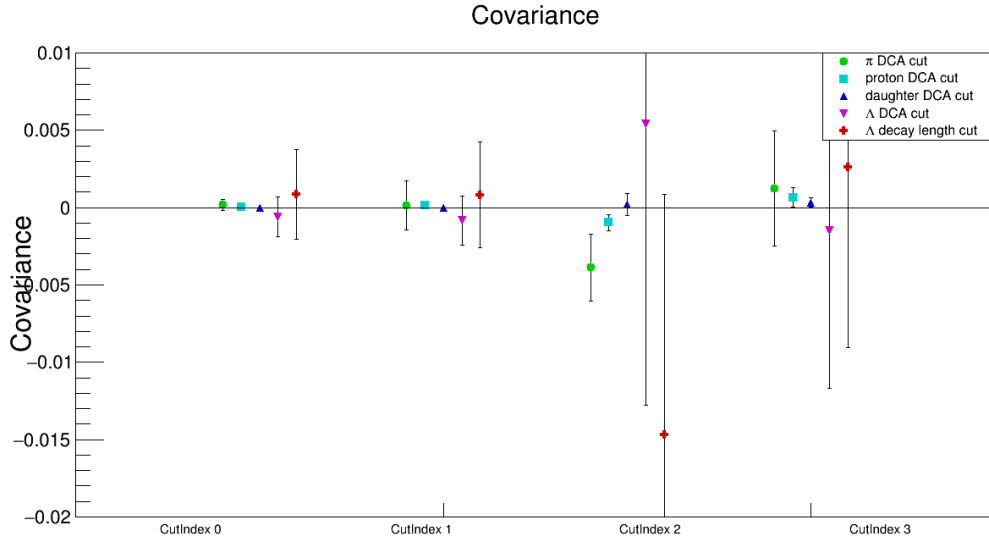


Fig. 98: Λ polarization covariance with cut quantities for each Λ cut index.

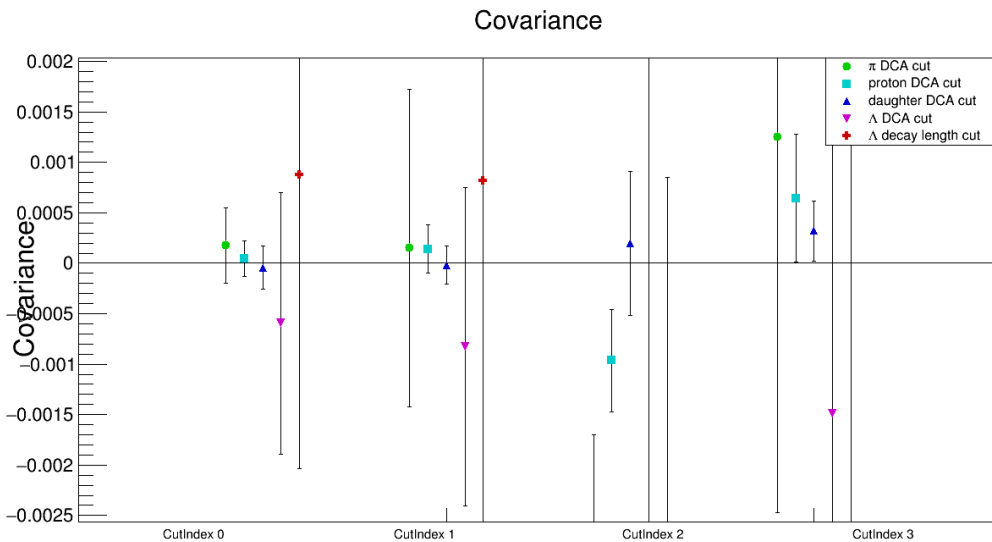


Fig. 99: Λ polarization covariance with cut quantities for each Λ cut index; zoomed in.

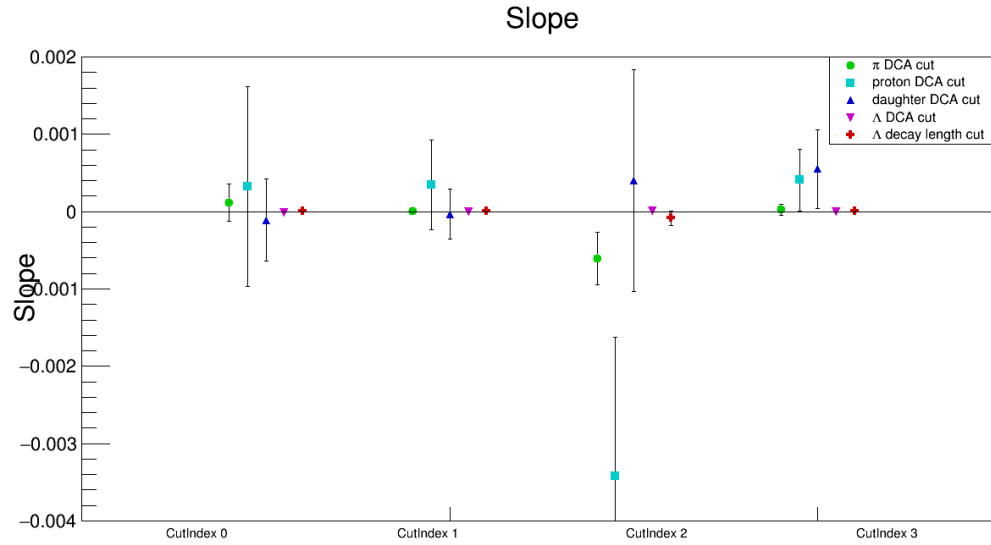


Fig. 100: Λ polarization “slope” from covariance with cut quantities for each Λ cut index. This is not corrected for mass purity.

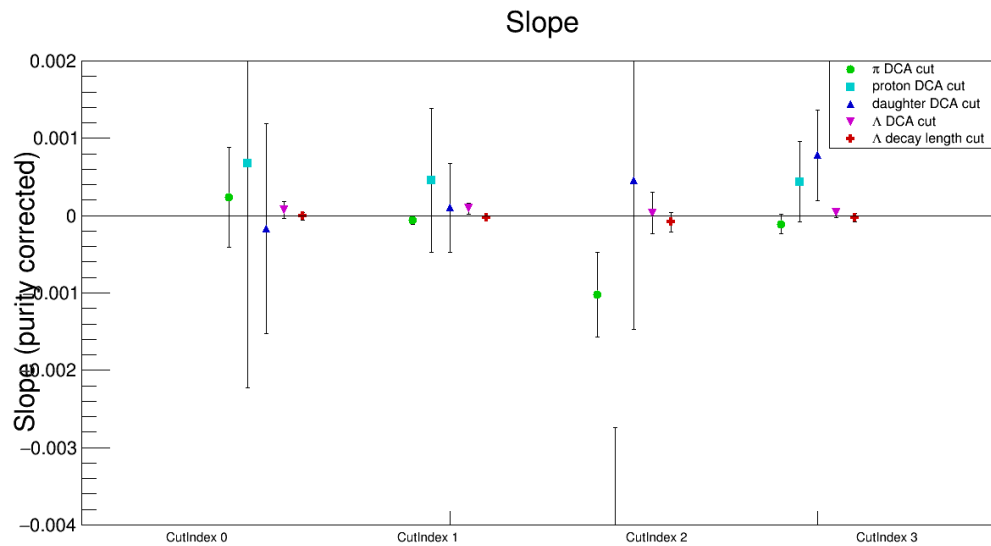


Fig. 101: Λ polarization “slope” from covariance with cut quantities for each Λ cut index. This is corrected for mass purity.

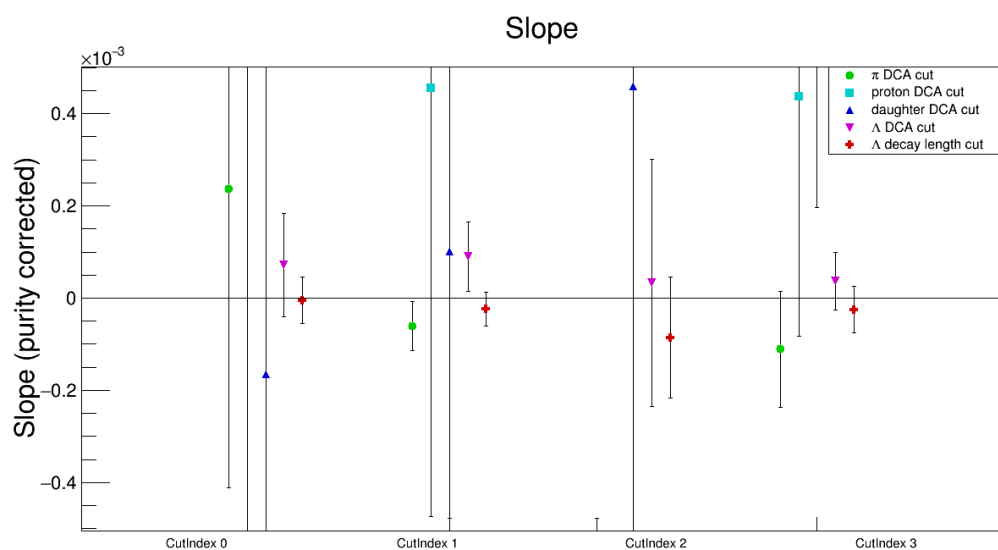


Fig. 102: Λ polarization “slope” from covariance with cut quantities for each Λ cut index; zoomed in. This is corrected for mass purity.

The only hints of non-statistical deviation comes from cut index 2, but cut index 2 is only 3% of the data! Cut index 2 represents Lambda's whose daughter proton has no ToF information while the pion daughter does. This is a very poor quantity Lambda candidate and since it is such a small percentage of the total number of Lambdas we can throw these Lambdas out with impunity. There is no bias introduced here, these are simply poor quality Lambdas. Therefore (throwing out cut index 2 Lambdas) there is no non-statistical deviations from covaration of the polarization and any of the cut quantities. To double check this conclusion I've increased/decreased the maximum of the fit range for the purity slope m_X . In the following plots the the maximum of the fit is multiplied by a rangefactor.

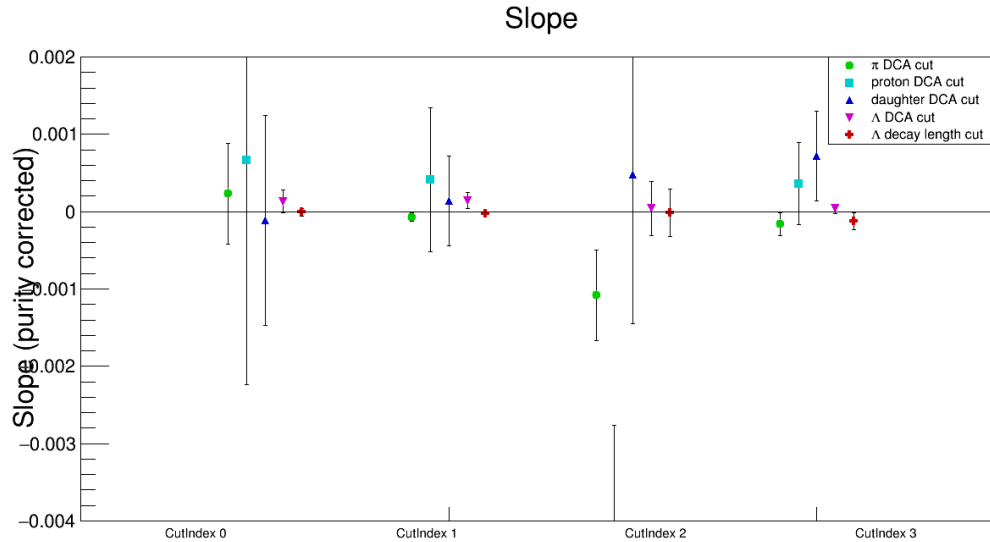


Fig. 103: Λ polarization “slope” from covariance with cut quantities for each Λ cut index. This is corrected for mass purity. The rangefactor is 0.5.

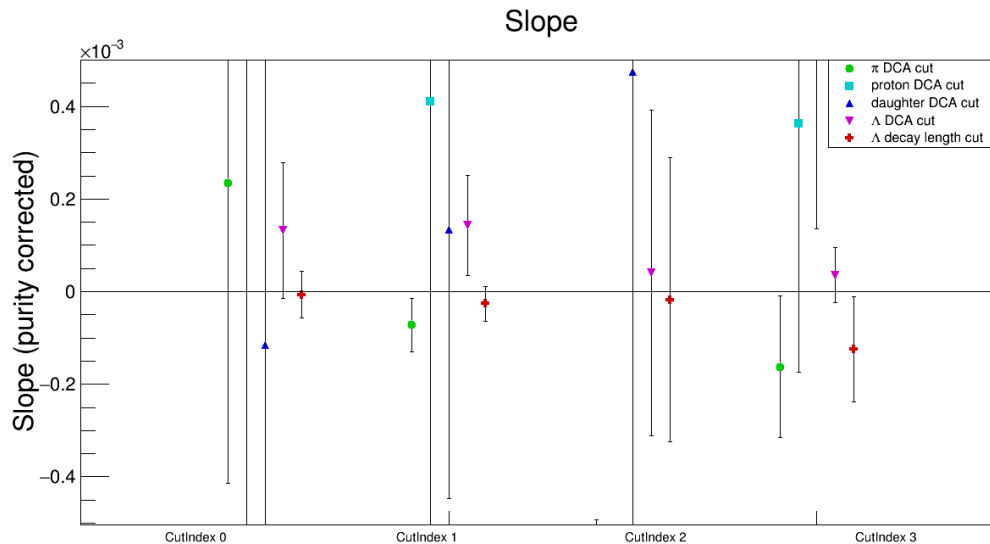


Fig. 104: Λ polarization “slope” from covariance with cut quantities for each Λ cut index; zoomed in. This is corrected for mass purity. The rangefactor is 0.5.

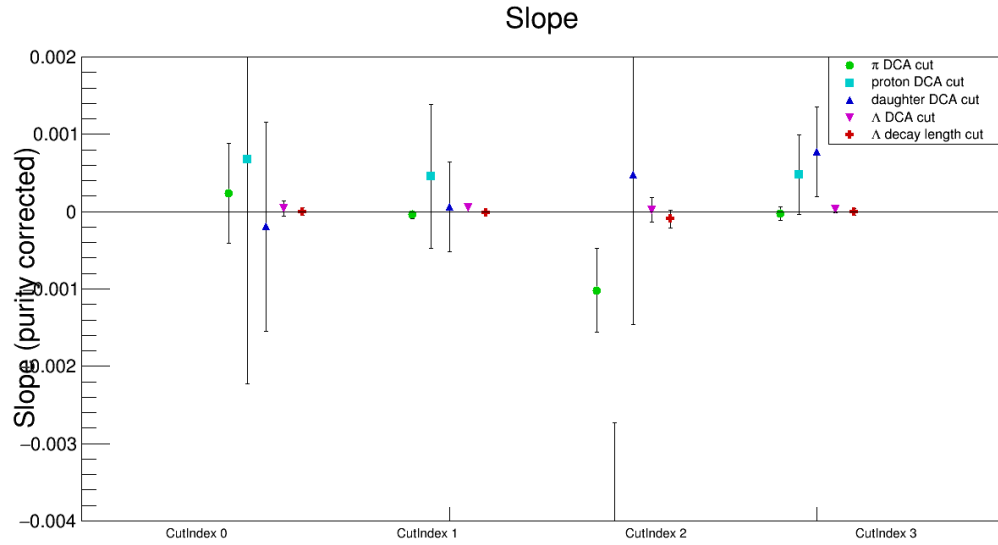


Fig. 105: Λ polarization “slope” from covariance with cut quantities for each Λ cut index. This is corrected for mass purity. The rangefactor is 2.

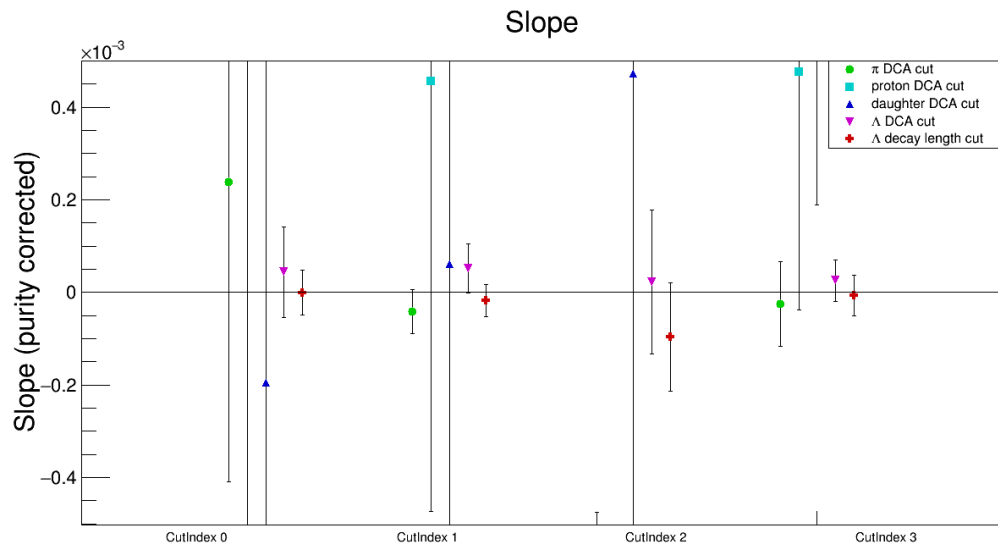


Fig. 106: Λ polarization “slope” from covariance with cut quantities for each Λ cut index; zoomed in. This is corrected for mass purity. The rangefactor is 2.

4.1.4 Simple cut variation

1945 This section is for historical purposes. The results shown here do not provide final systematic errors.

I'll focus on errors from the topology cuts for the Lambda as they are the ones specific to my analysis. To get a handle on the errors I varied each cut for 19GeV by either making the cut tighter so that I had 75% of the Lambdas as would be found using nominal cuts or I made the cut looser so that 125% of the Lambdas were found. The result for each cut for both Λ and $\bar{\Lambda}$ are shown below

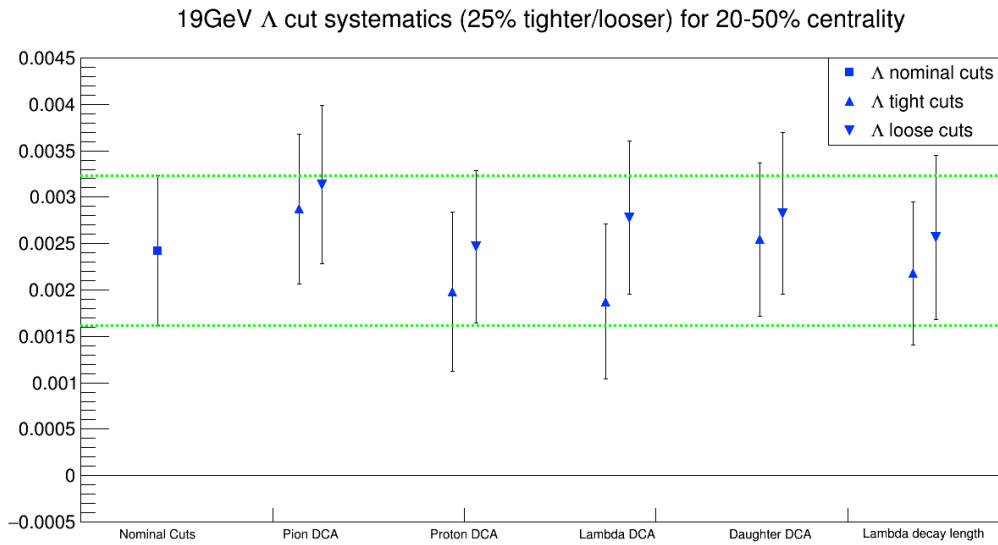


Fig. 107: $\langle \sin(\Psi_1 - \phi_{\Lambda}^*) \rangle$ as a function of cut variation. One cut at a time is loosened or tightened so that 125% or 75% of the Lambdas are found.

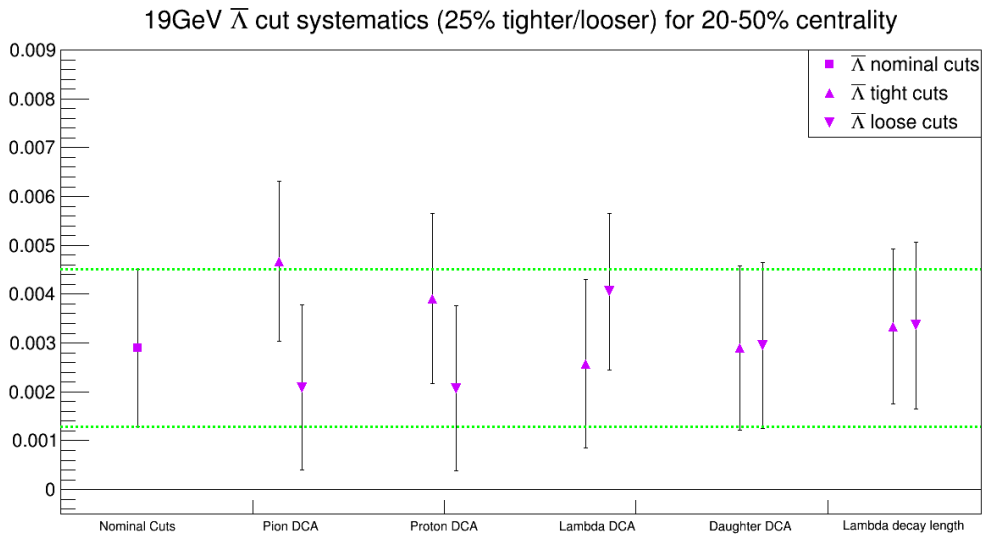


Fig. 108: $\langle \sin(\Psi_1 - \phi_{\Lambda}^*) \rangle$ as a function of cut variation. One cut at a time is loosened or tightened so that 125% or 75% of the Lambdas are found.

¹⁹⁵⁰ Note that in the previous two figures each data point is scaled by the (Signal+Background)/Signal of the mass distribution so that the results are not affected by the purity changes that would occur by loosening/tightening a cut. The systematic error is determined to be the largest variation between the tight cuts and loose cuts (eg. for Λ the difference between Lambda DCA tight and Lambda DCA loose). A covariance analysis is underway to get at these errors in a more sophisticated manner.

1955 **4.2 Residual effect**

There is a systematic error from the residual signal we see in the wings of the mass distribution which should be in the mass background of the results (see section 3.2). In section 3.2 we posit that this small residual effect comes from Lambdas which have proton daughters that get matched up with pion who does not come from a Lambda. Many of the protons in an event come from Lambdas and it is a much 1960 smaller percent of the pions. A Lambda candidate made from these particles might well have a small residual polarization since the proton carries the larger percentage of the Lambda momentum, and thus a fair bit of the spin information. The following are corrected for resolution.

$\sqrt{s_{NN}}$ (GeV)	$P\Lambda_{\text{uncorrected}} (\%)$	$P\bar{\Lambda}_{\text{uncorrected}} (\%)$
7.7	1.6%	6.6%
11.5	1.0%	2.3%
14.5	0.6%	0.9%
19.6	0.7%	1.2%
27	0.7%	1.1%
39	0.3%	0.8%

Table 11: Uncorrected results for Au+Au 20-50%.

$\sqrt{s_{NN}}$ (GeV)	$P\Lambda_{\text{noresidual}} (\%)$	$P\bar{\Lambda}_{\text{noresidual}} (\%)$	Level of correction Λ	Level of correction $\bar{\Lambda}$
7.7	2.4%	8.1%	155.4%	121.8%
11.5	1.5%	2.8%	151.7%	123.8%
14.5	1.2%	1.5%	192.3%	168.7%
19.6	1.0%	1.5%	151.5%	129.1%
27	1.1%	1.5%	153.0%	134.2%
39	0.5%	1.1%	149.2%	135.4%

Table 12: Results for Au+Au 20-50% corrected for mass purity without taking into account residual mass background polarization.

$\sqrt{s_{NN}}$ (GeV)	$P\Lambda_{\text{withresidual}} (\%)$	$P\bar{\Lambda}_{\text{withresidual}} (\%)$	Level of correction Λ	Level of correction $\bar{\Lambda}$
7.7	2.3%	7.0%	148.5%	106.0%
11.5	1.2%	2.7%	125.0%	116.7%
14.5	0.9%	2.2%	142.2%	245.9%
19.6	0.9%	1.7%	129.0%	138.4%
27	1.0%	1.3%	136.3%	119.9%
39	0.3%	1.2%	95.2%	136.6%

Table 13: Results for Au+Au 20-50% corrected for mass purity while taking into account residual mass background polarization.

$\sqrt{s_{NN}}$ (GeV)	$P\Lambda_{\text{withresidual}}/P\Lambda_{\text{noresidual}}$	$P\bar{\Lambda}_{\text{withresidual}}/P\bar{\Lambda}_{\text{noresidual}}$	$P\Lambda_{\text{noresidual}} - P\Lambda_{\text{withresidual}}$	$P\bar{\Lambda}_{\text{noresidual}} - P\bar{\Lambda}_{\text{withresidual}}$
7.7	95.6%	87.0%	-0.11%	-1.05%
11.5	82.4%	94.3%	-0.26%	-0.16%
14.5	73.9%	145.8%	-0.33%	0.69%
19.6	85.1%	107.2%	-0.15%	0.11%
27	89.1%	89.3%	-0.12%	-0.16%
39	63.8%	100.9%	-0.18%	0.01%

Table 14: Comparison between residual and non-residual corrections to data.

There are large statistical error bars associated with scale of the residual background correction. In fact this difference between considering and not considering the residual effect is well within statistical errors¹⁹⁶⁵ but we would like to associate a systematic error to our lack of understanding about the correct way of dealing with this residual effect. We can roughly average over the difference of the ratio of the two scaling methods to get final systematic errors. 15GeV is a special energy that will have an exception, but the average ratio not including 15GeV $\langle P\Lambda_{\text{withresidual}} / P\Lambda_{\text{noresidual}} \rangle \sim 0.85$ and $\langle P\bar{\Lambda}_{\text{withresidual}} / P\bar{\Lambda}_{\text{noresidual}} \rangle \sim 0.95$.

$\sqrt{s_{\text{NN}}}$ (GeV)	$P\Lambda_{\text{noresidual}}$ (%)	$P\bar{\Lambda}_{\text{noresidual}}$ (%)	$0.85P\Lambda_{\text{noresidual}}$	$0.95P\bar{\Lambda}_{\text{noresidual}}$ (%)	diff Λ	diff $\bar{\Lambda}$
7.7	2.4%	8.1%	2.019%	7.686%	0.4136%	0.4045%
11.5	1.5%	2.8%	1.228%	2.679%	0.2516%	0.1410%
14.5	1.2%	1.5%	1.036%	1.442%	0.2122%	0.0759%
19.6	1.0%	1.5%	0.8466%	1.471%	0.1734%	0.0774%
27	1.1%	1.5%	0.9172%	1.434%	0.1879%	0.0755%
39	0.5%	1.1%	0.4374%	1.083%	0.08959%	0.0570%

Table 15: Results for Au+Au 20-50% corrected for mass purity without taking into account residual mass background polarization. Diff is the difference between the first column and the previous relevant column.

Roughly averaging over the results in table 15 we get the following range of systematic errors (upper and lower)

$\sqrt{s_{NN}}$ (GeV)	Λ	Λ up sys	Λ down sys	$\bar{\Lambda}$	$\bar{\Lambda}$ up sys	$\bar{\Lambda}$ down sys
7.7	2.43%	0.00%	0.20%	8.09%	0.00%	1.00%
11.5	1.48%	0.00%	0.20%	2.82%	0.00%	0.15%
14.5	1.25%	0.00%	0.30%	1.52%	0.40%	0.15%
19.6	1.02%	0.00%	0.20%	1.55%	0.00%	0.15%
27	1.11%	0.00%	0.20%	1.51%	0.00%	0.15%
39	0.50%	0.00%	0.20%	1.14%	0.00%	0.15%

Table 16: Results for Au+Au 20-50% polarization results corrected for resolution correction and purity correction as well as systematic error.

4.3 Scaling errors

As discussed in the beginning of sec. 3 the data is subject to a few scalings: that of $\alpha_H = 0.647 \pm 0.013$ – the decay parameter, that of the resolution correction – as discussed in sec. 2.2.1, and the acceptance correction A_0 – as seen in table 1. All of these have associated errors, which are very very small compared to the statistical error of the measure. The α_H is the largest at 2%. These are included as a statement in the paper about the uncertainty in the scaling.¹⁹⁷⁵

Additionally given the interplay between helicity efficiency and non-zero polarization (discussed in sec. 3.4.2) we know (from simple simulation) that we should scale the data by about $7\% \pm 3.5\%$. This error is quoted from fig. 3.4.2.

1980 **4.4 Conservation of momentum effects on event plane resolution**

1985 There are possible conservation of momentum (MC) effects on the event plane determination. This was studied by Yadav Pandit in the run up of the BES v_1 paper using MevSim with and without MC (with the version used it could be turned off and on) using sub-event planes made by using different subsections of the BBC. As far as this analysis is concerned we expect this to be a roughly 2% systematic error on the event plane resolution for the BES. This study can be found on the paper webpage <http://www.star.bnl.gov/protected/bulkcorr/ypandit/BESv1Paper/> under “Support Documents” —→ “Momentum Conservation Effects”. It is also copied below:

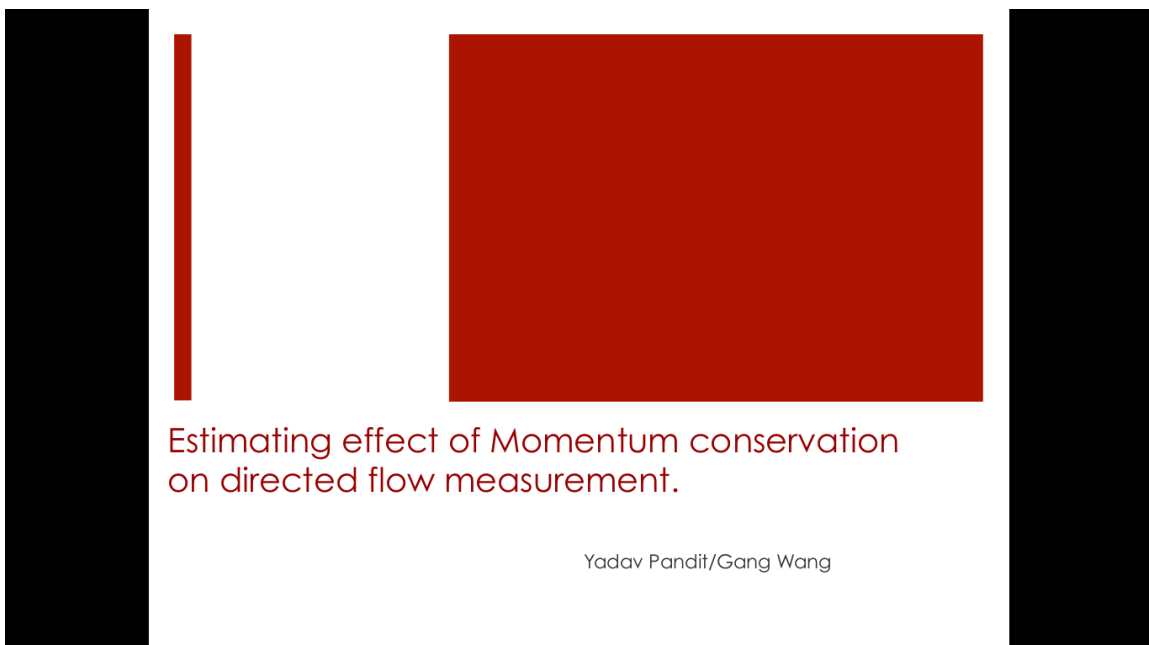


Fig. 109:

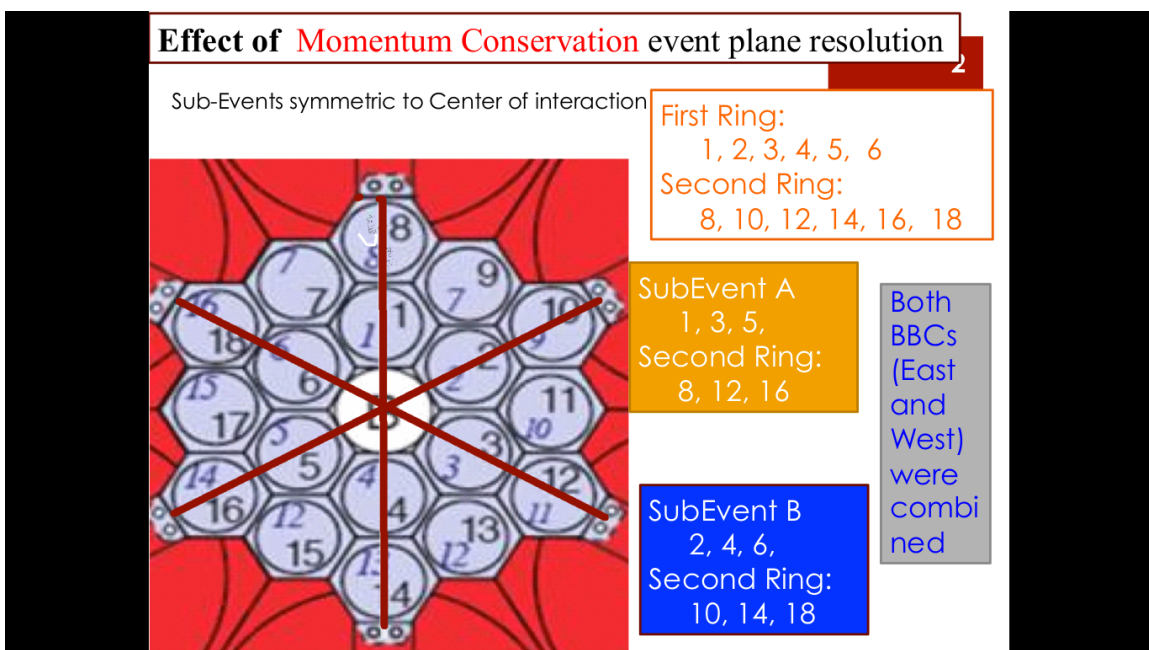
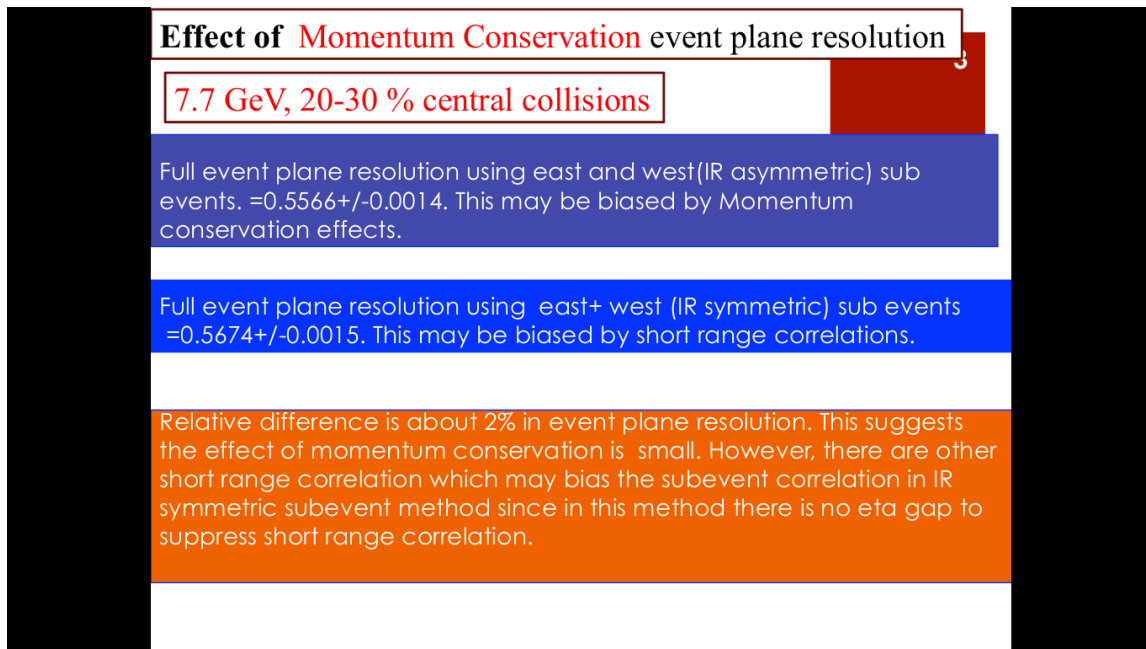
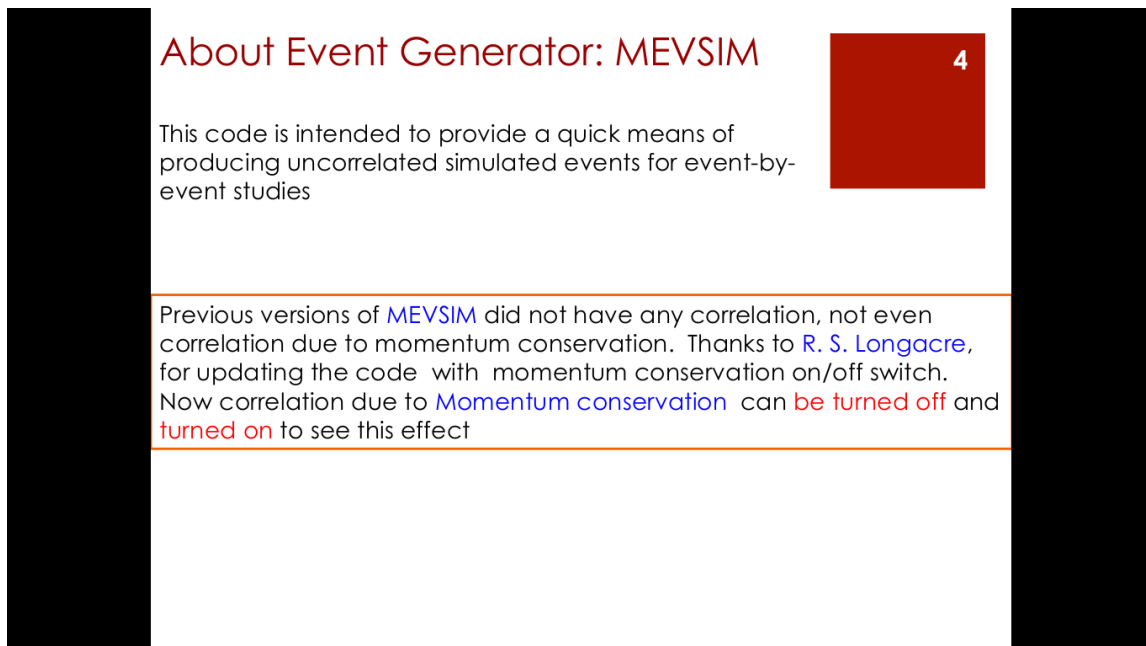


Fig. 110:

**Fig. 111:****Fig. 112:**

39 GeV: Central Collisions

5

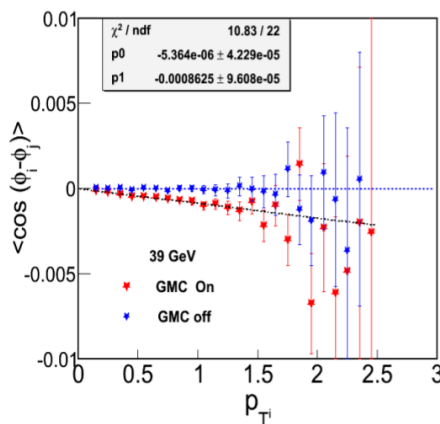
Input parameters:

1. $\pi^+ \cdot \pi^-$ spectra
2. Ratio of No of +ve Particles to -ve particles =1.09
3. Multiplicity

Fig. 113:

39 GeV: Central Collisions

6

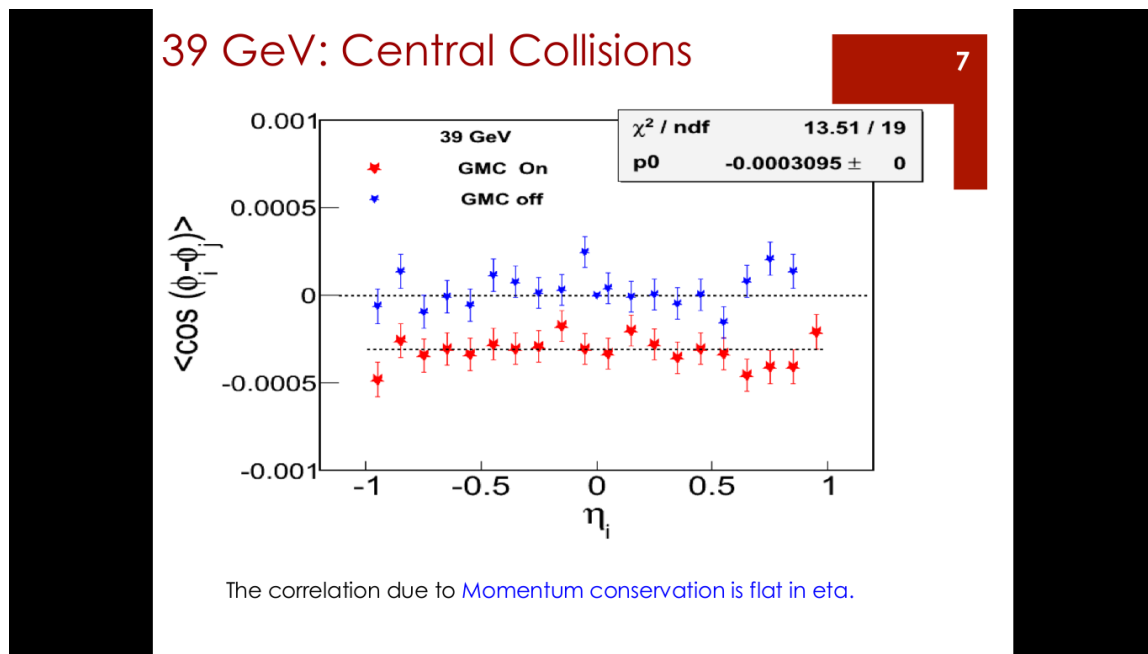
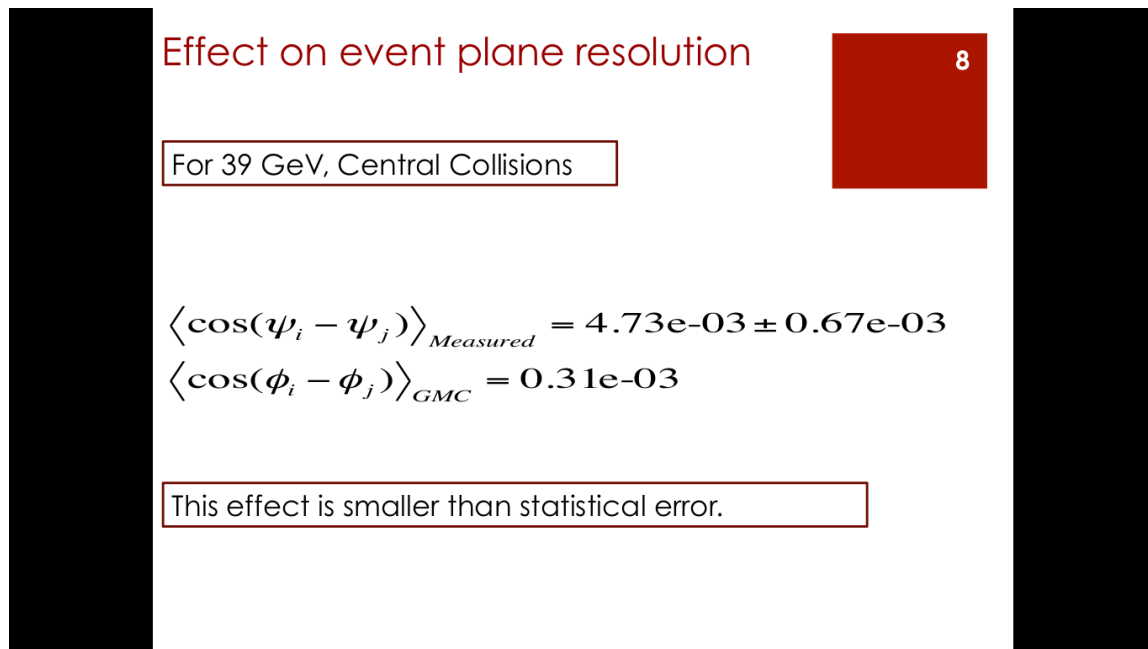


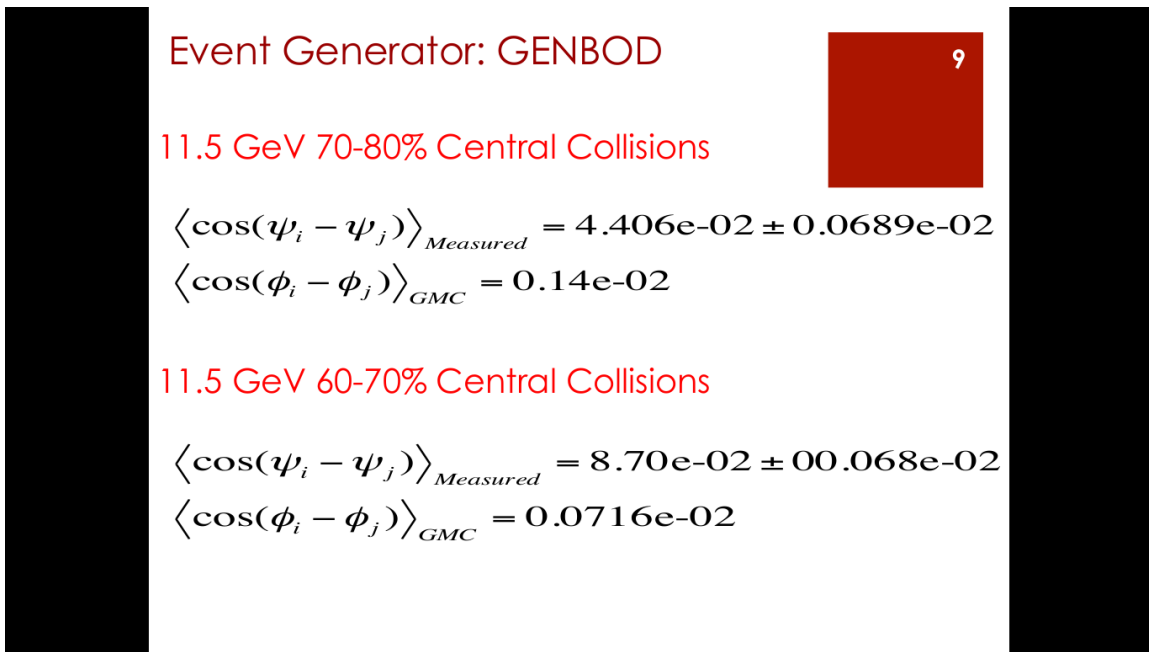
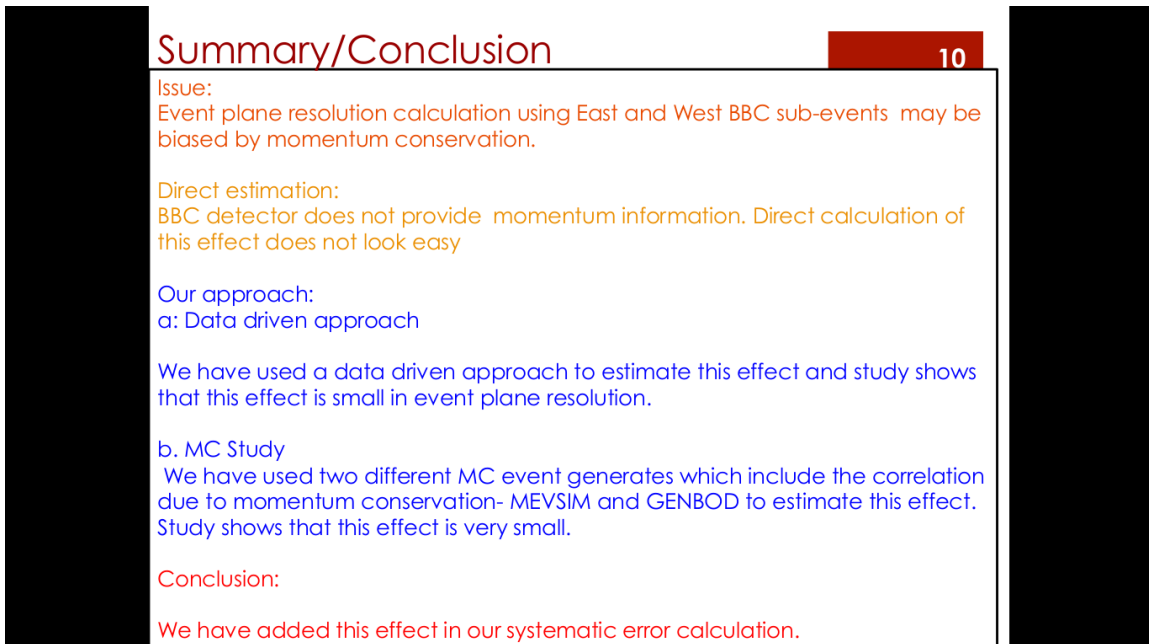
Slope at 200 GeV: Yi Li

0-5%	0.000358 ± 0.000005
5-10%	0.000457 ± 0.000006
10-20%	0.000644 ± 0.000006
20-30%	0.000973 ± 0.000008
30-40%	0.001515 ± 0.000013
40-50%	0.002458 ± 0.000021
50-60%	0.004227 ± 0.000037
60-70%	0.007593 ± 0.000073
70-80%	0.015889 ± 0.000204

The correlation due to Momentum conservation in simulated events. Slope is comparable to 20-30% central Au+Au events at 200 GeV(approximately similar no. of tracks)

Fig. 114:

**Fig. 115:****Fig. 116:**

**Fig. 117:****Fig. 118:**

4.5 Feeddown

There is uncertainty with our estimation of the yields for particles that feeddown into Lambdas. The feeddown is discussed in detail in section 3.5. Initially yield discrepancies between UrQMD and THER-MUS made our systematic errors. Now we are using a very explicitly thermal approach. The results for the feeddown corrected data are dependant on your choice of model, but this isn't exactly a systematic error.

5 Systematic Dependencies

In this section we intend to present any systematic dependency $\langle \sin(\Psi_1 - \phi_\Lambda^*) \rangle$ has on various quantities of interest. It has been posited that the measure may increase for Lambdas emitted in plane and at large momentum. It has also been claimed that this will not depend greatly on rapidity. There certainly should be some centrality dependence to the result as it depends on system angular momentum and thermalization. Because the analysis is so statistics limited this has become more a consistency check than a check for real dependence. The results are all corrected only for resolution. Higher order corrections (mass purity) are not taken into account. Additionally the results are not scaled by the factor of $8/(\pi\alpha)$.

Some of the figures in here are really of $\S_y \equiv \vec{S} \cdot \hat{L}$, that is with a boosted spin vector. In practice this result is nearly identical to the polarization measure. It is reasonable to expect they would have the same systematic dependencies. If these are still in the document I do intend to replace them at some point.

5.1 Centrality

This section is to show the centrality dependence of the signal. Many centrality windows are shown. The most peripheral collisions have the largest angular momentum but what is most important is the amount of angular momentum that gets transferred to the fireball at mid-rapidity. Additionally one must consider how thermalized the system is to know how the particle spin gets distributed. Stopping and thermalization mechanics are complicated so the dependence on centrality may well be difficult to predict. As a bit of a compromise one might expect the largest signal for mid-central collisions.

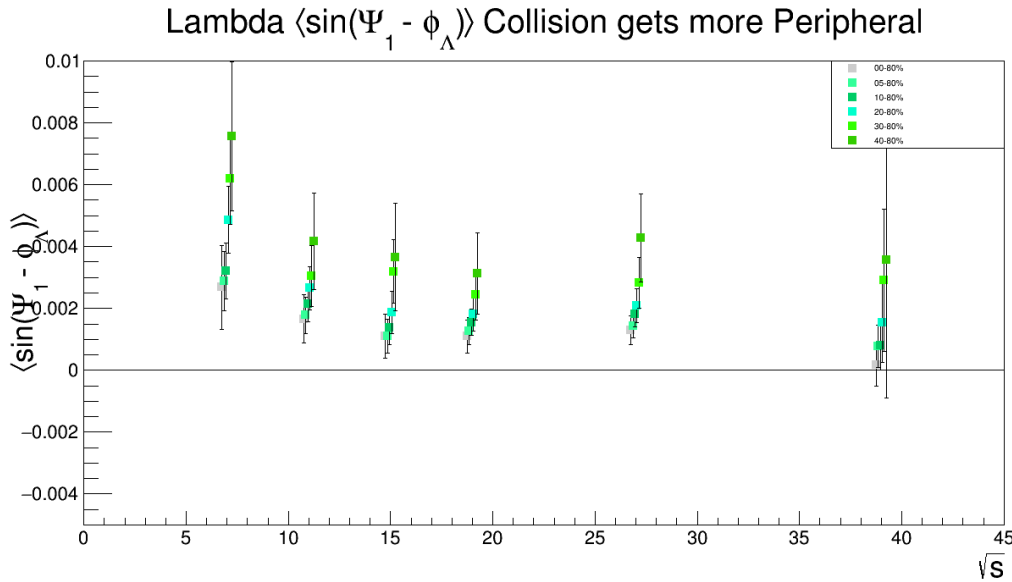


Fig. 119: $\langle \sin(\Psi_1 - \phi_\Lambda^*) \rangle$ as the collision gets more peripheral

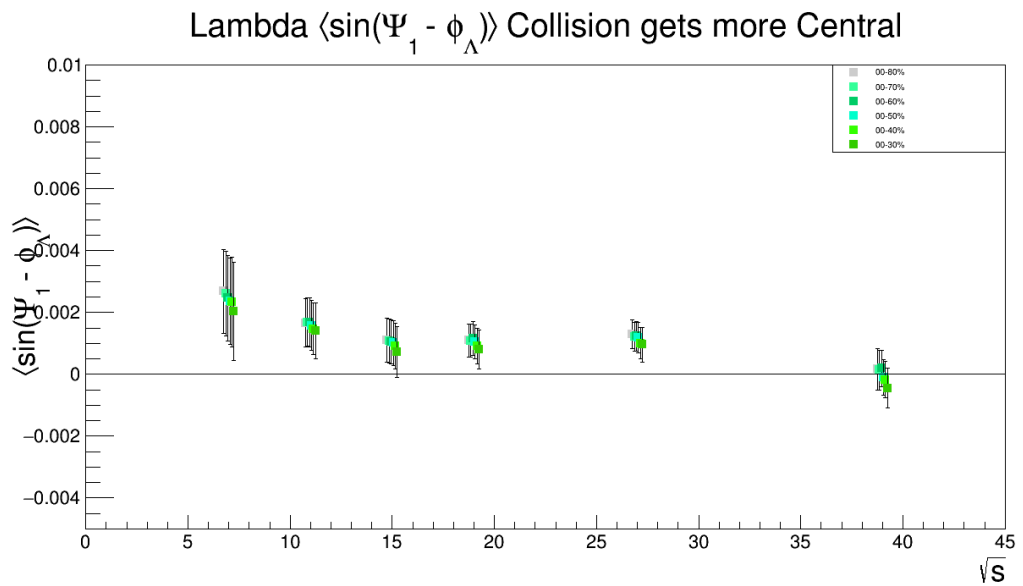


Fig. 120: $\langle \sin(\Psi_1 - \phi_\Lambda^*) \rangle$ as the collision gets more central

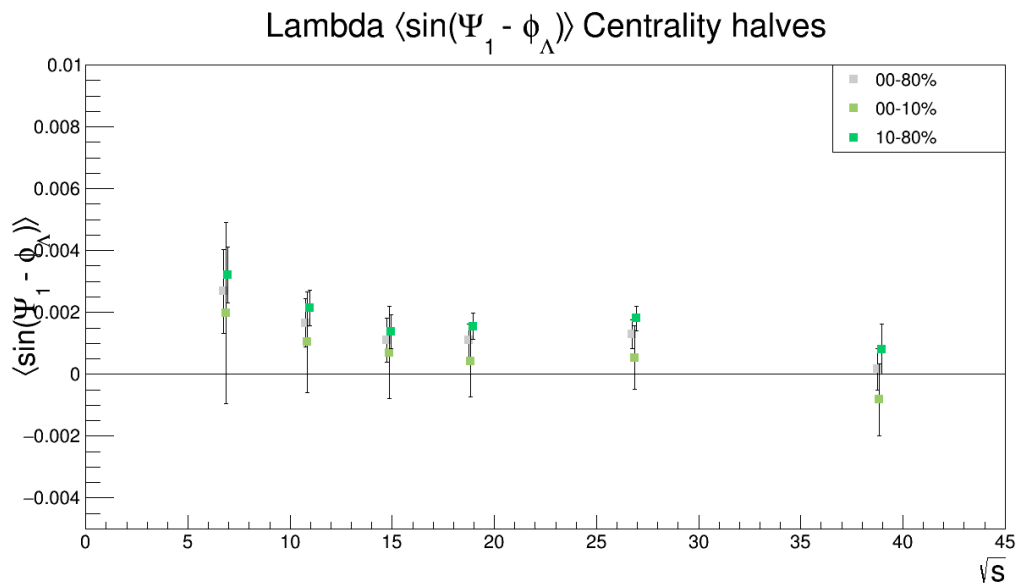


Fig. 121: $\langle \sin(\Psi_1 - \phi_\Lambda^*) \rangle$ for rough halves of centrality by yield

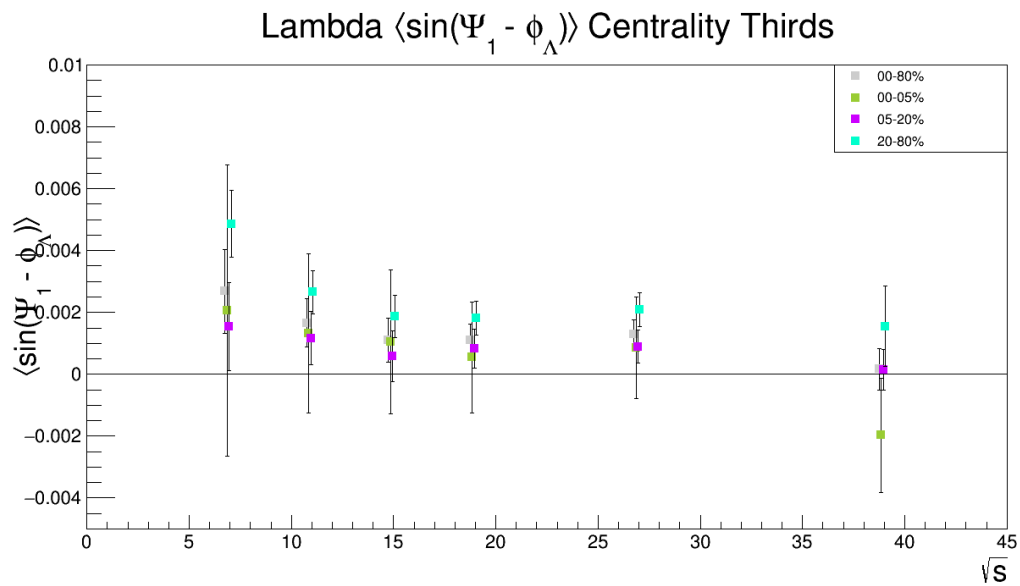


Fig. 122: $\langle \sin(\Psi_1 - \phi_{\Lambda}^*) \rangle$ for rough thirds of centrality by yield

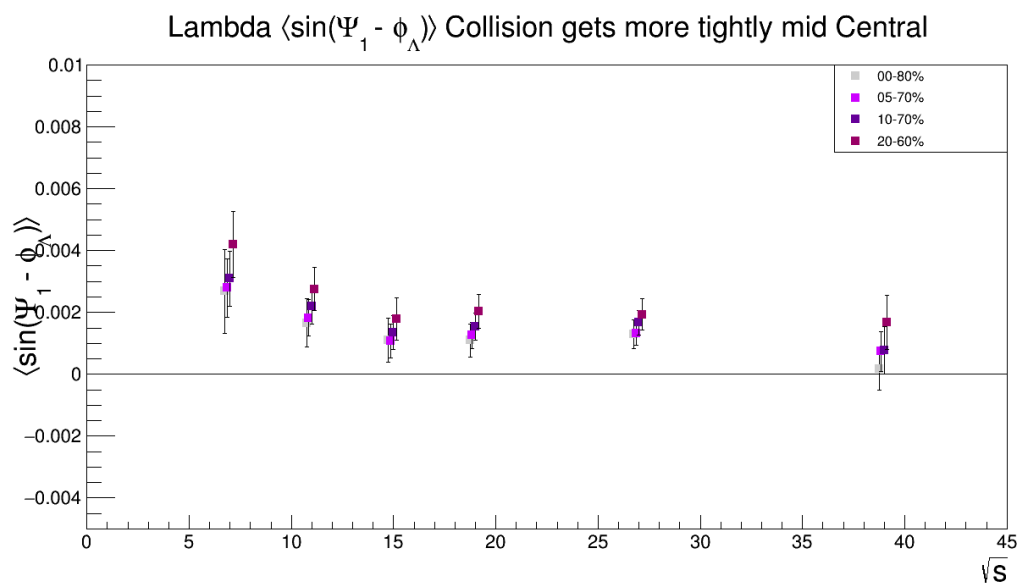


Fig. 123: $\langle \sin(\Psi_1 - \phi_{\Lambda}^*) \rangle$ as collisions get more mid-central

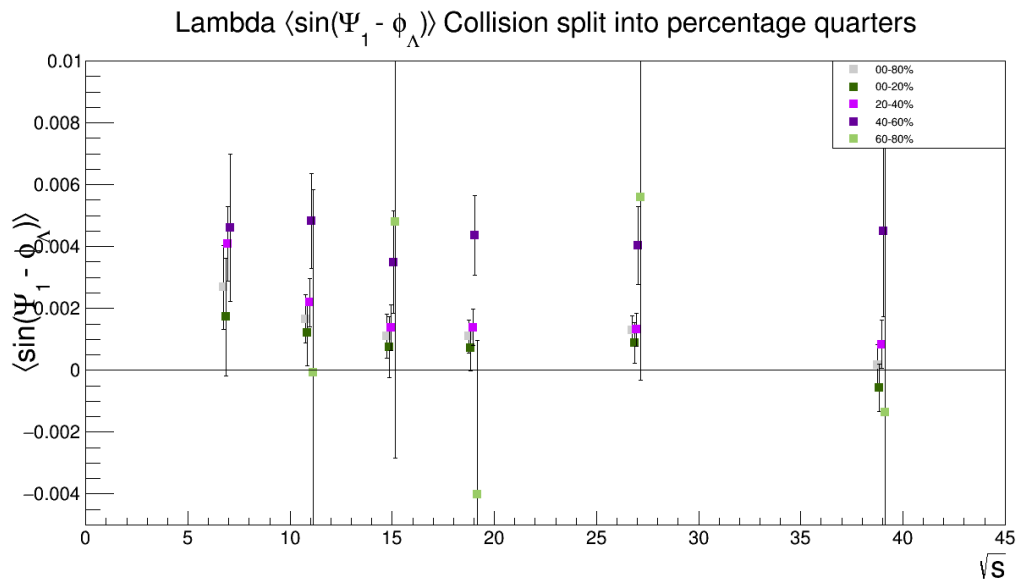


Fig. 124: $\langle \sin(\Psi_1 - \phi_\Lambda^*) \rangle$ for bins of 20% centrality

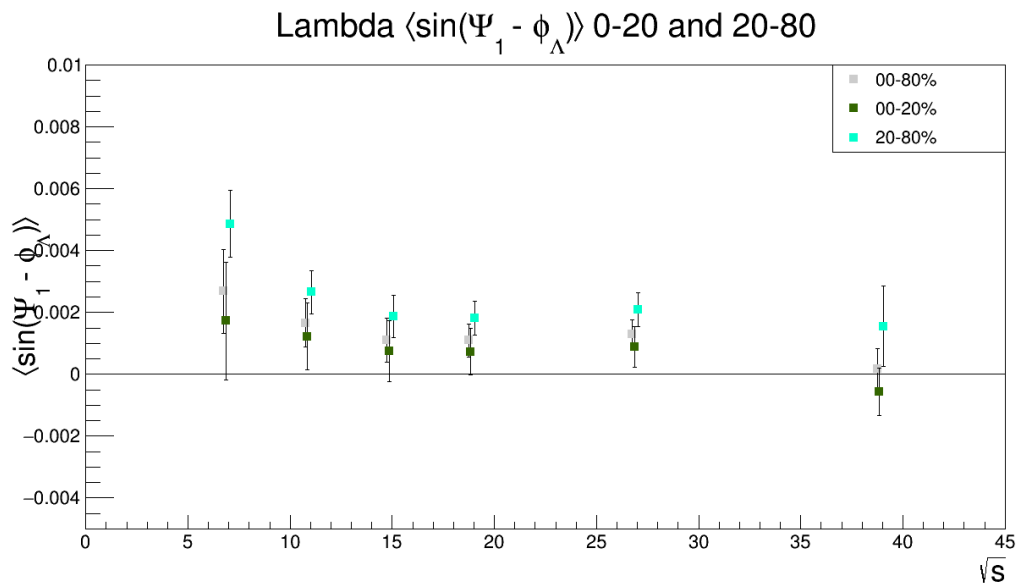


Fig. 125: $\langle \sin(\Psi_1 - \phi_\Lambda^*) \rangle$ for 0-20% and 20-80% centrality

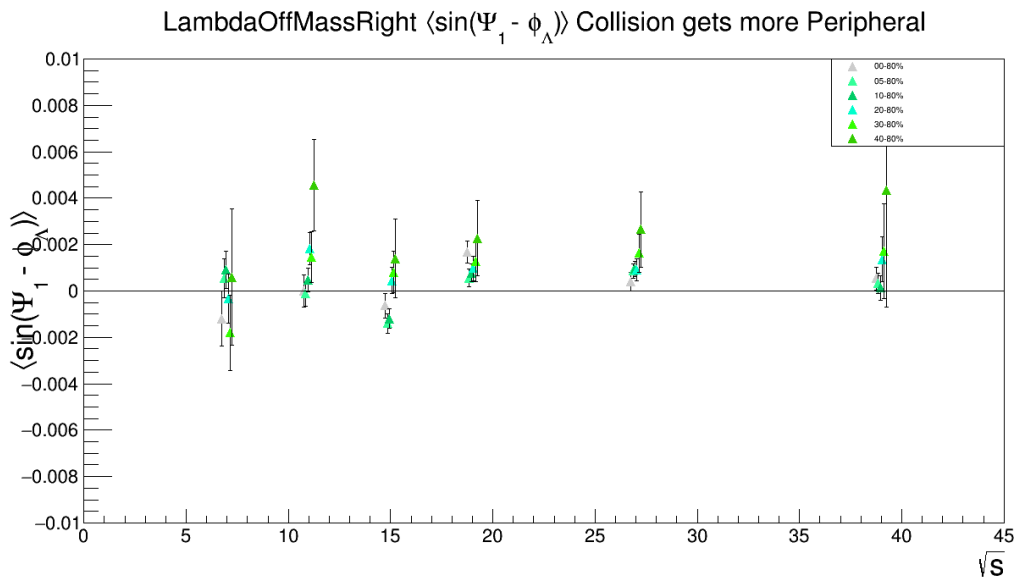


Fig. 126: $\langle \sin(\Psi_1 - \phi_\Lambda^*) \rangle$ right of mass peak ($m_{\text{inv}} > m_\Lambda$) as the collision gets more peripheral

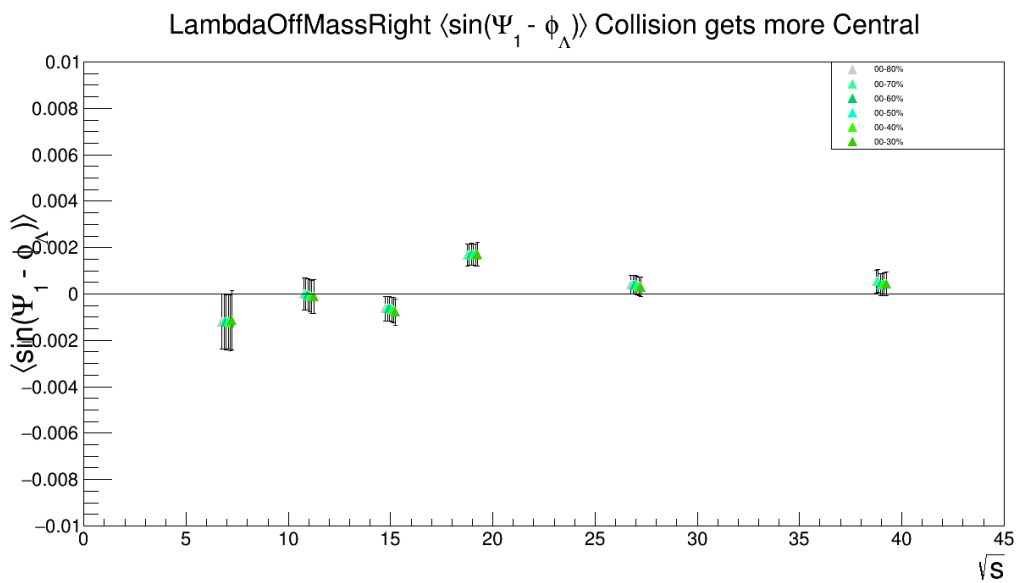


Fig. 127: $\langle \sin(\Psi_1 - \phi_\Lambda^*) \rangle$ right of mass peak ($m_{\text{inv}} > m_\Lambda$) as the collision gets more central

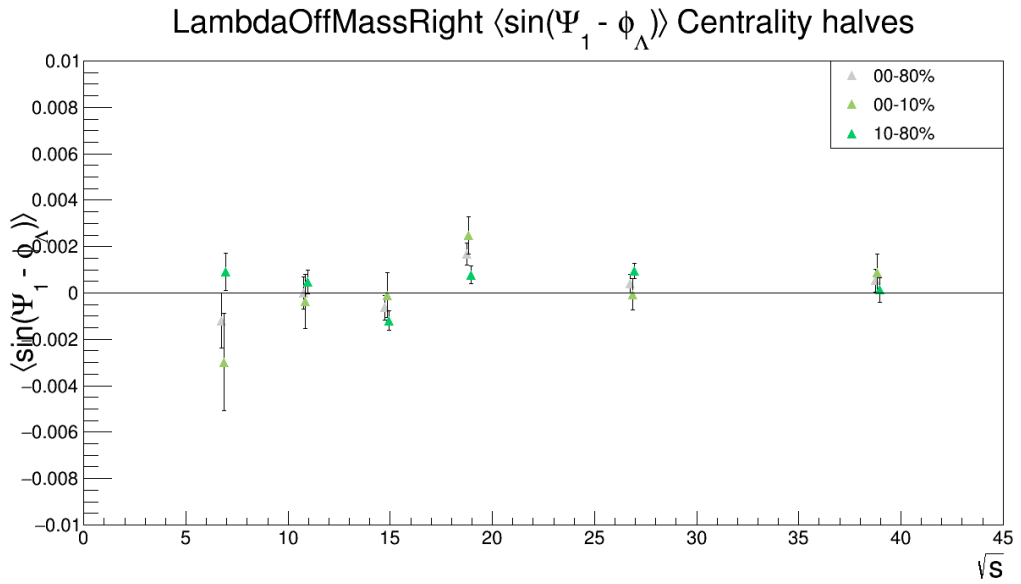


Fig. 128: $\langle \sin(\Psi_1 - \phi_\Lambda^*) \rangle$ right of mass peak ($m_{\text{inv}} > m_\Lambda$) for rough halves of centrality by yield

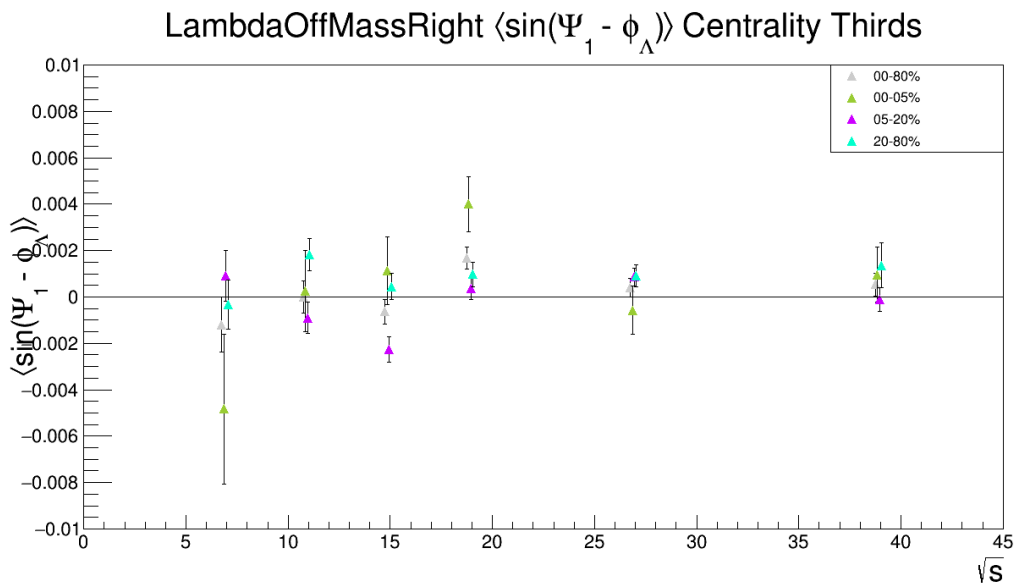


Fig. 129: $\langle \sin(\Psi_1 - \phi_\Lambda^*) \rangle$ right of mass peak ($m_{\text{inv}} > m_\Lambda$) for rough thirds of centrality by yield

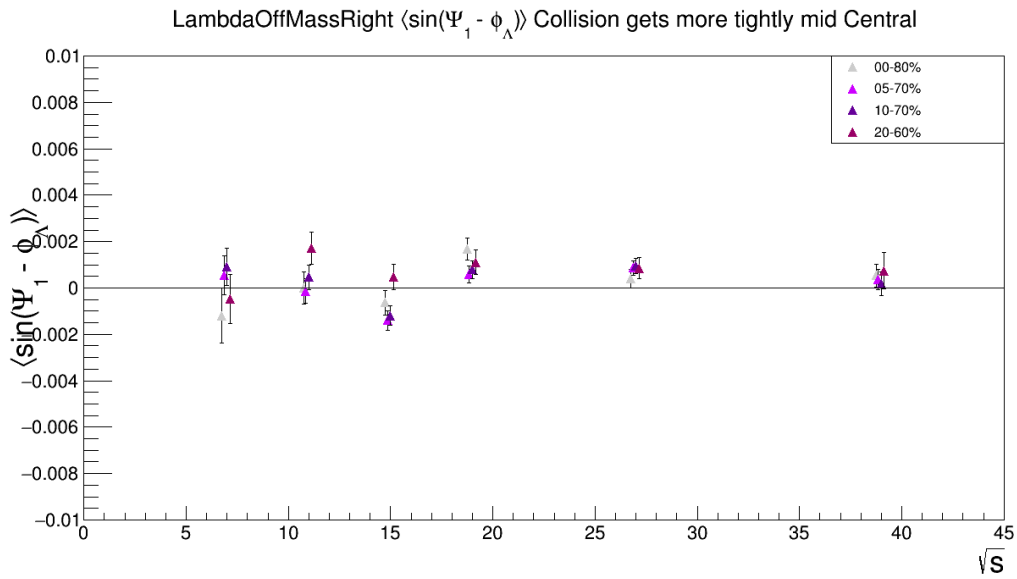


Fig. 130: $\langle \sin(\Psi_1 - \phi_\Lambda^*) \rangle$ right of mass peak ($m_{\text{inv}} > m_\Lambda$) as collisions get more mid-central

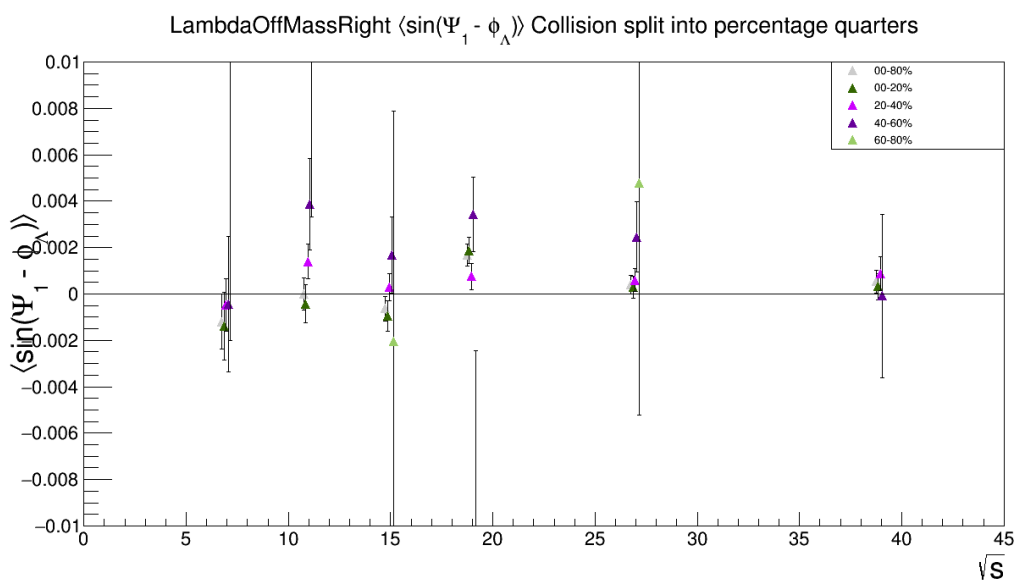


Fig. 131: $\langle \sin(\Psi_1 - \phi_\Lambda^*) \rangle$ right of mass peak ($m_{\text{inv}} > m_\Lambda$) for bins of 20% centrality

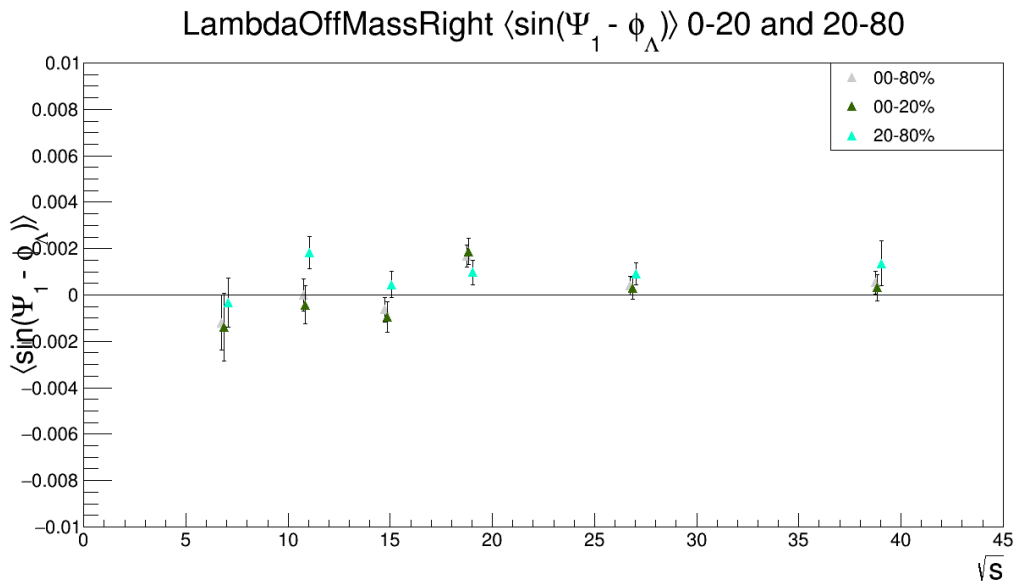


Fig. 132: $\langle \sin(\Psi_1 - \phi_\Lambda^*) \rangle$ right of mass peak ($m_{\text{inv}} > m_\Lambda$) for 0-20% and 20-80% centrality

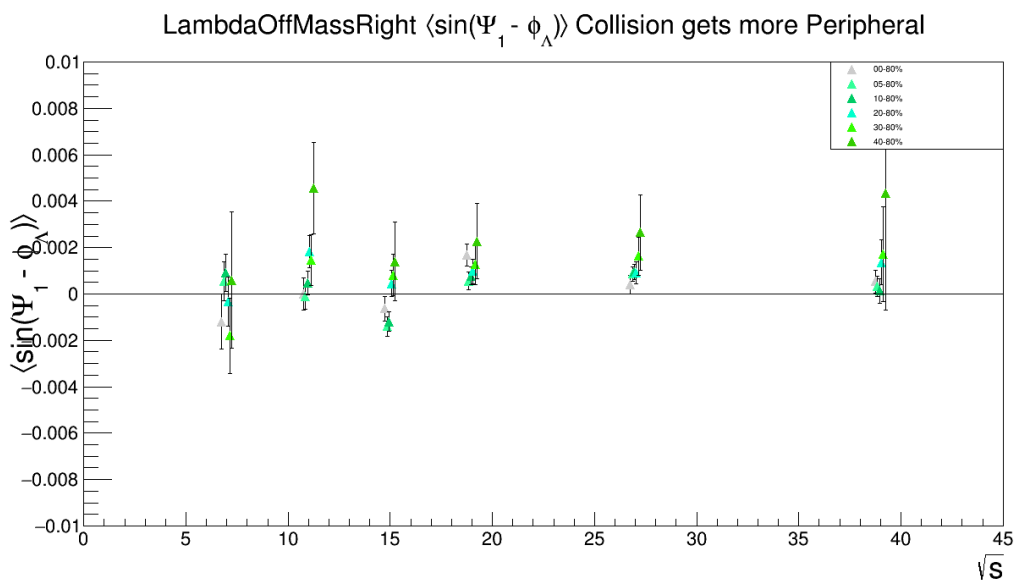


Fig. 133: $\langle \sin(\Psi_1 - \phi_\Lambda^*) \rangle$ left of mass peak ($m_{\text{inv}} < m_\Lambda$) as the collision gets more peripheral

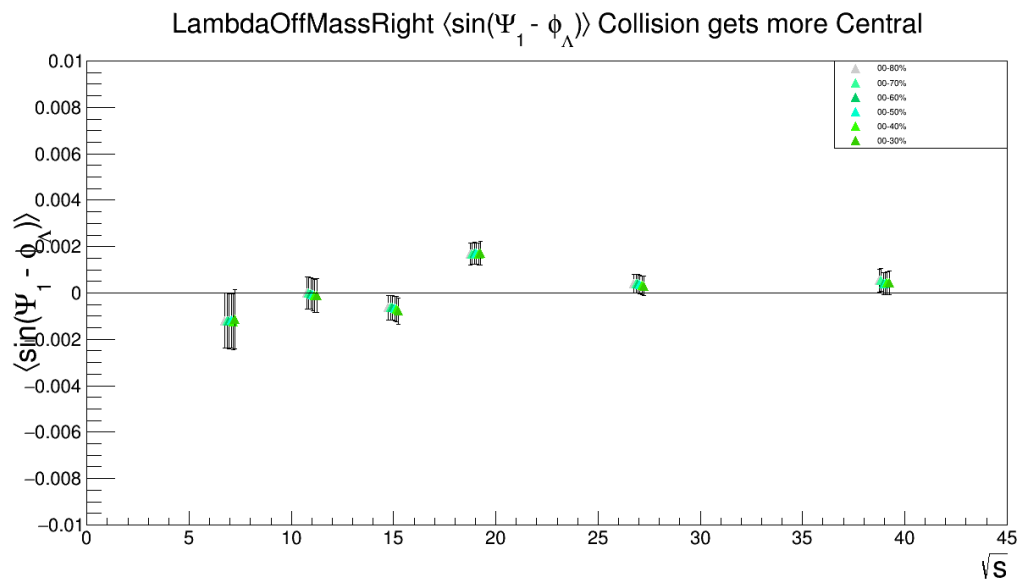


Fig. 134: $\langle \sin(\Psi_1 - \phi_\Lambda^*) \rangle$ left of mass peak ($m_{\text{inv}} < m_\Lambda$) as the collision gets more central

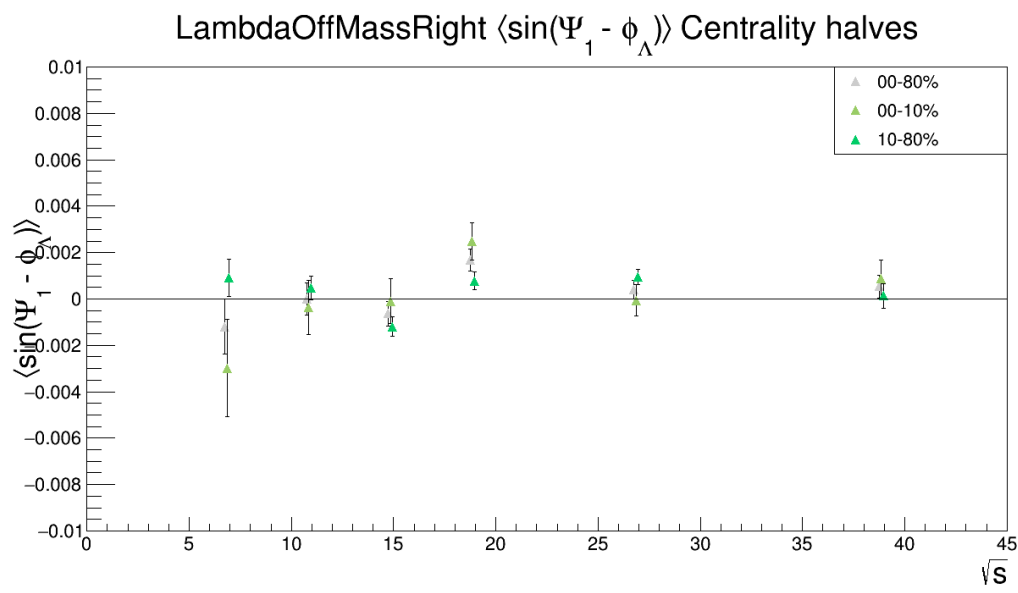


Fig. 135: $\langle \sin(\Psi_1 - \phi_\Lambda^*) \rangle$ left of mass peak ($m_{\text{inv}} < m_\Lambda$) for rough halves of centrality by yield

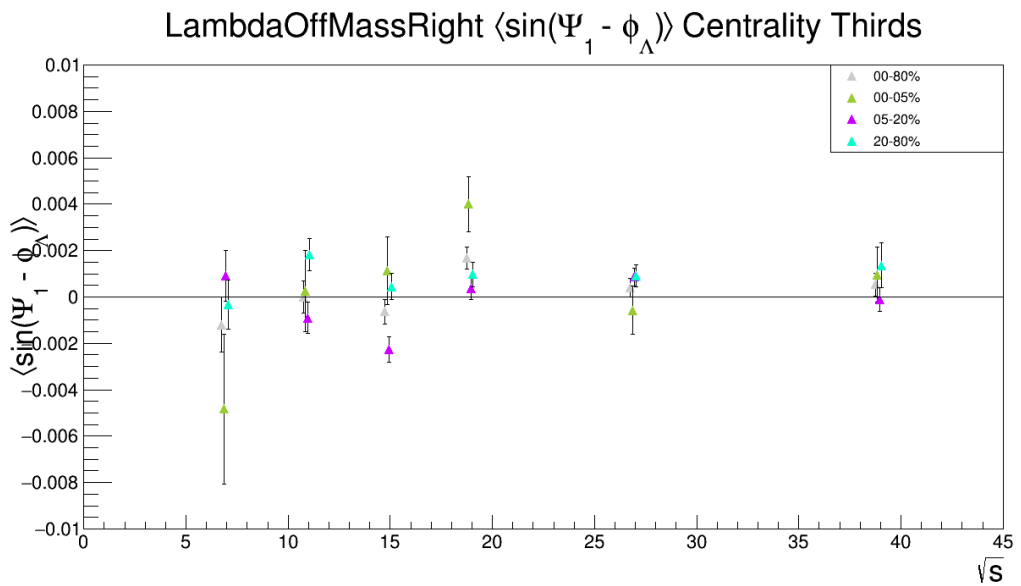


Fig. 136: $\langle \sin(\Psi_1 - \phi_\Lambda^*) \rangle$ left of mass peak ($m_{\text{inv}} < m_\Lambda$) for rough thirds of centrality by yield

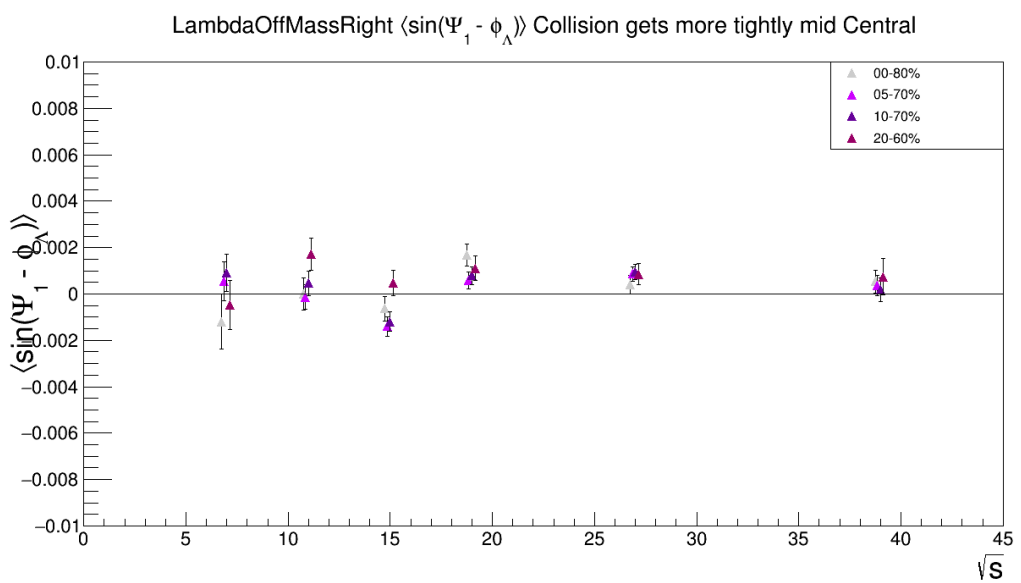


Fig. 137: $\langle \sin(\Psi_1 - \phi_\Lambda^*) \rangle$ left of mass peak ($m_{\text{inv}} < m_\Lambda$) as collisions get more mid-central

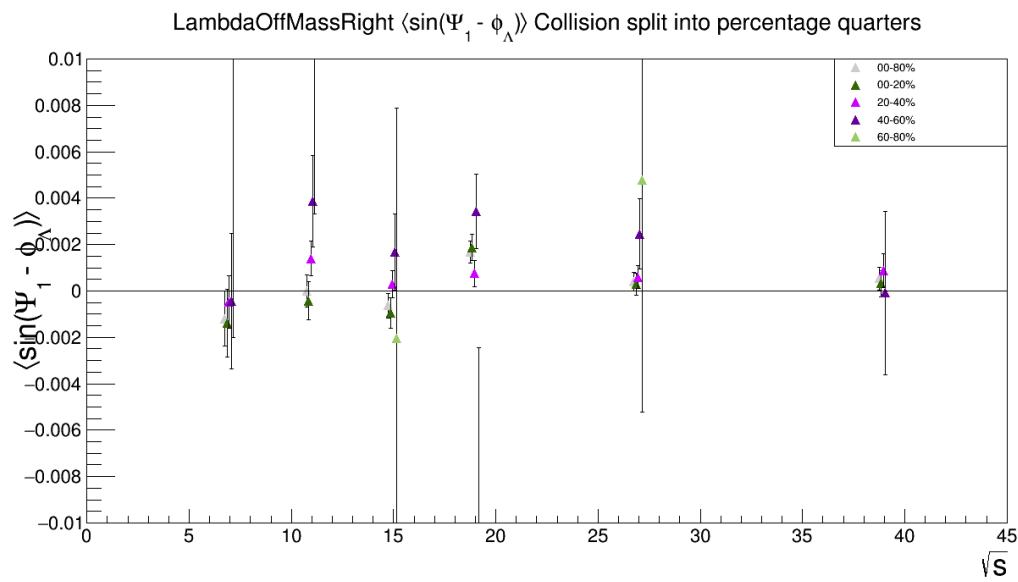


Fig. 138: $\langle \sin(\Psi_1 - \phi_\Lambda^*) \rangle$ left of mass peak ($m_{\text{inv}} < m_\Lambda$) for bins of 20% centrality

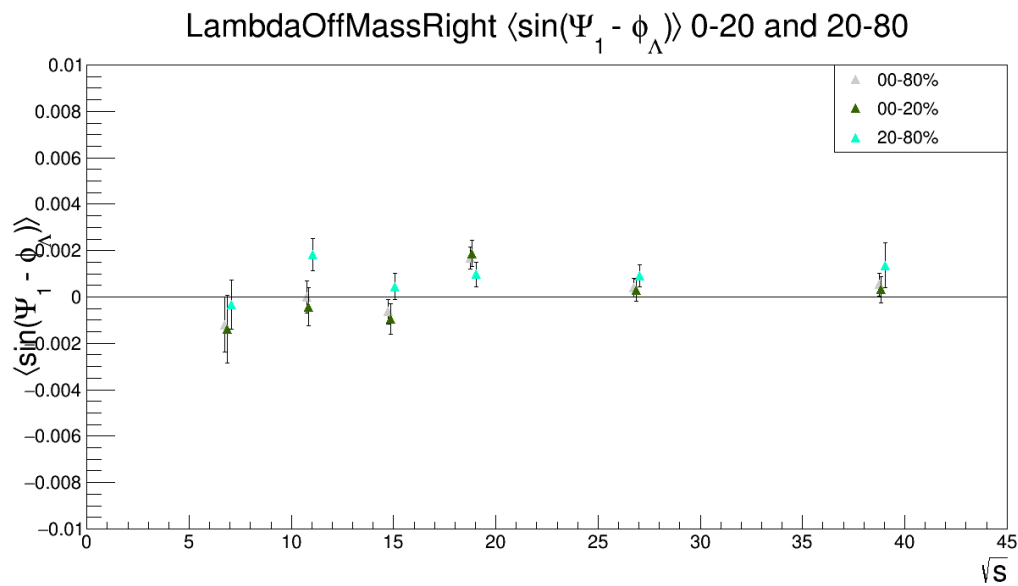


Fig. 139: $\langle \sin(\Psi_1 - \phi_\Lambda^*) \rangle$ left of mass peak ($m_{\text{inv}} < m_\Lambda$) for 0-20% and 20-80% centrality

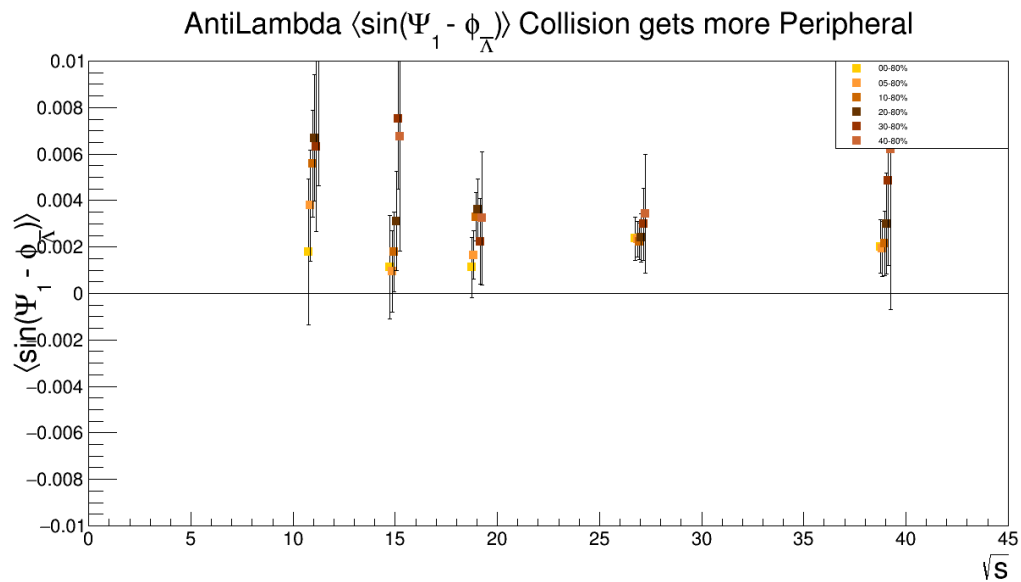


Fig. 140: $\langle \sin(\Psi_1 - \phi_{\bar{\Lambda}}^*) \rangle$ as the collision gets more peripheral

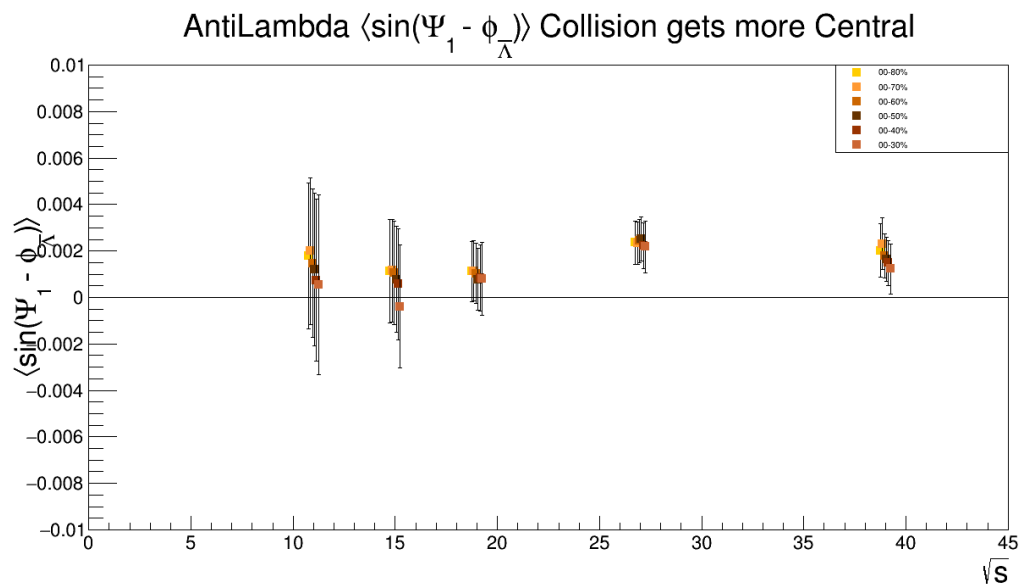


Fig. 141: $\langle \sin(\Psi_1 - \phi_{\bar{\Lambda}}^*) \rangle$ as the collision gets more central

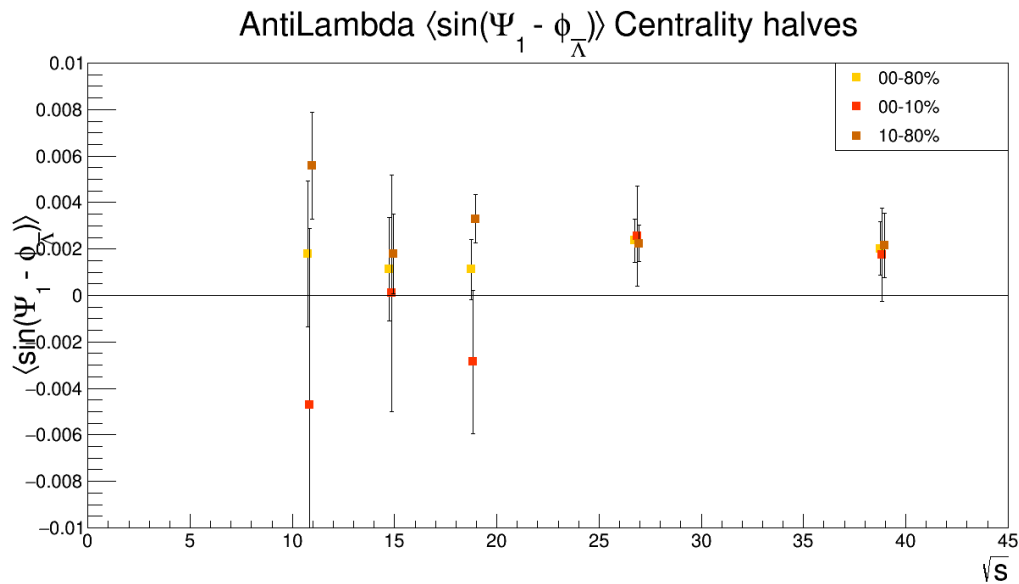


Fig. 142: $\langle \sin(\Psi_1 - \phi_{\bar{\Lambda}}^*) \rangle$ for rough halves of centrality by yield

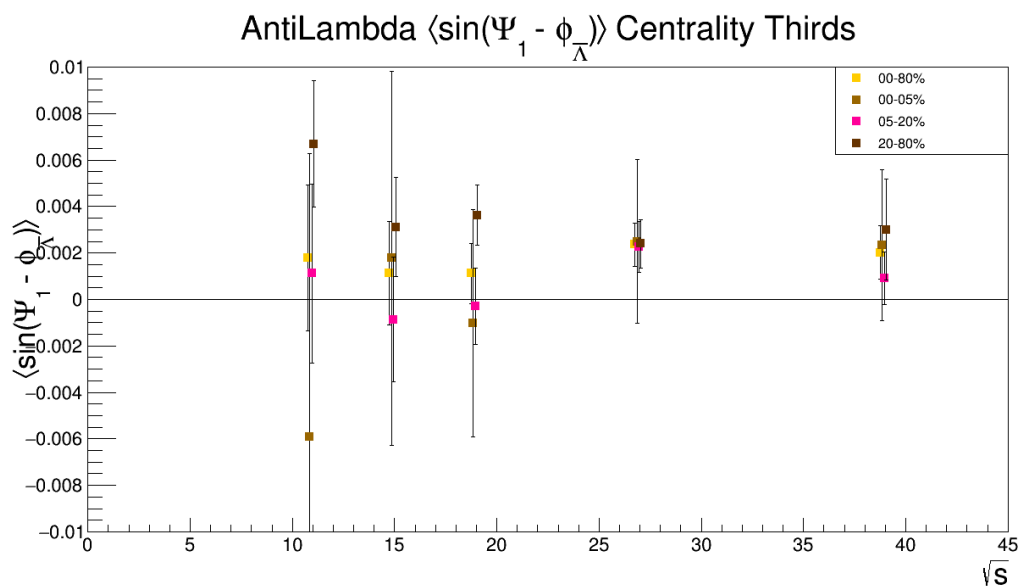


Fig. 143: $\langle \sin(\Psi_1 - \phi_{\bar{\Lambda}}^*) \rangle$ for rough thirds of centrality by yield

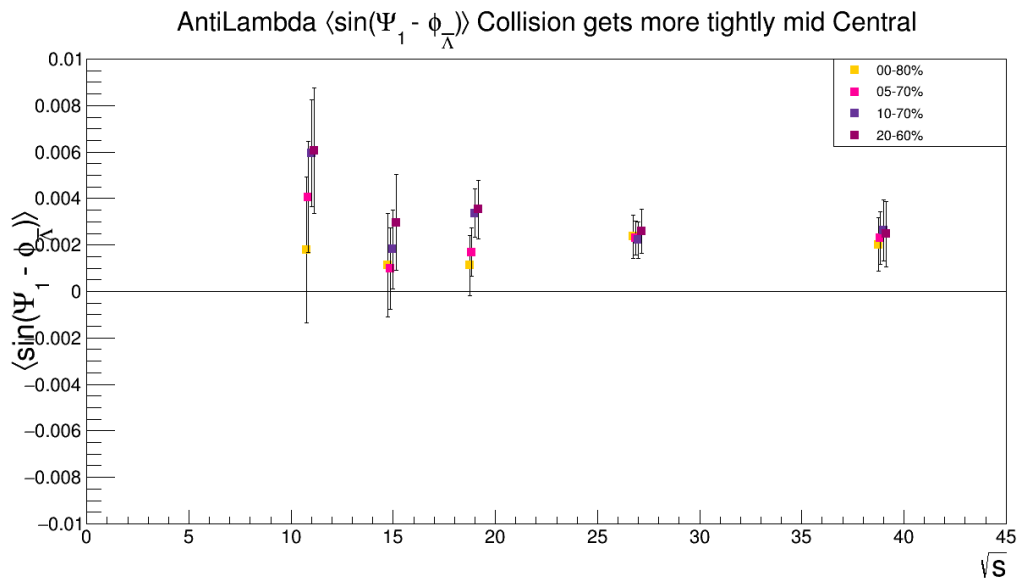


Fig. 144: $\langle \sin(\Psi_1 - \phi_{\bar{\Lambda}}^*) \rangle$ as collisions get more mid-central

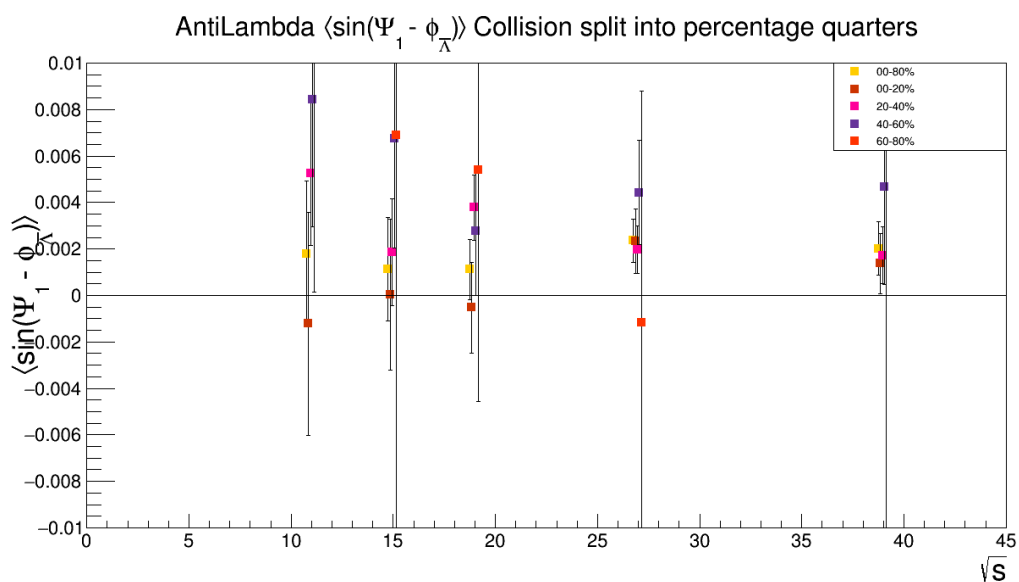


Fig. 145: $\langle \sin(\Psi_1 - \phi_{\bar{\Lambda}}^*) \rangle$ for bins of 20% centrality

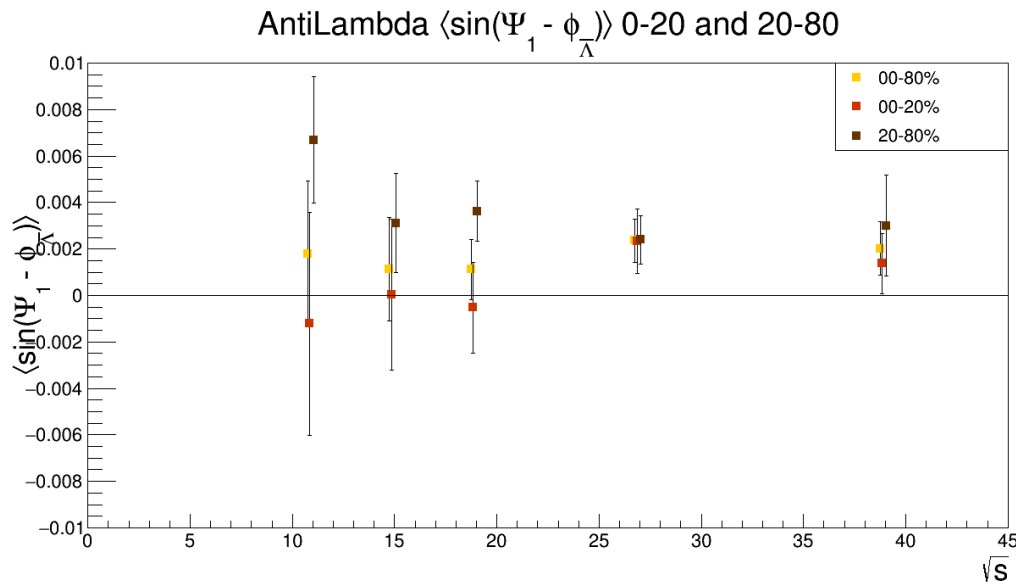


Fig. 146: $\langle \sin(\Psi_1 - \phi_{\bar{\Lambda}}^*) \rangle$ for 0-20% and 20-80% centrality

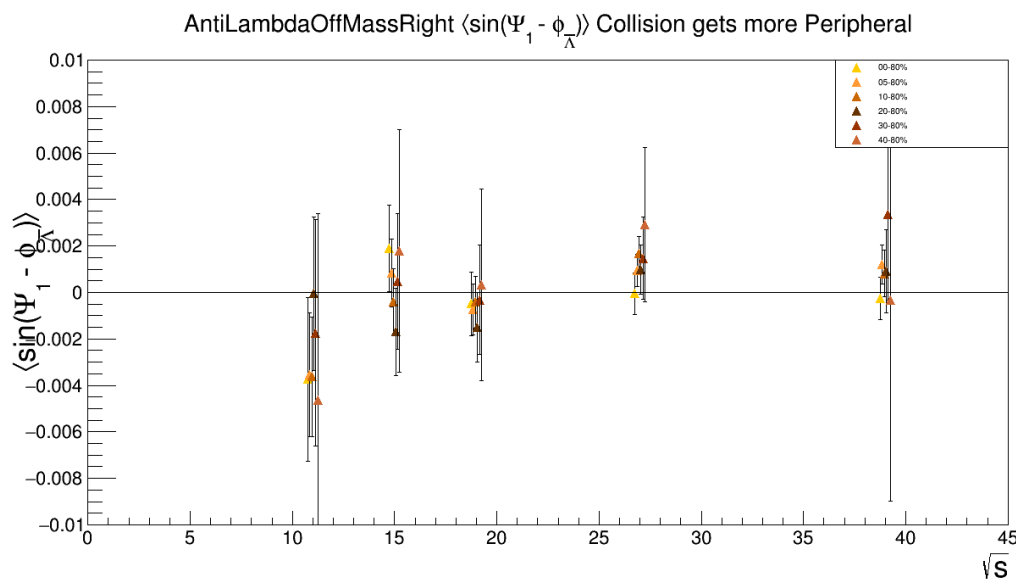


Fig. 147: $\langle \sin(\Psi_1 - \phi_{\bar{\Lambda}}^*) \rangle$ right of mass peak ($m_{\text{inv}} > m_{\bar{\Lambda}}$) as the collision gets more peripheral

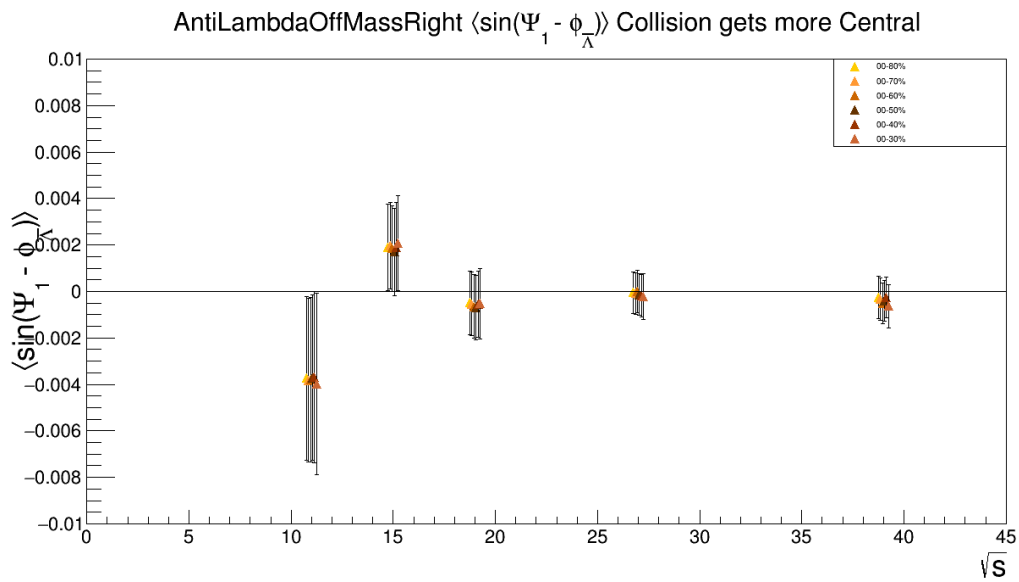


Fig. 148: $\langle \sin(\Psi_1 - \phi_{\bar{\Lambda}}^*) \rangle$ right of mass peak ($m_{\text{inv}} > m_{\Lambda}$) as the collision gets more central

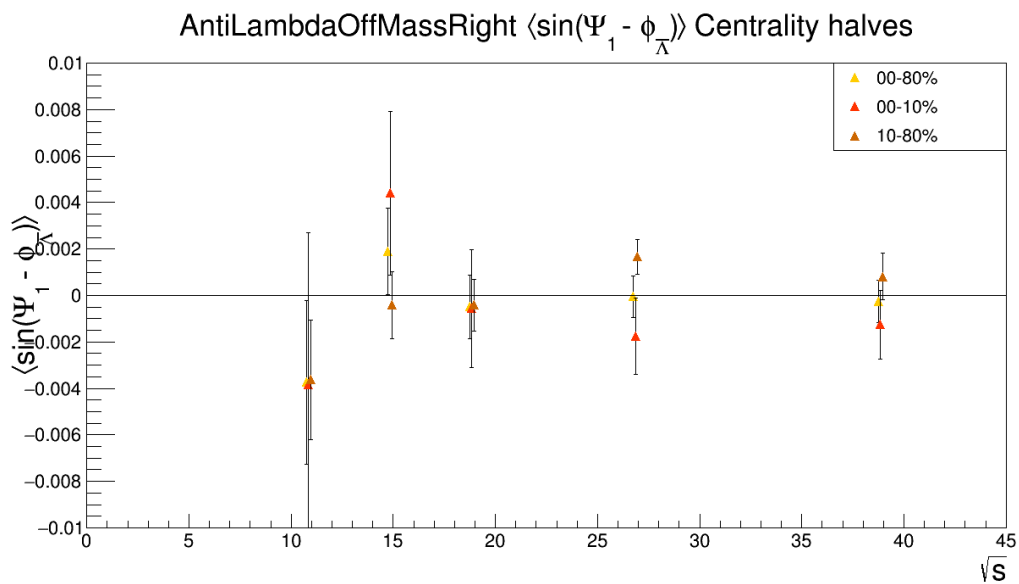


Fig. 149: $\langle \sin(\Psi_1 - \phi_{\bar{\Lambda}}^*) \rangle$ right of mass peak ($m_{\text{inv}} > m_{\Lambda}$) for rough halves of centrality by yield

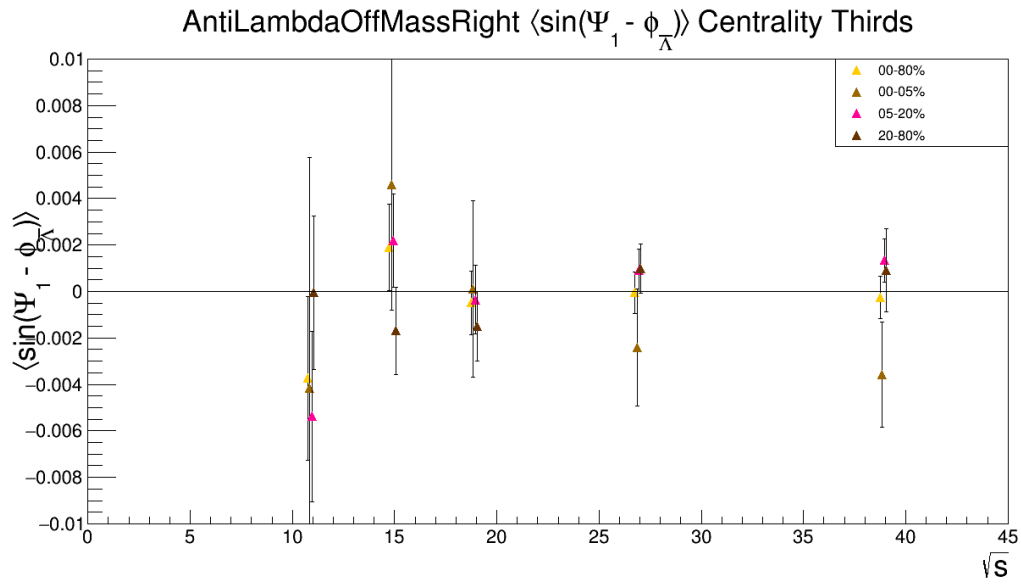


Fig. 150: $\langle \sin(\Psi_1 - \phi_{\bar{\Lambda}}^*) \rangle$ right of mass peak ($m_{\text{inv}} > m_{\Lambda}$) for rough thirds of centrality by yield

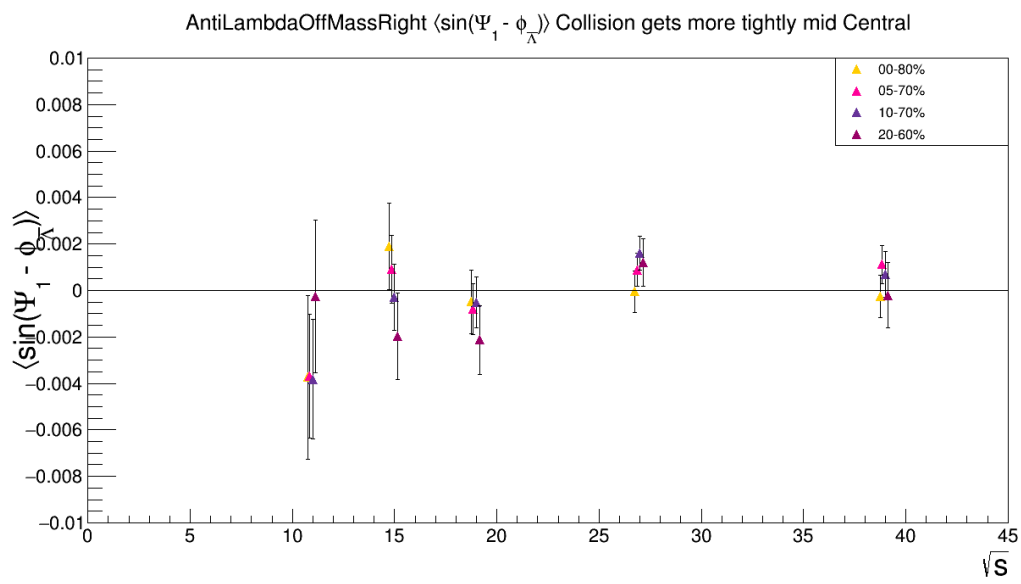


Fig. 151: $\langle \sin(\Psi_1 - \phi_{\bar{\Lambda}}^*) \rangle$ right of mass peak ($m_{\text{inv}} > m_{\Lambda}$) as collisions get more mid-central

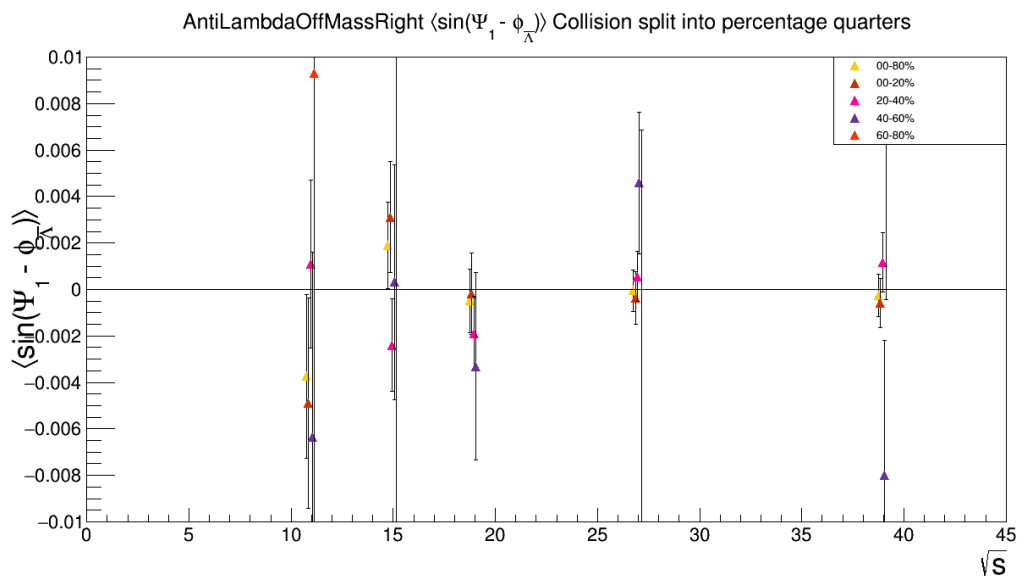


Fig. 152: $\langle \sin(\Psi_1 - \phi_{\bar{\Lambda}}^*) \rangle$ right of mass peak ($m_{\text{inv}} > m_{\Lambda}$) for bins of 20% centrality

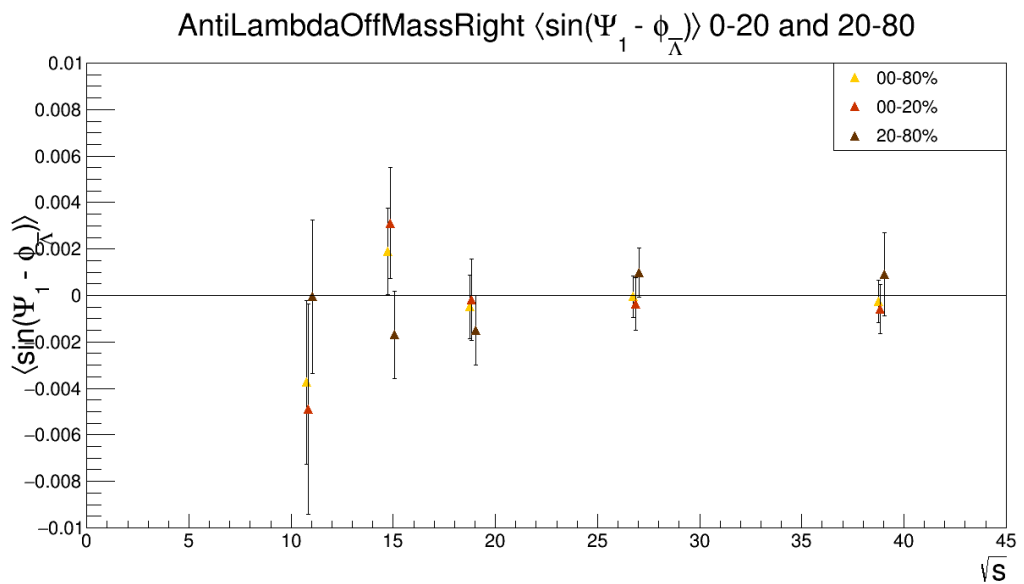


Fig. 153: $\langle \sin(\Psi_1 - \phi_{\bar{\Lambda}}^*) \rangle$ right of mass peak ($m_{\text{inv}} > m_{\Lambda}$) for 0-20% and 20-80% centrality

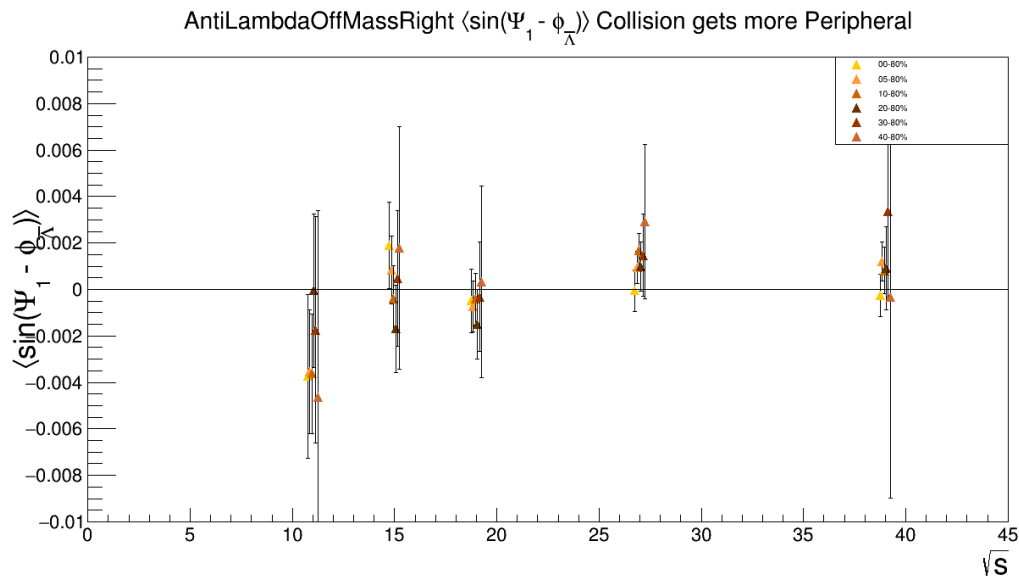


Fig. 154: $\langle \sin(\Psi_1 - \phi_{\bar{\Lambda}}^*) \rangle$ left of mass peak ($m_{\text{inv}} < m_{\Lambda}$) as the collision gets more peripheral

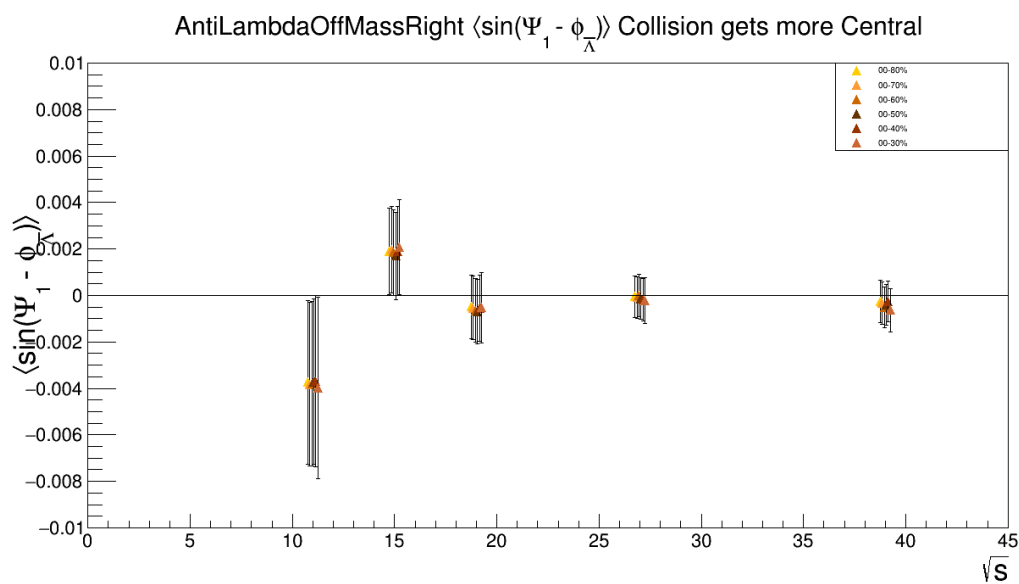


Fig. 155: $\langle \sin(\Psi_1 - \phi_{\bar{\Lambda}}^*) \rangle$ left of mass peak ($m_{\text{inv}} < m_{\Lambda}$) as the collision gets more central

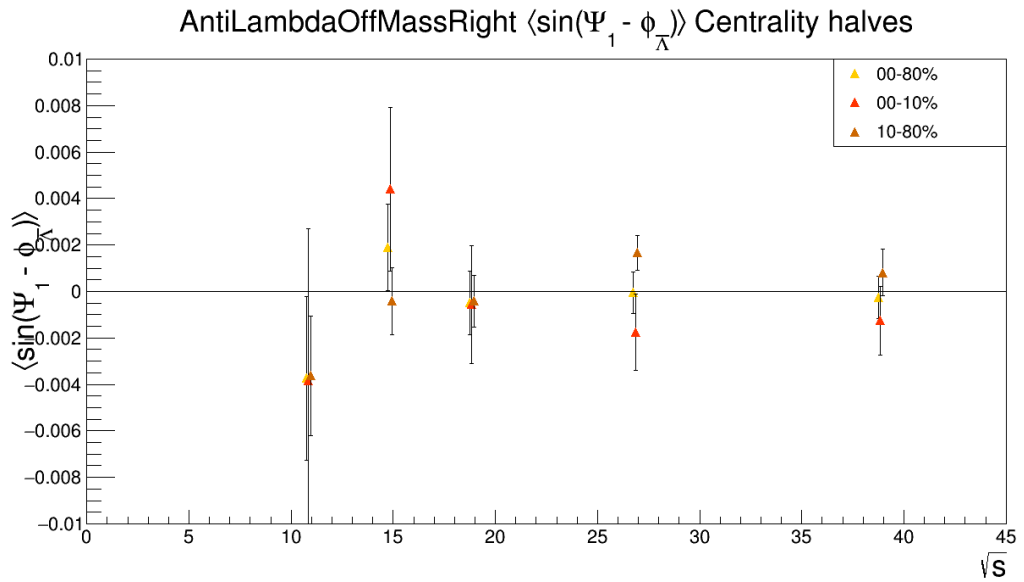


Fig. 156: $\langle \sin(\Psi_1 - \phi_{\bar{\Lambda}}^*) \rangle$ left of mass peak ($m_{\text{inv}} < m_{\Lambda}$) for rough halves of centrality by yield

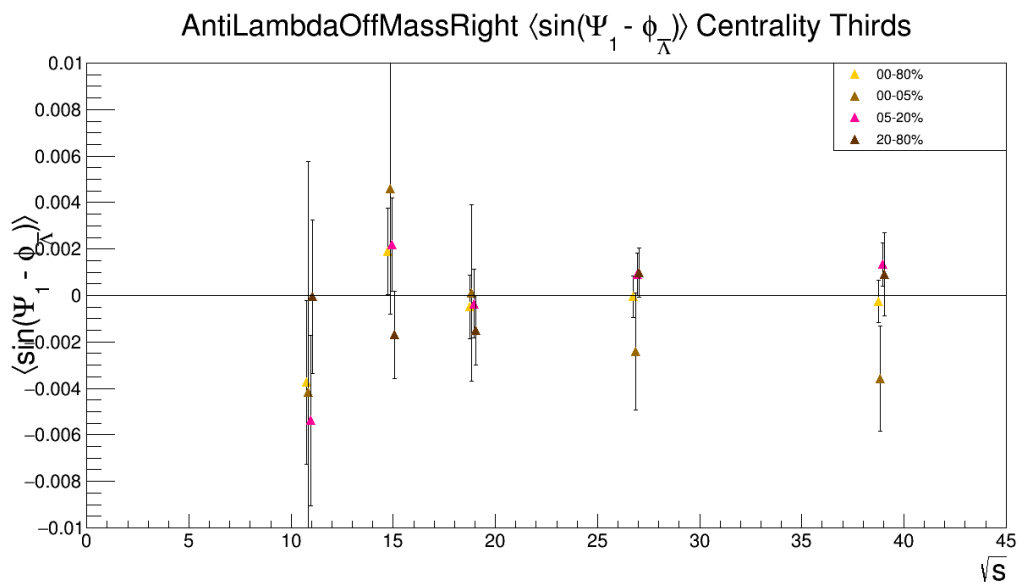


Fig. 157: $\langle \sin(\Psi_1 - \phi_{\bar{\Lambda}}^*) \rangle$ left of mass peak ($m_{\text{inv}} < m_{\Lambda}$) for rough thirds of centrality by yield

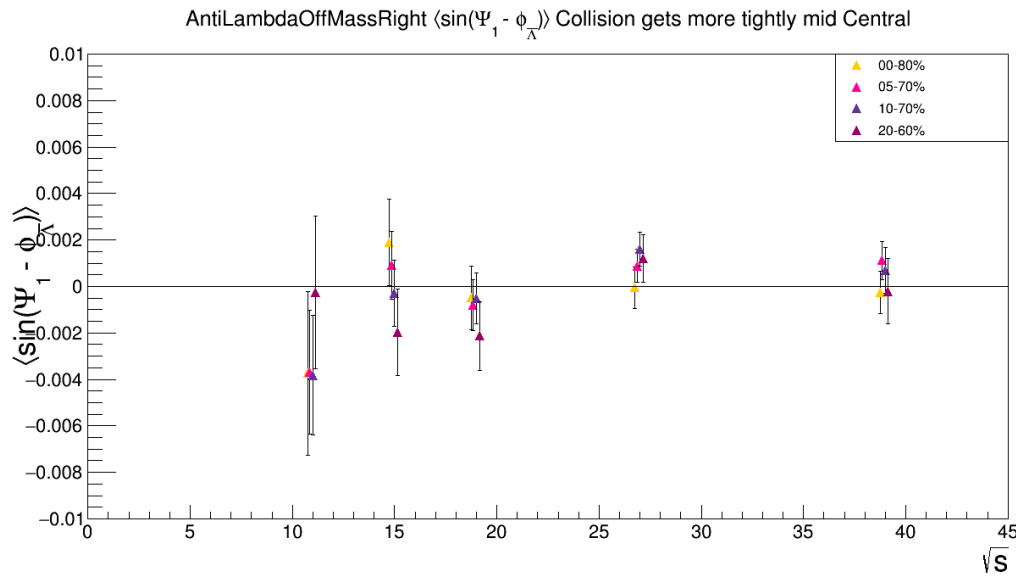


Fig. 158: $\langle \sin(\Psi_1 - \phi_{\bar{\Lambda}}^*) \rangle$ left of mass peak ($m_{\text{inv}} < m_{\Lambda}$) as collisions get more mid-central

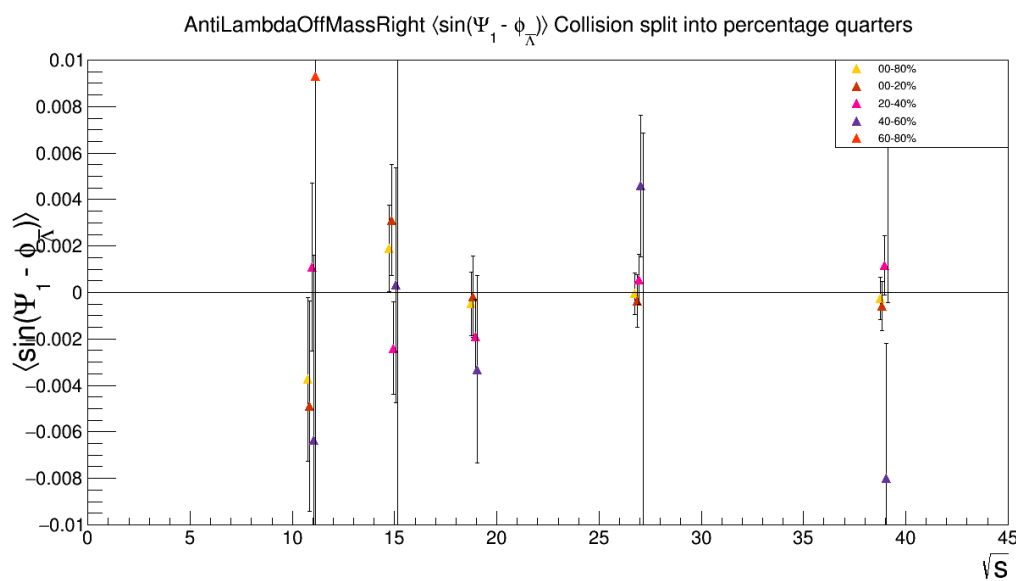


Fig. 159: $\langle \sin(\Psi_1 - \phi_{\bar{\Lambda}}^*) \rangle$ left of mass peak ($m_{\text{inv}} < m_{\Lambda}$) for bins of 20% centrality

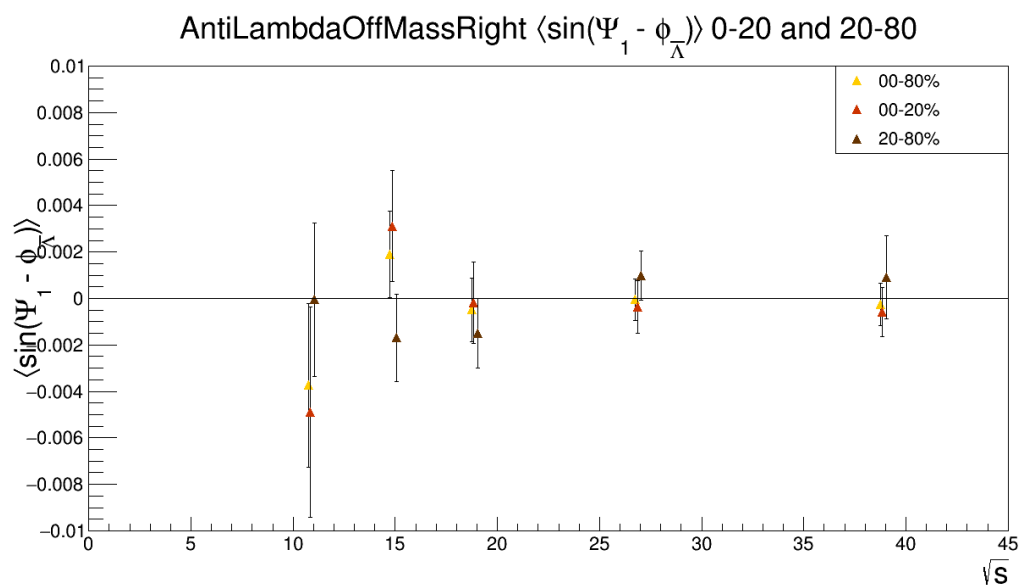


Fig. 160: $\langle \sin(\Psi_1 - \phi_{\bar{\Lambda}}^*) \rangle$ left of mass peak ($m_{\text{inv}} < m_{\Lambda}$) for 0-20% and 20-80% centrality

5.2 Energy

Higher momentum Lambdas have the opportunity to carry away a large fraction of the excess of angular momentum of the fireball. This may be energetically favored. It is generally predicted that the signal would increase with energy. What is shown here is the results when an attempt is made to split the data into statistically equal halves and thirds of Lambda energy (in GeV). The intentions of these cuts to make equal fractions may not be particularly well borne out because the cuts were chosen via histograms (it is a binning issue).

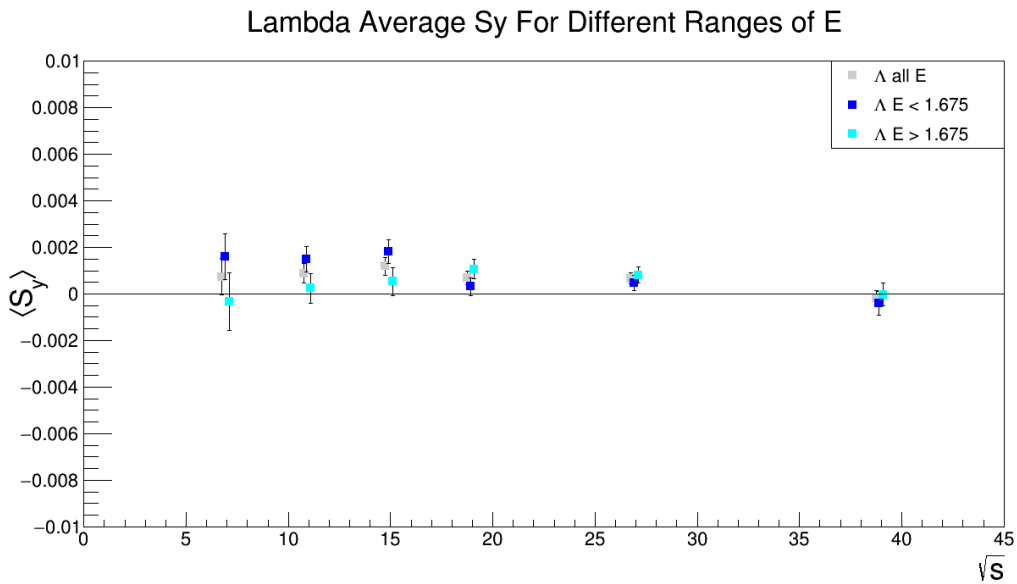


Fig. 161: Λ polarization cut into two energy bins. Energies quoted in legend are in GeV.

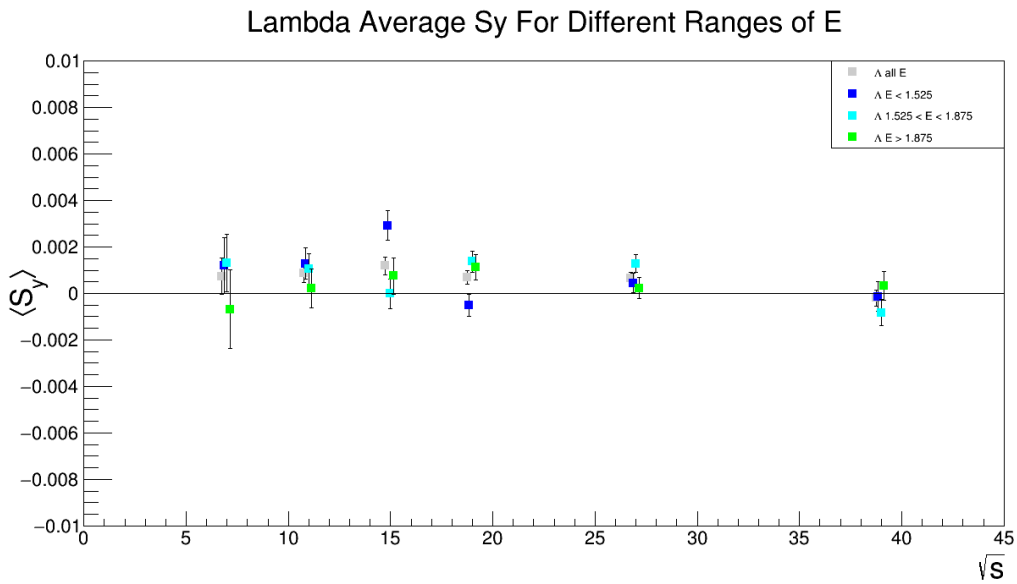


Fig. 162: Λ polarization cut into three energy bins. Energies quoted in legend are in GeV.

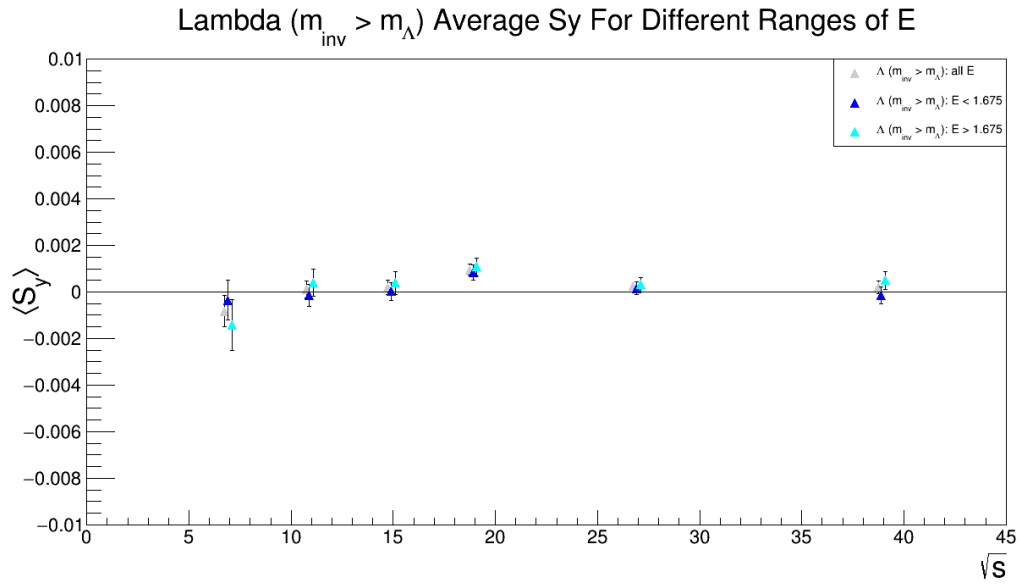


Fig. 163: Λ right of mass peak ($m_{\text{inv}} > m_{\Lambda}$) polarization cut into two energy bins. Energies quoted in legend are in GeV.

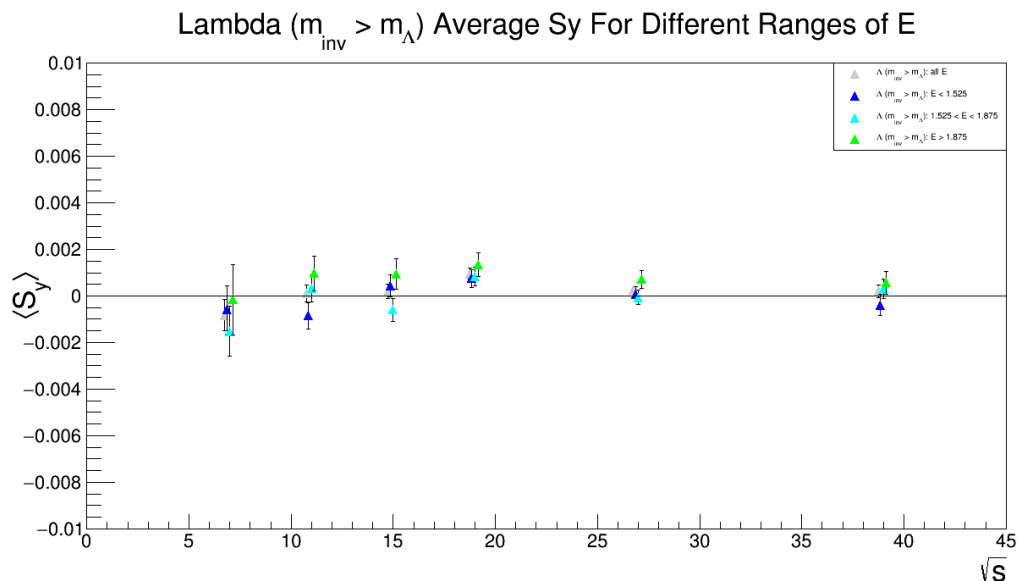


Fig. 164: Λ right of mass peak ($m_{\text{inv}} > m_{\Lambda}$) polarization cut into three energy bins. Energies quoted in legend are in GeV.

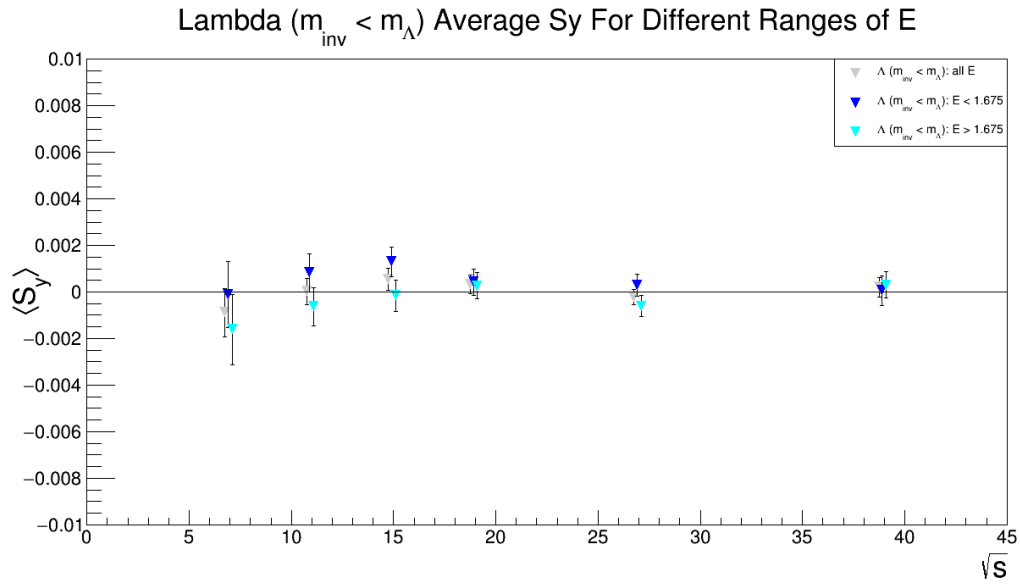


Fig. 165: Λ left of mass peak ($m_{inv} < m_\Lambda$) polarization cut into two energy bins. Energies quoted in legend are in GeV.

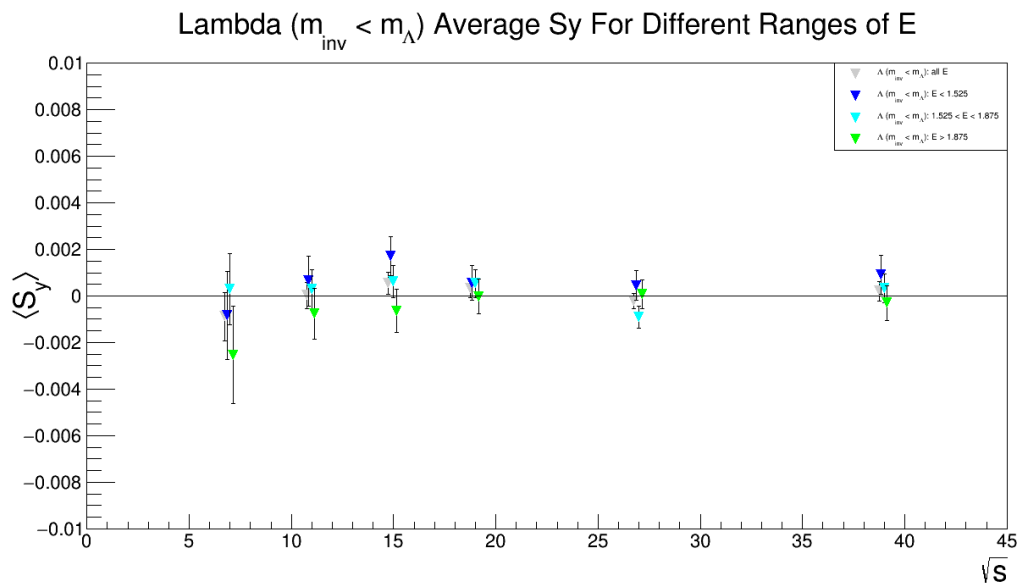


Fig. 166: Λ left of mass peak ($m_{inv} < m_\Lambda$) polarization cut into three energy bins. Energies quoted in legend are in GeV.

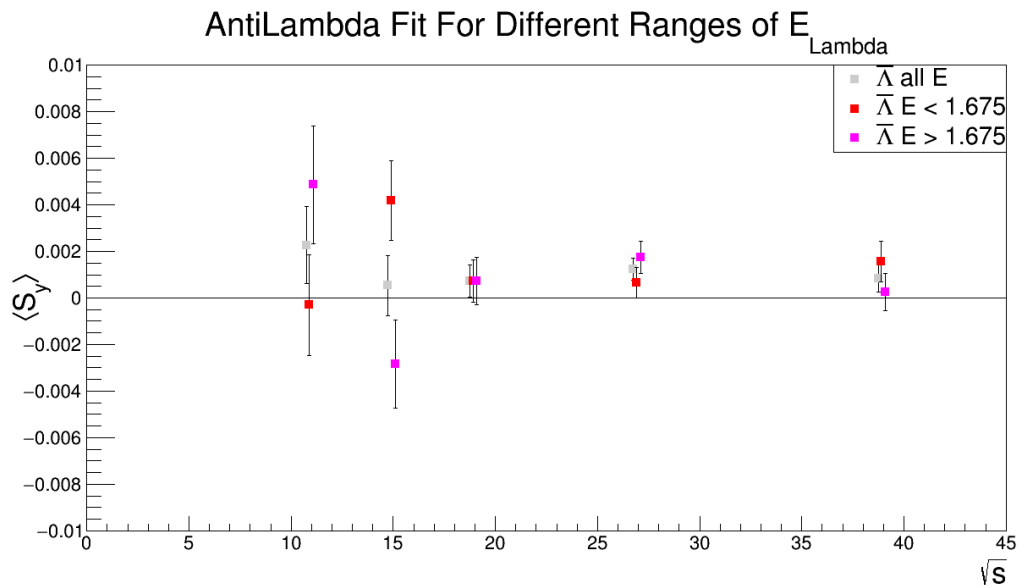


Fig. 167: $\bar{\Lambda}$ polarization cut into two energy bins. Energies quoted in legend are in GeV.

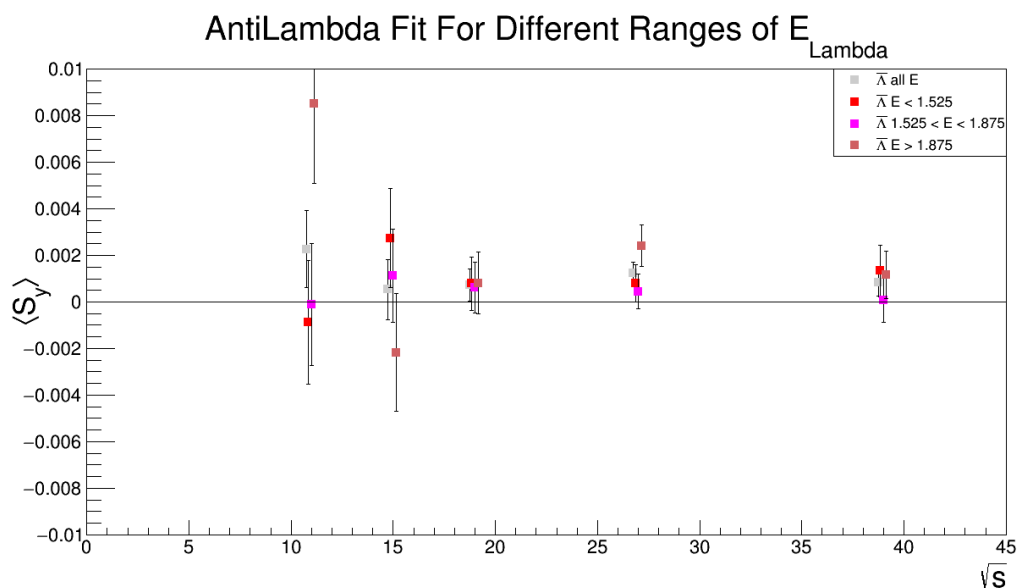


Fig. 168: $\bar{\Lambda}$ polarization cut into three energy bins. Energies quoted in legend are in GeV.

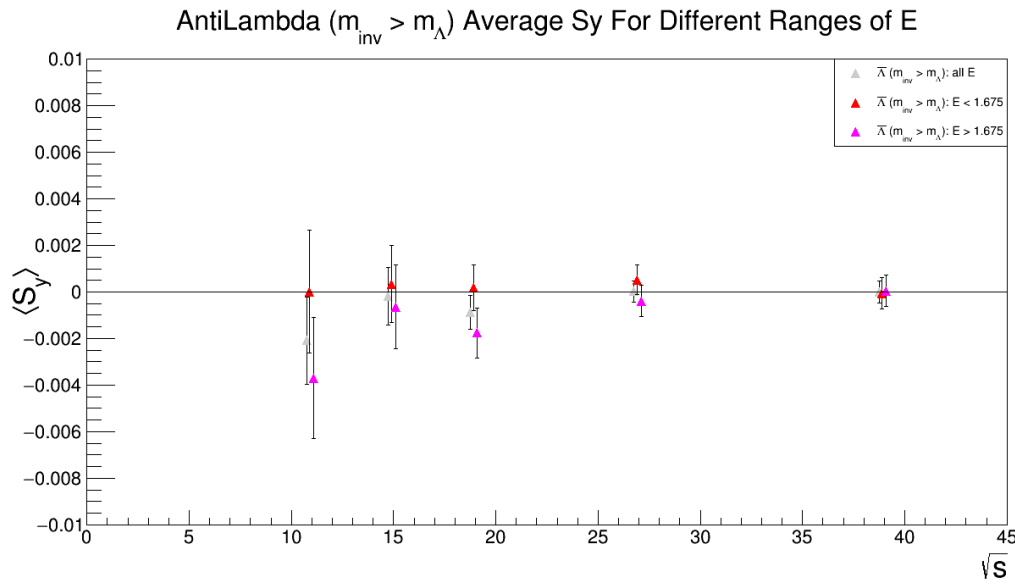


Fig. 169: $\bar{\Lambda}$ right of mass peak ($m_{inv} > m_\Lambda$) polarization cut into two energy bins. Energies quoted in legend are in GeV.

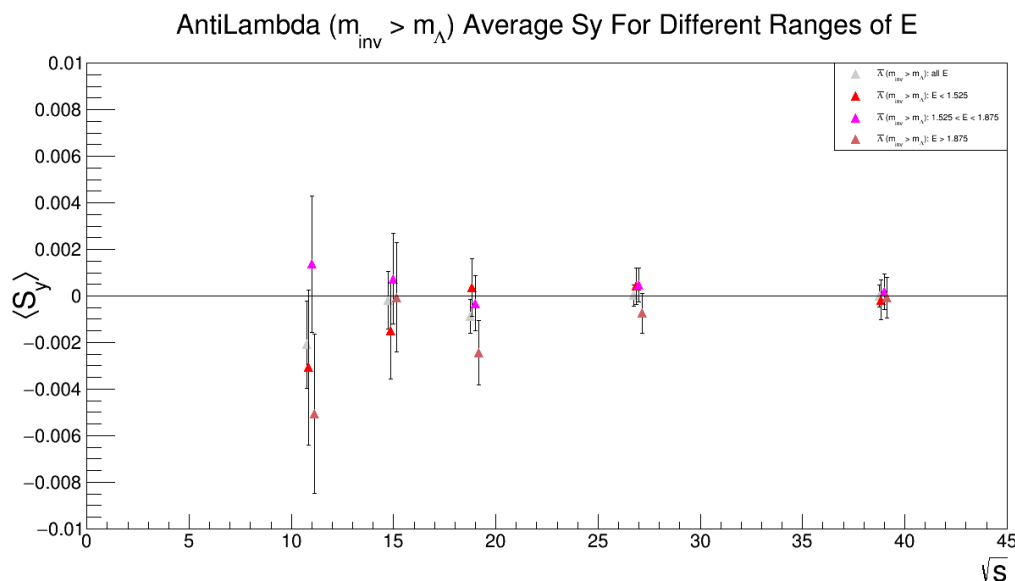


Fig. 170: $\bar{\Lambda}$ right of mass peak ($m_{inv} > m_\Lambda$) polarization cut into three energy bins. Energies quoted in legend are in GeV.

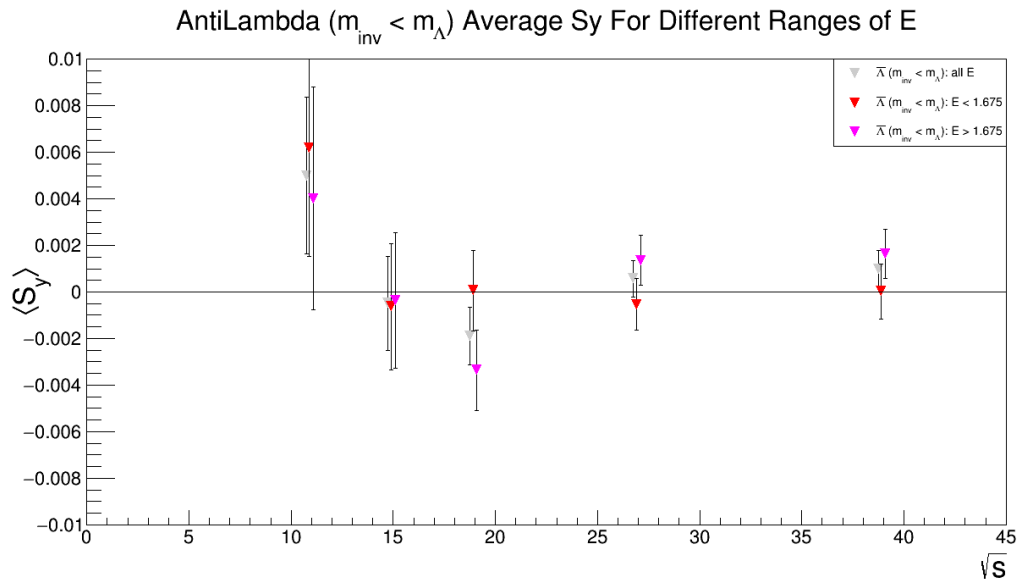


Fig. 171: $\bar{\Lambda}$ left of mass peak ($m_{inv} < m_\Lambda$) polarization cut into two energy bins. Energies quoted in legend are in GeV.

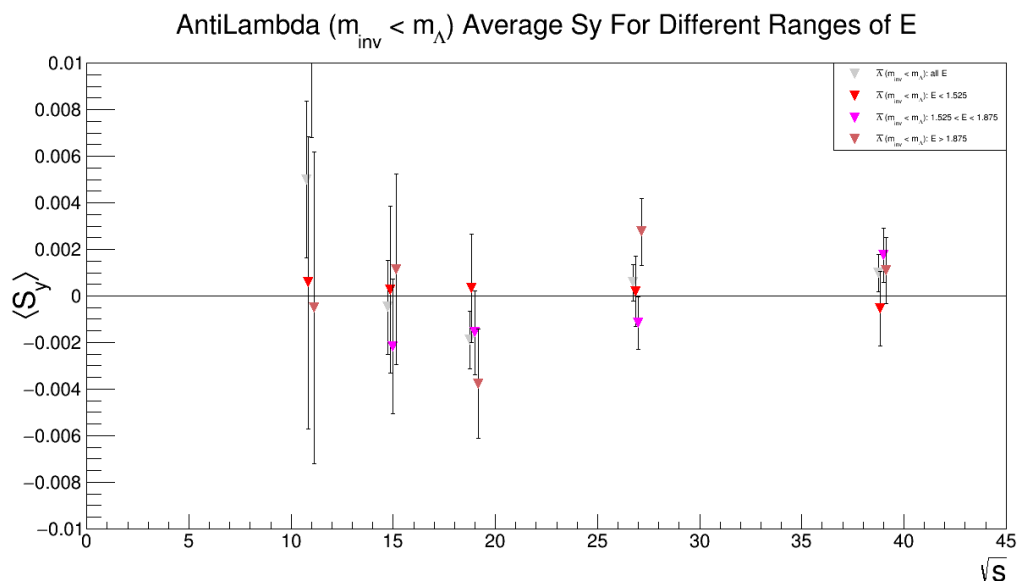


Fig. 172: $\bar{\Lambda}$ left of mass peak ($m_{inv} < m_\Lambda$) polarization cut into three energy bins. Energies quoted in legend are in GeV.

5.3 Rapidity

Hydrodynamic models see possible variation of the signal with Lambda rapidity magnitude. Naively the signal should not depend on the sign of the rapidity. It is possible that the production plane polarization coupled with first order flow could make this happen. What is shown here is the results when an attempt is made to split the data into statistically equal halves and thirds of Lambda rapidity. The intentions of these cuts to make equal fractions may not be particularly well borne out because the cuts were chosen via histograms (it is a binning issue).

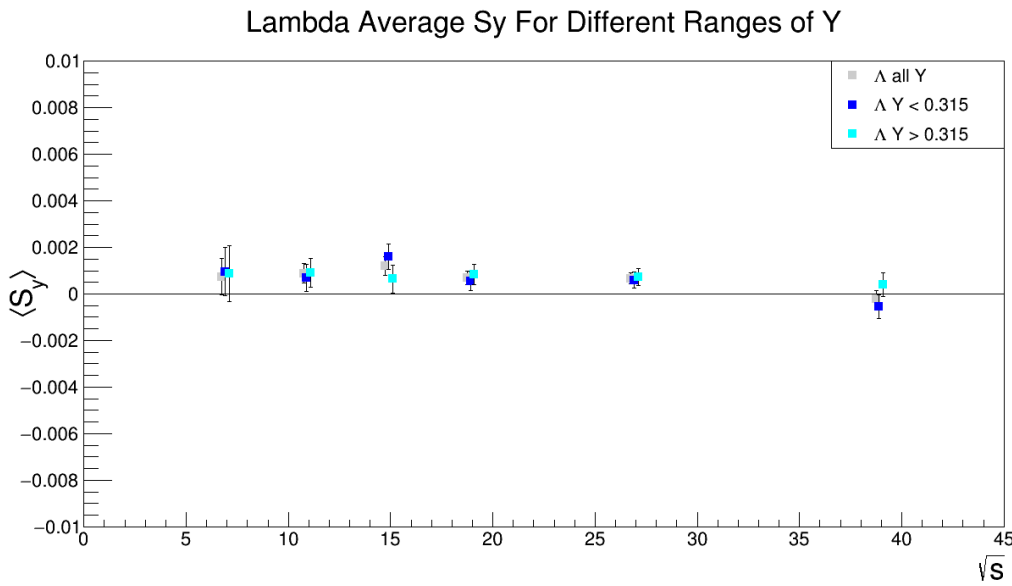


Fig. 173: Λ polarization cut into two rapidity bins.

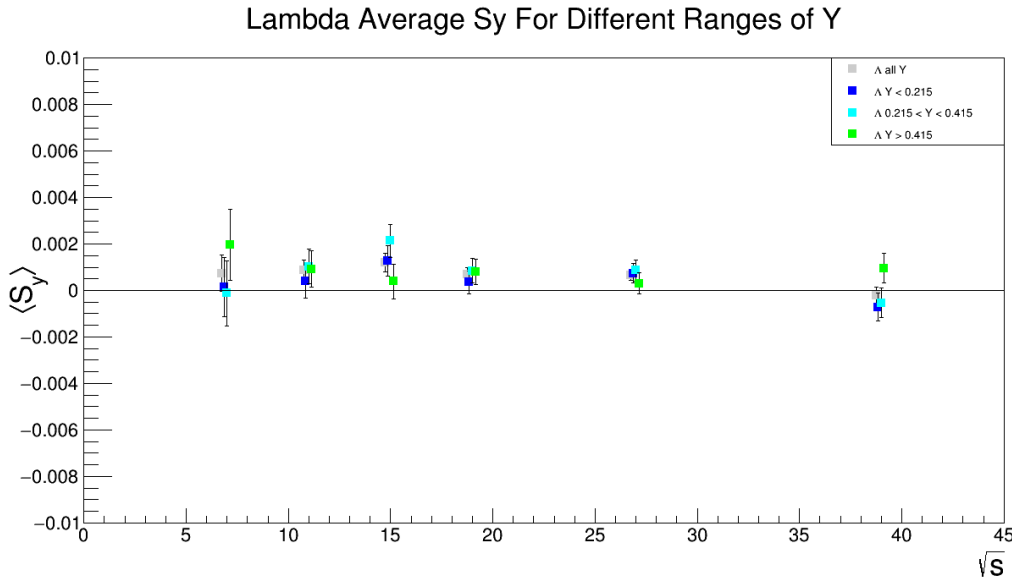


Fig. 174: Λ polarization cut into three rapidity bins.

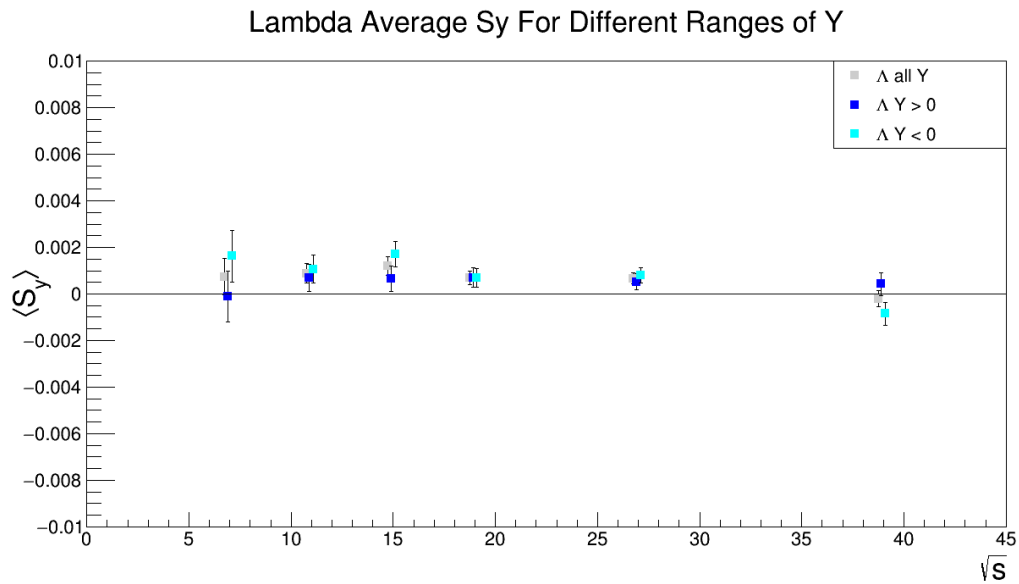


Fig. 175: Λ polarization cut into positive and negative rapidity bins.

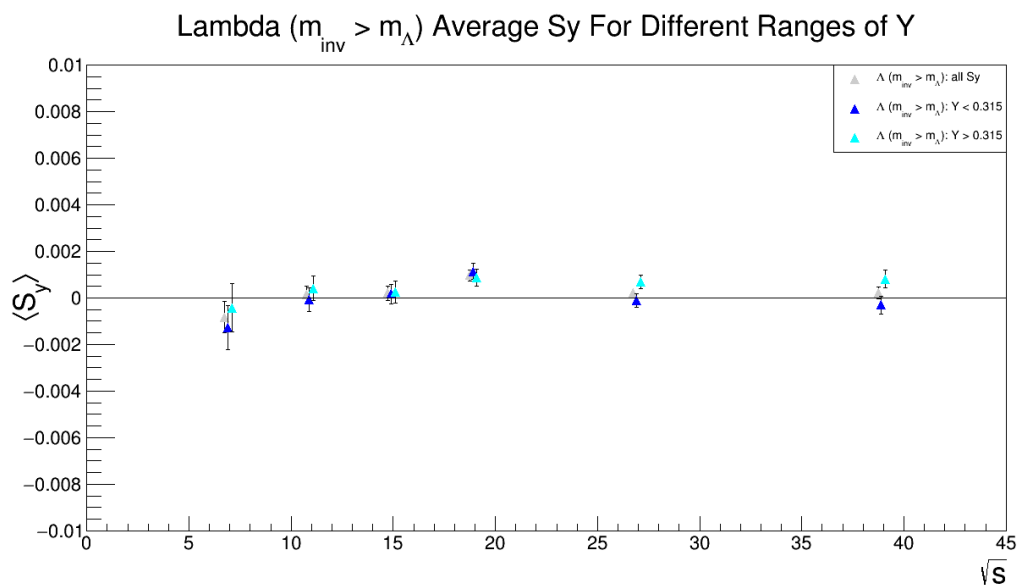


Fig. 176: Λ right of mass peak ($m_{inv} > m_\Lambda$) polarization cut into two rapidity bins.

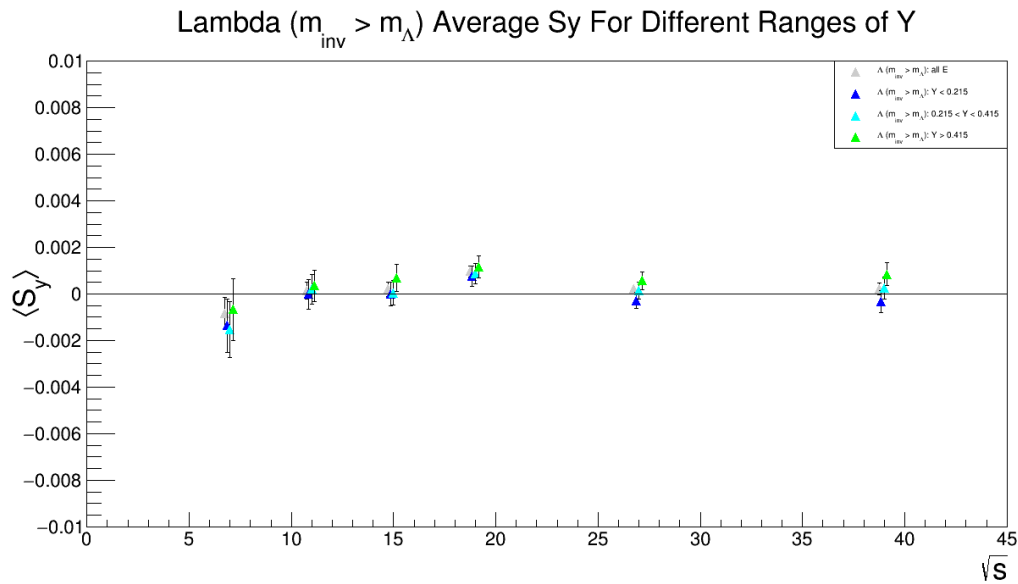


Fig. 177: Λ right of mass peak ($m_{inv} > m_\Lambda$) polarization cut into three rapidity bins.

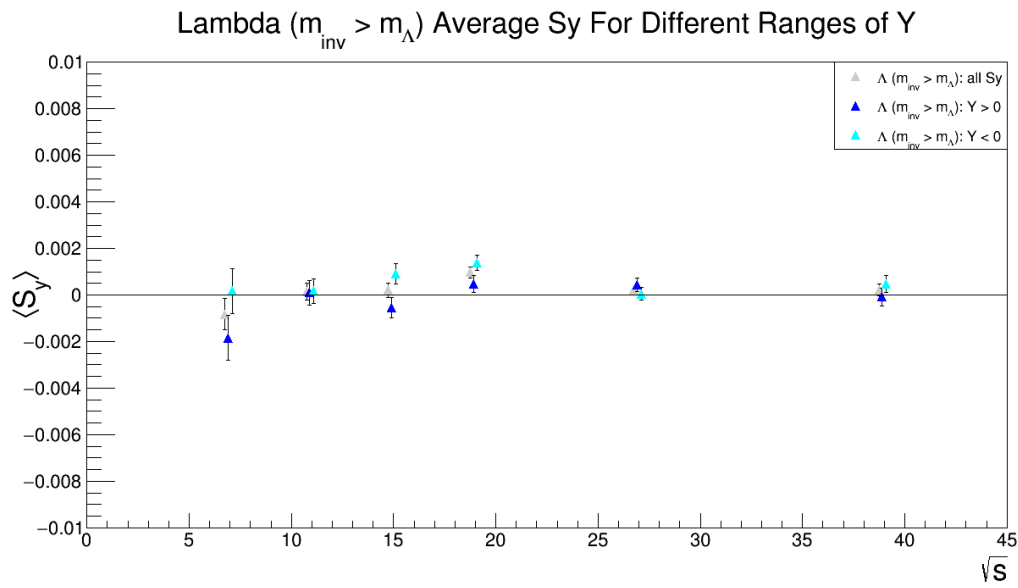


Fig. 178: Λ right of mass peak ($m_{inv} > m_\Lambda$) polarization cut into positive and negative rapidity bins.

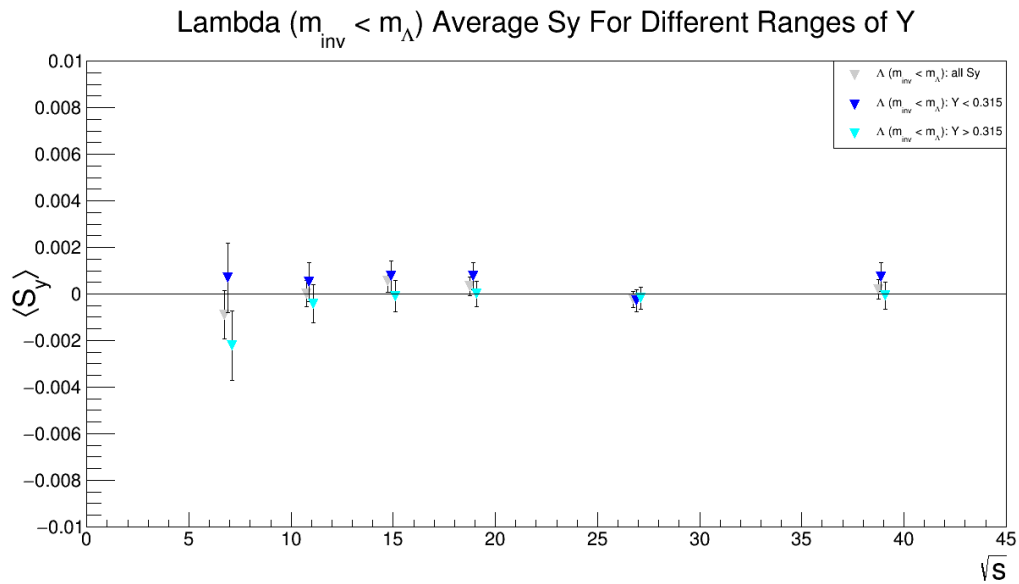


Fig. 179: Λ left of mass peak ($m_{\text{inv}} < m_{\Lambda}$) polarization cut into two rapidity bins.

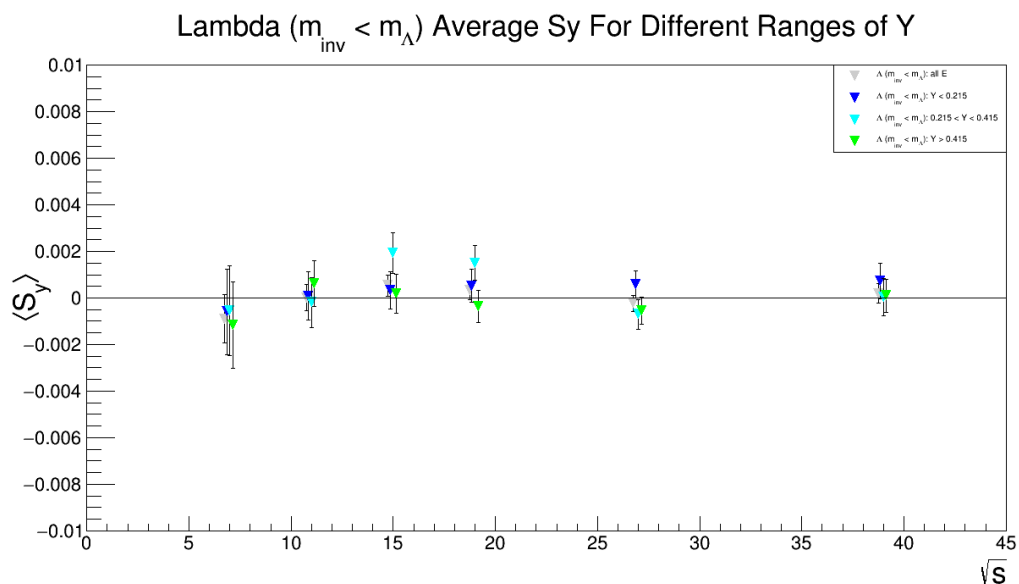


Fig. 180: Λ left of mass peak ($m_{\text{inv}} < m_{\Lambda}$) polarization cut into three rapidity bins.

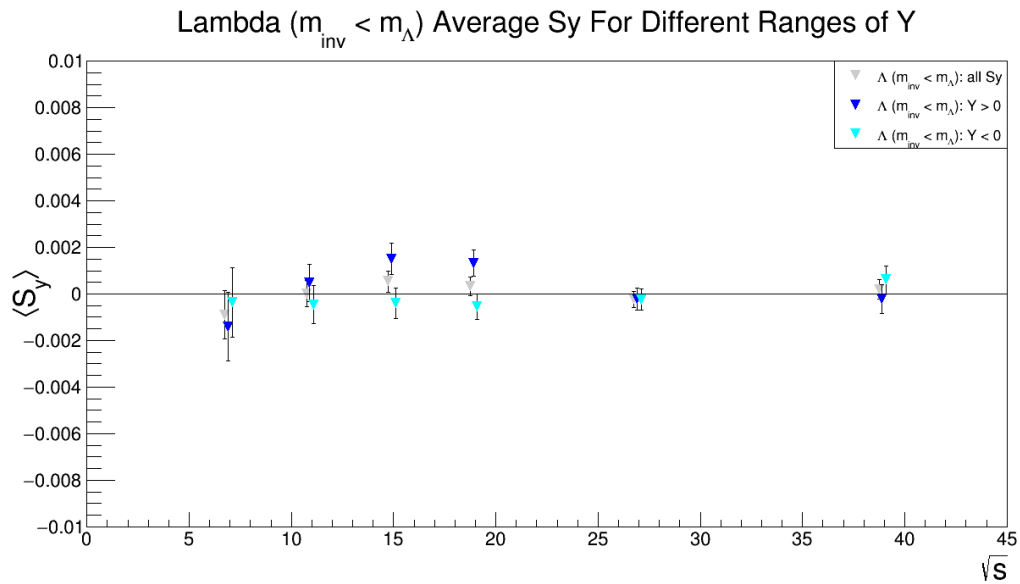


Fig. 181: Λ Left of mass peak ($m_{inv} < m_\Lambda$) polarization cut into positive and negative rapidity bins.

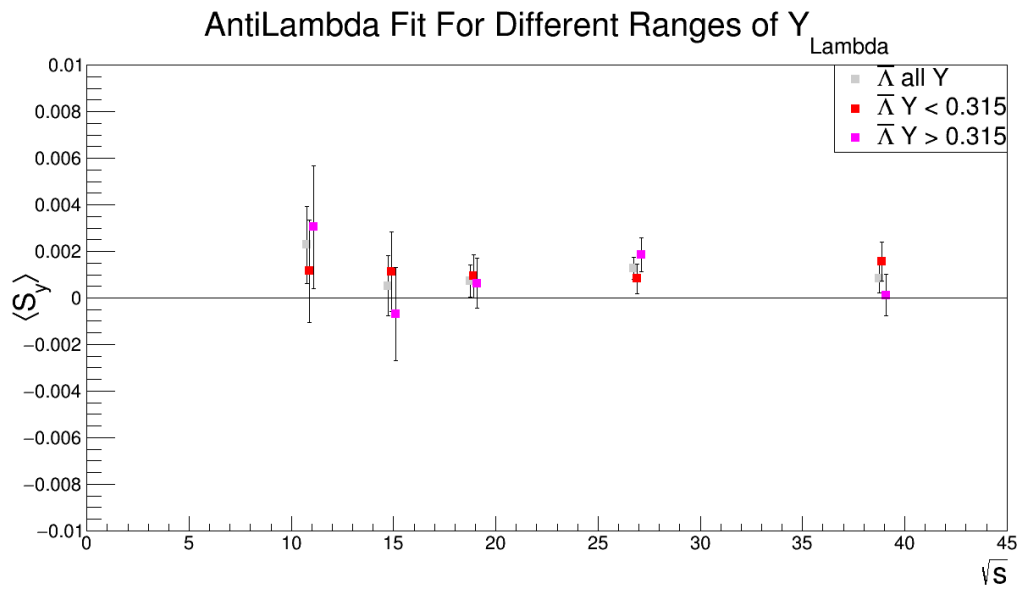


Fig. 182: $\bar{\Lambda}$ polarization cut into two rapidity bins.

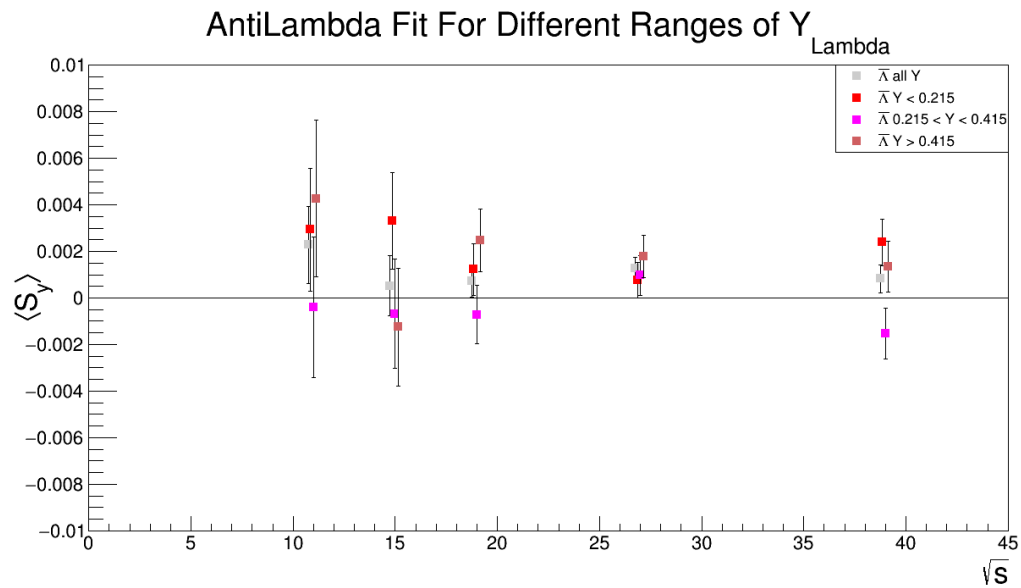


Fig. 183: $\bar{\Lambda}$ polarization cut into three rapidity bins.

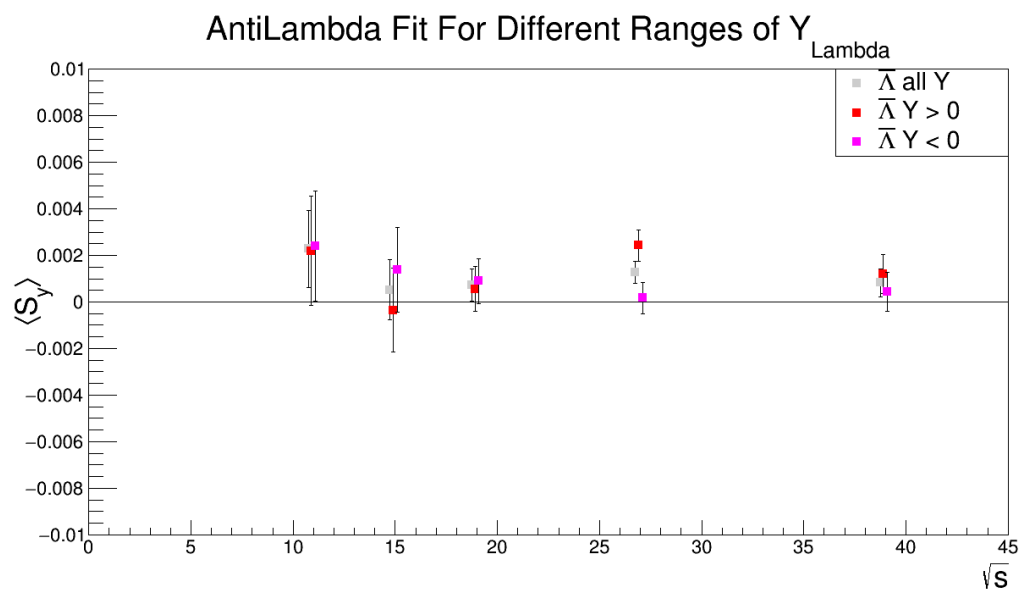


Fig. 184: $\bar{\Lambda}$ polarization cut into positive and negative rapidity bins.

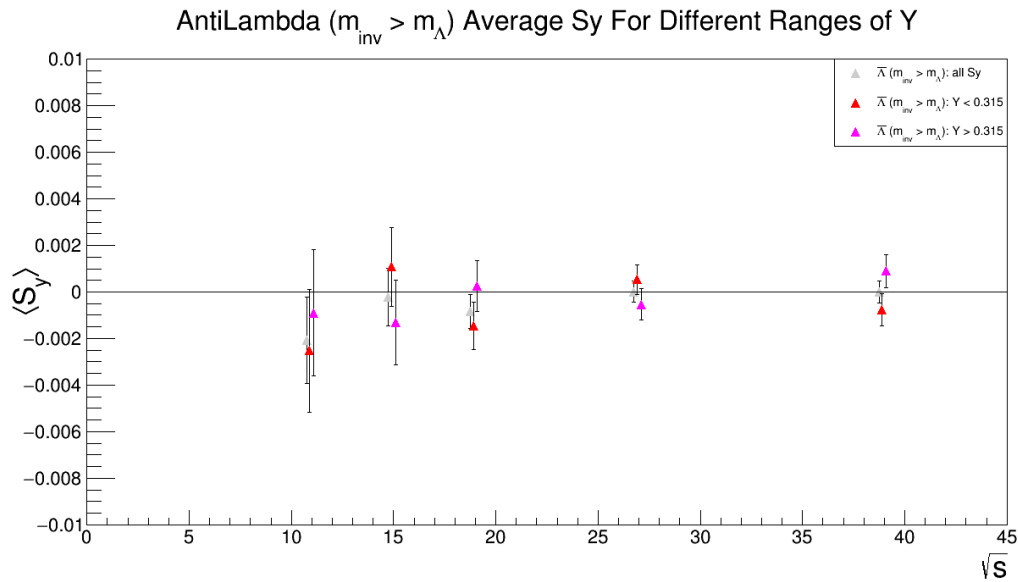


Fig. 185: $\bar{\Lambda}$ right of mass peak ($m_{inv} > m_\Lambda$) polarization cut into two rapidity bins.

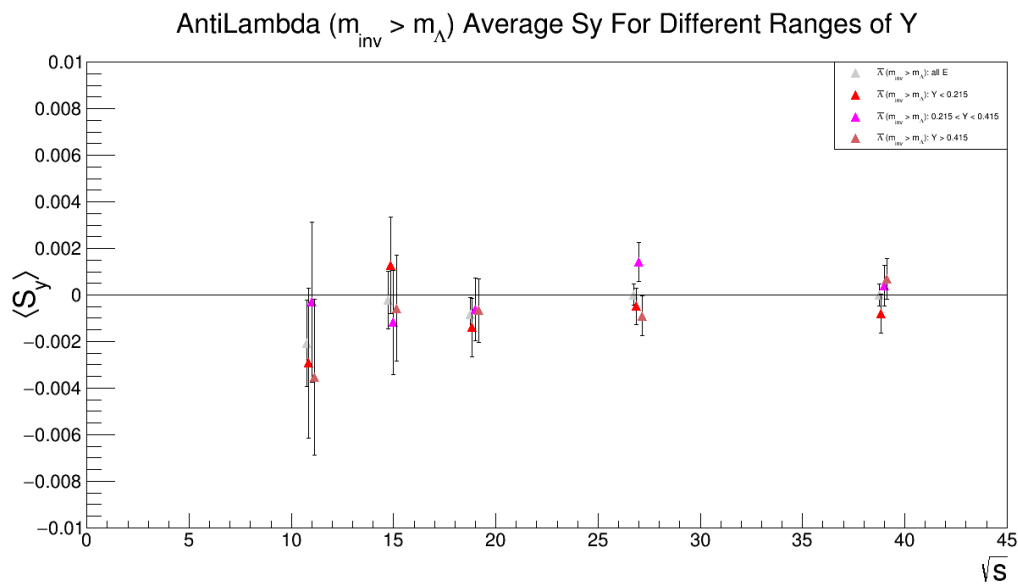


Fig. 186: $\bar{\Lambda}$ right of mass peak ($m_{inv} > m_\Lambda$) polarization cut into three rapidity bins.

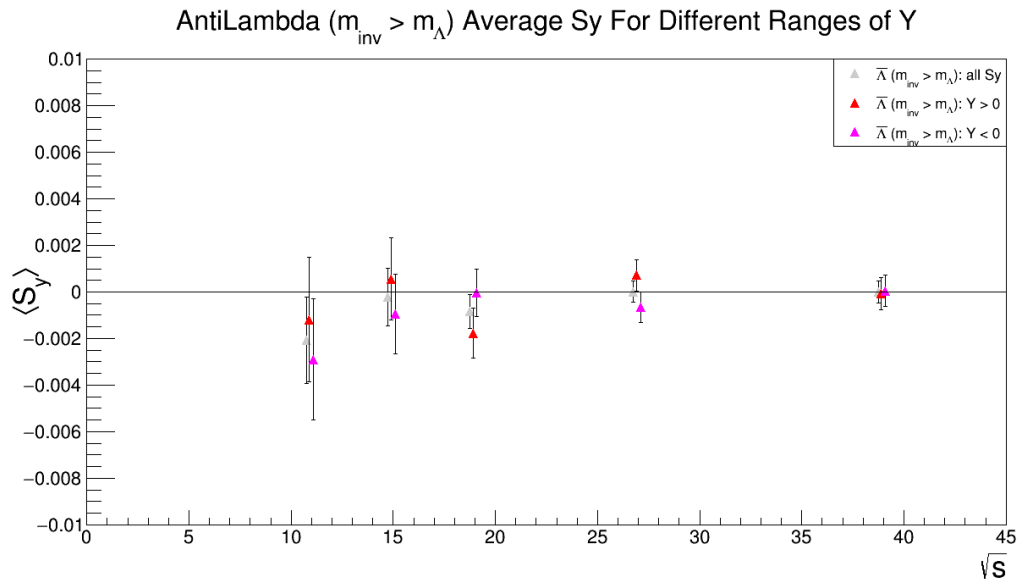


Fig. 187: $\bar{\Lambda}$ right of mass peak ($m_{inv} > m_\Lambda$) polarization cut into positive and negative rapidity bins.

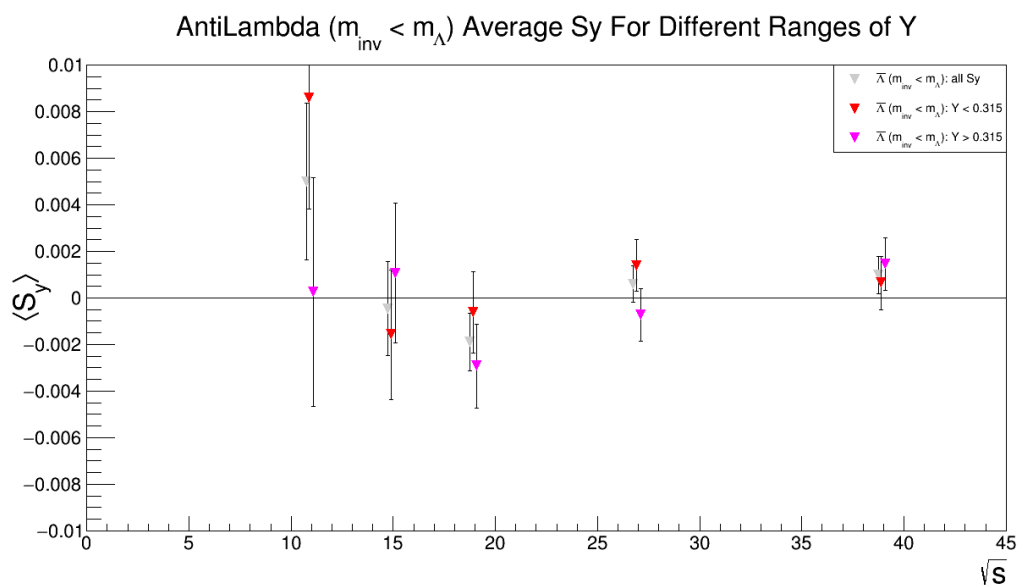


Fig. 188: $\bar{\Lambda}$ left of mass peak ($m_{inv} < m_\Lambda$) polarization cut into two rapidity bins.

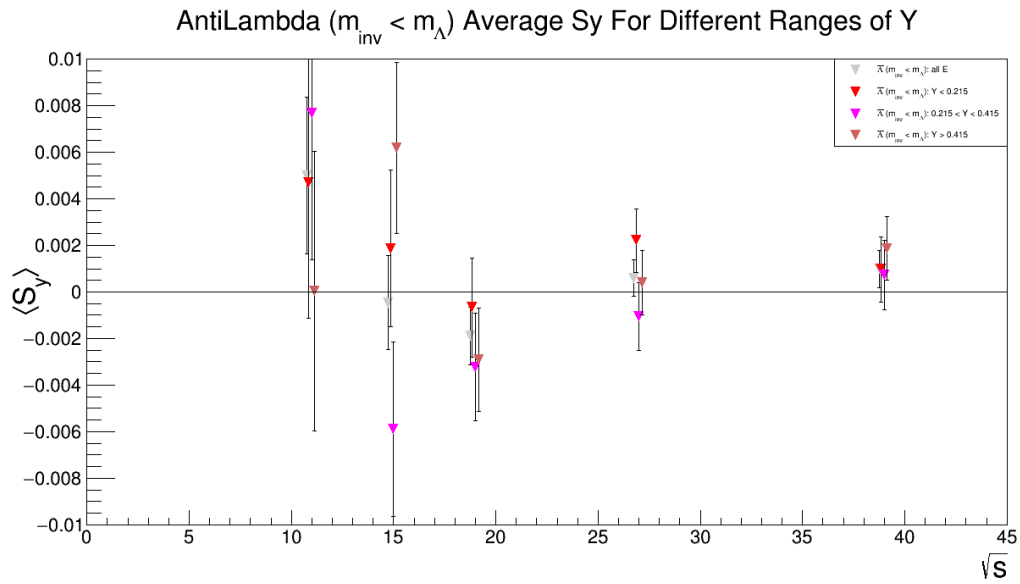


Fig. 189: $\bar{\Lambda}$ left of mass peak ($m_{inv} < m_\Lambda$) polarization cut into three rapidity bins.

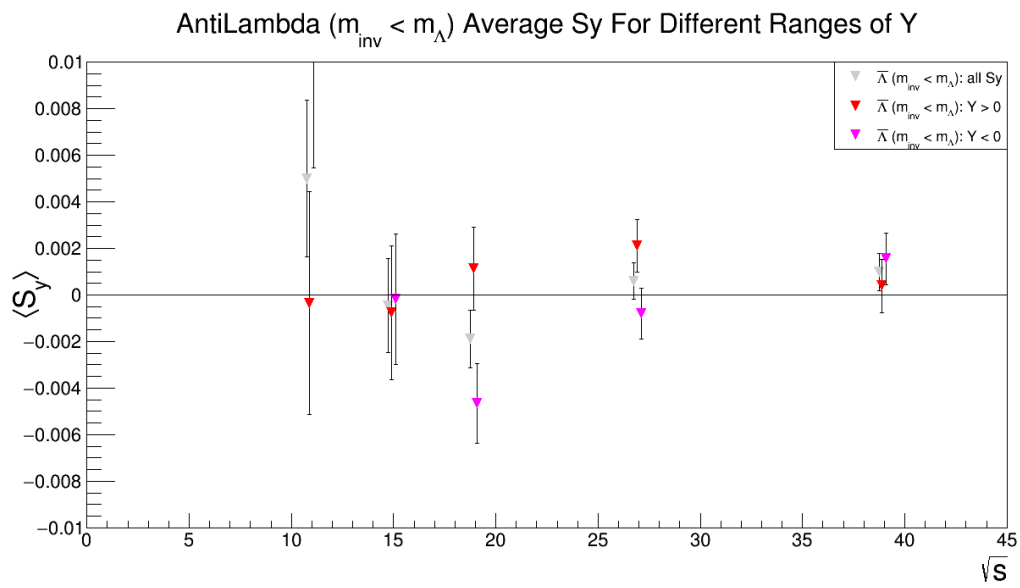


Fig. 190: $\bar{\Lambda}$ Left of mass peak ($m_{inv} < m_\Lambda$) polarization cut into positive and negative rapidity bins.

5.4 Azimuthal angle

Lambdas emitted in vs. out of plane may exhibit different polarization. One cannot look at the straight ϕ dependence of the signal because it would be dominated by the helicity efficiency effect described in section 3.4. To get around this we look at Lambdas in ($|\phi - \Psi_1| < \pi/4$ and $|\phi - (\Psi_1 + \pi)| < \pi/4$) compared to Lambdas emitted out of plane ($|\phi - \Psi_1/2| < \pi/4$ and $|\phi - (\Psi_1/2 + \pi)| < \pi/4$). In the figures I quote ϕ automatically with respect to Ψ_1 so this is $\cos(\phi) < 1/\sqrt{2}$ and $\cos(\phi) > 1/\sqrt{2}$ for space.

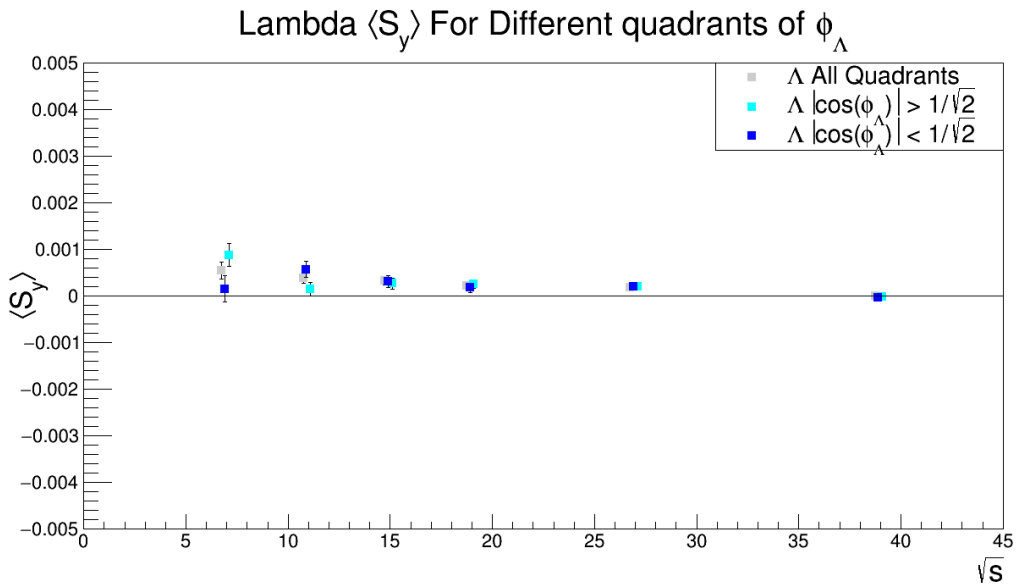


Fig. 191: Λ polarization cut into in and out of plane.

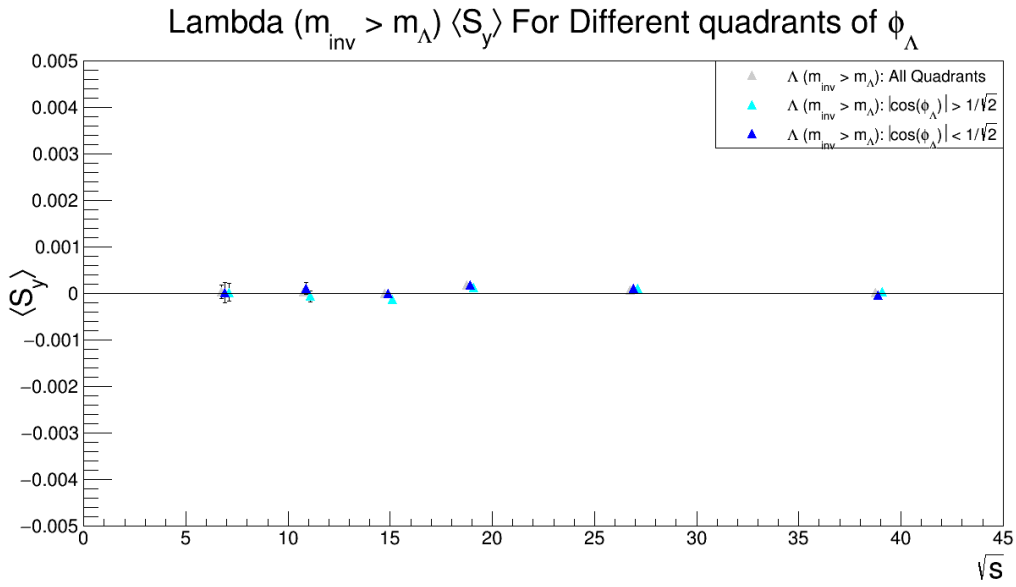


Fig. 192: Λ right of mass peak ($m_{\text{inv}} > m_\Lambda$) polarization cut into in and out of plane.

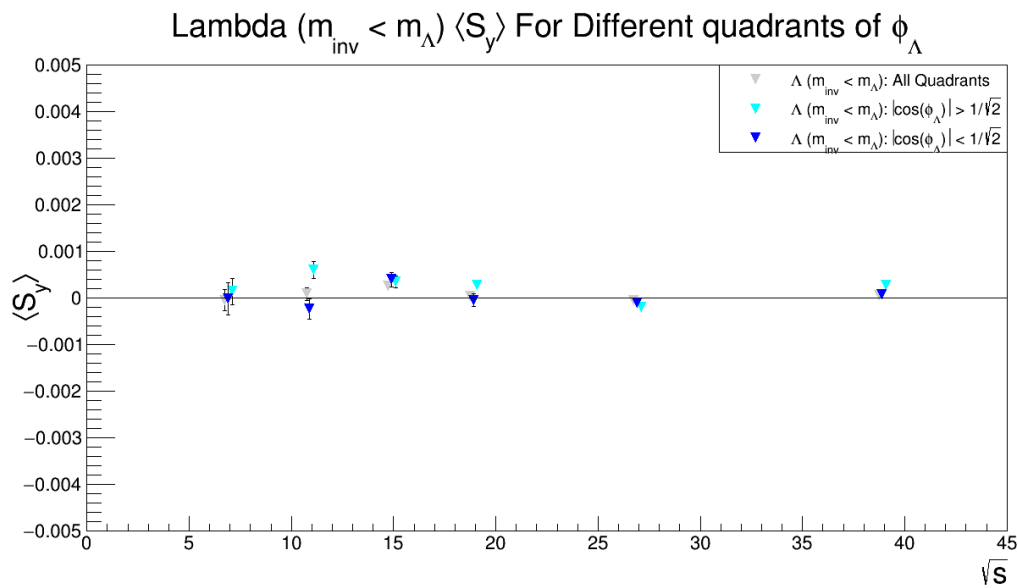


Fig. 193: Λ left of mass peak ($m_{inv} < m_\Lambda$) polarization cut into in and out of plane.

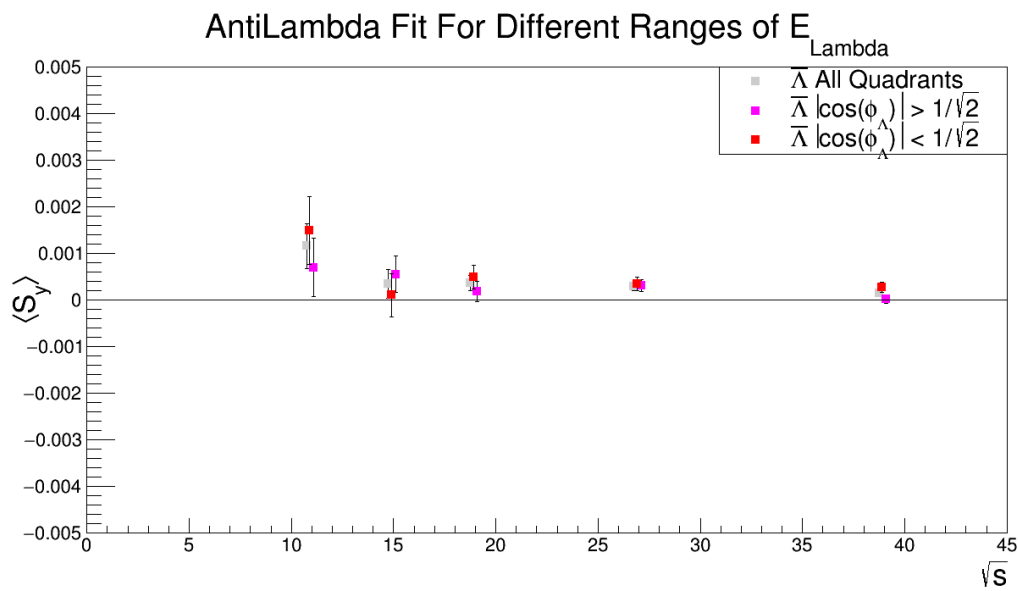


Fig. 194: $\bar{\Lambda}$ polarization cut into in and out of plane.

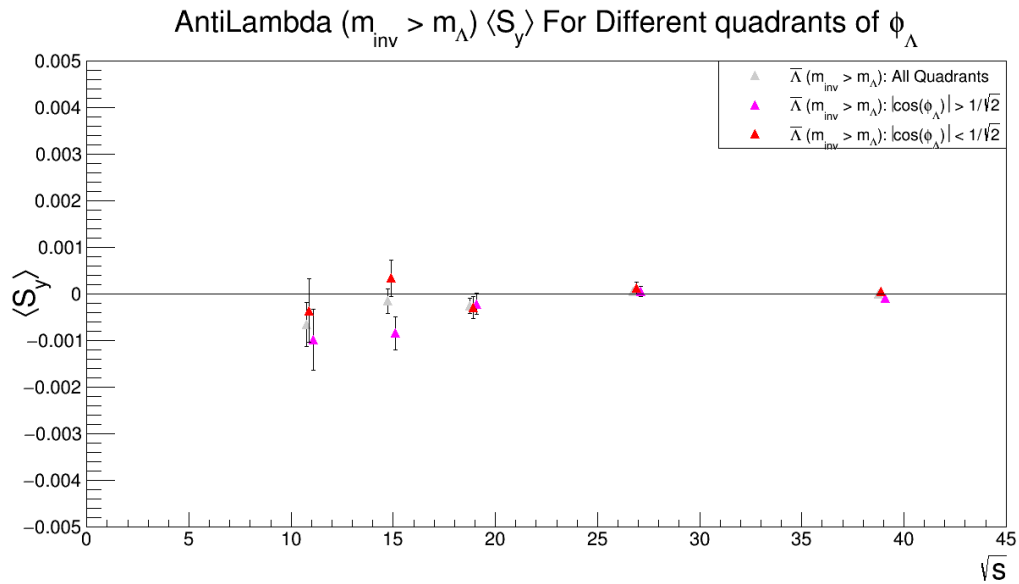


Fig. 195: $\bar{\Lambda}$ right of mass peak ($m_{inv} > m_\Lambda$) polarization cut into in and out of plane.

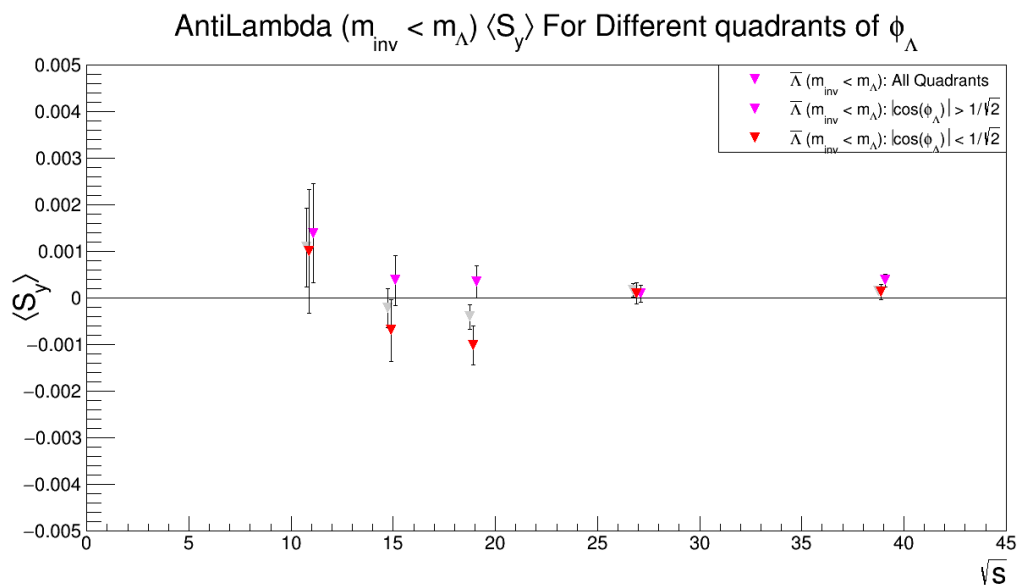


Fig. 196: $\bar{\Lambda}$ left of mass peak ($m_{inv} < m_\Lambda$) polarization cut into in and out of plane.

6 Signal falsification

The purpose of this section is to provide examples of work that was done to attempt to falsify the signal.
 2035 An important attempt to falsify the signal is from looking at the combinatoric background of the Lambda mass distribution. This is already discussed in section 3.2 so there is no corresponding check here.

6.1 Simulation comparison

Typically a natural place to look to verify or falsify an experimental signal are the many models that exist.
 2040 No available simulation (at least as far as I am aware) has vorticity or spin coupling so simulation can, at best, be used for falsifying the results and attempting to see if one sees the signal appear as a consequence of acceptance or kinematics. Since the analysis is so simple it is unlikely that such a falsification could occur. The tools available I have used in this analysis are HIJING, embedded Lambdas in real events, and UrQMD.

Since HIJING simulations in the STAR framework have included a cut such that primary particles have
 2045 $-4.5 < \eta < 2.5$ it isn't really possible to use the BBC and thus it is not possible to make any attempt at falsifying the results, aside from assuming that Ψ_1 is zero or random for every event. Because of the η cut many of the particles reaching the BBCs are secondary and thus there can be a large autocorrelation effect with daughters of Lambdas and the "measured" Ψ_1 . Assuming that Ψ_1 is zero for every event gives a result that falls right on zero.

2050 Embedding data is very statistically challenged. Since the Lambdas in embedding aren't polarized and are not made to have any correlation with Ψ_1 they can't give a number more sensitive than other simulation results.

UrQMD (in which the reaction plane is known) for 19.6GeV has given $S_y = 1.95^{-4} \pm 2.95^{-4}$ which means $N_\sigma = 0.66$ (S_y is a variable which is qualitatively consistent with $\sin(\Psi_1 - \phi_\Lambda^*)$). For UrQMD data
 2055 I am given a list of Lambdas and I have to decay them myself. I give them an isotropic decay geometry so it is hardly a surprise that the results fall on zero. I do not have UrQMD tracks run through the GEANT model of STAR so I can only analyze the data as similarly to real data up to a point.

6.2 Rotated pions

Another way to try to falsify the signal is the run the same code but rotate all of the pions in the event
 2060 by π in the $x - y$ plane. This should provide realistic Lambda candidates without providing any residual effects from real Lambdas leaking in. There should be a null signal in this measure. The following results are for resolution corrected polarization ($\sin(\Psi_1 - \phi_\Lambda^*)$) with no scaling by $8/(\pi\alpha)$.

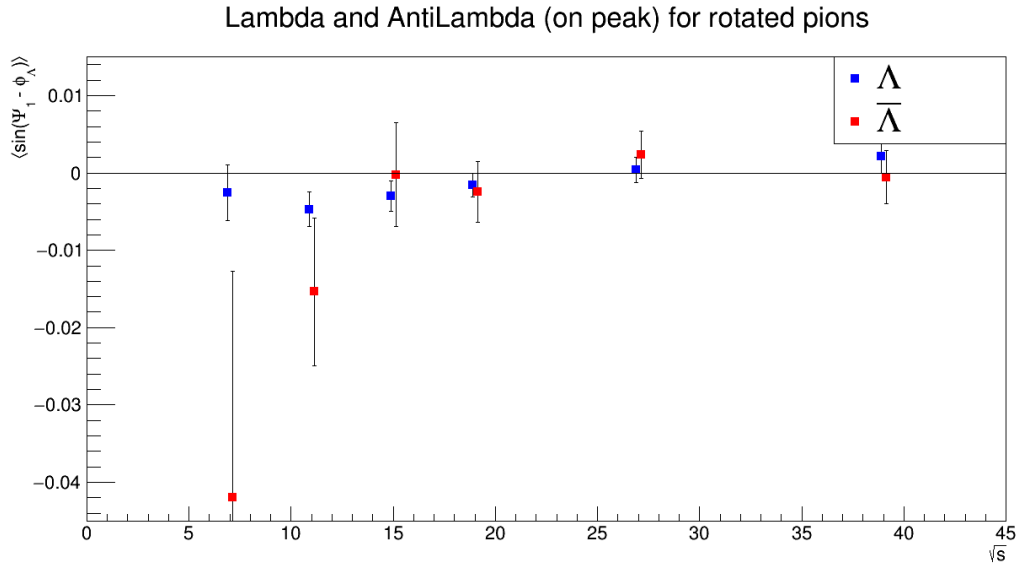


Fig. 197: $\sin(\Psi_1 - \phi_{\Lambda}^*)$ as a function of $\sqrt{s_{NN}}$ for Λ and $\bar{\Lambda}$ where the momenta of the pions in the events have been rotated 180 degrees in azimuth.

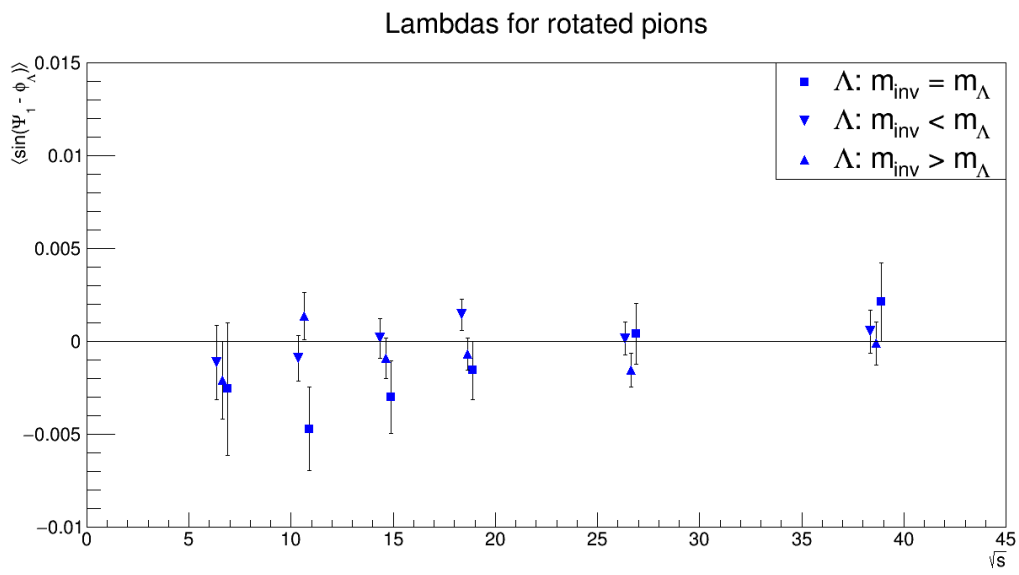


Fig. 198: $\sin(\Psi_1 - \phi_{\Lambda}^*)$ as a function of $\sqrt{s_{NN}}$ for Λ candidates that have large or small invariant mass - also referred to as off mass (both cases of $m_{inv} > m_{\Lambda}$ and $m_{inv} < m_{\Lambda}$) - where the momenta of the pions in the events have been rotated 180 degrees in azimuth.

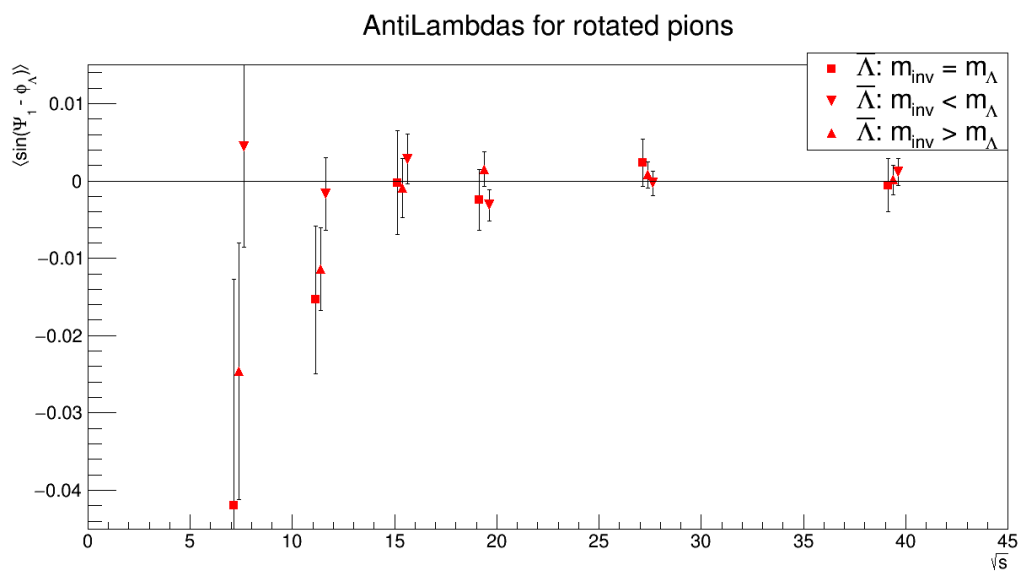


Fig. 199: $\sin(\Psi_1 - \phi_\Lambda^*)$ as a function of $\sqrt{s_{NN}}$ for $\bar{\Lambda}$ candidates that have large or small invariant mass - also referred to as off mass (both cases of $m_{inv} > m_\Lambda$ and $m_{inv} < m_\Lambda$) - where the momenta of the pions in the events have been rotated 180 degrees in azimuth.

7 STAR 2007 results

Part of the paper is quoting the 2007 (<https://arxiv.org/abs/0705.1691>) global polarization results from STAR. The first thing to make clear is that there is a sign error in the 2007 analysis due to a mistake about the angular momentum direction, so quoted results are going to be a sign off from what you see in the paper. To compare we need results integrated over p_T in 20-50% centrality. We got these numbers from the 2010 rows of <https://drupal.star.bnl.gov/STAR/files/starpublications/79/data.html>. To properly weight the centrality bins we assume that the number of Lambdas (AntiLambdas) in one bin centrality relative to another is the same as the ratio is for charged particles (RefMult). We get the refmult from “Centrality_def_refmult.txt” from StRefMultCorr averaging the two 5% centrality bins in the table.

Centrality	$62.4GeV$	$200GeV$
20-30%	167	226.5
30-40%	111.5	151.5
40-50%	71	96

Table 17: StRefMultCorr averaged tables for $62.4GeV$ and $200GeV$

Centrality	P_H	<i>error</i>	$RefMult \cdot P_H$	$(RefMult \cdot error)^2$
20-30%	-0.0001	0.0174	-0.0167	8.44367364
30-40%	0.044	0.02	4.906	4.9729
40-50%	-0.0032	0.0253	-0.2272	3.22669369

Table 18: $62.4GeV$ Λ results from 2007 paper

Centrality	P_H	<i>error</i>	$RefMult \cdot P_H$	$(RefMult \cdot error)^2$
20-30%	0.0096	0.024	1.6032	16.064064
30-40%	0.0282	0.027	3.1443	9.06311025
40-50%	0.0174	0.034	1.2354	5.827396

Table 19: $62.4GeV$ $\bar{\Lambda}$ results from 2007 paper

Centrality	P_H	<i>error</i>	$RefMult \cdot P_H$	$(RefMult \cdot error)^2$
20-30%	0.000177	0.015	0.0400905	11.54300625
30-40%	-0.016	0.0178	-2.424	7.27219089
40-50%	0.031	0.0221	2.976	4.50118656

Table 20: $200GeV$ Λ results from 2007 paper

Centrality	P_H	<i>error</i>	$RefMult \cdot P_H$	$(RefMult \cdot error)^2$
20-30%	-0.00795	0.017	-1.800675	14.82635025
30-40%	-0.011	0.02	-1.6665	9.1809
40-50%	-0.0022	0.025	-0.2112	5.76

Table 21: $200GeV$ $\bar{\Lambda}$ results from 2007 paper

Type	P_H	<i>error</i>
$62.4GeV$ Λ	0.0133393419	0.0116727212
$62.4GeV$ $\bar{\Lambda}$	0.0171184549	0.015918979
$200GeV$ Λ	0.0012491361	0.0101871395
$200GeV$ $\bar{\Lambda}$	-0.0077602848	0.0115104159

Table 22: 2007 final 20-50% centrality results tabulated from tables 18-21